

***The Effect of High Hydrostatic Pressure on
Hydrogen Bond Scaffolds***

Dissertation

Zur Erlangung des Doktorgrades der Naturwissenschaften

Dr. rer. nat.

an der

**Fakultät für Chemie und Pharmazie-
der Universität Regensburg**



vorgelegt von

Thomas Weinbender

aus Traunreut

im Jahre 2020

Die Arbeit wurde angeleitet von:

Prof. Dr. Oliver Reiser

Promotionsgesuch eingereicht am:

17.06.2020

Promotionskolloquium am:

07.08.2020

Prüfungsausschuss

Vorsitz : Apl. Prof. Dr. Rainer Müller

1. Gutachter : Prof. Dr. Oliver Reiser

2. Gutachter : Prof. Dr. Frank-Michael Matysik

3. Prüfer : Prof. Dr. Alexander Breder

Der experimentelle Teil der vorliegenden Arbeit wurde in der Zeit von November 2016 bis Januar 2020 unter der Leitung von Herrn Prof. Dr. Oliver Reiser am Institut für Organische Chemie der Universität Regensburg angefertigt.

Herrn Prof. Dr. Oliver Reiser möchte ich herzlich für die Aufnahme in seinen Arbeitskreis, die Überlassung des interessanten Themas, die anregenden Diskussionen und seine stete Unterstützung während der Durchführung dieser Arbeit danken.

Für meine Familie und Freunde

Table of Contents

1	Introduction	10
2	Aim of the Work.....	33
3	Main Part.....	34
3.1	High-Pressure-mediated Thiourea-Organocatalyzed Asymmetric Michael Addition to (Hetero)Aromatic Nitroolefins	34
3.2	Synthesis of a γ -Aminobutyric Acid (GABA) Derivative.....	45
3.3	Influence of High Pressure on Hydrogen Bonds	48
3.3.1	NMR Studies of Hydrogen Bonds.....	51
3.3.2	IR Studies of Hydrogen Bonds	57
4	Summary.....	66
4.1	Summary in English	66
4.2	Summary in German	68
5	Experimental Part.....	70
5.1	General Information.....	70
5.2	Experimental Procedures and Analytical Data	72
5.2.1	High Pressure Technique.....	72
5.2.2	Nitroolefin Synthesis.....	76
5.2.3	General Procedure for High Pressure/ambient Pressure Reactions	86
5.2.4	Michael Addition Products	87
5.2.5	Synthesis of γ -amino acid 4-amino-3-(2-methyl-1 <i>H</i> -indol-3-yl)butanoic acid....	93
5.2.6	Amide Synthesis	94
5.3	NMR Spectra.....	100
5.4	HPLC Chromatograms	159
6	References.....	181
7	Appendix	189
7.1	Curriculum Vitae.....	189
8	Acknowledgement.....	191
9	Declaration.....	193

Abbreviations

2-HPP	2-hydroxypropiophenone	ESI	electrospray ionization
AcOH	acetic acid	Et	ethyl
AF	amyloid fibrils	EtOAc	ethyl acetate
APCI	atmospheric pressure chemical ionization	FTIR	fourier-transform infrared spectroscopy
aq.	aqueous	GABA	γ -aminobutyric acid
ASP	aspartic Acid	Glu	glutamic acid
BFD	benzoylformate decarboxylase	H	histidine
Bn	benzyl	h	hour
Boc	<i>tert</i> -butyloxycarbonyl	His	histidine
Bu	butyl	HOBt	hydroxybenzotriazole
d	day	HPLC	high-performance liquid chromatography
d.r.	diastereomeric ratio	HQ	hydroquinone
DCC	<i>N,N</i> - dicyclohexylcarbodiimide	HRMS	high-resolution mass spectroscopy
DCE	1,2-dichloroethane	I	isoleucine
DCM	dichloromethane	IR	infrared
DEAEA	<i>N,N</i> - diethylaminoethylamine	L	leucine
DEM	diethyl malonate	LBHB	low barrier hydrogen bond
DENPEM	diethyl 2-(2-nitro-1- phenylethyl)malonate	Me	methyl
DMAP	4-dimethylaminopyridine	min	minute
DMF	<i>N,N</i> -dimethylformamide	Mp	melting point
DMS	dimethyl sulfide	NCS	<i>N</i> -chlorosuccinimide
DMSO	dimethyl sulfoxide	NHS	<i>N</i> -hydroxysuccinimide
dTGS	deuterated triglycine sulfate	NMR	nuclear magnetic resonance
E _a	activation energie	NST	trans- β -nitrostyrene
EDC	1-ethyl-3-(3- dimethylaminopropyl)carbo diimid hydrochloride	PCP-	perturbed-chain polar
ee	enantiomeric excess	SAFT	statistical associating fluid theory
EI	electron ionization	PDA	photodiode array
equiv	equivalents	Ph	phenyl
		ppm	parts per million
		PTFE	polytetrafluoroethylene

Abbreviations

Q	glutamine
Q-TOF	quadrupole time-of-flight
R	arbitrary rest
rt	room temperature
Ser	serine
SWHB	single well hydrogen bond
TBAB	tetra- <i>n</i> -butylammonium bromide
tBu	<i>tert</i> -butyl
TEMPO	(2,2,6,6-tetramethylpiperidin-1-yl)oxyl
ThDP	homotetrameric thiamine diphosphate
THF	tetrahydrofuran
TLC	thin layer chromatography
TOF	time-of-flight
TS	transition state
UV	ultraviolet
β -ACC	β -aminocyclopropane carboxylic acids

1 Introduction‡

With around 7.79 billion human beings on our planet, living in 193 sovereign states and practicing dozens of different religions, one can definitely say: every individual is unique and different from each other. Certainly, there is one particular thing we, as humans, all have in common which was sung by the Bee Gees in 1977: “Stayin’ Alive”. Once a human being is born the main goal is to stay alive. To achieve this, the supply of oxygen, water and nourishment needs to be ensured. The latter developed mainly by the food industry and food processing, making groceries accessible from all around the world.

The consumers choices are predominantly affected by two factors, safety and quality of food products. The quality can easily be determined by smell, color, flavor, texture and their nutritional values. However, the determination of food contaminations is more complicated since they are not detectable with the naked eye. When conventional food preservation and sterilization methods (thermal processing) are used to denature proteins and inactivate enzymes and microorganisms, several undesired changes in the food’s quality are often inevitable. A novel non-thermal food processing method is the treatment with high pressures up to 1000 MPa being applicable to both liquid and solid goods, with or without their packaging. It is a valuable germ-destroying method without any loss of quality and therefore without altering the nature of the food.^[2]

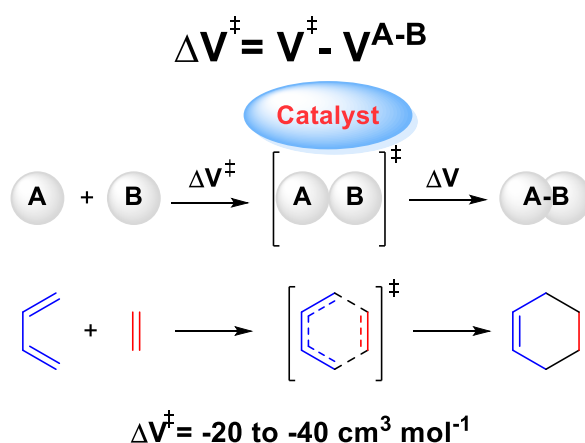
High pressure, or hydrostatic pressure, finds its applications not only in industrial processes but also in academic research in the fields of chemistry and physics. Chemical reactions do not occur spontaneously, in most cases, activation energy is required for the reaction to proceed with reasonable reaction rates. Going back to the 1950’s only a few laboratories all around the world were able to do proper high pressure research in organic chemistry. In these times, the misapprehension that high pressure experiments were exceptionally intricate to examine led to the dispartment of this research topic as an outstanding discipline in science, only accessible for the well-versed. However, these circumstances have drastically changed in the recent years. Equipment for high pressure experiments is now more affordable and more readily available than before. Additionally, due to technical innovations, conducting and carrying out these experiments became less challenging rendering high pressure a prominent method of activation.^[3]

The direct observation of hydrostatic pressure effects on (bio)organic molecules by spectroscopic methods such as IR or NMR is still labor and equipment intensive and finds quickly its

‡This chapter is partially based on T. Weinbender, M. Hofmann, O. Reiser, *Biophys. Chem.* **2019**, 106280.^[1]

limitation by the spectroscopically transparent materials available for a given solvent to carry out such measurements. On the other hand, many functional biomolecules such as enzymes display catalytic activity to promote organic reactions. Along these lines, various classes of small organic molecules have been identified that display catalytic activity related to enzymes, thus, such compounds might be considered as enzyme models. Given their much simpler structure, such entities, coined as organocatalysts, are readily available and moreover, the understanding of their mode of action is greatly simplified. Thus, evaluating reactivity (kinetics) and selectivity (chemo- and stereoselectivity) of enzymes and organocatalysts might provide an indirect approach to deduce the effect of pressure on such molecules and might be especially meaningful given that the catalytic process takes place in the active center of the enzyme.

Moreover, a given reaction catalyzed by an enzyme or an organocatalyst might benefit from applying pressure, being a mild and non-destructive activation mode, thus enabling significant rate accelerations and the possibility of suppressing the formation of side products. Generally, acceleration of reactions by pressure is only possible if the volume of activation ΔV^\ddagger , being defined as the difference of the volume of the transition state V^\ddagger and the volume of the corresponding reactants V^{A-B} (Scheme 1) possesses a negative value.^[4-6] Responsible for the negative volume of activation is the packing coefficient η , which is defined as the ratio of the van der Waals volume V_w (intrinsic molar volume) to the partial molar volume V . Given that the packing coefficient η of cyclic entities is larger than of the corresponding acyclic entities, the negative activation volume ΔV^\ddagger of reactions proceeding through cyclic transition states such as pericyclic reactions can be rationalized.^[7]



Scheme 1. Definition of the volume of activation and the Diels-Alder-reaction of butadiene and ethylene as a model reaction.

Addition reactions, best established for cycloadditions such as the Diels-Alder reaction, generally fulfill this criterion (Table 1), and many examples demonstrate the beneficial effect of

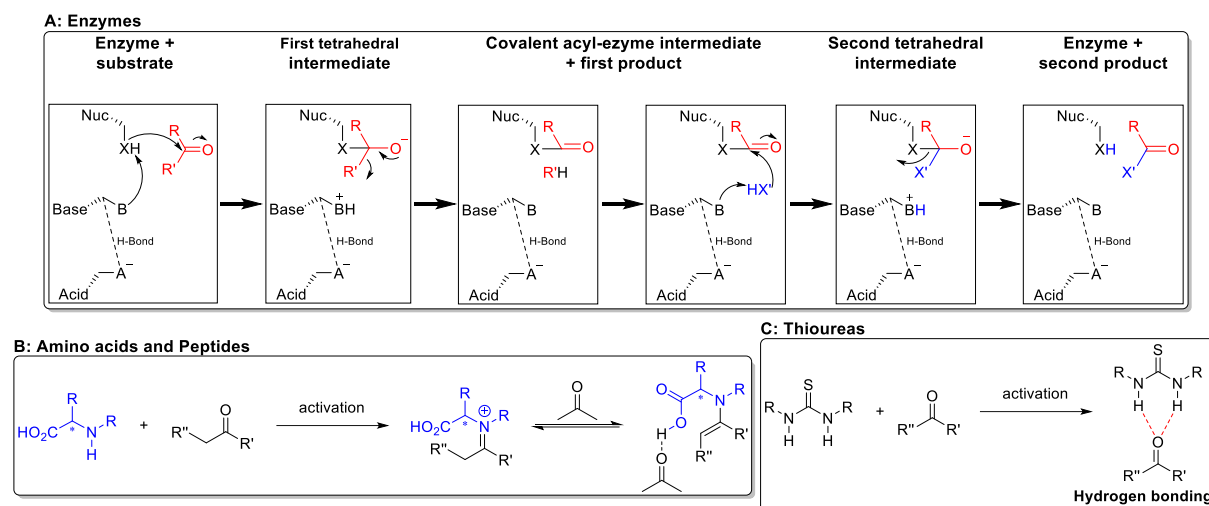
pressure for these processes. The especially large negative ΔV^\ddagger values that are found for Baylis-Hillman reactions illustrate the effect of electrostriction on the activation volume of a reaction: The occurrence of ionic intermediates causes an ordering of the components in solution based on charge attraction, thus resulting in a decrease of volume. In contrast, the formation of radicals by homolytic bond cleavage goes along with a positive ΔV^\ddagger value, conveniently rationalized by the increasing number of molecules in the rate determining step.

Table 1. Estimated range of ΔV^\ddagger of selected reactions.

Reaction	Estimated range for ΔV^\ddagger (cm ³ mol ⁻¹)
Diels-Alder ^[5]	-20 to -40
Baylis-Hillman ^[8]	-40 to -50
Menshutkin ^[9]	-10 to -30
[2+2] Cycloaddition ^[10]	-10 to -30
Michael-like ^[11]	-5 to -40
Homolysis ^[9]	0 to +15
Activation Volumes for selected reaction classes of organic compounds ^[12]	

Since many organic reactions proceed with high selectivity being possible through a defined arrangement of substrates, changes of selectivity might reflect geometrical perturbations of the active center of a catalyst, e.g. of an enzyme, by pressure. Thus, analyzing the pressure dependence on selectivity, especially on stereoselectivity such as dia- and enantioselectivity, might be a sensitive tool to directly identify geometrical changes in the transition state. In turn, an increase of the rate of a reaction might serve as an indication for pressure to shift a conformational equilibrium towards an assembly with higher packing coefficients.

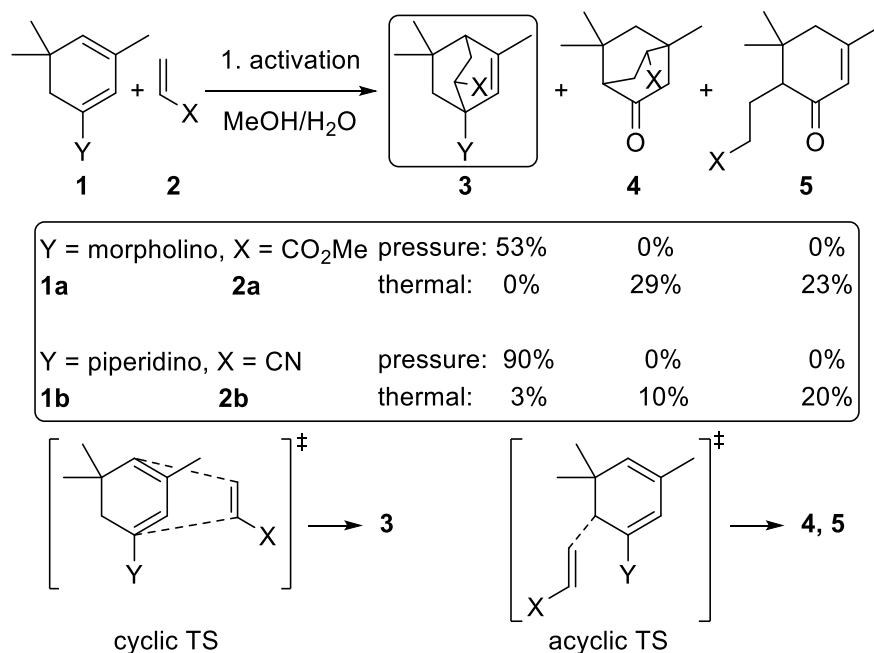
Hereinafter, the development of high hydrostatic pressure in organic chemistry, aiming to deduce effects of pressure on bio(organo)molecules by analyzing their catalytic performance with respect to reaction rates and selectivities, is highlighted. Four different classes of catalysts are presented: (a) Enzymes, representing the catalysts of Nature, (b) amino acids and peptides, representing key building blocks of life, (c) primary amines and cinchona alkaloids, found in plants and, (d) thiourea derivatives, known as inhibitors of enzymes (Scheme 2).



Scheme 2. (A) General reaction mode of a catalytic triad of enzymes (black), (B) activation mode of amino acids and peptides via iminium/enamine intermediates, (C) activation mode of thioureas through hydrogen bonding with the substrate.

Uncatalyzed reactions at high pressure – Diels-Alder and aldol reactions

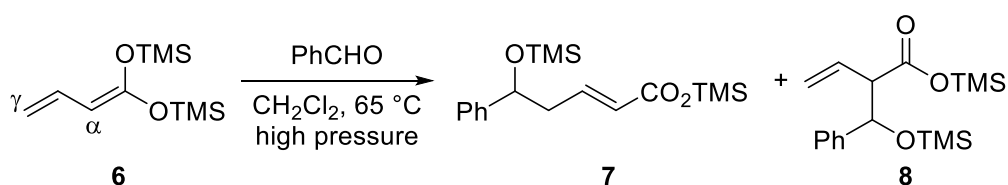
The preference for compact or more ordered transition states under pressure being reflected by larger packing coefficients became apparent in early studies on Diels-Alder reactions. Dauben and coworkers demonstrated that pressure not only affects the rate, but also the course of such a reaction in that the formation of products arising through open chain, i.e. less compact transition states, are suppressed. The pressure induced reaction of isophorone dienamines **1** with methyl acrylate (**2a**) or acrylonitrile (**2b**) exclusively gave the Diels-Alder adduct **3** (Scheme 3), while under heating only products **4** and **5** arising from enamine addition to the Michael acceptors **2** are observed.^[13]



Scheme 3. Reaction of isophorone dienamine **1** with methyl acrylate (**2a**) and acrylonitrile (**2b**).

Several years later Bellassoued et al. investigated the uncatalyzed Mukaiyama aldol reaction of trimethylsilyl ketene acetals **6** and benzaldehyde under ambient and high pressure conditions^[14] (Table 2).

Table 2. Condensation reaction of unsaturated silyl ketene acetal **6** with benzaldehyde.



Entry	Conditions	γ -adduct 7	α -adduct 8	Yield
1	200 MPa, 3 d	88	12	41%
2	500 MPa, 6 d	83	17	57%
3	1200 MPa, 3 d	35	65	51%
4	1700 MPa, 3 d	25	75	68%

Under „low pressure“ conditions (200 – 500 MPa) the γ -adduct **7** was predominantly formed, whereas the application of high pressure (1200 – 1700 MPa) favored the formation of the corresponding α -adduct **8**. This preference for the latter under high pressure might be a consequence of a more compact six-membered Zimmermann-Traxler transition state **9**

(Figure 1), while the formation of the conjugated, thus thermodynamically more favored **7**, proceeds via a less dense, presumably open chain transition state.^[14]

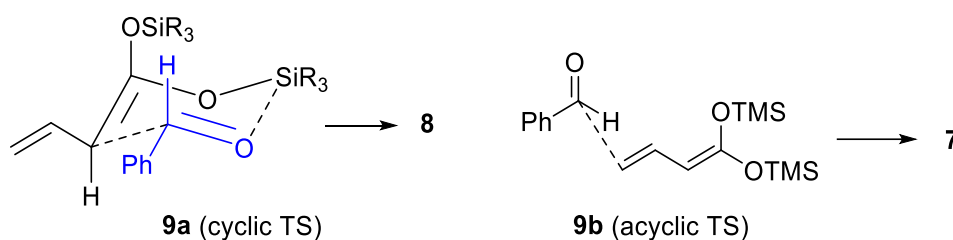


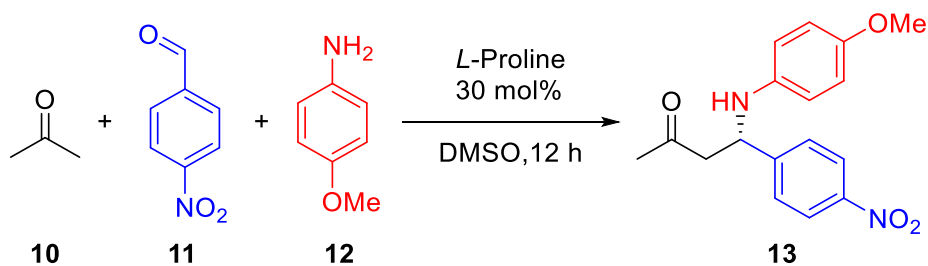
Figure 1. Transition state **9** towards the α -adduct and γ -adduct.

This preference for the latter under high pressure might be a consequence of a more compact six-membered Zimmerman-Traxler transition state **9** (Figure 1), while the formation of the conjugated, thus thermodynamically more favored **7**, proceeds via a less dense, presumably open chain transition state.^[14]

Amino acids and peptides

In 2000, List et al. and MacMillan et al. impressively demonstrated that small organic molecules can efficiently catalyze asymmetric reactions, rivaling the performance of enzymes.^[15,16] For example, asymmetric aldol reactions can be catalyzed by *L*-proline acting as a micro-aldolase mimic.^[15] Subsequently, Hayashi and coworkers investigated such reactions catalyzed by *L*-proline under pressure, e.g. the three-component List-Barbas-Mannich reaction.^[17]

It was shown that high pressure decreases the enantioselectivity but considerably enhances the reaction rate (Table 3).

Table 3. The three-component List-Barbas-Mannich reaction of *p*-nitrobenzaldehyde (**11**), *p*-anisidine (**12**) and acetone (**10**) under different conditions.

Entry	Pressure	Temperature	Yield	e. r.
1	0.1 MPa	23 °C	20%	95:5
2	0.1 MPa	-20 °C	5%	99:1
3	200 MPa	-20 °C	58%	95.5:4.5

Here, the Mannich reaction follows again a compact Zimmerman-Traxler type transition state, in which the sterically less hindered but also less compact (*E*)-imine explains the sense of optical induction in the products. A key feature of the transition state is the hydrogen bond between the carboxylic acid and the imine, necessary for the activation of the latter towards nucleophilic attack. The increased rate being observed under pressure might be an indication of a more efficient formation of that bond. While conceivable, promoting an uncatalyzed pathway through pressure (control experiments without *L*-proline at high pressure were not reported) which could also explain the loss of selectivity, seems to be less likely given this way no hydrogen bond induced activation of the imine would take place. The loss of selectivity at high pressures could be explained by the partial formation of the more compact (*Z*)-imine, which would then give the other enantiomer, following the corresponding Zimmerman-Traxler transition state^[18] (Figure 2).

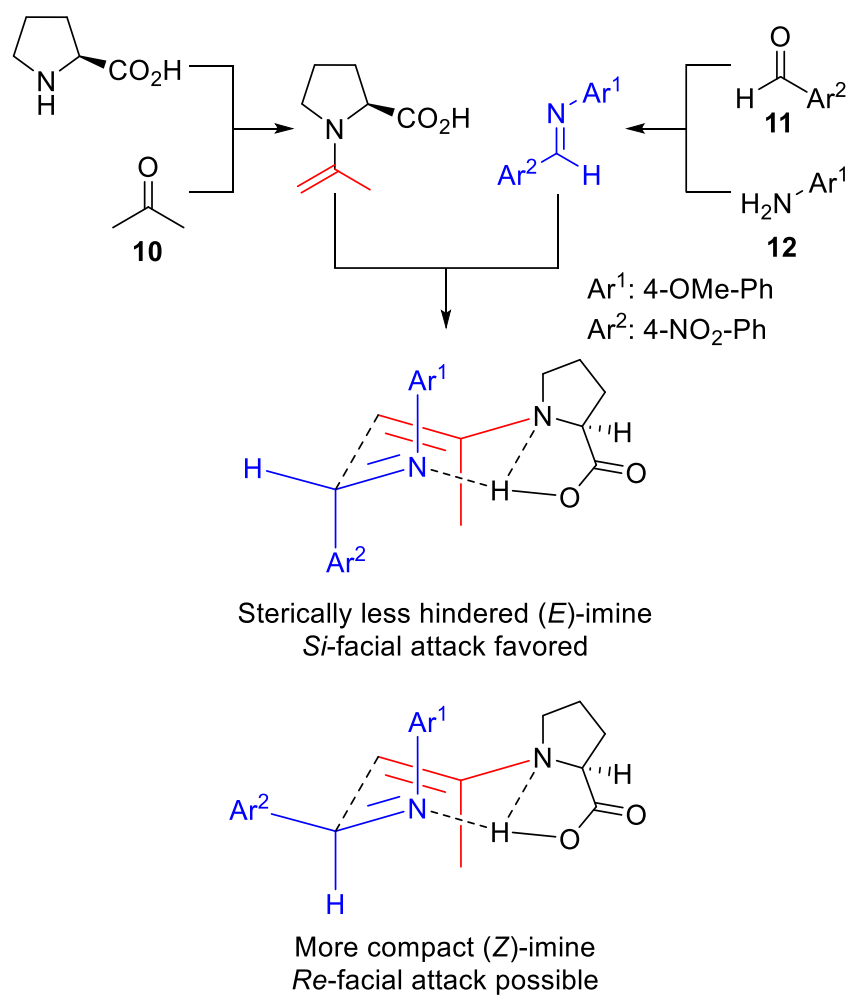
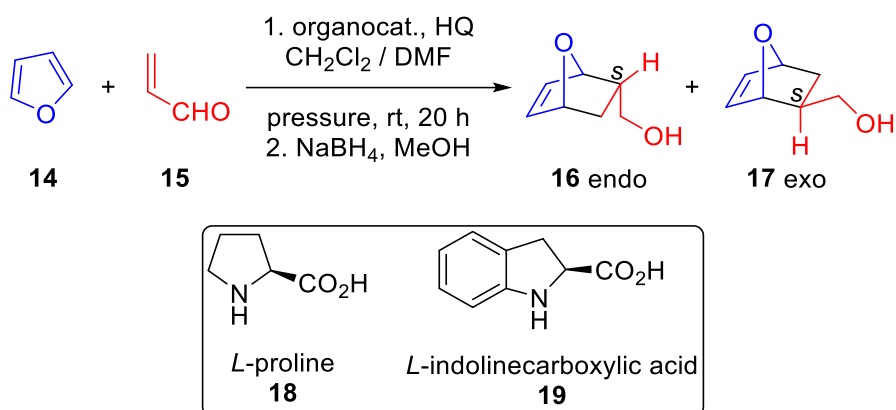


Figure 2. Zimmermann-Traxler transition state with (*E*)- and (*Z*)-imine.

Kotsuki et al. studied the organocatalyzed asymmetric Diels-Alder reaction between furan (**14**) and acrolein (**15**) under high pressure.^[19]

Table 4. The Diels-Alder reaction of furan (**14**) and acrolein (**15**) under different pressures (HQ = hydroquinone).

Entry	Catalyst	Pressure	Yield	e.r.		16:17 ratio
				16	17	
1	18	200 MPa	5%	55.4:45.5	60.5:39.5	56:44
2	18	400 MPa	33%	51.5:48.5	51:49	51:49
3	19	200 MPa	22%	52:48	63:37	48:52
4	19	400 MPa	33%	56.5:43.5	57:43	41:59
5	19	800 MPa	45%	55:45	53:47	44:56

Although furans as dienes for Diels-Alder reactions show low reactivity due to their aromaticity, it was possible to obtain products with reasonable yields, while only traces of product were formed at ambient pressure in all cases. An increase of the reaction rate was observed along with a decrease of enantioselectivity at high pressures, although the effect was small. Ratio of *endo/exo* was by and large unaffected by pressure^[19] (Table 4).

The increased reaction rate at high pressure is attributed to the iminium ion intermediate, since bond formation and ionization both have negative values for the volume of activation ΔV^\ddagger .^[19] The drop of selectivity could be explained by pressure induced spatial rearrangement of substrate and catalyst-iminium species. At lower pressures the *si*-face is predominantly exposed to cycloaddition in the *endo* transition state, presumably representing the match between catalyst and substrate by minimizing steric interactions. With increasing pressure the sterically more hindered but also more compact transition state favoring the *re*-face is accessed for cycloaddition, thus resulting in a decrease of the enantiomeric excess (Figure 3).

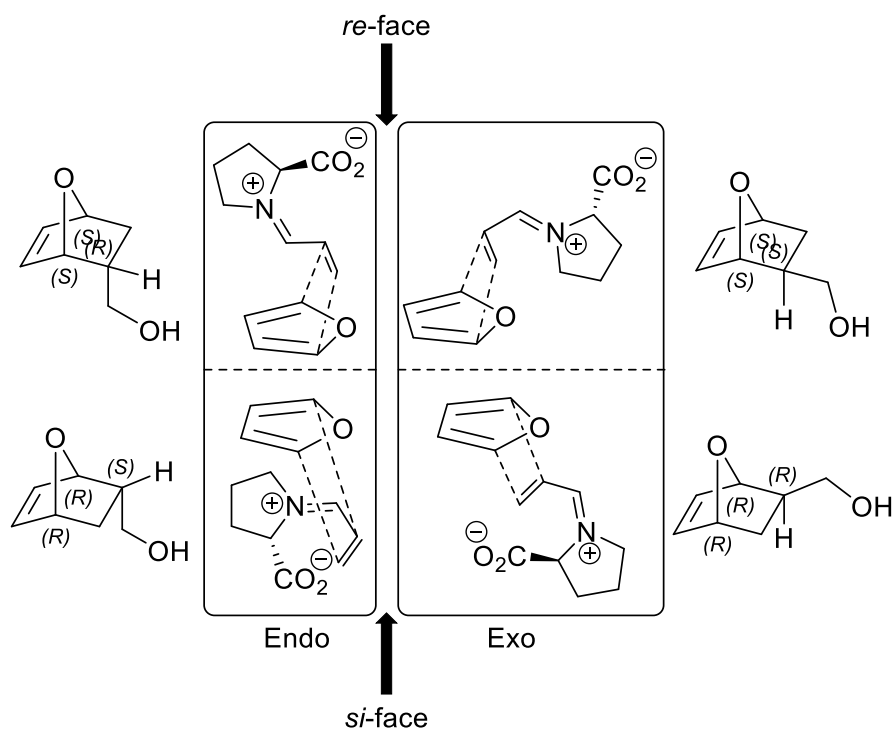


Figure 3. *Si*- and *re*-face cycloaddition of furan (**14**) and the iminium intermediate formed from acrolein with *L*-proline.

While the examples discussed so far made use of organocatalysts that had little degree of conformational freedom and thus there was little opportunity to observe pressure induced changes in selectivity, the situation is different in enzymes, given the many rotatable bonds present. Small peptides, i.e. short segments of amino acid monomers connected by amide bonds, that are able to catalyze organic reactions might serve as models for enzymes. Wennemers and coworkers demonstrated that tripeptides can show remarkable activity in conjugate additions and aldol reactions.^[20,21,22] The impact of spatial proximity of functional groups to make a thriving catalysis was demonstrated in these studies, calling for the close positioning of the amino group at the *N*-terminus (NH) and the carboxylic acid (CO₂H) group at the *C*-terminus to each other.^[20,22,23] Based on this work Reiser et al. implemented rigid *cis*- β -aminocyclopropane carboxylic acids (β -ACC, \blacktriangle)^[24] as the central unit into tripeptide catalysts, to limit the number of possible conformations to a compact, presumably catalytically active one, in which the C- and N-terminus would be close together, and to an extended, presumably inactive one (Figure 4).^[25]

H-Pro- \blacktriangle -Pro-OH (**20**) catalyzed aldol reactions at ambient pressure in up to 91% *ee*^[25], however, for a comparative study to deduce pressure effects, the aldol reaction between acetone (**10**) and *p*-nitrobenzaldehyde (**24**) was chosen, which proceeded in 69% *ee*. An NMR study suggested that the extended *trans*-conformation *trans*-**20** is in a 3:1 equilibrium with

cis-**20**, the latter bringing the C- and N-terminus in close proximity and thus deemed to be decisive for allowing the aldol reaction to proceed.

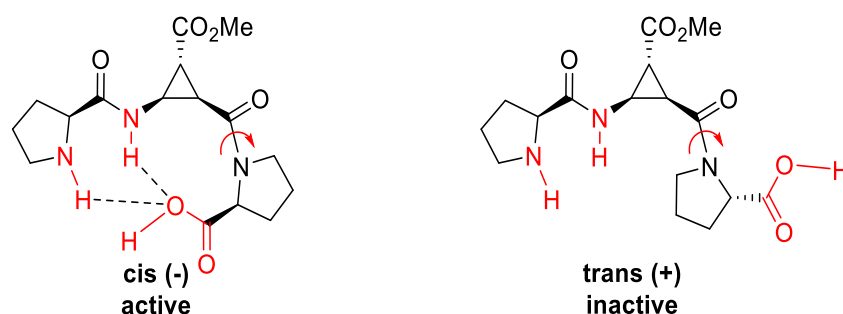
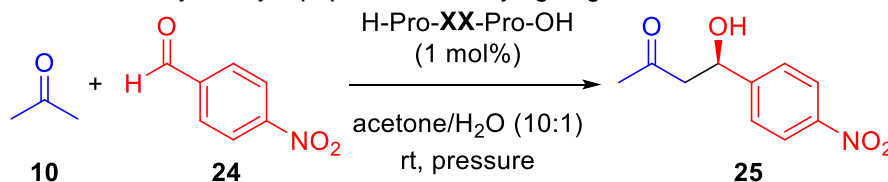


Figure 4. The two major conformers *cis/trans* (1:3) of H-Pro- Δ -Pro-OH (**20**).

Upon applying pressure (Table 5, entries 1, 2), a six-fold rate acceleration was observed. Since the enantioselectivity remained at the same level^[26], this rate acceleration can not be a consequence of a pressure induced uncatalyzed background reaction. We therefore reason that the more compact *cis*-conformation becomes populated to a larger extent under pressure, being necessary for the catalytic turnover of the reaction.

Table 5. Aldol reaction catalyzed by tripeptides with varying ring size.



Entry	Catalyst [XX]	Conditions	Yield	e.r.
1	(-)- \blacktriangle 20	0.1 MPa, 24 h	68%	85:15
2	(-)- \blacktriangle 20	480 MPa, 4 h	73%	84:16
3	(-)- \blacksquare 21	0.1 MPa, 24 h	45%	74:26
4	(-)- \blacksquare 21	500 MPa, 7 h	66%	71:29
5	(-)- \blacklozenge 22	0.1 MPa, 24 h	82%	66:34
6	(-)- \blacklozenge 22	460 MPa, 6 h	57%	71:29
7	(-)- \blacklozenge 23	0.1 MPa, 24 h	71%	57:43
8	(-)- \blacklozenge 23	480 MPa, 7 h	65%	61:39

Corroboration comes from NMR-studies with H-Pro- Δ -Pro-OH (**20**) up to 200 MPa. The amide NH-signal region H-Pro- Δ -Pro-OH (**20**) (Figure 5) clearly indicated the vanishing of one

conformer upon applying pressure, although a definite structural assignment was not possible yet.

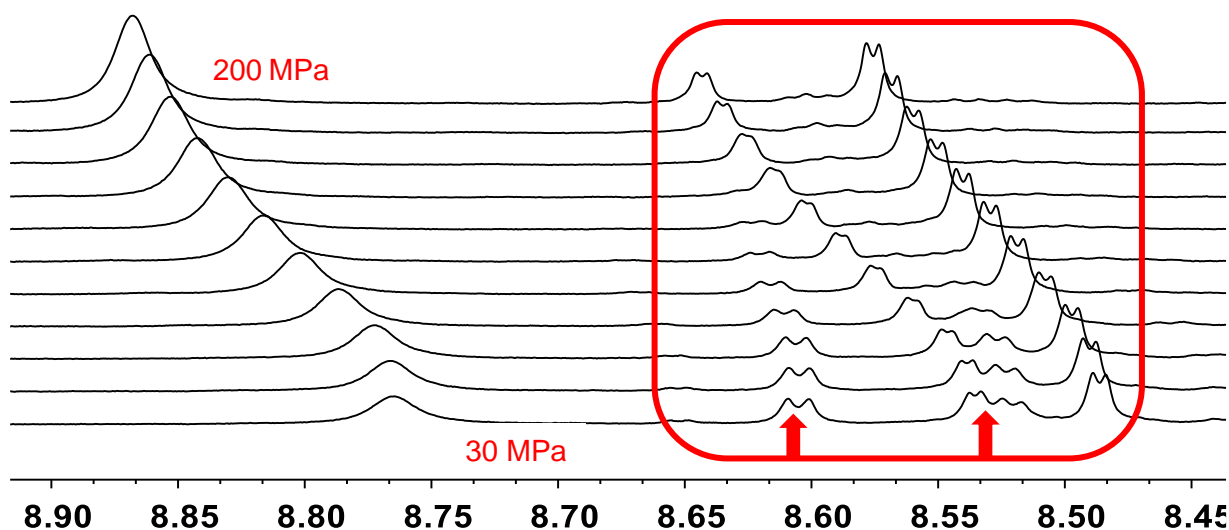


Figure 5. $^1\text{H-NMR}$ spectral region of the amide signal of H-Pro- Δ -Pro-OH (**20**) at different pressures.

Extending incrementally the ring size of the central β -amino acid from three to six in the tripeptides (Figure 6) allowed gradually a greater degree of freedom due to the different conformations possible in the larger rings, which includes different conformations in which the C- and N-terminus are in close enough proximity to catalyze the aldol reaction. Following this rational, not unexpectedly a drop in the e.r. values was observed, but now for the first time slight increases of the e.r. values were observed upon applying pressure (Table 5, entries 5-8). Apparently, in these cases the number of conformations is reduced by shifting their equilibrium towards the most compact one, which results in an increased level of enantioselectivity.^[27]

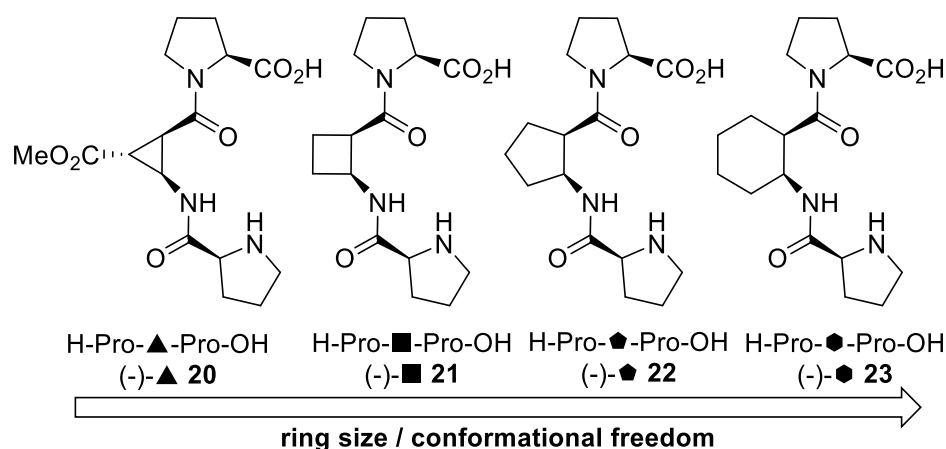
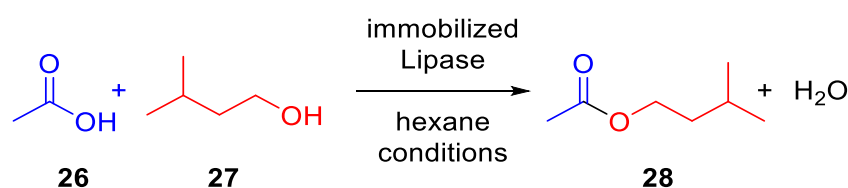


Figure 6. Different tripeptides containing cyclic β -amino acids of various ring sizes.

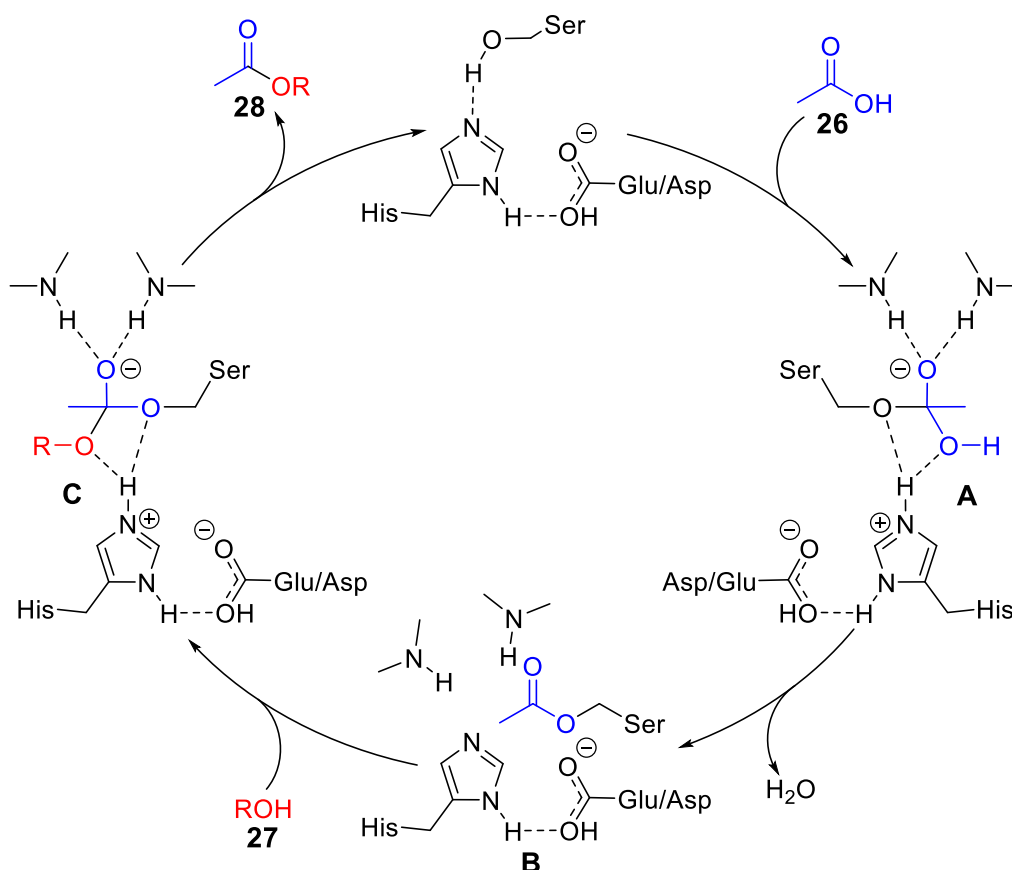
Enzymes

The vast majority of enzymes are proteins. Although many proteins suffer from denaturation and thus losing their functionality when exposed to high pressure, approximately two dozen of enzymes have been so far discovered that show improved activity under such conditions.^[28] Lipases itself often exhibit remarkable properties in terms of thermal stability, enantioselectivity and solvent-resistance and are, therefore, widely employed in industrial processes. Eisenmenger and Reyes-De-Corcuera were able to show that thermal stability along with increased activity might be further increased under high hydrostatic pressure.^[29]



Scheme 4. Lipase catalyzed esterification of acetic acid (**26**) with isoamyl alcohol (**27**) to isoamyl acetate (**28**).

The question emerged whether this observation can be attributed to high pressure induced perturbances in the enzyme, e.g. to conformational changes along with a change in the reaction mechanisms, or to alterations of substrate and/or solvent packing, therefore having influence on the enzyme structure.^[29] The catalytic triad is a set of three synergistically working amino acids found in the active site of the enzyme, and herein, the Ser-His-Asp/Glu triad is a well-studied catalytic motif in lipases. Taking the esterification of acetic acid (**26**) with isoamyl alcohol (**27**) as a representative example (Scheme 4), the reaction is initiated by the attack of a Ser-residue to **26** to form a tetrahedral intermediate **A** (Scheme 5). An acyl-enzyme complex **B** is subsequently formed by loss of a water molecule. **B** is attacked by alcohol **27** to form tetrahedral intermediate **C**, followed by release of ester **28** with concurrent regeneration of the lipase. The tetrahedral intermediates are stabilized by hydrogen bonds of the protein backbone amides with the transient oxyanion (Scheme 5).^[30] This highly ordered assembly could be favored by pressure, which would account for the observed activity enhancement.



Scheme 5. The mechanism of lipase-catalyzed esterification of acetic acid (**26**) and isoamyl alcohol (**27**).

However, besides a direct rate acceleration based on a pressure favored transition state different factors must also be taken into account. Exposure of the immobilized lipase at ambient and high pressure (Scheme 4) in the absence of substrate revealed that pressure protects the enzyme to be irreversibly inactivated, i.e. no inactivation of the lipase after 4 h at 80 °C and 400 MPa was observed, while at ambient pressure under otherwise unchanged conditions a drop in activity by 60% was observed (Table 6).

Table 6. Thermal inactivation of lipase after 4 h at 80 °C at different pressures.

Temperature	Pressure	Residual activity
80 °C	0.1 MPa	40%
	400 MPa	99%

In line with this observation, it was found that the initial lipase activity increases only slightly at ambient pressure, while at 350 MPa the activity is more than twice as high upon moving from 40 to 80 °C (Table 7).

Table 7. Influence of pressure and temperature on the activity of immobilized lipase catalyzing the esterification of acetic acid (**26**) and isoamyl alcohol (**27**) in hexane at 40 °C and 80 °C.

Temperature gradient	Pressure	Activity increased by
40 to 80 °C ($\Delta T = 40$ °C)	0.1 MPa	110%
	350 MPa	240%

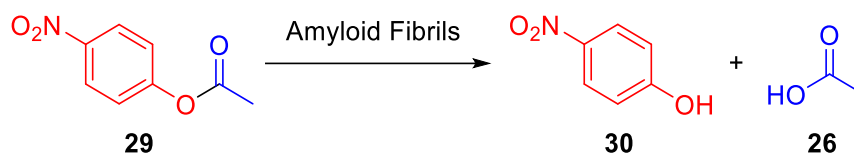
Calculations of activation energies E_a from the rate constant of the reaction (Scheme 4) at different pressures did not show significant differences, pointing to similar and pressure independent transition states. While the volume of activation ΔV^\ddagger was positive and did not significantly change upon variation of the temperature (range 40 to 80 °C between 300 and 500 MPa; approx. $+15 \text{ cm}^3 \text{ mol}^{-1}$), the volume of activation was found to be negative between ambient pressure and 200 MPa, suggesting again that a more ordered conformation goes along with an enhanced activity.^[29] The same authors reported even more pronounced pressure effects when the unimmobilized enzyme was investigated in an ionic liquid – alcohol biphasic system (1-butyl-3-methylimidazolium hexafluorophosphate, isoamyl alcohol) instead of hexane.^[29] A rate acceleration of the free lipase by a factor of 14 to 15 was observed upon applying a pressure of 500 MPa (Table 8).

Table 8. Influence of pressure and temperature on the rate of free lipase catalyzing the esterification of acetic acid (**26**) and isoamyl alcohol (**27**) in an ionic liquid.

Temperature	Pressure gradient	Rate acceleration
40 °C	0.1 to 500 MPa ($\Delta P = 499.9$ MPa)	15-fold
80 °C		14-fold

Again, based on the observed rate constant of the reaction, the activation energy was calculated to be by and large unaffected by pressure. The activation volume ΔV^\ddagger however was determined to be significantly negative in value (0.1 MPa to 500 MPa) (40 °C: $-16 \text{ cm}^3 \text{ mol}^{-1}$; 80 °C: $-17 \text{ cm}^3 \text{ mol}^{-1}$).^[31]

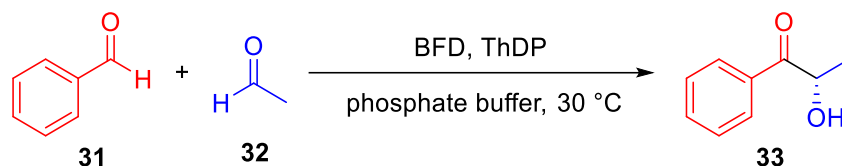
Winter and coworkers examined the dependence of the catalytic activity of de novo designed amyloid fibrils Ac-LHLHLRL-CONH₂ (AF1) and Ac-IHIHIQI-CONH₂ (AF2). Exposing these to pressures up to 200 MPa led to an enhancement of the esterase activity for the hydrolysis of *p*-nitrophenyl acetate (**29**, *p*NPA) (Scheme 6), being reflected by a negative volume of activation (approx. $-14 \text{ cm}^3 \text{ mol}^{-1}$).^[32]



Scheme 6. Hydrolysis of pNPA (**29**) catalyzed by amyloid fibrils.

Investigating the enzyme activity in a pressure range from 0.1 to 200 MPa, the reaction rate for both AF1 and AF2 was increased 3.5-fold at all temperatures (22 – 38 °C) and substrate concentrations (0.2 – 0.8 mM) in comparison to the ambient pressure reaction.^[32]

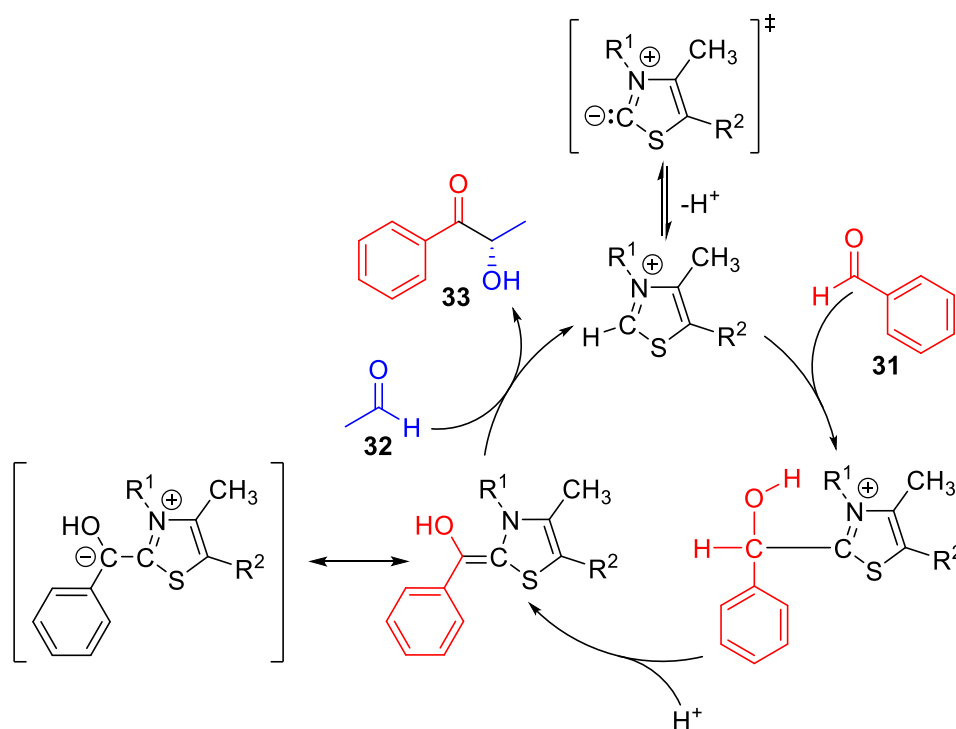
Beside esterifications and hydrolyses also biocatalyzed C-C bond formations are growing in importance. Benzoylformate decarboxylase (BFD) is a homotetrameric thiamine diphosphate (ThDP)-dependent enzyme, important for the mandelate catabolism.^[33]



Scheme 7. Carbonylation of benzaldehyde (**31**) and acetaldehyde (**32**) catalyzed by BFD.

Liese et al. showed the carbonylation of benzaldehyde (**31**) and acetaldehyde (**32**) catalyzed by three different BFD species (BFD F464I, BFD A460I and the hybrid BFD A460I-F464I) to form 2-hydroxypropiophenone (2-HPP, **33**, Scheme 7). Reactions were run at different pressures in the range of 50 MPa to 290 MPa. Besides the reaction rate, the enantioselectivity in favor of (*R*)-2-HPP significantly increased with pressure. The hybrid species BFD A460I-F464I performed especially well at high pressure (271 MPa), providing a (*R*)-2-HPP to (*S*)-2-HPP ratio of 9:1 compared to 3.9:1 at 50 MPa.^[33]

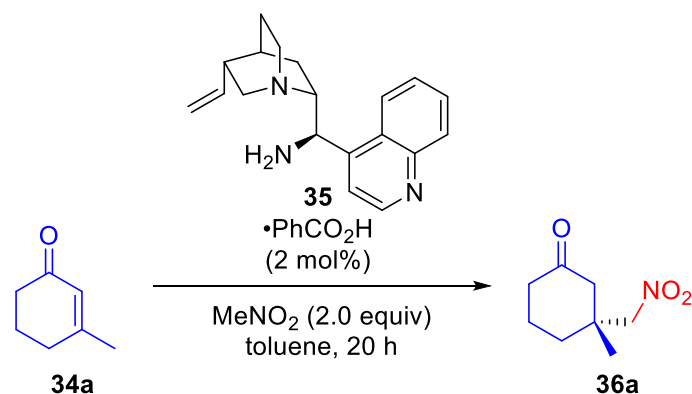
Since the BFD-mediated carbonylation reaction shows an enamine-carbanion species and other ionic intermediates, it is conceivable that reaction rates are increased under high pressure due to charge attraction, resulting in a decrease of volume (Scheme 8). The pressure-induced increase in enantioselectivity is not fully rationalized yet. Non-enzymatic background reactions and self-racemization of the product could be excluded by appropriate control experiments. Further experiments towards the changes in the active site or in the hydrophobicity and substrate binding are ongoing in the authors laboratory.^[33]



Scheme 8. BFD-mediated carbonylation mechanism.

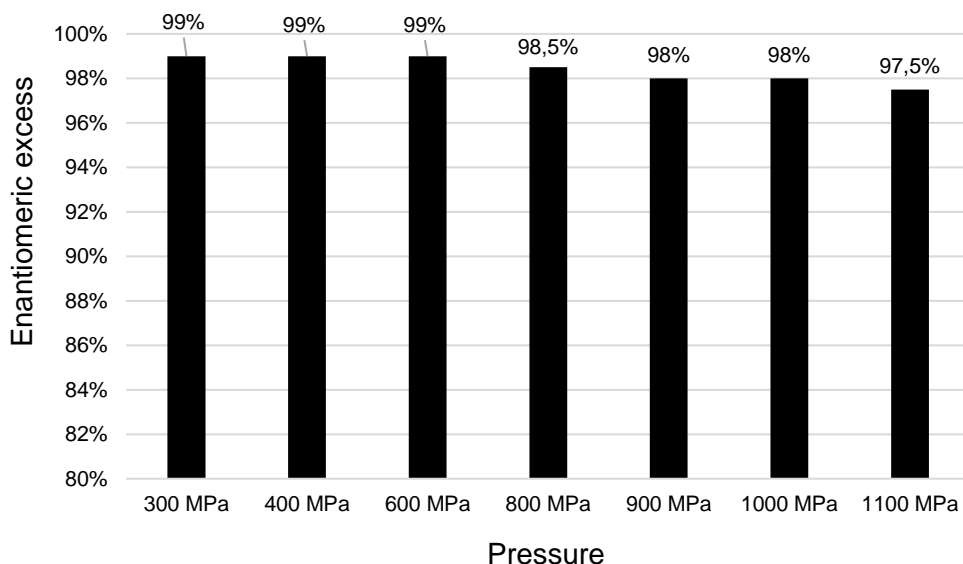
Cinchona alkaloids

Seminal contributions to organocatalysis with primary amines and cinchona alkaloids under high pressure were made by Kwiatkowski and coworkers. They investigated different reaction types like asymmetric Michael additions^[34], Friedel-Crafts alkylations^[35] and hydroxyalkylations^[36], demonstrating that pressure is especially beneficial to overcome steric crowding in such transformations. For example, the 1,4-conjugate addition of nitroalkanes to prochiral β,β -disubstituted enones **34** proceeded in excellent yields to γ -nitroketones **36** bearing a quaternary center (Table 9), while under ambient pressure conditions only low yields (1 – 9%) were obtained.

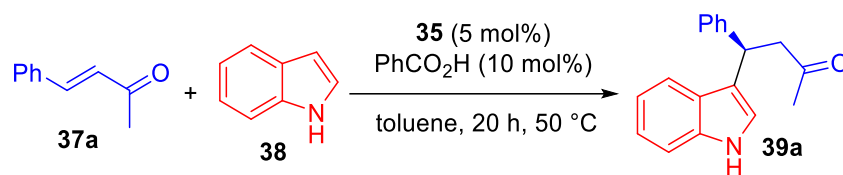
Table 9. The 1,4-conjugate addition of nitromethane to β,β -disubstituted enone (**34a**) under pressure.

Entry	Pressure	Yield	e.r.
1	0.1 MPa	<2%	99:1
2	1000 MPa	80%	99:1

Remarkably, the enantioselectivity kept at a high level ($98 \pm 1\%$ ee) within the whole pressure range up to 1000 MPa (Figure 7). The reaction of **34a** with MeNO₂ is a bimolecular reaction which is assumed to be favored by pressure. Furthermore, ionic species are involved in this reaction so that a contraction of the overall volume by electrostriction can be expected during the course of reaction.

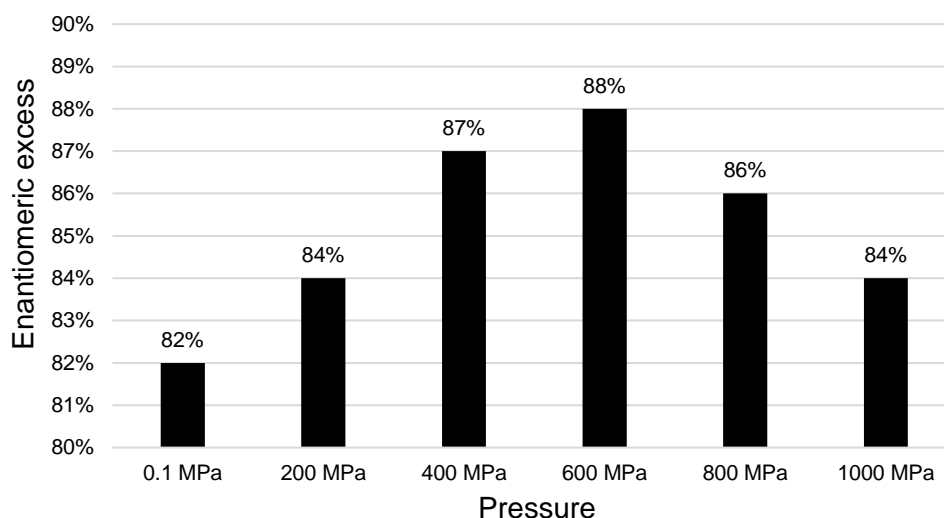
**Figure 7.** Enantiomeric excess of **36a** in dependence of pressure.

A similar trend was observed for the high pressure induced organocatalytic Friedel-Crafts alkylation of indole (**38**) with α,β -unsaturated ketones **37**, the latter process providing derivatives **39** (Table 10).^[35]

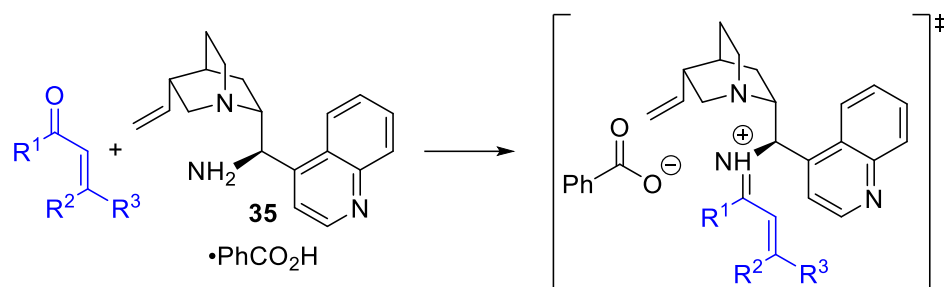
Table 10. Pressure effect on the Friedel-Crafts alkylation of indole (**38**).

Entry	Pressure	Yield	e.r.
1	0.1 MPa	6%	91:9
2	1000 MPa	95%	92:8

In contrast to the Michael addition of MeNO₂ to **34a** (Table 9), the enantioselectivity was slightly but consistently altered by pressure. The highest value for enantioselectivity was observed at 600 MPa, pressures below and above that point resulted in a reduction (Figure 8). A possible explanation for this observation could be an influence on the *E/Z*-ratio of the iminium salt formed, which would expose opposite enantiotopic faces of the reacting C-C- π -bond to the incoming nucleophile, however, further investigations are necessary to understand the underlying mechanisms.

**Figure 8.** Enantiomeric excess of **39a** in dependence of pressure.

The observed rate acceleration under pressure should be a result of the formation of the ionic iminium salt (Scheme 9), which should therefore result in a negative volume of activation due to electrostriction.

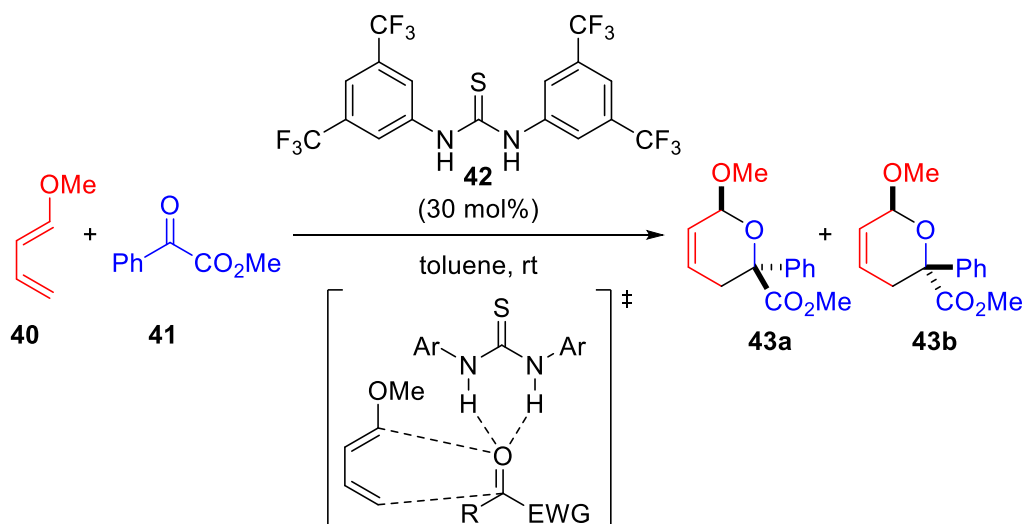


Scheme 9. Iminium transition state of amines and aldehydes/ketones.

Thiourea derivatives

In 2009, seven years after Schreiner et al.^[37] introduced the first widely applicable thiourea catalyst **42**, Kotsuki and coworkers investigated the influence of pressure in hetero-Diels-Alder reaction with carbonyl derivatives **41**.^[38] In difference to the activation of carbonyl compounds by iminium ion formation discussed in the previous chapter with cinchona alkaloids, the activation mode for carbonyl compounds with thiourea derivatives proceeds through hydrogen bonding.^[38]

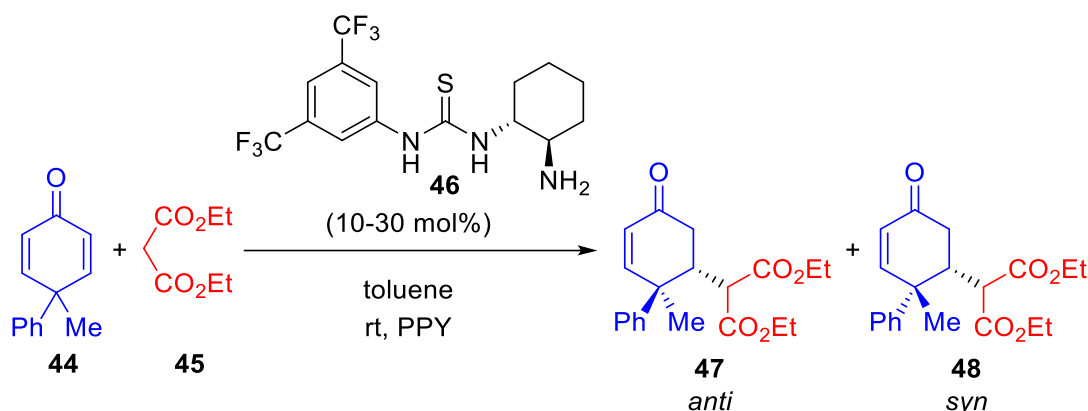
The observed rate acceleration as a consequence of high hydrostatic pressure can be rationalized with the negative volume of activation for the hetero-Diels-Alder reaction that is generally observed. While only traces of product **43** were obtained at ambient pressure conditions, yields up to 91% were obtained at 1000 MPa (Table 11).^[38] However, the fact that the reaction hardly proceeds in the absence of the thiourea catalyst even at 1000 MPa clearly indicates that no pressure accelerated, *uncatalyzed* background reaction takes place but rather that the catalyst is involved in the transition state. The d.r. of **43** was increased in the range of 400 – 800 MPa from 3.6:1 to 4.9:1 but experienced a decrease at 1000 MPa to 3.4:1. The assignment of the diastereomers was not done by the authors, but it seems plausible to assume that the transition state in which the sterically less compact but electronically preferred positioning of the smaller ester group in the *endo* position (**43a**) is competing at higher pressures with the more compact transition state placing the larger phenyl group *endo* (**43b**).

Table 11. Diels-Alder reaction of 1-methoxybutadiene (**40**) and methyl 2-oxo-2-phenylacetate (**41**) under different high pressure conditions.

Entry	Conditions	Yield (d.r.)
1	0.1 MPa, 72 h	trace
2	400 MPa, 72 h	58% (3.6:1)
3	800 MPa, 72 h	82% (4.9:1)
4	1000 MPa, 10 h	91% (3.4:1)
5 ^[a]	1000 MPa, 10 h	8% (1:2.1)

[a]: no catalyst was used.

Besides Diels-Alder reactions, asymmetric conjugate additions of stabilized nucleophiles to α,β -unsaturated carbonyl systems were also investigated utilizing a combination of thiourea catalysis and high-pressure. This way, sterically highly congested cyclohexenones could be synthesized in high yield and stereoselectivity^[39], contrasting the sluggish reaction that is observed at ambient pressure (Table 12).

Table 12. Thiourea **46** catalyzed asymmetric desymmetrization of 4,4-disubstituted cyclohexadienone **44** under high pressure.

Entry	44:45	Conditions	Yield	dr (47/48)	ee [%] (47/48)
1 ^[a]	1:1.5	0.1 MPa, 108 h	11%	9.0:1	92/82
2 ^[a]	1:1.5	800 MPa, 24 h	22%	7.3:1	94/86
3 ^[b]	1:1.5	800 MPa, 48 h	54%	6.7:1	88/82
4 ^[b]	3:1	800 MPa, 48 h	82%	5.2:1	92/86

[a] Catalyst loading 10 mol%. [b] Catalyst loading 30 mol%.

The diastereoselectivity, being most likely a consequence of substrate control, was decreased upon applying pressure, indicating that transition state leading to the sterically more congested product, i.e. placing phenyl and malonate on the same side of the cyclohexane ring, is populated to a larger extent. In contrast, the enantioselectivity of the reaction appears to be by and large unaffected by applying pressure, suggesting that the preferred catalyst-substrate interaction which dictates the selection between the two enantiotopic faces of the cyclohexadienone substrate is already compact.^[39] Again, it is important to note that pressure does not deter the catalyst-substrate interaction or induces a non-catalyzed reaction pathway, which would have led to an erosion of enantioselectivity.

The effect of hydrostatic pressure on organic transformations such as Diels-Alder reactions (as an example for a pericyclic reaction), Aldol and Mannich reactions, esterifications and hydrolyses, bimolecular reactions catalyzed by bio- and organocatalysts were described in the latter. The main activation modes of small molecules through the catalysts occur through hydrogen bonding or formation of covalently linked intermediates. All of the mentioned organic reactions benefit from high pressure with respect to rate acceleration. Especially a negative value for the volume of activation ΔV^\ddagger , which is attributed to the different packing coefficients of cyclic and acyclic compounds, electrostriction of ionic intermediates, or steric hindrance is responsible for rate accelerations. In contrast, only little changes in stereoselectivity are

observed when moving from ambient to high pressure. A rationale for these observations might be that the catalyzed reactions already occur through compact assemblies of substrate-catalyst species. Moreover, the chiral information of an organo- or biocatalyst is defined within a network of covalent bonds. This is different to metal asymmetric catalyzed processes, in which ligand exchange at the metal with solvent, generally accelerated by pressure^[40], can lead to different, catalytically active but non stereoselective metal species.^[41] Thus, an increased reaction rate along with unchanged selectivity might serve as evidence for pressure to shift a conformational equilibrium towards the more compact catalyst-substrate transition state which needs to be populated in any case for the catalyzed pathway to proceed.

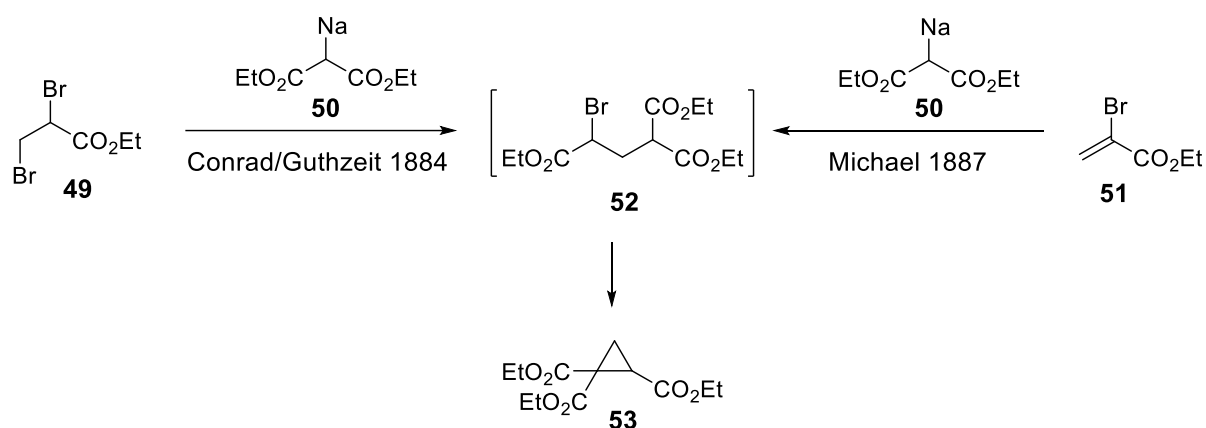
2 Aim of the Work

In the present work, the effect of high hydrostatic pressure on hydrogen bond acceptor-donor complexes was investigated. Firstly, thiourea-organocatalyzed Michael additions of diethyl malonate to various heteroaromatic nitroolefins have been studied under high-pressure conditions (up to 800 MPa), being conducive to enhanced product yields, high reaction rates, and high enantioselectivity. Elucidating the effects of solvents for maximizing reaction rates and yields has been carried out using the Perturbed-Chain Polar Statistical Associating Fluid Theory (PCP-SAFT), allowing for the first time a prediction of the kinetic profiles under high-hydrostatic-pressure conditions. The PCP-SAFT modeling and all *in-silico* screenings were envisioned by Prof. Sadowski and co-workers at the TU Dortmund in the Laboratory of Thermodynamics. In addition, NMR- and IR-studies were conducted to examine the influence of high pressure on the hydrogen bond properties of acceptor-donor complexes as well as on intramolecular hydrogen bonds in different amides.

3 Main Part

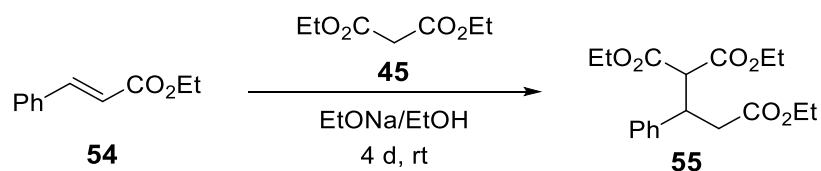
3.1 High-Pressure-mediated Thiourea-Organocatalyzed Asymmetric Michael Addition to (Hetero)Aromatic Nitroolefins[‡]

Michael addition reactions are an extremely powerful and convenient tool to build up molecular complexity by forming C-C bonds. This reaction, firstly discovered by Arthur Michael in 1887^[43], describes the nucleophilic addition to an α,β -unsaturated carbonyl compound. In his initial study, Michael was able to obtain cyclopropane derivative **53**, the same product which was described and published by Conrad & Guthzeit in 1884.^[44] When dibromo ester **49** was replaced by olefin **51** it became apparent during the course of the reaction that, prior to the cyclopropane formation, an addition of diethyl sodiomalonate (**50**) to the double bond of **51** must proceed (Scheme 10).



Scheme 10. Cyclopropane synthesis by Conrad & Guthzeit vs. Michael.

To prove his hypothesis, Michael conducted the reaction of cinnamic acid and diethyl malonate. With his successful reaction the figurehead of the Michael addition or 1,4-conjugate addition was born (Scheme 11). The launch of the Michael addition was the beginning of a powerful tool to form C-C bonds and henceforth different variants, as well as asymmetric ones, were developed.



Scheme 11. Diethyl malonate (**45**) addition to cinnamic acid (**54**).

[‡]This chapter is partially based on T. Weinbender, M. Knierbein, L. Bittorf, C. Held, R. Siewert, S. P. Verevkin, G. Sadowski, O. Reiser, *ChemPlusChem* **2020**.^[42]

Nowadays, Michael additions, especially the addition of 1,3-dicarbonyl compounds to nitroolefins, are well-explored transformations, as the resulting nitroalkanes can be easily transformed into a broad variety of synthetically useful building blocks harboring a wide assortment of functional groups^[45] such as hydrogen^[46], nitrile oxide^[47], amine^[48], ketone or carboxylic acid.^[49]

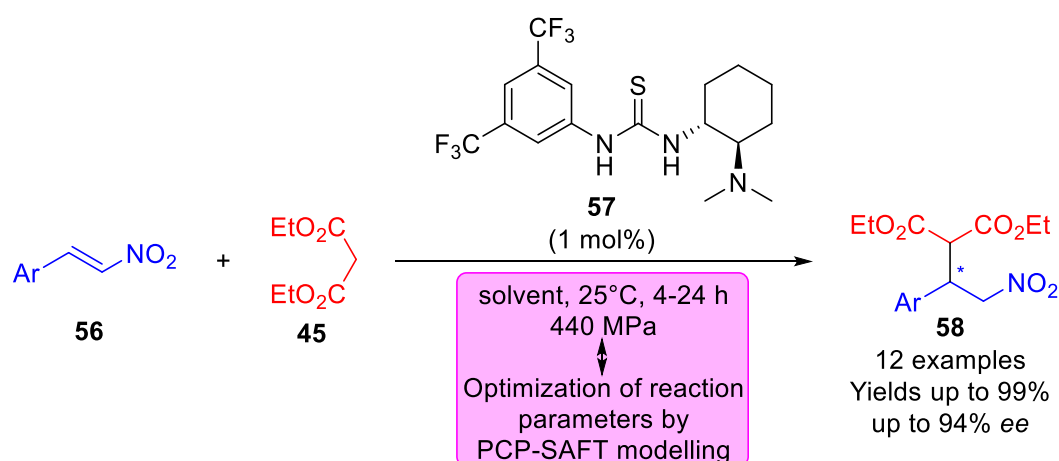
In the following, the influence of high hydrostatic pressure on the previous discussed Michael addition reactions is investigated on the example of thiourea-organocatalyzed asymmetric Michael addition to (hetero)aromatic nitroolefins supported by *in-silico* solvent predictions by PCP-SAFT.

In general, the efficiency of chemical reactions in terms of reaction rate, yield and selectivity is influenced by several factors such as temperature, pressure, concentration, and solvent. Therefore, precise information and understanding of these factors are of paramount importance for fine-tuning reaction conditions in order to enhance rates and yields of the desired transformation. Following the first report in 1862 of Berthelot et al.^[50], solvent effects on chemical reactions were correlated with the solvent's polarity and were later explained by the solvation of the reacting agents.^[51] Several groups have studied the effects of solvents on reaction rates and equilibria for chemical reactions^[52] as well as for biochemical reactions.^[53] The reaction medium strongly influences molecular interactions of the given reactants. Thus, analysis of thermodynamic activities, e.g. by computational thermodynamic models of the reagents in the given solvent allow precise prediction of certain solvent effects on the reaction performance. Therefore, different models have been proven to correctly predict the influence of solvent on liquid-phase reactions at atmospheric pressure.^[54–56,57] However, the applicability of these computational methods for very-high-pressure conditions in liquid phases (100-800 MPa) has not been validated until today.

The effects of high pressure in solution on the reaction equilibria were first explored by Planck in 1887^[58] followed by investigations regarding the reaction rates by Rothmund in 1896.^[59] Since then, many groups explored pressure effects on biochemical^[60] as well as on chemical reactions^[9,61], whereas the pioneering study of Matsumoto and Uchida^[62] stands out as the first report of pressure effects on asymmetric organocatalytic reactions. Apart from purely academic interest, high-pressure applications have also gained substantial industrial significance, e.g. in food processing.^[63] High pressure is capable of improving reactions either indirectly by phase transition (especially towards supercritical fluids) or directly by volume effects. The latter typically occurs in liquid-phase reactions and is known to depend on the employed solvent. Hence, it was set out whether the effects of solvent on reactions are altered at high pressure and whether they can be predicted by thermodynamic models. Thus, in this

study Perturbed-Chain Polar Statistical Associating Fluid Theory (PCP-SAFT) was applied for the first time to an organic reaction at very-high-pressure conditions of up to 800 MPa. PCP-SAFT was chosen for this purpose as it has been successfully applied to compute the reacting agent's interactions in solution under ambient pressure and up to 2 MPa.^[55]

As a model system for this approach, the Michael addition of 1,3-dicarbonyl compounds to nitroolefins was chosen. In 2003, Takemoto and co-workers^[64,65] developed an efficient method for the highly enantio- and diastereoselective, conjugate addition of 1,3-dicarbonyl compounds to nitroolefins. Thereby, in the presence of the newly designed bifunctional thiourea catalyst **57**, the transformation proceeds at ambient pressure and room temperature, however, prolonged reaction times and high catalyst loadings (10 mol%, 12-72 h) are required.

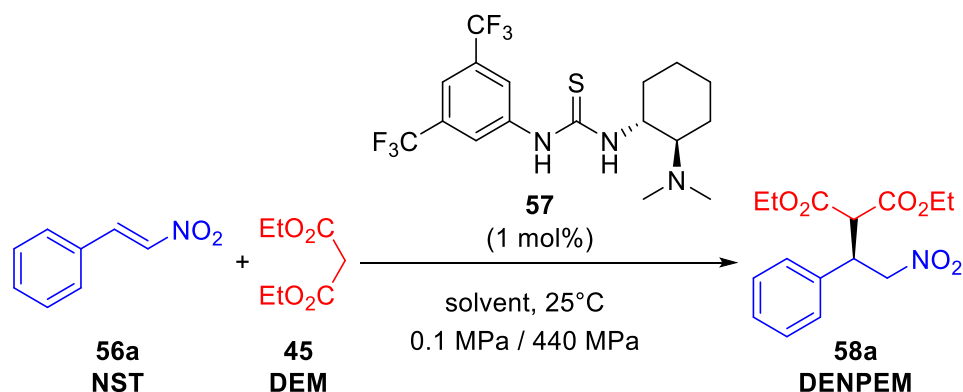


Scheme 12. 1,4-Conjugate addition of diethyl malonate (**45**) to *N*-, *S*- and *O*-containing aromatic nitroolefins **56** catalyzed by thiourea derivative **57** at high pressure.

Taking this precedent into account, it was investigated whether a rate acceleration can be achieved at high-pressure conditions without erosion of enantioselectivity and moreover, if solvent effects on reaction rate and yield at high pressure can be predicted using Perturbed-Chain Polar Statistical Associating Fluid Theory^[66] (PCP-SAFT) (Scheme 12). Michael-type reactions belong to the class of bimolecular addition reactions, which are known to be accelerated by high pressure due to a negative volume of activation (in the range of -5 to -40 $\text{cm}^3 \text{mol}^{-1}$).^[1,4] The volume of activation is defined as the difference of the volume of the transition state V^\ddagger and the volume of the corresponding reactants V^{A-B} .^[4,6,67]

Aiming to find the optimal solvent for the title reaction, PCP-SAFT to the Michael additions between diethyl malonate (**45**) and trans- β -nitrostyrene (**56a**) was applied (Scheme 13). The following theoretical work was carried out by Michael Knierbein (Prof. Gabriele Sadowski, TU Dortmund University).

The pure-component thermodynamic data such as vapor pressure, density data and activity coefficients of the reacting agents were available in the literature^[68], except for Michael adduct **58a**, which were therefore determined experimentally. Based on these reaction-independent data PCP-SAFT parameters were fitted.



Scheme 13. Model reaction of diethyl malonate (DEM, **45**) and trans-β-nitrostyrene (NST, **56a**) in different solvents and at various pressures.

Thermodynamics limits the equilibrium-yield of chemical reactions, depending on the reaction conditions. Further, reaction kinetics depend on the solvent, which can be expressed via thermodynamic activities of the reacting agents. These effects of solvent and pressure on yield and kinetics were investigated for the reaction shown in Scheme 13. The equilibrium constant for this reaction is given by Equation 1.

$$K_{th} = \frac{a_{DENPEM}}{a_{NST} \cdot a_{DEM}} \quad (1)$$

Equation (1) is based on thermodynamic activities of the reacting agents **56a**, **45** and **58a**, which are defined as the product of the equilibrium mole fractions and activity coefficients of the respective component. K_{th} is a function of temperature and pressure, however, it is independent of concentrations and solvents. Consequently, solvent effects on the reaction-equilibrium concentrations can be predicted for known K_{th} values based on the molecular interactions of the reagents with the solvent. Thermodynamic models, e.g. PCP-SAFT, give access to thermodynamic activities and are therefore well-suited tools that allow precise predicting of solvent effects on reaction equilibria.^[54,55]

Reaction kinetics are expressed in Equation (2) as change of the product mole fraction with time.

$$\frac{dx_{DENPEM}}{dt} = k_1 \cdot a_{NST} \cdot a_{DEM} - k_{-1} \cdot a_{DENPEM} \quad (2)$$

Here, k_1 and k_{-1} denote the rate constants of the forth and back reactions, respectively, that are directly linked to the thermodynamic equilibrium constant according to Equation 3.

$$K_{th} = \frac{k_1}{k_{-1}} \quad (3)$$

Owing to the activity-based expressions in Equation (1) and (2), also the kinetic constants k_1 and k_{-1} are independent of both concentration and solvent. Based on these physical relationships, thermodynamic models can be used to predict solvent effects on reaction kinetics.^[54,56]

The equilibrium constant K_{th} and the kinetic constants k_1 and k_{-1} depend on pressure. These pressure effects on the reaction equilibrium are quantified by the standard volume of reaction $\Delta^R v^0$:

$$\left(\frac{\partial \ln(K_{th})}{\partial p} \right)_T = \frac{-\Delta^R v^0}{R \cdot T} \quad (4)$$

Applying transition-state theory allows quantifying pressure effects on the reaction rate as a function of the volume of activation:

$$\left(\frac{\partial \ln(k)}{\partial p} \right)_T = \frac{-\Delta v^\ddagger}{R \cdot T} \quad (5)$$

In order to determine the equilibrium constant as well as the kinetic constants, the reaction rate and the reaction-equilibrium mole fractions for the addition of diethyl malonate (DEM, **45**) to trans- β -nitrostyrene (NST, **56a**) were measured experimentally in toluene as the solvent at 0.1 MPa and at 440 MPa, respectively. Based on these data, solvent effects on the reaction rate and equilibrium yield were predicted *via* activity coefficients at 0.1 MPa as well as at high-pressure conditions: First, the *in-silico* solvent screening was performed at 0.1 MPa for solvents covering different solvent classes. The screening results showed that *n*-hexane has the strongest beneficial effect on the reaction. That is, among the solvents studied, PCP-SAFT predicted that *n*-hexane should lead to the fastest reaction rate and to the highest product yield at reaction equilibrium. In contrast, it was predicted that dichloromethane would have the most disadvantageous effect on the reaction yield and kinetics (Figure 9, lines).

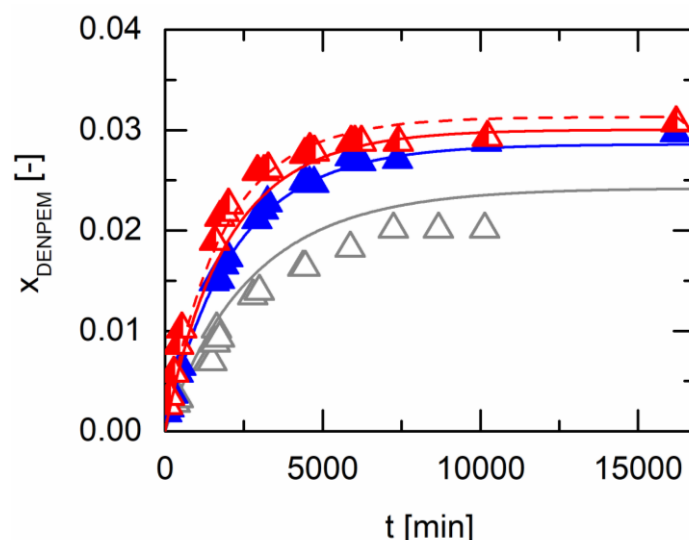


Figure 9. Mole fraction of the reaction product DENPEM plotted against reaction time at 0.1 MPa and 25 °C in different solvents. Symbols: experimental data (gray empty triangles: dichloromethane, blue triangles: toluene, red half-filled triangles: *n*-hexane/toluene). Lines: PCP-SAFT predictions (gray: dichloromethane, blue: toluene, solid red line: *n*-hexane/toluene, dashed red line: *n*-hexane). Reaction conditions: Nitroolefin **56a** (1.0 equiv), diethyl malonate (DEM, **45**) (2.0 equiv), catalyst **57** (1 mol%) in solvent (0.5 M, with respect to nitroolefin **56a**).

In order to validate the PCP-SAFT predictions, the kinetic profiles were measured in different solvents (see Figure 9, triangles). Dichloromethane, toluene and a solvent mixture of *n*-hexane/toluene mixture (1:1, %_v) were chosen for this purpose. The latter was necessary due to the insufficient solubility of the reactants in pure *n*-hexane as solvent. The experimental results were in excellent agreement with the PCP-SAFT predictions, both with respect to kinetics but also reflected the trend in yield at equilibrium for a given solvent. The data show that PCP-SAFT is a meaningful tool for solvent screening using thermodynamic activities as proposed in equations (1) and (2).

Subsequently, the *in-silico* solvent screening was performed at 440 MPa to evaluate if PCP-SAFT can also be used to predict the reactants and product activities in Equations (1) and (2) at high hydrostatic pressure (Figure 10).

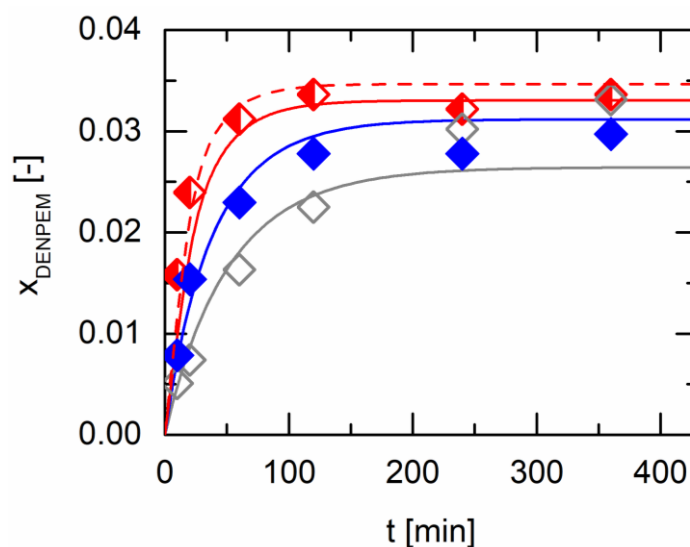


Figure 10. Mole fraction of the reaction product DENPEM plotted against reaction time at 440 MPa and 25 °C in different solvents. Symbols: experimental data (gray empty diamonds: dichloromethane, blue diamonds: toluene, red half-filled diamonds: *n*-hexane/toluene). Lines: PCP-SAFT predictions (gray: dichloromethane, blue: toluene, solid red line: *n*-hexane/toluene, dashed red line: *n*-hexane). Reaction conditions: Nitroolefin **56a** (1.0 equiv), diethyl malonate (DEM, **45**) (2.0 equiv), catalyst **57** (1 mol%) in solvent (0.5 M, with respect to nitroolefin **56a**).

Also under high-pressure conditions, PCP-SAFT again predicts the influence of solvent with respect to kinetics with high accuracy (Figure 10, lines), being in strong agreement with the experimental results (Figure 10, diamonds). Yet, PCP-SAFT slightly underestimates the equilibrium endpoint in dichloromethane.

The approach followed in this study was finally evaluated at even higher pressure (800 MPa), taken the reaction of **56a** and **45** in toluene as a representative example (Figure 11). PCP-SAFT predicted a further rate acceleration but no significant change in the equilibrium compared to the reaction at 440 MPa, which was again verified by the experimental data obtained.

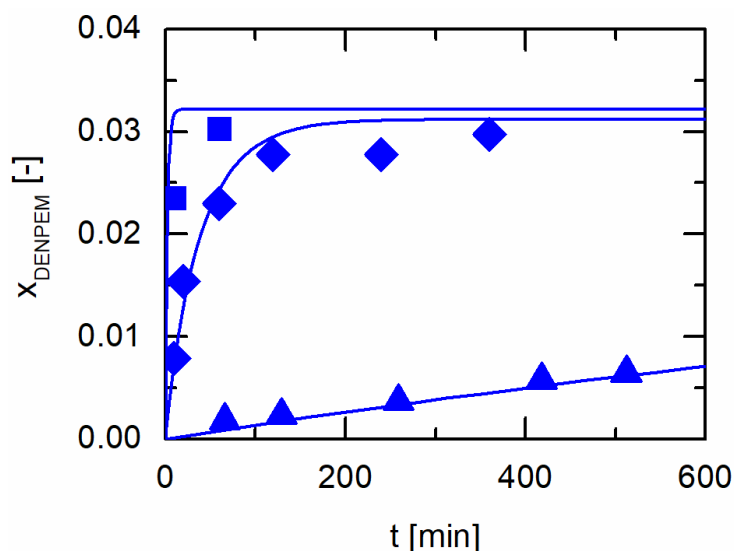
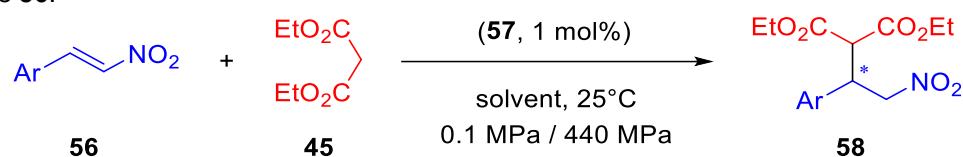
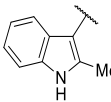
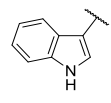


Figure 11. Mole fraction of the reaction product DENPEM plotted against reaction time at 25 °C in toluene. Symbols: experimental data at different pressures (triangles: 0.1 MPa, diamonds: 440 MPa, squares: 800 MPa), lines: PCP-SAFT predictions. Reaction conditions: Nitroolefin **56a** (1.0 equiv), diethyl malonate (DEM, **45**) (2.0 equiv), catalyst **57** (1 mol%) in solvent (0.5 M, with respect to nitroolefin **56a**).

Next, the scope of the Michael addition of diethyl malonate (DEM, **45**) and various heteroaromatic nitroolefins **56a** at 440 MPa was explored.^[69] PCP-SAFT predicted dichloromethane to be an inferior solvent, which was consequently not chosen. Due to solubility reasons, it had to compromise to run all reactions in toluene. The loading of the catalyst **57** was reduced from the typically employed 10 mol%^[15,16] to 1 mol%, and for comparison, ambient pressure reactions under the same conditions were run in parallel. Under these reaction conditions, the corresponding Michael adducts **56b-j** (Table 13, entries 1-9) were obtained at ambient pressure as well as at high pressure in a clean reaction: lower yields obtained are the results of an incomplete conversion of the reaction partners. Gratifyingly, the high enantioselectivities obtained at ambient pressures are mirrored at 440 MPa, indicating that pressure is not inducing an uncatalyzed background reaction or altering the catalyst-substrate arrangement necessary for asymmetric induction. The benefit of the high-pressure conditions becomes apparent when comparing conversion and yield at a given time, being higher by a factor of 2-12, suggesting that the necessary, but entropically disfavored ternary arrangement of nitroolefin **56a**, DEM **45** and catalyst **57** in the transition state has a negative volume of activation.

Table 13. Substrate scope of the Michael reaction of diethyl malonate (DEM, **45**) with various nitroolefins **56**.

Entry	Ar	Pressure (MPa)	Time	Solvent	Yield ^[a]	ee ^[b]
1		0.1	4 h	toluene	58b , 50%	94%
		440			58b , 99%	94%
2		0.1	24 h	toluene	58c , 20%	[c]
		440			58c , 50%	[c]
3		0.1	24 h	toluene	58d , 28%	92%
		440			58d , 93%	93%
4		0.1	24 h	toluene	58e , 18%	86%
		440			58e , 67%	91%
5		0.1	24 h	toluene	58f , 22%	91%
		440			58f , 79%	91%
6		0.1	24 h	toluene	58g , 8%	85%
		440			58g , 80%	85%
7		0.1	24 h	toluene	58h , 40%	91%
		440			58h , 83%	90%
8		0.1	24 h	toluene	58i , 25%	88%
		440			58i , 32%	90%
9		0.1	24 h	toluene	58j , 28%	87%
		440			58j , 67%	87%
10		0.1	24 h	THF	58k , 5%	60%
		440			58k , 62%	60%

11		0.1	24 h	THF	58l , 9%	70%
		440			58l , 92%	70%
12		0.1	24 h	THF	58m , 10%	69%
		440			58m , 84%	69%

Reaction conditions: Nitroolefin **56** (0.40 mmol, 1.0 equiv), diethyl malonate (DEM, **45**) (0.80 mmol, 2.0 equiv), catalyst **57** (1 mol%) in solvent (0.8 mL, 0.5 M with respect to nitroolefin **56**). [a] Isolated yield. [b] Enantiomeric excess was determined by chiral HPLC. [c] HPLC analysis was not possible due to the instability of the product.

In the case of pyridyl- (**58k**) and unprotected indolyl nitroolefins (**58l** and **58m**) the solvent had to be changed to THF. The substitute solvent had to be more polar to overcome solubility limitations without interacting to much with the thiourea catalyst **57**. While the reactions were greatly accelerated under pressure, a significant reduction in enantioselectivity (Table 13, entries 10-12) was observed. Interactions of solvent and catalyst **57** via hydrogen bonding lead to erosion of stereinduction, which was kept at a minimum when THF was used, compared to MeOH or MeCN. Since it was shown that high pressure does not disrupt the stereinduction but enhances the product formation enormous, THF represents a viable compromise as a solvent for the Michael addition at high pressures. Besides the aforementioned results, solvent effects of THF on reaction kinetics and equilibrium were also predicted (see Figure 12).

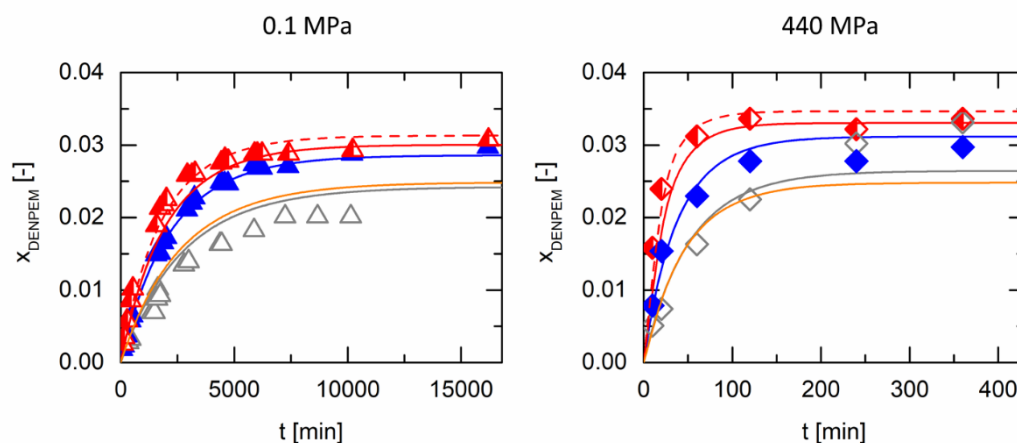


Figure 12. Mole fraction of the reaction product DENPEM plotted against reaction time at 0.1 MPa (left) and 440 MPa (right) and 25 °C in different solvents. Symbols: experimental data (gray: dichloromethane, blue: toluene, red: *n*-hexane/toluene). Lines: PCP-SAFT predictions (gray: dichloromethane, orange: tetrahydrofuran, blue: toluene, solid red line: *n*-hexane/toluene, dashed red line: *n*-hexane). Reaction conditions: Nitroolefin **56a** (1.0 equiv), diethyl malonate (DEM, **45**) (2.0 equiv), catalyst **57** (1 mol%) in solvent (0.5 M, with respect to nitroolefin **56a**).

In conclusion, it is demonstrated for the first time that thermodynamic-based PCP-SAFT screening can be applied at high hydrostatic pressures (up to 800 MPa) in liquid phase to predict solvent effects relevant for the reaction outcome with respect to kinetics and yield. Thus, the asymmetric Michael addition reaction of diethylmalonate to various heteroaromatic nitroolefins was significantly enhanced with respect to catalyst loading (from 10 down to 1 mol%) and reaction time (from 24-72 h down to 4-24 h). No erosion of enantioselectivity is observed, proving that the application of pressure did not induce an uncatalyzed background reaction. The obtained products are valuable for the synthesis of analogs of Baclofen, a pharmaceutical agent used to treat spastic movement disorders such as multiple sclerosis, as demonstrated with the conversion of **58I** (see next chapter). The combination of PCP-SAFT and high hydrostatic pressure appears to be promising for improving on the major drawbacks of sluggish process cycles generally encountered in organocatalyzed reactions.

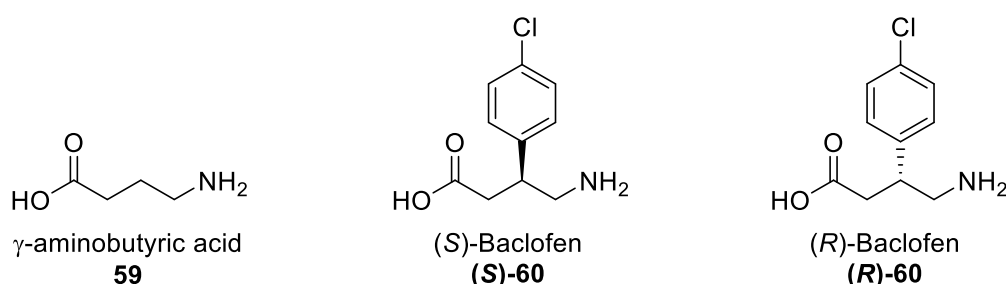
3.2 Synthesis of a γ -Aminobutyric Acid (GABA) Derivative

Approximately 70 years have passed since γ -aminobutyric acid (**59**) (GABA) (Scheme 14) was first discovered as a chief inhibitory neurotransmitter in the mammalian (vertebrate and invertebrate) central nervous system by Awapara^[70], Udenfried^[71], Roberts and Frankel.^[72]

Not just accumulation at presynapses as well as in postsynaptic densities, various GABA receptors were shown in extrasynaptic locations on different types of neurons and non-neuronal cells.

Moreover, beside the aforementioned excitatory neurotransmitter function, GABA serves as a paracrine/autocrine signal molecule, and plays an important role in the entire period of neural development.

Baclofen (**60**) (Scheme 14), sold under the brand name Lioresal®, Liofen®, Gablofen® and others, is a pharmaceutical agent used to treat spastic movement disorders such as multiple sclerosis, and finds further application in the treatment of alcohol dependence.^[73] It was first synthesized by the chemist Heinrich Keberle^[74] in 1962 and was designed as a drug for epilepsy treatment. Although the effect on treating epilepsy was disappointing, it was found that certain spastic disorders can be successfully treated.



Scheme 14. Structures of GABA (**59**), (S)- and (R)-Baclofen (**60**).

To valorize the synthetic protocol of the Michael addition described in the previous chapter, a multi-step transformation towards a new γ -aminobutyric acid analogue was examined. Therefore, the racemic indolyl Michael adduct **58i** (*N,N*-bis[[3,5-bis(trifluoromethyl)phenyl]thiourea (**42**) and NEt_3 as catalyst) was transformed. Adduct **58i** was chosen as the model substrate due to its immanent indolyl moiety, which is known to be widely distributed in nature and producible by various bacterial cultures. The corresponding γ -amino acid is not known in literature and hence could show a promising pharmacologic activity.

Furthermore, adduct **58i** exhibits an increased inertness towards polymerization under acidic conditions compared to similar derivatives like adduct **58m**^[75], since its preferential linkages sites C2 and C3 are blocked through the methyl and the nitroalkane group. The only accessible

position for polymerization remains the N1-position through the unprotected NH-moiety. The formation of possible di- and tri- and oligomers is not considered here.

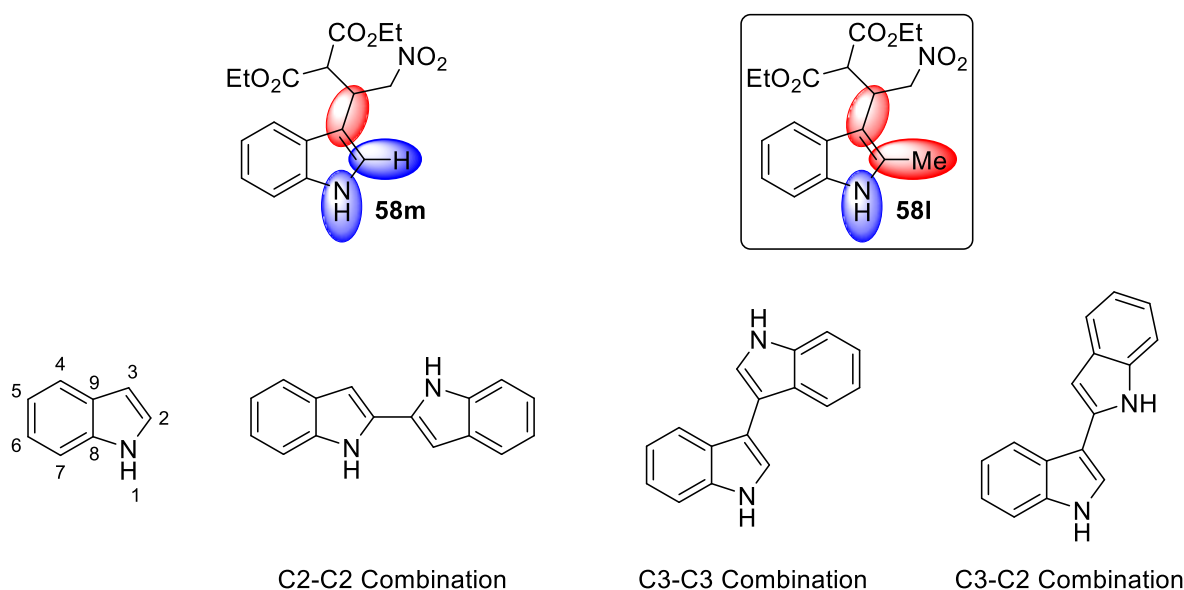
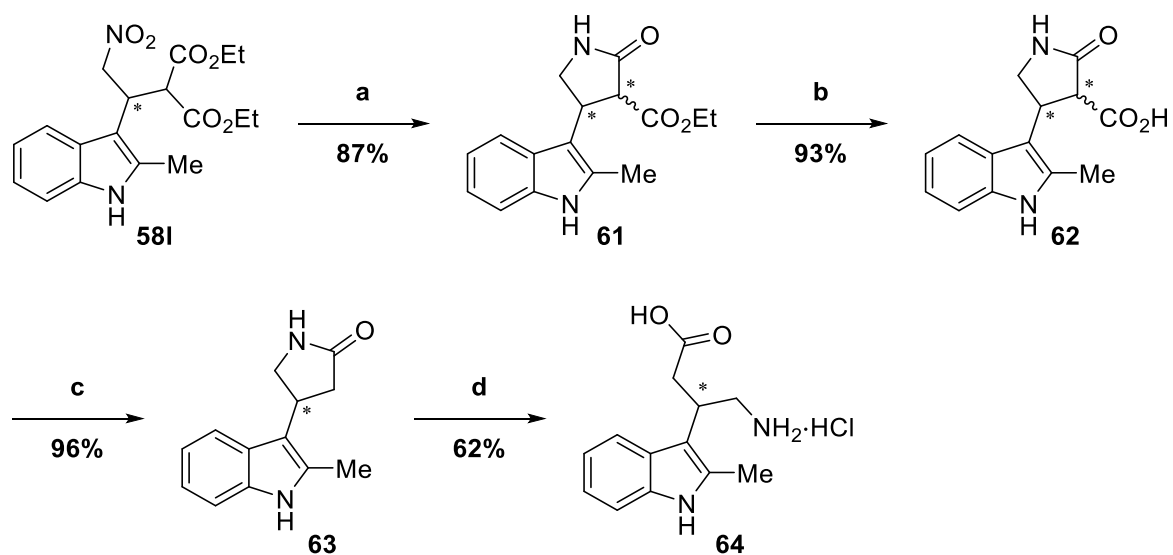


Figure 13. Polymerization positions of indole. Red circled position: blocked. Blue circled position: accessible.

In the first step of the GABA-analogue synthesis, the nitro group was reduced to provide lactam **61** after intramolecular lactamization in 87% yield. NaBH_4 and NiCl_2 in MeOH was used as reducing agent, forming the active species Ni_2B *in situ*. Nitroaliphatic compounds have traditionally been reduced in autoclaves by high-pressure hydrogenation. Research in reduction methods revealed that amorphous transition metal borides are of paramount importance as heterogeneous catalysts when it comes to the reduction of aliphatic nitro compounds^[76]. Subsequently, the ester group was hydrolyzed by NaOH in EtOH and the corresponding carboxylic acid **62** was obtained in an almost quantitative yield of 93%. Conventional thermal decarboxylation of the carboxylic acid in high-boiling solvents was not successful. Compound **62** had to be heated over its melting point of 192° C to approximately 230 °C with a heat gun to achieve a nearly quantitative decarboxylation with 96% yield. Lactams are known to hydrolyze under acid conditions and therefore the open chain species can be obtained. The desired γ -amino butyric acid derivative was formed after hydrolyzation with 6 M HCl under reflux conditions as its corresponding hydrochloric salt **64** with 62% yield. The moderate yield in the last step of the total synthesis can be attributed to undesired polymerization side reactions (Scheme 15).



Scheme 15. Synthesis of GABA analogue. Reaction conditions: [a] $\text{NiCl}_2 \cdot 6\text{H}_2\text{O}$, NaBH_4 , MeOH, rt, 6 h. [b] NaOH, EtOH, rt, 16 h. [c] $230\text{ }^\circ\text{C}$, 5 min. [d] 6 M HCl, reflux, 24 h.

In summary, Michael addition adduct **58I** was successfully used as a starting point for the four step synthesis of γ -aminobutyric acid derivative **64** in 48% overall yield, clearly stating the synthetic utility of the obtained Michael adducts in the previous chapter.

3.3 Influence of High Pressure on Hydrogen Bonds

The phenomenon of hydrogen bonding is an intermediate range inter- or intramolecular interaction between an electron-deficient hydrogen atom and an area of high electron density. These non-covalent bonds are quintessential for secondary and tertiary structures of proteins and the DNA, carrying the genetic instructions for the development of life.

Table 14. Dissociation energy of different bond types.

Bond type	Dissociation energy
Ionic lattice ^[77]	41 – 360 kcal mol ⁻¹ [a]
Covalent bond ^[78]	34 – 256 kcal mol ⁻¹
Hydrogen bond ^[79,80]	2 – 40 kcal mol ⁻¹
van der Waals forces ^[81]	0.5 – 1 kcal mol ⁻¹

[a] Cited ranges for ionic dissociation energies vary.

A hydrogen atom is formally capable of forming only a single chemical bond, according to the well-known valence bond theory. Frequently, the hydrogen atom is forming an additional bond, the so called “hydrogen bond”, becoming pseudo two-valent. In general, hydrogen bonds can connect atoms with higher electronegativity than hydrogen itself, which can be observed in water as $\text{H}_2\text{O} \cdots \text{H}-\text{OH}$, as well as with atoms with lower electronegativity such as bonds in boranes $\text{B}-\text{H}-\text{B}$.^[82]

Besides the different types, hydrogen bonds can also be classified in two categories specifying the corresponding bonding symmetry. On the one hand, so called “single well hydrogen bonds” (SWHBs) describe symmetrical hydrogen bonds, the strongest of all hydrogen bonds, where the hydrogen atom is located equidistant in line with the heteroatoms and is ideally as close as possible to an 180° angle. The potential energy function for hydrogen consists of a single well between the heteroatoms, additionally SWHBs are very short in distance. On the other hand, the so called “low barrier hydrogen bonds” (LBHBs) were defined as shorter and asymmetric in character and hence possessing an intermediate strength. When it comes to LBHBs, the distance between one heteroatom and hydrogen atom is shorter than a “conventional” hydrogen bond. Here, the hydrogen atom is located in a double minimum potential well, where its zero point vibrational state is close to the barrier.^[83,84] The “conventional” hydrogen bond is characterized as a weak dipolar attraction between a hydrogen and a heteroatom. The strongest representatives SWHBs are very rare, but both,

SWHBs as well as LBHBs can be referred to strong hydrogen bonds. However, the majority of hydrogen bonds are weak and are assigned to conventional hydrogen bonds.^[85]

The energy of the strongest covalent bond ($C\equiv O$ 256 kcal mol⁻¹) is about 7.5- fold higher than the weakest ($O-O \approx 34$ kcal mol⁻¹).^[78] In comparison, the energy of hydrogen bonds ranges from 2 to 40 kcal mol⁻¹.^[79,80] Accordingly, the strongest hydrogen bond is 20-fold higher than the weakest, a huge gap compared to covalent bonds. Based on these data, it is important to combine the concept of SWBHs and LBHBs together with the model of dipolar attractions to understand the physiochemical properties of hydrogen bonds. Weak hydrogen bonds with nitrogen and oxygen usually exhibit enthalpies between 4 to 10 kcal mol⁻¹. The enthalpy, for instance, of the $O-H\cdots O$ hydrogen bond in alcohols and water has a value of 5 to 6 kcal mol⁻¹, whereas for carboxylic acids the enthalpy is approximately 7 kcal mol⁻¹.^[80] The bond strength of LBHBs lies in the range of 12 to 24 kcal mol⁻¹. However, the strength of stronger SWHBs starts at 24 kcal mol⁻¹ and can reach values up to 40 kcal mol⁻¹.^[84] All these energies refer to the enthalpy of heteroatoms with and without the interaction of the hydrogen bond. The length of the corresponding hydrogen bond is directly correlated to its strength and thus, in general, the stronger a hydrogen bond the shorter its bonding distance. Moreover, the longer a covalent bond ($O-H$), the shorter the corresponding hydrogen bond ($O\cdots H$). In some cases, the covalent as well as the hydrogen bond become equal in distance forming a perfect symmetrical bond.^[85]

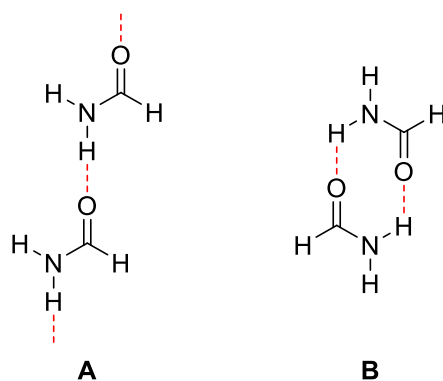
As a tool for detecting intra- and intermolecular hydrogen bonds, Raman spectroscopy, infrared (IR) spectroscopy as well as nuclear magnetic resonance (NMR) are the methods of choice. Raman scattering utilizes inelastic scattering of photons to detect vibrational modes as well as rotational and various low-frequency modes of molecules. The excitation wavelengths used for Raman spectroscopy ranges from the high-energy ultra-violet through the region of visible light to the low-energy infrared^[86]. Related to Raman spectroscopy, IR spectroscopy yields similar and complementary molecular information, using wavelengths from the near IR to the far IR to provide insight into functional groups and their possibly concentration^[87]. In contrast, the NMR spectroscopy is a technique to detect magnetic fields around atomic nuclei, and thus, the location of the detected nuclei in the spectrum is dependent on the shielding of electron density^[88]. Hydrogen bonding interactions strongly influence the vibrational modes as well as the shielding of the involved nuclei and therefore detection with the techniques described in the latter are possible.

The importance and influence of physiochemical properties of hydrogen bonds were already investigated to a large extent. Despite the fundamental role, the influence of high pressure on hydrogen bonds is an insufficient investigated area, especially when interactions in solution are considered. Since the application of high pressure in the solid state is more common,

scientists already explored that pressure can reduce the intermolecular distances and therefore can reach a higher packing resulting in a strengthening of hydrogen bonds in the crystal. The crystals force field perturbs the position of hydrogen bonds. Hence, pressure can “push” hydrogen bonds in a more optimal geometry.^[89]

Ohtaki et al.^[90] investigated the effects of temperature and pressure on hydrogen bonds in water and formamide in their liquid structure. The liquid structure of formamide consists as a mixture of a ring- and open-chain dimer (Table 15). By applying pressure, the content of ring-dimer was enriched and became predominant. Additionally, the ¹H-chemical resonance of the formamide was shifted downfield with increasing pressure, indicating a strengthening of the respective hydrogen bonds.

Table 15. Linear-chain A and ring-dimer B structure of liquid formamide.



Entry	Temperature	Pressure	mol%	
			Linear A	Ring B
1	25 °C	0.1 MPa	57	43
2	25 °C	20 MPa	50	50
3	25 °C	40 MPa	43	57

3.3.1 NMR Studies of Hydrogen Bonds

Oh and co-workers^[91] investigated a highly diastereo- and enantioselective strategy for an Aldol reaction of methyl 2-isocyanoacetate using thiourea derivatives as hydrogen bond donor catalysts. To prove the existence of the hydrogen bonded catalyst-substrate complexes, NMR studies were examined (Figure 14). In favor to run this experiment, thiourea derivative **42** was used as a hydrogen bond donor. The advantage of thiourea **42** is its C₂-symmetry resulting in only three different signals in the ¹H-NMR spectrum and therefore simplifying subsequent NMR analysis.

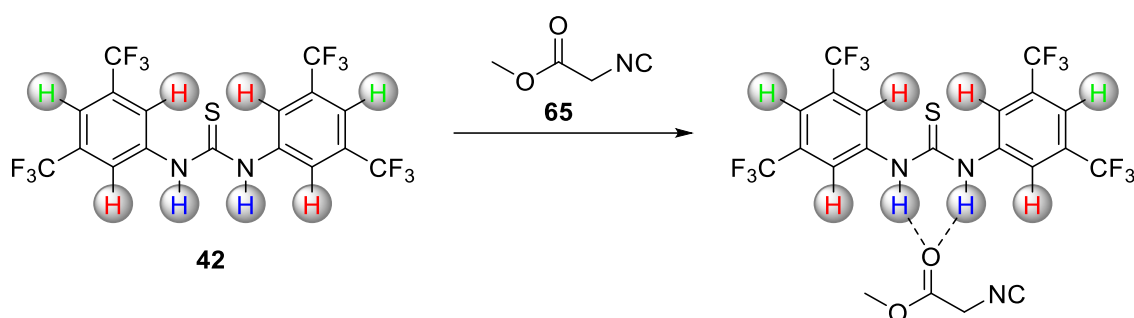


Figure 14. Thiourea **42**, a hydrogen bond donor, and methyl 2-isocyanoacetate (**65**), a hydrogen bond acceptor, forming a catalyst-substrate complex.

Thiourea **42** (0.04 mmol) was measured in THF-*d*₈ (0.7 mL) prior to the addition of the hydrogen bond acceptor **65**. After the addition of **65** (0.08 mmol) the NH-signal of thiourea **42**, which is directly involved into the hydrogen bond, was shifted downfield from δ 8.00 to 8.02 ppm. The signal of the four aromatic protons (Figure 14, red) were shifted from δ 6.39 to 6.40 ppm. Only the signal of the two aromatic protons (Figure 14, green) remained unaffected by the hydrogen bond and remained at δ 6.07 ppm. These downfield shifts are giving evidence for the formation of a complex consisting of the hydrogen bond donor **42** and acceptor **65**.

Based on these literature precedence, high pressure NMR studies were performed to investigate the influence of pressure on hydrogen bonds, especially on similar hydrogen-donor-acceptor-complexes as described in the latter. The NMR study was carried out in the institute of biophysics and physical biochemistry in collaboration with Dr. Markus Beck-Erlach, member of the working group of Prof. Sprangers.

Hence, the same thiourea derivate **42** (0.04 mmol) was used as a hydrogen bond donor and nitroolefin **56a** (0.08 mmol) as a hydrogen bond acceptor. These compounds are inspired by the reaction conditions of the Michael addition mentioned in Chapter 3.1. CD₃CN was chosen

as the solvent, due to its low costs compared to THF- d_8 , but slightly higher hydrogen bond acceptor properties. Figure 15 shows the influence of pressure on the NH-resonance shift of thiourea **42**. Notably, every signal in the NMR is shifted by pressure and signals need to be adjusted by the intrinsic pressure effect. Therefore, thiourea **42** had to be measured in the full pressure range up to 180 MPa with and without the addition of nitroolefin **56a** (Figure 15).

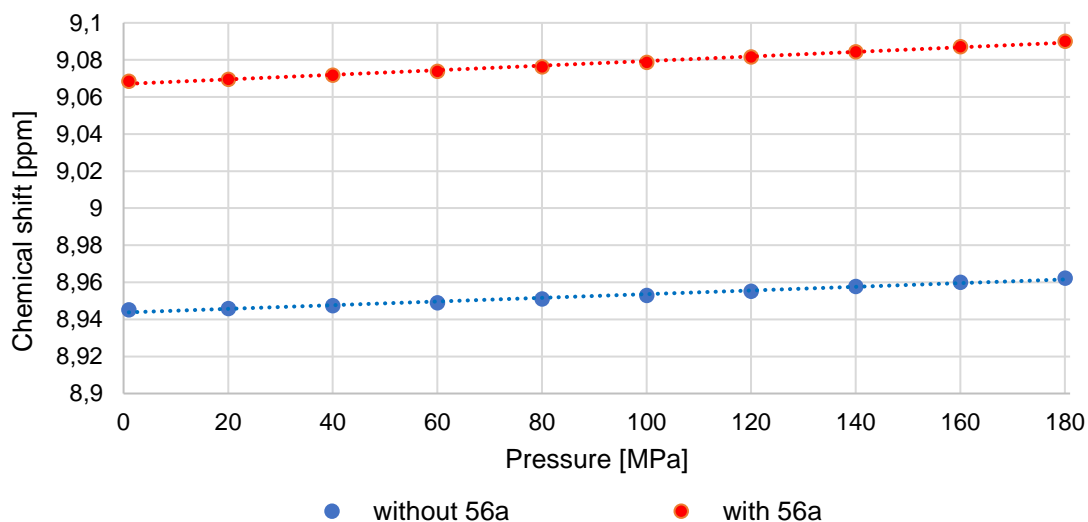


Figure 15. NH-Signal of thiourea **42** in dependence of pressure with and without the addition of hydrogen bond acceptor **56a**.

When the pressure induced signal shift of the red data-line (thiourea **42** with nitroolefin **56a**) is subtracted with the blue data-line, the adjusted and absolute pressure shift can be obtained. A total signal downfield-shift of 0.0045 ppm in the pressure range from 0.1 to 180 MPa was observed (Figure 17). This value might seem very low and insufficient but, indeed, is already significant. The pressure induced shift of the NH-signal is presented in Figure 16.

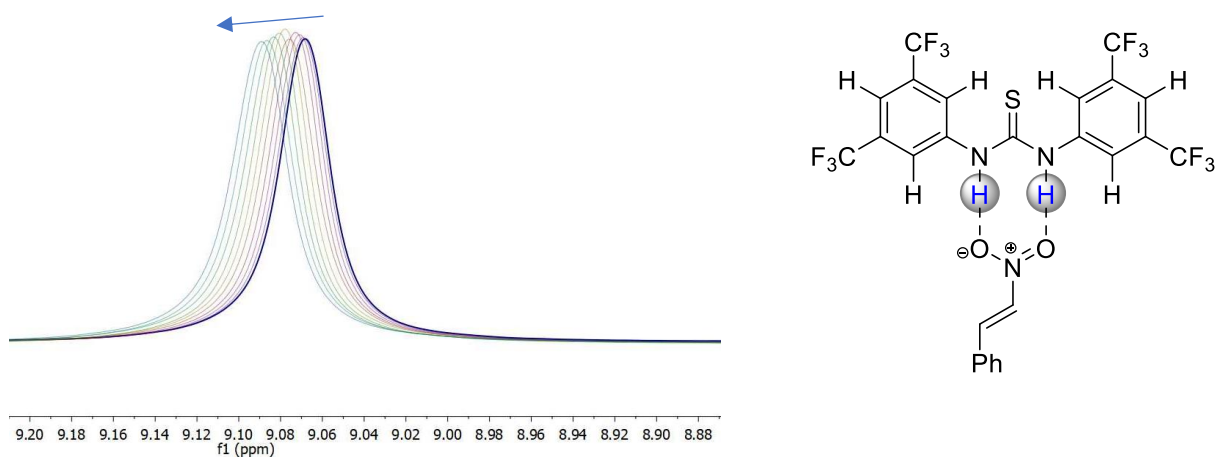


Figure 16. NH-signal shift of thiourea **42** influenced by pressure.

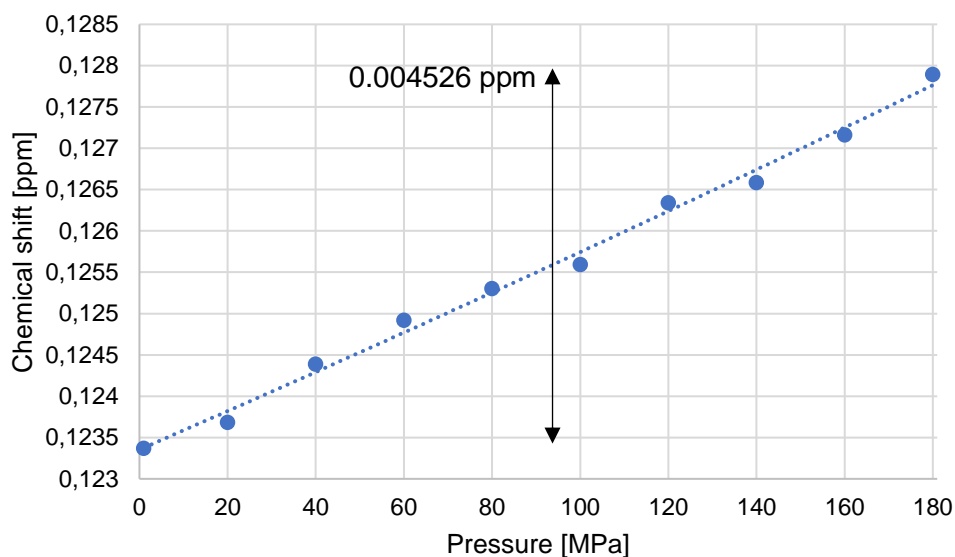


Figure 17. Absolute pressure shift of the NH-signal of thiourea **42** in presence of nitroolefin **56a**.

The same procedure was applied to the aromatic signals of thiourea **42** (Figure 14, red). The signal shift of the four aromatic protons in dependence of pressure with and without nitroolefin **56a** are displayed in Figure 18.

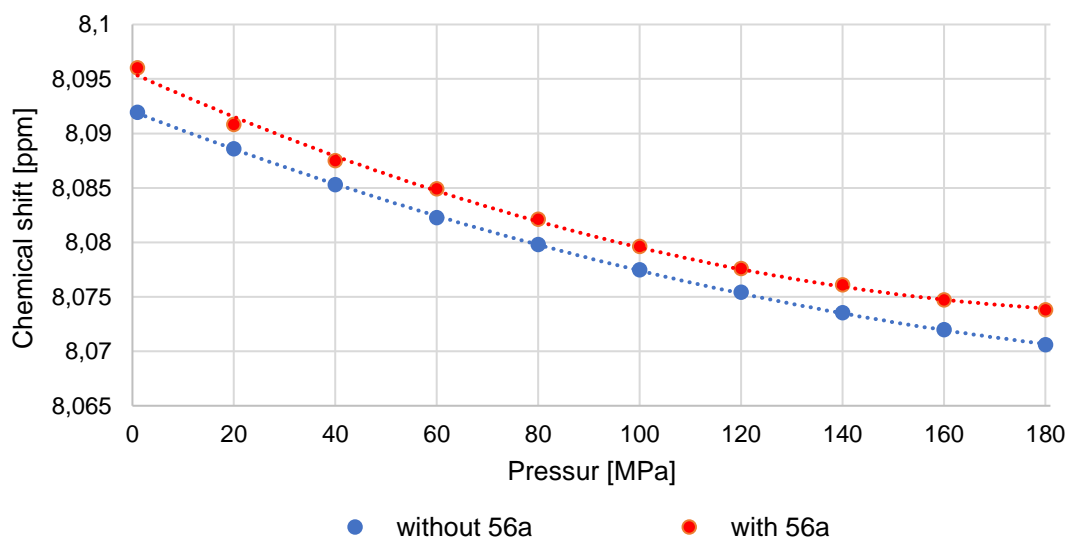


Figure 18. Signal of the four aromatic protons of thiourea **42** in dependence of pressure with and without the addition of hydrogen bond acceptor **56a**

A total signal downfield-shift of 0.00086 ppm in the pressure range from 0.1 to 180 MPa was observed (Figure 20). This value is too low to be significant and can be neglected. The pressure induced shift of the four aromatic signal is presented in Figure 19.

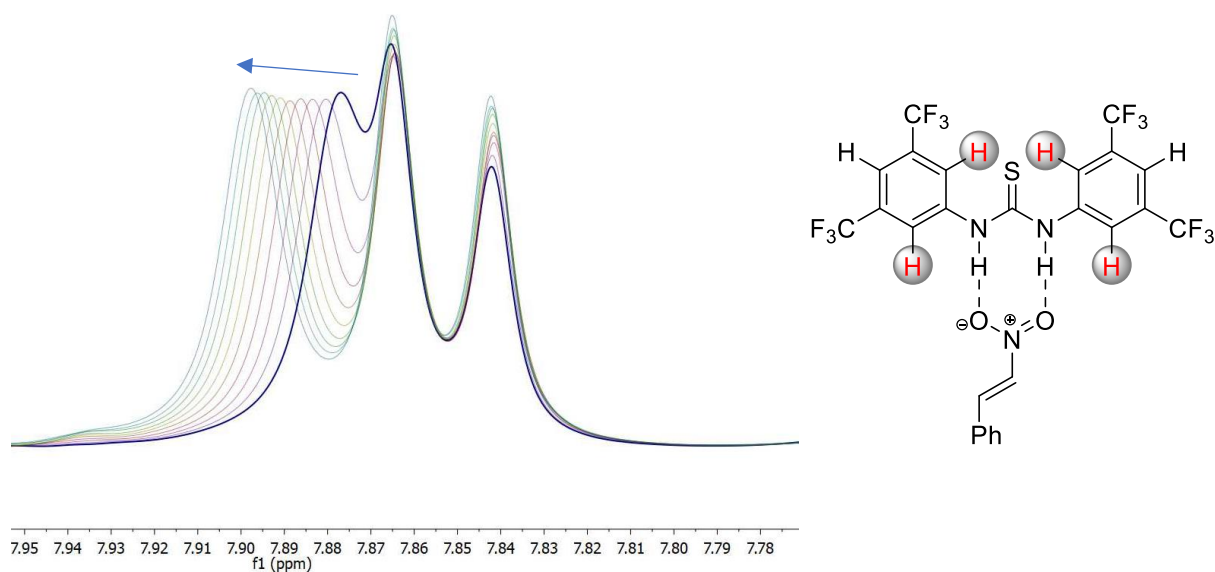


Figure 19. Signal shift of the four aromatic protons of thiourea **42** by pressure.

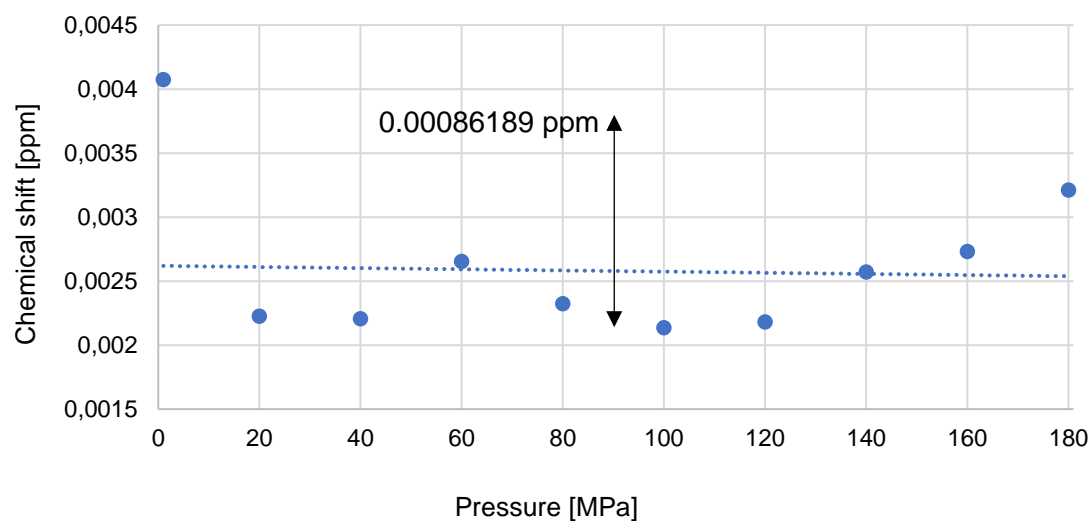


Figure 20. Absolute pressure shift of the four aromatic signals of thiourea **42** in presence of nitroolefin **56a**.

The signal shift of the last two aromatic protons (Figure 14, green) in dependence of pressure with and without nitroolefin **56a** is displayed in Figure 21.

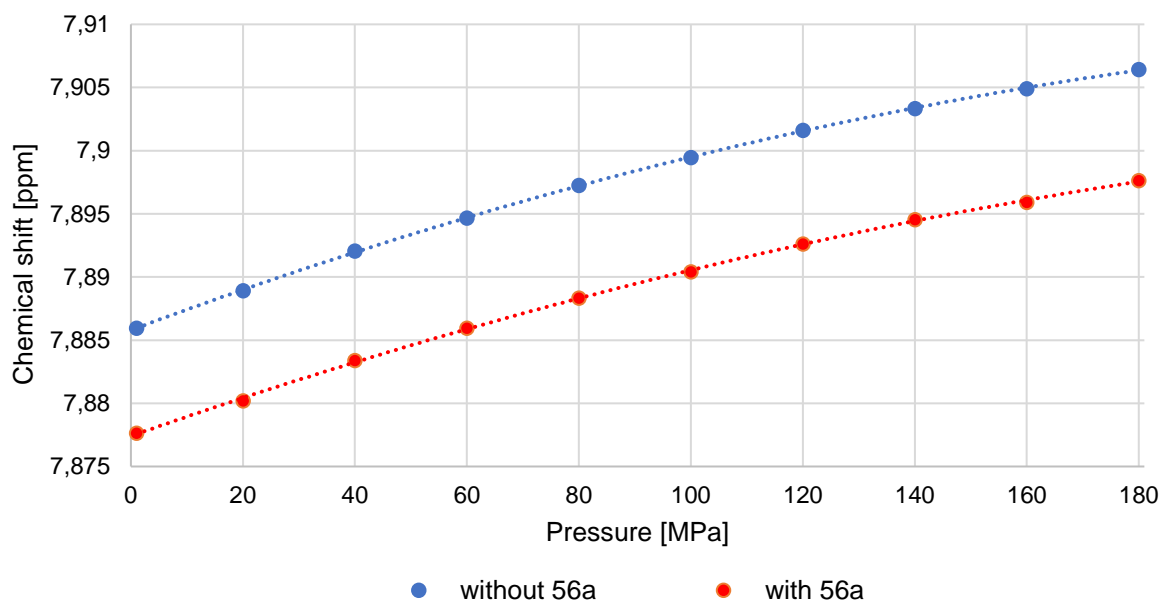


Figure 21. Signal of the two aromatic protons of thiourea **42** in dependence of pressure with and without the addition of hydrogen bond acceptor **56a**.

A total signal upfield-shift of 0.00048 ppm in the pressure range from 0.1 to 180 MPa was observed (Figure 23). This value is too low to be significant and therefore neglected due to its upfield shift. The pressure induced shift of the two aromatic signal is presented in Figure 22.

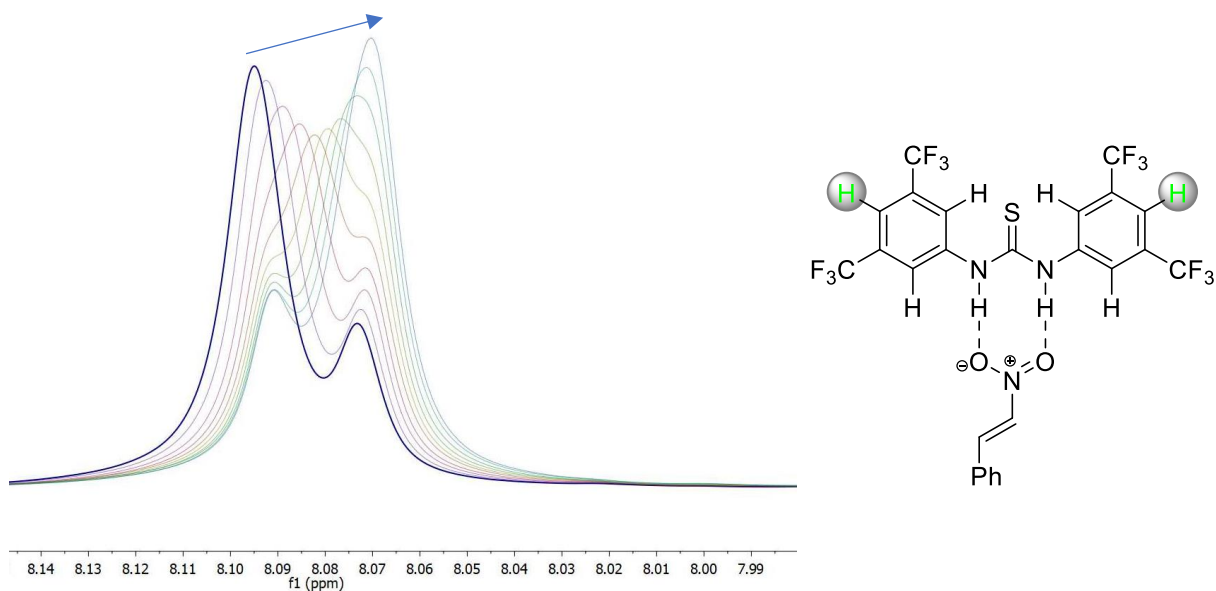


Figure 22. Signal shift of the two aromatic protons of thiourea **42** by pressure.

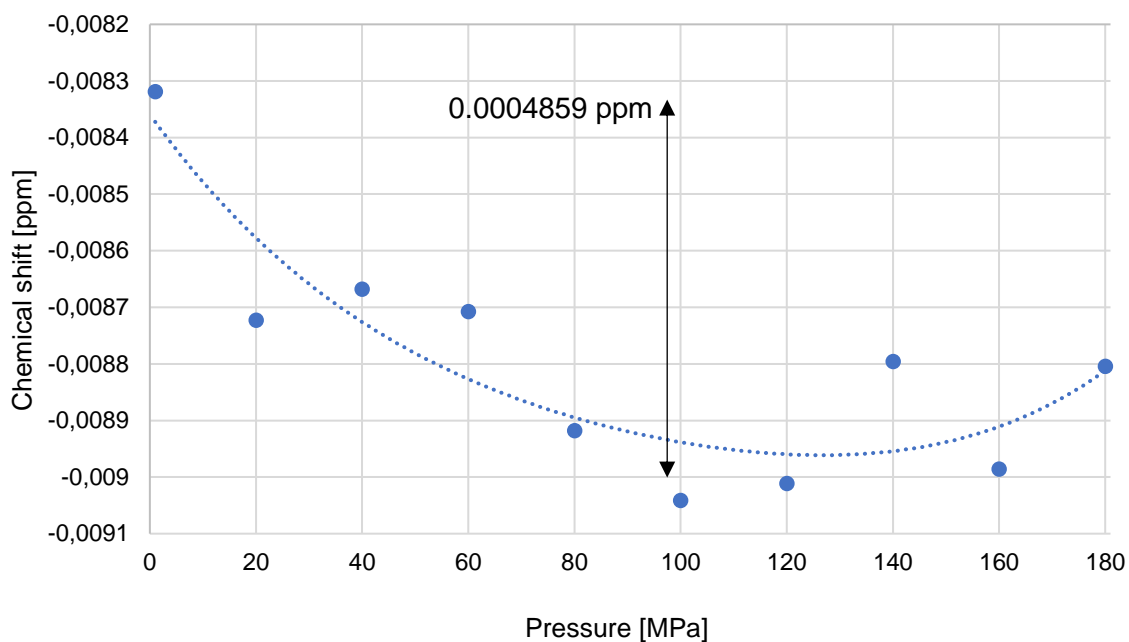


Figure 23. Absolute pressure shift of the two aromatic signals of thiourea **42** in presence of nitroolefin **56a**.

In conclusion, the consideration of the aromatic protons of thiourea **42** and the pressure induced shifts are negligible due to the low ppm-values as well as their rather long distance to the hydrogen bond. The pressure induced shift of the NH-signal is indeed significant, but the assignment of the effect's nature is ambiguous. The investigated downfield-shift of the NH-signal could be contributed to two different phenomena. On the one hand, the amount of the formed substrate-catalyst-complex could be increased by increasing pressure what would lead to the resulted downfield-shift. In exchange, it has to be assumed, that at ambient pressure a certain percentage of the thiourea **42** exists without a formed hydrogen bond towards the nitroolefin **56a**. To exclude the possibility that already the entire amount of thiourea is bound to the nitroolefin, appropriate experiments with a molar ratio of thiourea and nitroolefin of 1:1 and 2:1 were carried out. Unfortunately, a downfield-shift with a lower molar ratio at ambient pressure was not observed and therefore it can be assumed that, to a certain extent, the thiourea compounds also exist without hydrogen bonding. On the other hand, the resulted downfield-shift could also indicate a strengthening of the formed hydrogen bond. The intramolecular distance is decreased by pressure, also decreasing the length of the hydrogen bond. The shorter a hydrogen bond, the stronger it is. Due to this ambiguous result received by NMR spectroscopy additional IR measurements were conducted.

3.3.2 IR Studies of Hydrogen Bonds

For further mechanistic insights, in addition to the aforementioned NMR studies, also IR measurements were carried out to investigate the effect of pressure on hydrogen bonds on an expanded basis. IR measurements were examined in the inorganic chair of Prof. Scheer at the University of Regensburg. Spectra were recorded on a Thermo Scientific™ Nicolet™ iS™5 FTIR, optics with KBr windows, high performance dTGS-detector, germanium coated KBr-beam splitter and iD1 transmission with KBr cuvette.

Oh^[91] and co-workers investigated a strategy for an efficient Aldol reaction supported by NMR studies, but also extended their examination by IR measurements for further insights into the hydrogen bond donor-acceptor interaction. The free NH-signal of neat thiourea **42** (hydrogen bond donor) without hydrogen bonding interactions is located at a wavenumber of approximately 3435 cm⁻¹. When methyl α -isocyanoacetate is added, a catalyst-substrate complex with hydrogen bond interactions is formed and the NH-signal at approximately 3435 cm⁻¹ completely disappears. The vanishing of the free NH-signal indicates a quantitative formation of a hydrogen bonded catalyst-substrate complex. The bonded NH-signal was shifted to lower wavenumbers in the range of 2985-3204 cm⁻¹. When the NH group serves as a hydrogen bond donor, the length of the covalent bond between N and H is increased resulting in the weakening of the covalent bond through the hydrogen bond leading to a shift to lower wavenumbers. When acetone was employed as a weaker hydrogen bond acceptor, the signal of the free NH as well as the bonded NH are coexisting at the same time indicating a partial formation of a catalyst-substrate complex.

Based on this work^[91], high pressure IR measurements were conducted to investigate the influence of pressure on hydrogen bonds for comparison with the prior described and obtained results by NMR studies. At first, ambient pressure measurements, similar to the work of Oh and coworkers, were performed. Prior to the addition of hydrogen bond acceptors, a solution of thiourea **42** in dichloromethane (17.33 mM) was measured. The signal of the free NH was found at a wavenumber of 3374 cm⁻¹ (Figure 24).

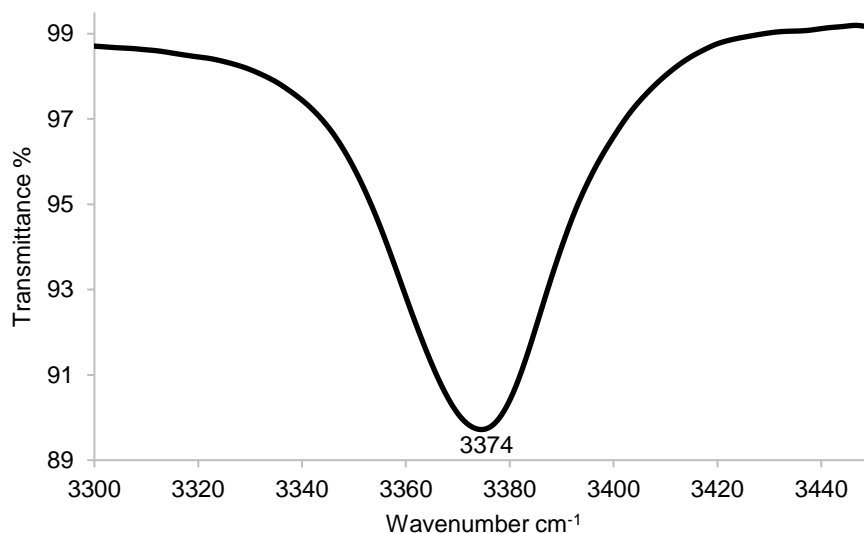


Figure 24. NH-spectral region of thiourea **42** in dichloromethane (17.33 mM) without hydrogen bond acceptors.

Subsequently, acetone (**10**) as well as methyl 2-cyanoacetate (**66**) were used as hydrogen bond acceptors in a range of 2.0 to 4.0 equivalents (Figure 25, Figure 26).

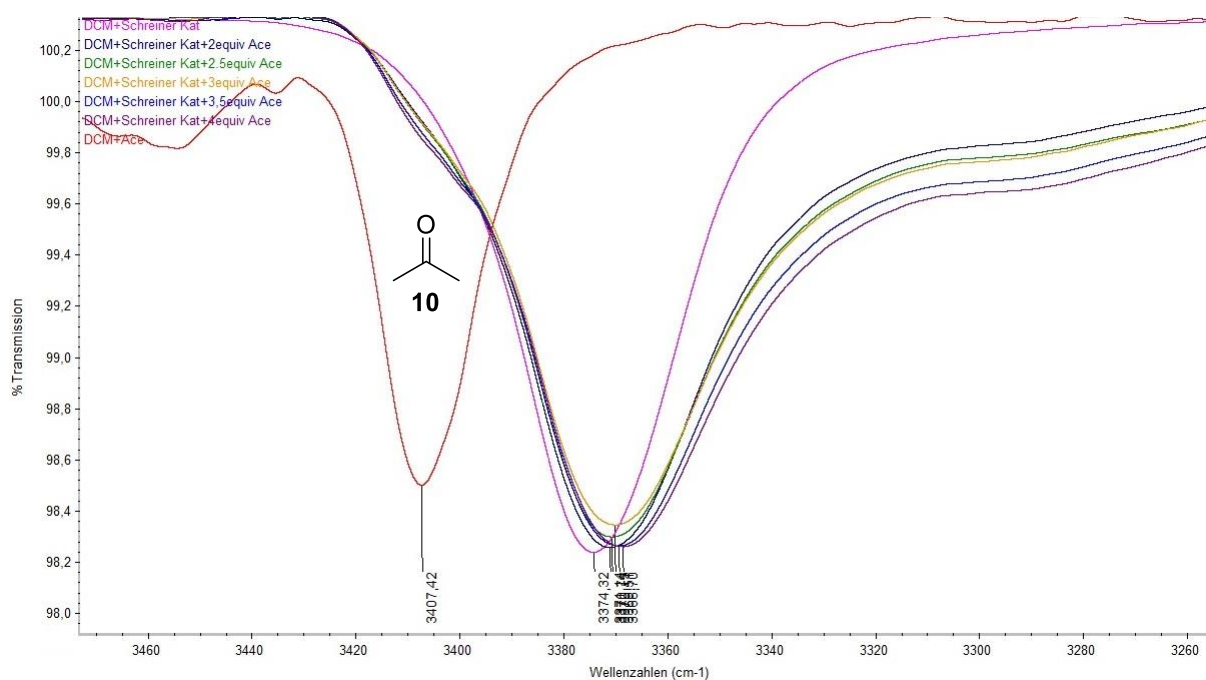


Figure 25. Stacked IR spectrum with NH-spectral region of thiourea **42** with different equivalents of acetone. Left signal (red curve): acetone without thiourea **42** in dichloromethane (17.33 mM) for comparison.

Unfortunately, the ambient pressure measurements did not show the expected interactions of hydrogen bond donor and acceptor with respect to a spectral shift to lower wavenumbers. Even when 4.0 equivalents of hydrogen bond acceptor were used, the spectral shift was too low to be significant. However, the high pressure IR measurements conducted at the TU-Dortmund with supervision of a co-worker from Prof. Winters group were more surprising. The high pressure measurements were conducted with the same conditions described in the latter. Here, it was not possible to detect signals and functional groups of the corresponding thiourea **42** in solution. Even when a saturated solution in dichloromethane or chloroform was used the corresponding thiourea signals were not detectable.

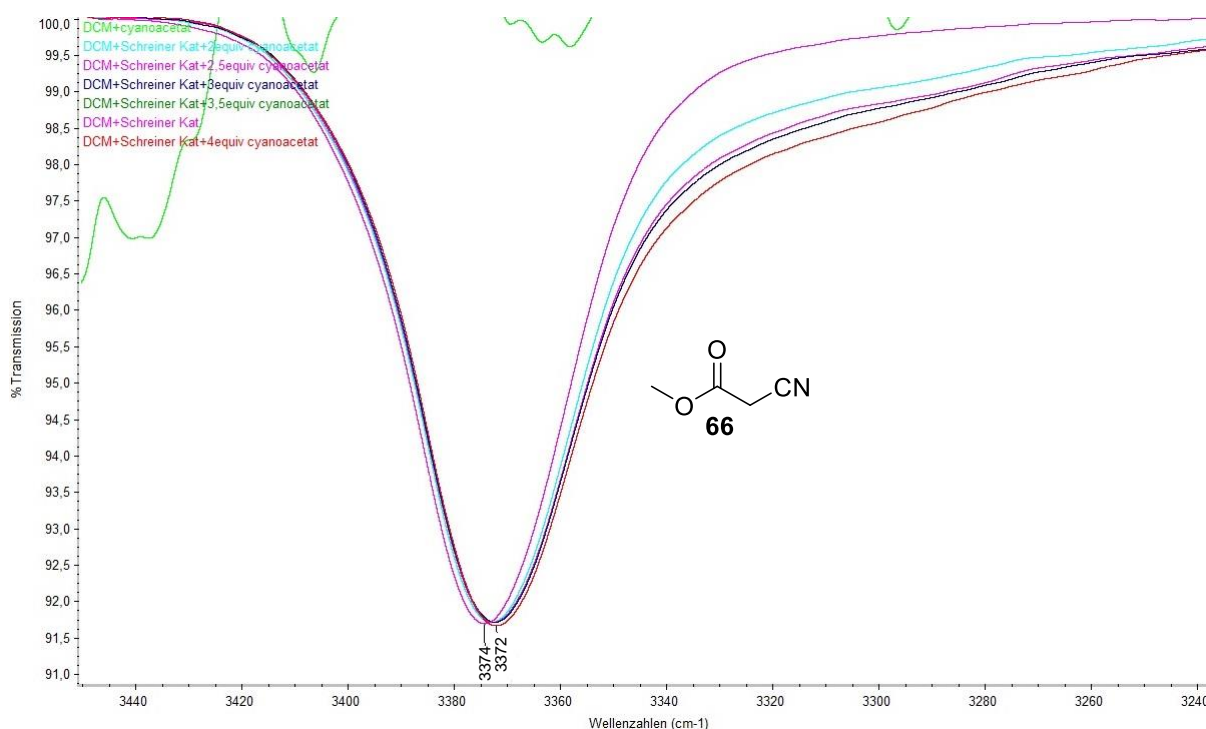


Figure 26 Stacked IR spectrum with NH-spectral region of thiourea **42** in dichloromethane (17.33 mM) with different equivalents of methyl 2-cyanoacetate (**66**).

However, in order to gain reasonable information about hydrogen bonds and their properties under hydrostatic pressure, the concept of hydrogen bond acceptor-donor complexes had to be replaced by another more suitable and detectable system.

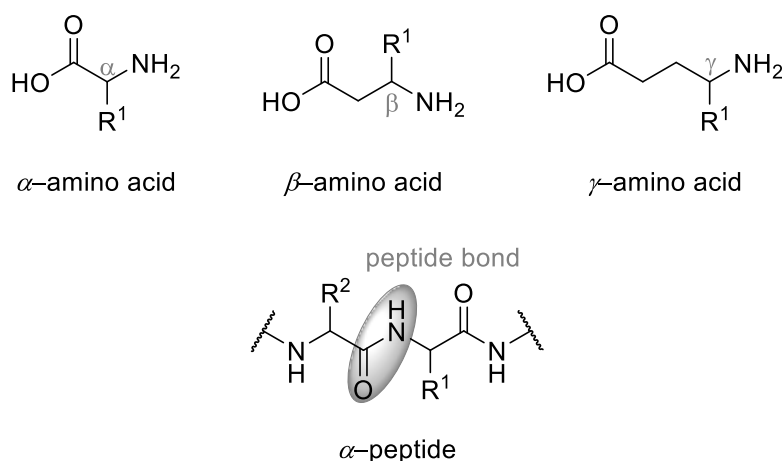


Figure 27: Different amino acids and a α -peptide showing the peptide bond.

Therefore, the intramolecular formed hydrogen bonds of different small amides were studied. Small amide molecules are particularly suitable to be investigated and accessible for fundamental investigations since they can be considered as peptide mimics as well as mimics for oligoamides, proteins, enzymes and foldamers.^[92] Amides as mimics are advantageous since these “model compounds” are structurally closely related to large peptides without harboring an enormous variety of functional groups or protons. This fact allows simple analysis by NMR or IR and therefore provides conformational information as well as hydrogen bond properties without the interference of unnecessary moieties. Accordingly, Gellman counts as a pioneer in the research field of foldamers and examined model studies for the folding of a variety of peptide backbones. In 1994, Gellmann^[93] investigated the intramolecular hydrogen bond properties of β -alanine and γ -amino butyric acid derivatives with the aim to design unnatural polyamides and examine the specific folding pattern. Variable-temperature FTIR was the method of choice. The most beneficial solvent to perform IR measurements in the amide A region are alkyl halides such as CH₂Cl₂ or CHCl₃. These alkyl halides are exhibiting low polarities and do not interact or interfere with hydrogen bonds. An amide concentration down to 1.0 mM was essential to avoid interference of intermolecular hydrogen bonds.

When Using *N*-acetyl- β -alanine *N,N'*-dimethylamide (**67**) only a single NH-resonance at approximately 3440 cm⁻¹ (293 K) was observed. This indicates, that a non-hydrogen-bonded NH is present, and thus, the formation of the six-membered-ring, usually available to β -alanine derivatives, does not occur. Additionally, aggregation of **67** can also be excluded. When the molecule length is increased by one carbon atom to *N*-acetyl- γ -aminobutyric acid *N,N'*-dimethylamide (**68**), the intramolecular hydrogen bond properties changed dramatically. In this case, two distinct NH-signals were observed at the same time at approximately 3446 and 3323 cm⁻¹ (294 K). Again, the higher energy band can be attributed to the non-hydrogen-

bonded NH, the lower energy band indicates an intramolecular hydrogen bonded NH. The signal with lower wavenumbers proves the formation of a seven-membered-ring available in γ -aminobutyric acid derivatives (Figure 28).

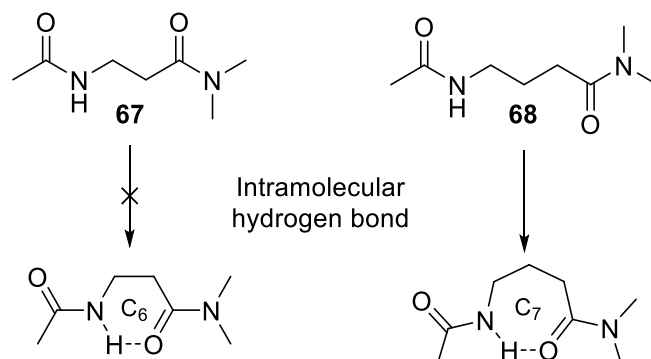
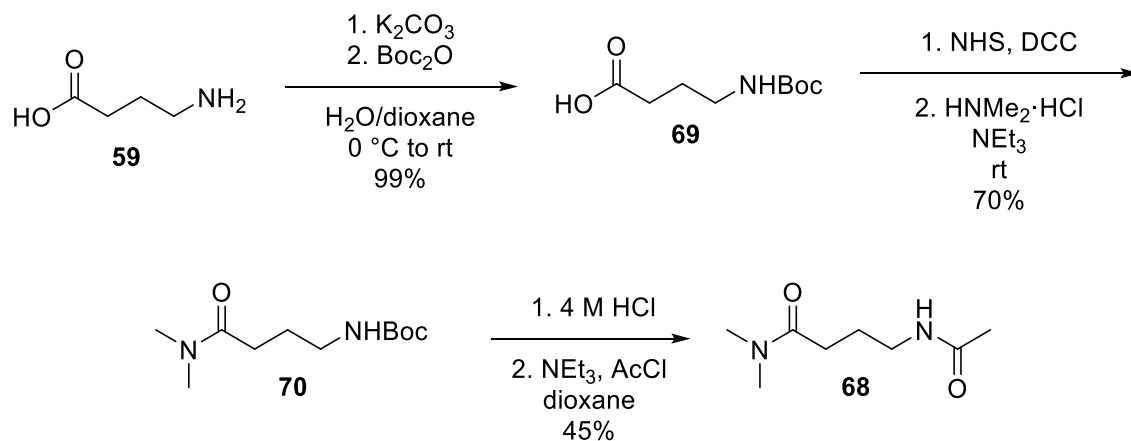


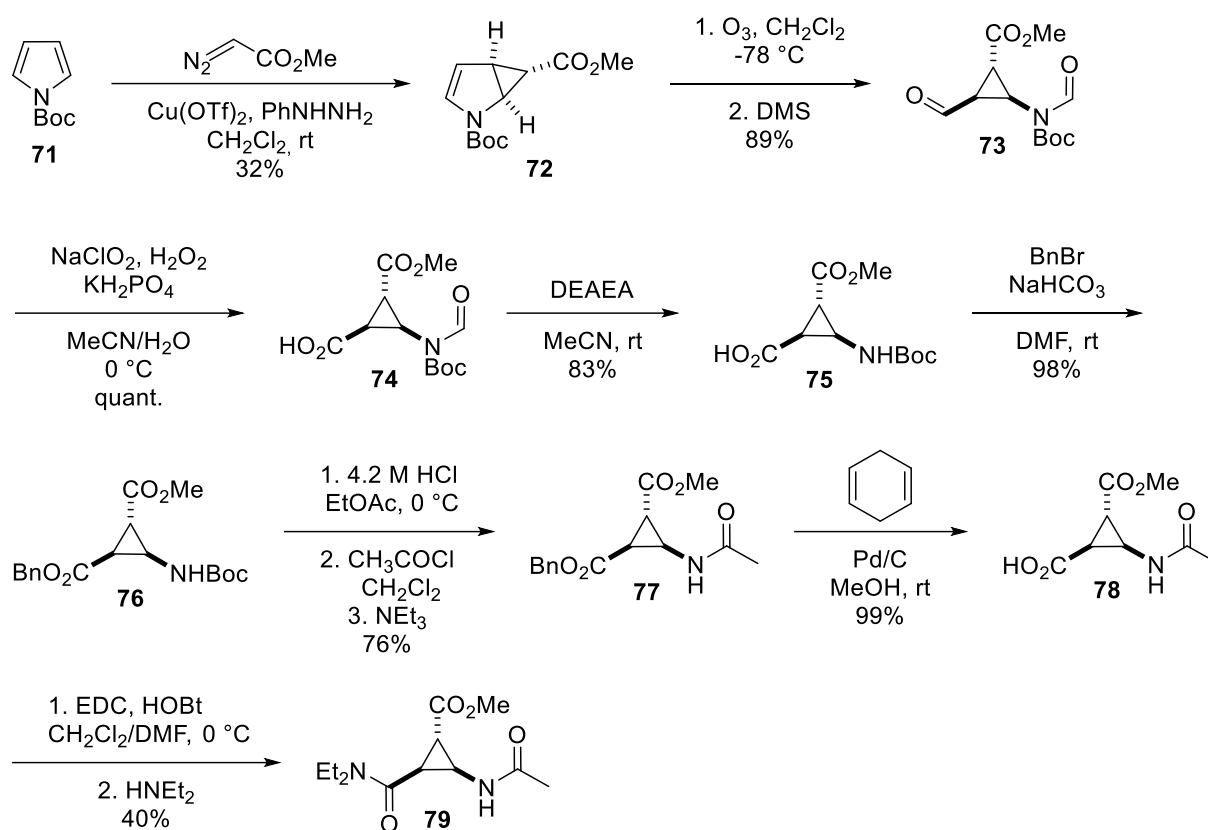
Figure 28. Amide **67** and **68** with a potentially formed intramolecular hydrogen bond.

Based on Gellmans findings^[93], the effect of pressure on intramolecular hydrogen bonds were investigated. During the course of this evaluation, amides **68** and **79** were synthesized according to literature known procedures^[26,93,94] (Scheme 16, Scheme 17).



Scheme 16. Three step synthesis of amide **68**.

Both amides are present in their non-bonded species as well as in their hydrogen bonded species at the same time in solution, making them extremely valuable for this purpose. The special feature of amide **79** is particularly noteworthy. This compound was synthesized by Reiser et al.^[94] for the first time and is structurally closely related to amide **67** but, other than amide **67**, it exists predominantly in its hydrogen bonded form.



Scheme 17. Eight step synthesis of amide **79**.

The ambient pressure IR spectra were recorded on a Thermo Scientific™ Nicolet™ iS™5 FTIR, optics with KBr windows, high performance dTGS-detector, germanium coated KBr-beam splitter and iD1 transmission with KBr cuvette. An amide concentration of 1.0 mM in dichloromethane was chosen for both **68** and **79**, inspired by Gellmans investigation set up. Both spectra are in a good agreement with the ones reported in literature^[93,94] (Figure 29, Figure 30).

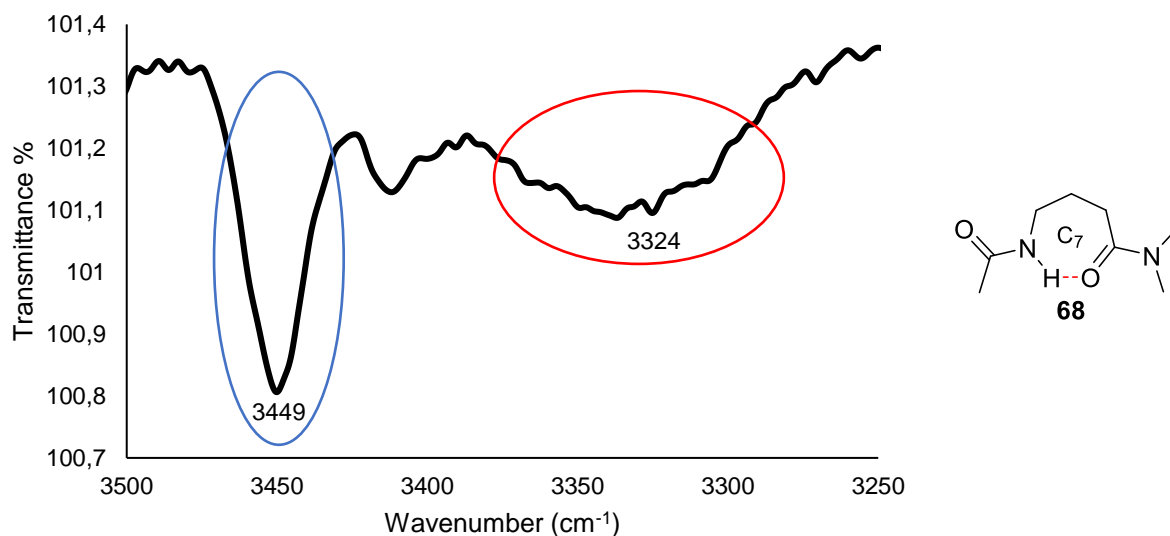


Figure 29. IR amide A region of amide **68**. Blue circled signal: non-bonded NH. Red circled signal: hydrogen bonded NH.

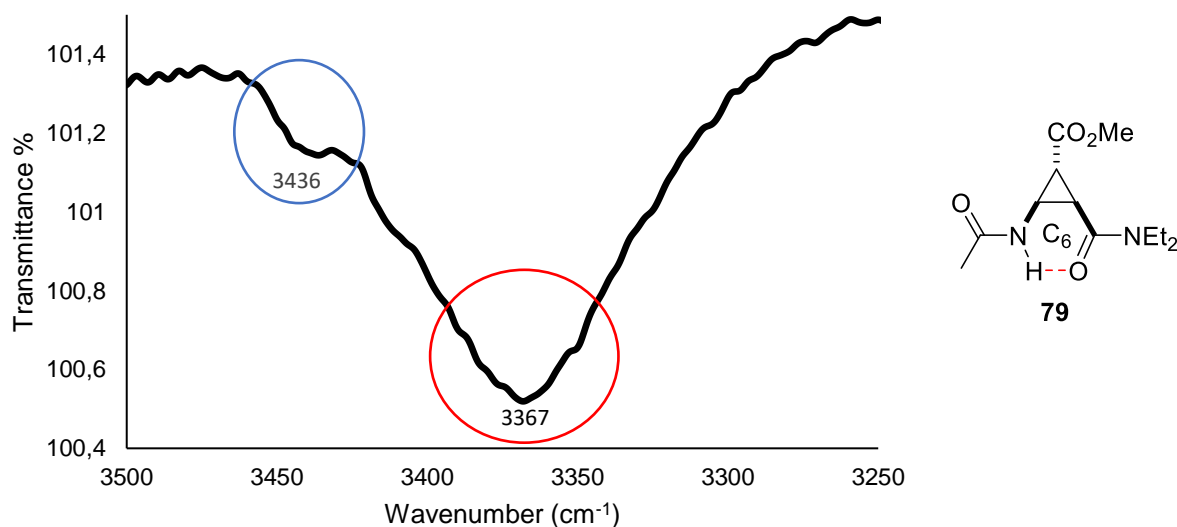


Figure 30. IR amide A region of amide **79**. Blue circled signal: non-bonded NH. Red circled signal: hydrogen bonded NH.

In order to investigate the effect of pressure on the intramolecular hydrogen bond, both samples of **68** and **79** were sent to the TU Dortmund under supervision of a co-worker from Prof. Winters group. Unfortunately, the measurements in organic solvents, especially in dichloromethane or chloroform, were no longer permissible due to the high risk of damaging the diamond window. Organic solvents would simply dissolve the glue, making high pressure measurements in organic solvents currently not possible.

Due to the unambiguous solvent problem, a theoretical discussion as well as a prognosis of the pressure effects will be evaluated in the following. When those amide solutions are put under pressure basically four phenomena could occur:

- The system stays unchanged and the distribution of the bonded and non-bonded species do not alter.
- The strength of the hydrogen bonds already formed at ambient pressure will increase without altering the distribution of the bonded and non-bonded species. The stronger a hydrogen bond the shorter its length is, therefore prolonging and weakening the covalent NH-bond. The weakening of the NH-bond would result in a shift to even lower wavenumbers. This phenomenon is relatively likely to happen since pressure forces molecules into a more compact packing by decreasing the total volume (Figure 31).

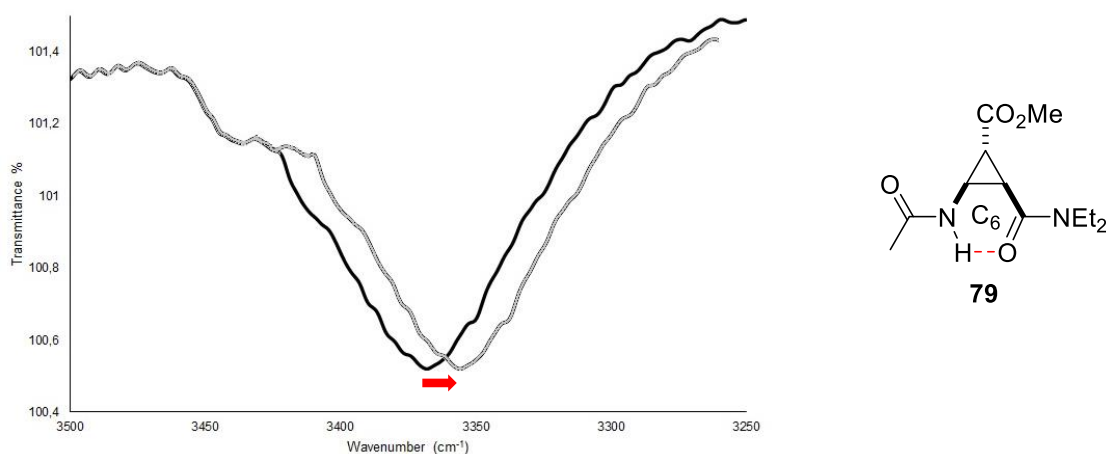


Figure 31. Processed IR spectrum (gray) in the amide A region of amide **79** with a shift of the lower energy band to lower wavenumbers.

- Pressure induces a change in the distribution of bonded and non-bonded species. As the hydrogen bonded species is expected to possess a smaller volume than the open chained form, pressure could shift the equilibrium towards the hydrogen bonded and compact species. This would result in a decrease of the higher energy band signal (non-bonded NH) and simultaneously in an increase of the lower energy band signal (bonded NH) (Figure 32).

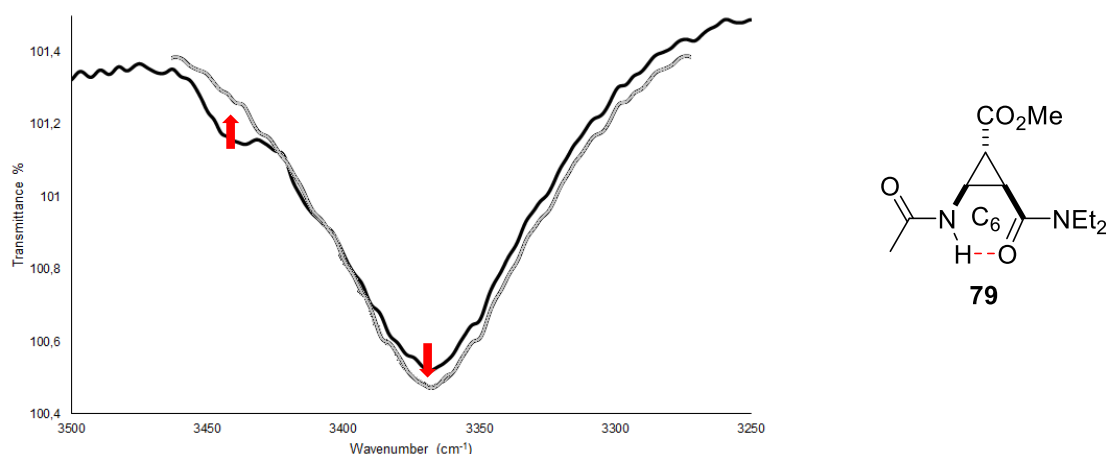


Figure 32. Processed IR spectrum (grey) in the amide A region of amide **79** with decreasing of the higher energy band signal and increasing of the lower energy band signal.

- The fourth phenomenon could be a mixture of enhancing the strength of the hydrogen bond and shifting the equilibrium towards the hydrogen bonded species. Both effects would benefit from pressure and exhibit a more compact assembly than the open chain amides.

As soon as a suitable setup for high pressure IR measurements with the use of organic solvents is available, these investigations remain to be determined to shed light on this interesting field which could provide important information about the behavior of hydrogen bonds under pressure. Scientists working in different disciplines like enzyme catalysis, peptide folding and biochemical processes would benefit from these valuable information.

4 Summary

4.1 Summary in English

In the present PhD thesis, the thiourea-organocatalyzed Michael addition of diethyl malonate to various heteroaromatic nitroolefins has been studied under high-pressure conditions up to 800 MPa, being conducive to enhanced product yields, high reaction rates, and high enantioselectivity. Elucidating the effects of solvents for maximizing reaction rates and yields has been carried out using the Perturbed-Chain Polar Statistical Associating Fluid Theory (PCP-SAFT), allowing a prediction of the kinetic profiles under high-hydrostatic-pressure conditions for the first time. The thermodynamic-based PCP-SAFT solvent and pressure screening were conducted by Prof. Sadowski and coworker (Michael Knierbein) at the Laboratory of Thermodynamics, TU Dortmund University. To demonstrate the synthetic utility of the synthesized Michael adducts as valuable building blocks in organic chemistry, racemic indolyl adduct **58I** was transformed to its corresponding γ -amino acid analogue, a derivative of Baclofen (**60**) which serves as a highly bioactive pharmaceutical.

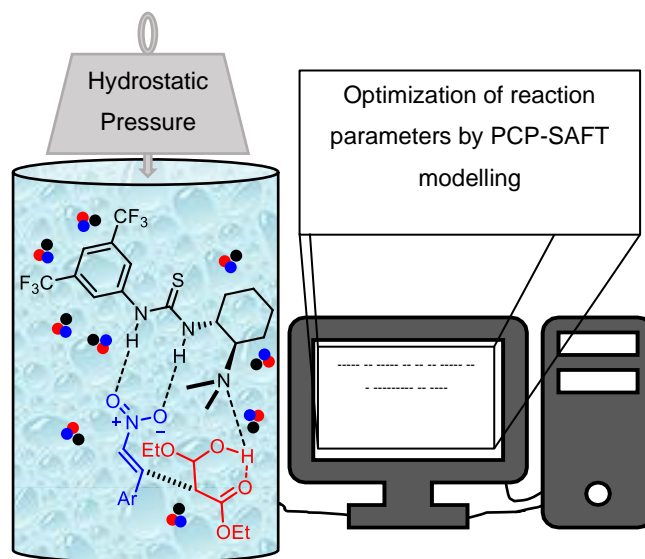


Figure 33. Graphical representation of the Michael addition of diethyl malonate to various heteroaromatic nitroolefins supported by PCP-SAFT predictions.

Based on these studies, high pressure NMR measurements were performed to investigate the influence of pressure on hydrogen bonds, especially on hydrogen-donor-acceptor-complexes similar to the prior described Michael addition conditions. In favor to run this experiment, thiourea derivative **42** served as a hydrogen bond donor and nitroolefin **56a** as a hydrogen bond acceptor. The NMR study was carried out in the institute of biophysics and physical

biochemistry in collaboration with Dr. Markus Beck-Erlach, member of the working group of Prof. Sprangers.

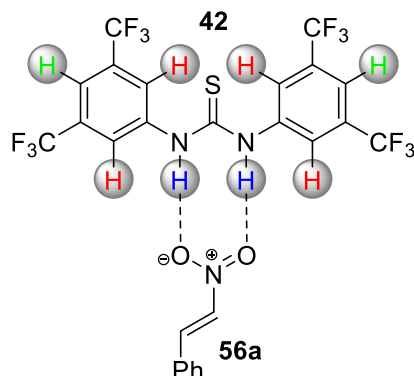


Figure 34. Thiourea **42**, a hydrogen bond donor, and trans- β -nitrostyrene (**56a**), a hydrogen bond acceptor, forming a catalyst-substrate complex.

Furthermore, additional IR measurements were conducted regarding the examination of the effect of pressure on hydrogen bonds with the aim to gain deeper mechanistic insights and understanding. Therefore, the same hydrogen bond-donor-acceptor-complexes were employed with dichloromethane serving as the solvent. Unfortunately, ambient pressure as well as the high pressure measurements did not show the expected interactions of hydrogen bond donor and acceptor with respect to a spectral shift to lower wavenumbers. Since the concept of hydrogen bond acceptor-donor-complexes did not lead to reasonable information, small amide molecules and their intramolecular formed hydrogen bonds were investigated. Ambient pressure measurements and their corresponding results were in good agreement with the ones reported in literature. Unfortunately, high pressure measurements in organic solvents, especially in dichloromethane or chloroform, were no longer permissible due to the high risk of damaging the diamond window and remain to be determined.

4.2 Summary in German

In der vorliegenden Doktorarbeit wurde die Addition von Diethylmalonat an verschiedenen heteroaromatischen Nitroolefinen unter Hochdruckbedingungen (bis zu 800 MPa) untersucht. Die Verwendung von Hochdruck führte zu einer erhöhten Produktausbeute, kürzeren Reaktionszeiten und einer hohen Enantioselektivität. Mit Hilfe der sogenannten Perturbed-Chain Polar Statistical Associating Fluid Theory (PCP-SAFT) konnten zum ersten Mal Vorhersagen in Bezug auf Ausbeute, Reaktionsrate und den dementsprechenden kinetischen Profilen sogar unter Hochdruckbedingungen gemacht werden. Die *in-silico* Vorhersagen zeigten dabei eine besonders gute Übereinstimmung mit den Laborergebnissen. Diese thermodynamischen PCP-SAFT Lösungsmittel- und Druckscreensings wurden von Prof. Sadowski und Mitarbeitern (Michael Knierbein) am Lehrstuhl für Thermodynamik an der TU Dortmund durchgeführt. Um das Konzept der Michael Addition aufzuwerten wurde das Michael Adduct **58I** in dessen entsprechende γ -Aminosäure, ein Baclofenderivat, transformiert.

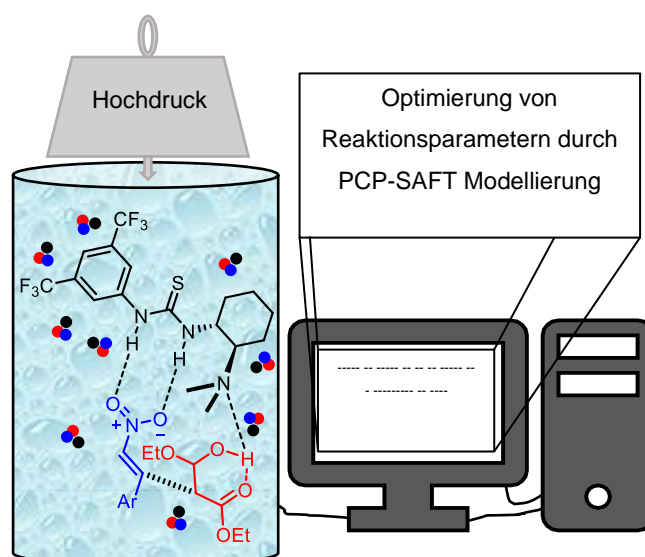


Abbildung 1. Grafische Darstellung der Michael Addition von Diethylmalonat an verschiedene heteroaromatische Nitroolefine mit der PCP-SAFT gestützten Optimierung der Reaktionsparameter.

Angelehnt an dieses Projekt wurden Hochdruck NMR Untersuchungen an Wasserstoffbrücken-Donor-Akzeptor-Komplexen durchgeführt, um Informationen über den Einfluss von Druck auf Wasserstoffbrücken zu erhalten. Bei diesen NMR Untersuchungen wurde darauf geachtet, ein System zu wählen, das dem der Michael Addition ähnlich ist. Im Zuge dessen wurde das Thioharnstoffderivat **42** als Wasserstoffbrücken-Donor und das Nitroolefin **56a** als Wasserstoffbrücken-Akzeptor verwendet. Die NMR Messungen wurden am

Institut für Biophysik und physikalische Biochemie in Zusammenarbeit mit Dr. Markus Beck-Erlach, Mitarbeiter von Prof. Sprangers, durchgeführt.

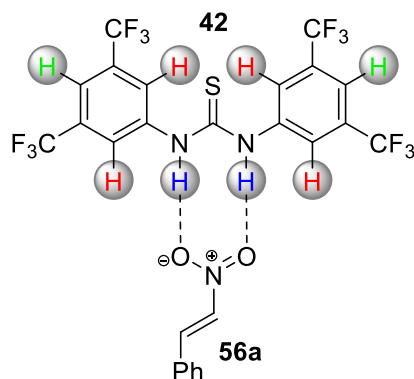


Abbildung 2. Thioharnstoff **42**, ein Wasserstoffbrücken-Donor, und trans-β-nitrostyrol (**56a**), ein Wasserstoffbrücken-Akzeptor. Bildung eines Katalysator-Substrat-Komplex.

Abschließend wurden zusätzlich zu den NMR Messungen IR Messungen durchgeführt, um den Effekt von Druck auf Wasserstoffbrückennetzwerke zu untersuchen. Der Einsatz von Infrarotspektroskopie war notwendig, um die uneindeutigen Ergebnisse der Kernspinresonanz zu ergänzen. Dazu wurden dieselben Wasserstoffbrücken-Donor-Akzeptor-Komplexe verwendet, jedoch kam Dichlormethan als Lösungsmittel zum Einsatz. Unglücklicherweise sah man die zu erwartenden Effekte von H-Brücken-Donor und Akzeptor sowohl unter Normaldruck als auch unter Hochdruck nicht und somit auch nicht die damit verbundenen Spektralverschiebung zu geringeren Wellenzahlen. Da das Konzept der H-Brücken-Komplexe nicht die erwünschten Ergebnisse lieferte wurden kleine Amide und deren intramolekulare Wasserstoffbrücken untersucht. Die Ergebnisse der Normaldruckmessungen zeigten dabei eine hohe Übereinstimmung mit den Ergebnissen der Literatur. Unglücklicherweise konnten die Hochdruckmessungen in organischen Lösungsmitteln, besonders in Dichlormethan und Chloroform, nicht durchgeführt werden, da das Risiko das Diamantfenster zu beschädigen zu hoch war. Sobald eine geeignete Alternative gefunden wird sollten diese Untersuchungen nachgeholt werden.

5 Experimental Part

5.1 General Information

Commercially available chemicals were purchased in high quality and were used without further purification. Reactions with moisture or oxygen sensitive reagents were carried out in flame dried glassware under an atmosphere of predried nitrogen. Anhydrous solvents were prepared by established laboratory procedures. CH_2Cl_2 , EtOAc and hexanes (40–60 °C) for chromatography were distilled prior to use.

Thin Layer Chromatography

Thin layer chromatography was performed with TLC precoated aluminum sheets (Merck) Silica gel 60 F254, 0.2 mm layer thickness. Visualization was done with UV light ($\lambda = 254 \text{ nm}$) and staining with vanillin (6.0 g vanillin, 100 mL ethanol (95%), 1 mL conc. sulfuric acid), ninhydrin (300 mg ninhydrin, 3 mL conc. acetic acid, 100 mL ethanol) or potassium permanganate (1.0 g KMnO_4 , 2.0 g Na_2CO_3 , 100 mL H_2O) followed by heating.

Column Chromatography

Column chromatography was performed with silica gel (Merck, 0.063–0.200 mm particle size) and flash silica gel 60 (Merck, 0.040–0.063 mm particle size).

NMR Spectroscopy

^1H -NMR spectra were recorded on FT-NMR-spectrometer of the type Bruker Avance 300 (300 MHz for ^1H , 75 MHz for ^{13}C) or BRUKER Avance III 400 “Nanobay” (400 MHz for ^1H , 101 MHz for ^{13}C). Chemical shifts for ^1H -NMR were reported as δ , parts per million (ppm), relative to the signal of CHCl_3 at 7.26 ppm, H_2O at 4.79 ppm, D_3COD pentet at 3.31 ppm and relative to the center line signal of the DMSO-d_6 quintet at 2.50 ppm. Spectra were evaluated in 1st order and coupling constants J were reported in Hertz (Hz). The following notations indicate the multiplicity of the signals: s = singlet, bs = broad singlet, d = doublet, t = triplet, q = quartet and m = multiplet, and combinations thereof. Chemical shifts for ^{13}C -NMR were reported as δ , parts per million (ppm), relative to the center line signal of the CDCl_3 triplet at 77.2 ppm, DMSO-d_6 septet at 39.5 ppm and D_3COD septet at 49.0 ppm. NMR-yields were determined using diphenoxymethane as internal standard.

IR Spectroscopy

FTIR spectroscopy was carried out on a Cary 630 FTIR Spectrometer. Solid and liquid compounds were measured neatly and the wave numbers are reported as cm^{-1} .

Mass Spectrometry

Mass spectra were recorded by the Central Analytical Laboratory (University of Regensburg) using Jeol AccuTOF GCX and Agilent Q-TOF 6540 UHD. High-resolution mass spectra were measured using atmospheric pressure chemical ionization (APCI), electron ionization (EI), electrospray ionization (ESI) with a quadrupole time-of-flight (Q-TOF) detector.

Optical Rotation

Determination of optical rotation was carried out on a MCP 500 Modular Circular Polarimeter by Anton Paar using 589 nm (Na-D-line) as measurement wavelength.

Chiral-HPLC

Enantiomeric excess was determined by chiral HPLC using Varian 920-LC with a photodiode array (PDA). For each compound a specified chiral stationary phase was used (Phenomenex Lux Cellulose-1/Phenomenex Lux Cellulose-2, 4.6 x 250 mm, particle size 5 μm).

High Pressure Reactions

High pressure reactions up to 440 MPa were performed using a self-custom-built hydraulic high pressure apparatus from Unipress (Warsaw) using melted PTFE tubes as reaction vessels. A 1:1 (v/v) mixture of decahydronaphthalene (mixture of cis and trans) and 2,2,4-trimethylpentane was used as a pressurizing medium.

Melting Points

Melting points were measured on an SRS MPA 100 OptiMelt instrument. Values thus obtained were not corrected.

5.2 Experimental Procedures and Analytical Data

All Substrates were prepared following the reported procedures and their analytical data were consistent with those published in the literature.

5.2.1 High Pressure Technique

The pressure vessel is a piston-cylinder reactor made of solid steel (Figure 35) including the reaction mixture encapsulated in sealed reaction vessels. The pressure vessel is then filled with a pressurizing medium. In this case, the reaction vessels are made from PTFE (Figure 36). As PTFE is thermoplastic, tubes can be processed through thermal impact providing cheap reaction vessels. A certain set of know-how and practice is required for proper sealing to prevent leaking. Alternatively, screw cap vials consisting of thicker double-walled PTFE material can be used instead. These vials are indeed reusable, but they have a fixed reaction volume which cannot be adapted. In the figure below a step-by-step guidance for the thermal processing of PTFE tubes is given.

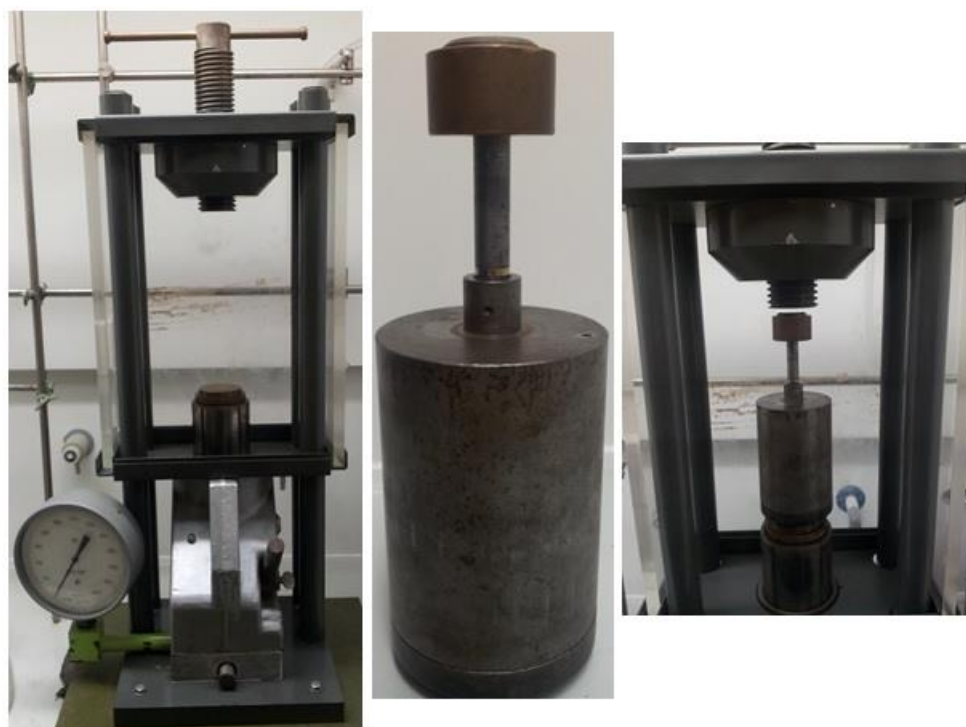


Figure 35. A self-custom-built hydraulic high pressure apparatus from Unipress (Warsaw), middle: pressure vessel (cylinder) with the piston on top, right: pressure vessel inserted in the high pressure apparatus.

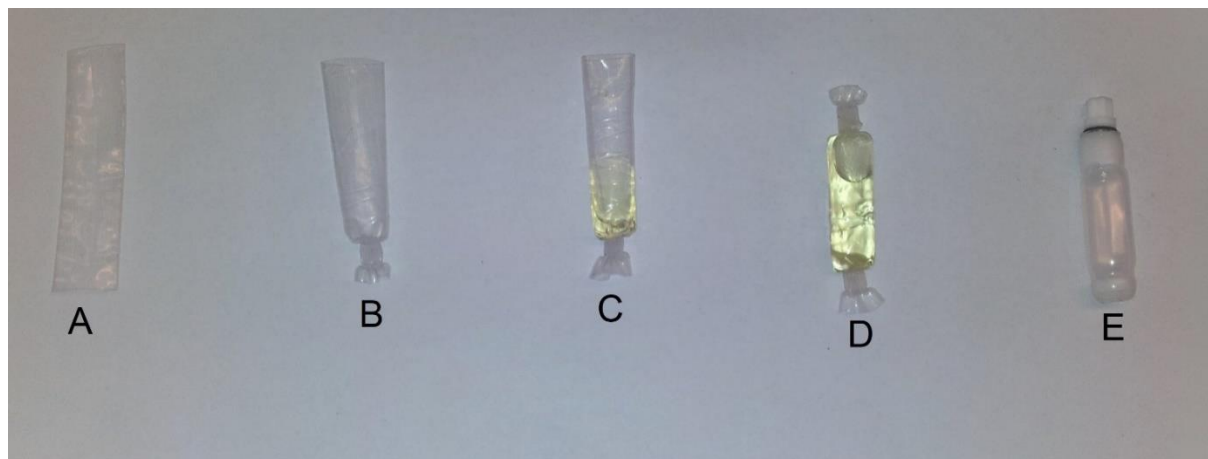
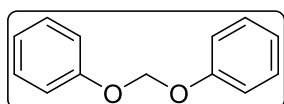


Figure 36. **A:** Little piece of the bulk stock PTFE tubes. **B:** One-sided thermally sealed PTFE tube. **C:** One-sided sealed tube filled with reaction mixture. **D:** Completely sealed tube containing the reaction mixture with a little residual air left. **E:** Self-made custom screw cap vial consisting of a double-walled PTFE tube sealed by two plugs.

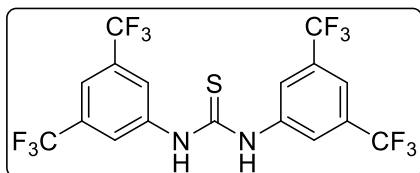
Diphenoxymethane (**S1**)^[95]



A 500 mL round bottom flask equipped with a magnetic stirring bar was charged with KOH (33.0 g, 590 mmol, 8.0 equiv) and H₂O (100 mL) under cooling with an ice bath. After complete dissolving phenol (7.00 g, 74.4 mmol, 1.0 equiv) was added, then CH₂Cl₂ (70 mL, 93.0 g, 1.1 mol, 15.0 equiv) and TBAB (2.88 g, 8.90 mmol, 0.1 equiv). After the reaction mixture was stirred for 30 h at 50 °C the crude mixture was transferred to a separatory funnel, the organic layer was washed with sat. NaHCO₃ (5 × 100 mL) and brine (5 × 100 mL), dried over anhydrous MgSO₄, filtered and the solvent was removed under reduced pressure to give **S1** (6.00 g, 37.2 mmol, 81%) as a colorless oil.

¹H-NMR (300 MHz, CDCl₃): δ 7.35 – 7.30 (m, 4H), 7.17 – 7.11 (m, 4H), 7.08 – 7.02 (m, 2H), 5.75 (s, 2H). ¹³C-NMR (75 MHz, CDCl₃): δ 157.1, 129.69, 122.57, 116.61, 91.29.

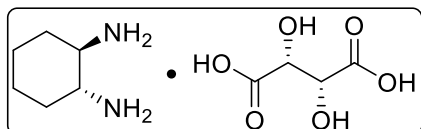
1,3-bis(3,5-bis(trifluoromethyl)phenyl)thiourea (**42**)^[96]



A 25 mL round bottom flask equipped with a magnetic stirring bar and a reflux condenser was charged with 3,5-bis(trifluoromethyl)aniline (619 mg, 2.70 mmol, 1.0 equiv) in anhydrous THF (5 mL). 1-Isothiocyanato-3,5-bis(trifluoromethyl)benzene (732 mg, 2.70 mmol, 1.0 equiv) in anhydrous THF (5 mL) was added dropwise and the resulting mixture was heated to 50 °C for 115 h. The crude product was purified by recrystallization from CHCl₃ to give **42** (1.35 g, 2.70 mmol, 99%) as a colorless solid.

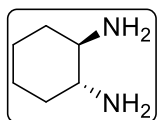
¹H-NMR (300 MHz, CD₃CN): δ 8.79 (bs, 2H), 8.10 (s, 4H), 7.83 (s, 2H).

(1*R*,2*R*)-(+)-1,2-Diaminocyclohexane *L*-tartrate (S2**)^[97]**



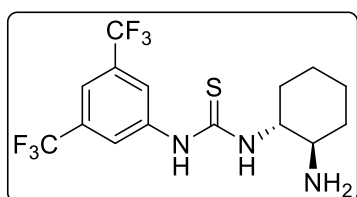
A 100 mL Erlenmeyer assembled with a stirring bar and a thermometer was charged with H₂O (25 mL). *L*-(+)-Tartaric acid (7.5 g, 50.0 mmol, 0.5 equiv) was added with stirring in one portion. The solution was stirred as racemic *trans*-1,2-diaminocyclohexane (11.4 g, 12 mL, 100 mmol, 1.0 equiv) was added carefully in one portion. A slurry was formed initially but complete dissolution was observed once addition was complete. Glacial acetic acid (5 mL) was then added in one portion. The product began to precipitate during the addition and continued to precipitate while the reaction mixture was allowed to cool to 5 °C, with stirring, overnight. The product was isolated by filtration, the filter cake was washed with cold H₂O followed by MeOH (4 × 15 mL) at room temperature. The product was dried under reduced pressure to give **S2** (8.5 g, 32.0 mmol, 32%) as a white powder. **S2** obtained exhibits enantiomeric pure. The product was used without further purification in the next step.

(1*R*,2*R*)-Cyclohexane-1,2-diamine (S3**)^[97]**



A 100 mL round bottom flask equipped with a magnetic stirring bar was charged with a suspension of **S2** (2.00 g, 7.57 mmol, 1.0 equiv) and CH₂Cl₂ (40 mL). While this mixture was stirred vigorously NaOH (728 mg, 18.2 mmol, 2.4 equiv) in a mixture of H₂O (5 mL) and brine (5 mL) was added dropwise. After stirring for 30 min at room temperature the mixture was transferred to a separating funnel and the organic layer was separated. The aqueous layer was extracted with CH₂Cl₂ (4 × 20 mL). The combined organic layers were dried over anhydrous MgSO₄, filtered and concentrated to give crude **S3**. The crude product was sublimated to give **S3** (640 mg, 5.60 mmol, 74%) as a colorless solid
¹H-NMR (300 MHz, CDCl₃) δ 2.30 – 2.16 (m, 2H), 1.88 – 1.76 (m, 2H), 1.73 – 1.59 (m, 2H), 1.45 (s, 4H), 1.34 – 1.01 (m, 4H). **¹³C-NMR** (75 MHz, CDCl₃) δ 57.81, 35.64, 25.58.

1-((1*R*,2*R*)-2-Aminocyclohexyl)-3-(3,5-bis(trifluoromethyl)phenyl)thiourea (46**)^[98]**

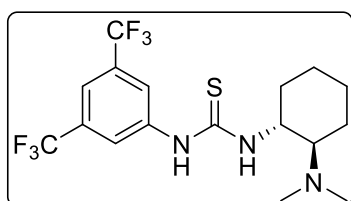


A flame dried 50 mL Schlenk flask equipped with a magnetic stirring bar was charged with **S3** (327 mg, 2.87 mmol, 1.0 equiv) in anhydrous THF (10 mL) and stirred under N₂ atmosphere while cooling with an ice bath. 1-Isothiocyanato-3,5-bis(trifluoromethyl)benzene (777 mg, 2.87 mmol, 1.0 equiv) in anhydrous THF (10 mL) was

added dropwise to the stirred solution over 30 min. After the reaction mixture reached room temperature it was stirred for another 15 h. The solvent was removed under reduced pressure and the resulting residue was purified on silica ($\text{CH}_2\text{Cl}_2/\text{MeOH}/\text{NEt}_3$ 40:1:0.1) to give **46** (902 mg, 2.34 mmol, 82%) as a colorless solid. Spectral data are in agreement with those reported in literature.^[99]

¹H-NMR (300 MHz, CDCl_3): δ 8.03 (s, 2H), 7.58 (s, 1H), 6.27 (bs, 1H), 3.39 (bs, 1H), 2.79 – 2.63 (m, 1H), 2.13 – 1.87 (m, 2H), 1.87 – 1.66 (m, 2H), 1.41 – 1.13 (m, 4H).

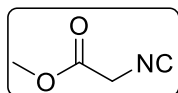
1-(3,5-bis(Trifluoromethyl)phenyl)-3-((1*R*,2*R*)-2-(dimethylamino)cyclohexyl)thiourea (57)^[100]



A 25 mL round bottom flask equipped with a magnetic stirring bar was charged with **46** (500 mg, 1.30 mmol, 1.0 equiv) in 1,4-dioxane (3 mL). To this mixture Zn powder (339 mg, 5.19 mmol, 4.0 equiv), AcOH (623 mg, 10.4 mmol, 8.0 equiv) and aq. formaldehyde (37%, 117 mg, 3.89 mmol, 3.0 equiv) were added and the resulting reaction mixture was stirred for 72 h at room temperature. After the stirring aq. NH_3 solution (32%, 3 mL) was added. The mixture was transferred to a separatory funnel, the aqueous phase was extracted with CH_2Cl_2 (3 \times 10 mL), the organic layers were combined, dried over anhydrous MgSO_4 , filtered and the solvent was removed under reduced pressure. The residue was purified on silica ($\text{EtOAc}/\text{NEt}_3$ 100:1) to give **57** (227 mg, 548 μmol , 42%) as a colorless solid. Spectral data are in agreement with those reported in literature.^[101]

¹H-NMR (300 MHz, CDCl_3): δ 7.84 (s, 2H), 7.62 (s, 1H), 2.52 – 2.41 (m, 1H), 2.34 (bs, 6H), 1.97 – 1.68 (m, 3H), 1.37 – 1.10 (m, 4H).

Methyl 2-isocyanoacetate (66)^[102]

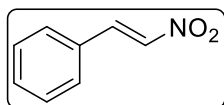


A 100 mL round bottom was charged with 2-isocyanoacetic acid (851 mg, 10.0 mmol, 1.0 equiv) in methanol (40 mL) and Amberlyst 15 (1.6 g). The resulting mixture was stirred at room temperature for 7 h, Amberlyst 15 was filtered, washed with Et_2O and the solvent was removed under reduced pressure to give **66** (624 mg, 6.29 mmol, 63%) as a colorless oil.

¹H-NMR (300 MHz, CDCl_3) δ 3.82 (s, 3H), 3.47 (s, 2H). **¹³C-NMR** (75 MHz, CDCl_3) δ 163.50, 113.08, 53.71, 24.62.

5.2.2 Nitroolefin Synthesis

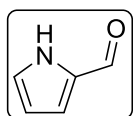
(*E*)-(2-Nitrovinyl)benzene (**56a**)^[103]



A 250 mL Erlenmeyer flask equipped with a magnetic stirring bar, a thermometer and a dropping funnel was charged with benzaldehyde (10.2 mL, 10.6 g, 100 mmol, 1.0 equiv), nitromethane (5.4 mL, 6.16 g, 101 mmol, 1.0 equiv) and EtOH (20 mL). The mixture was cooled to 0 °C in an ice bath and a 2 M NaOH (55 mL, 4.40 g, 110 mmol, 1.1 equiv) was added dropwise, keeping the temperature below 5 °C. After complete addition, the mixture was stirred for further 30 min at the same temperature, then diluted with H₂O (50 mL). The reaction mixture was poured into a mixture of ice (50 g) and conc. HCl (16 mL, 37wt%, 1.9 equiv) and the resulting yellow precipitate was filtered and washed with cold H₂O (2 × 10 mL). The crude product was recrystallized from EtOH to give **56a** (10.6 g, 68.8 mmol, 69%) as yellow needles.

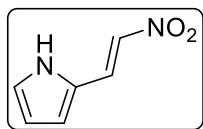
¹H-NMR (400 MHz, CDCl₃) δ 8.02 (d, *J* = 13.8 Hz, 1H), 7.59 (d, *J* = 13.6 Hz, 1H), 7.57 – 7.42 (m, 5H). ¹³C-NMR (75 MHz, CDCl₃) δ 139.18, 137.19, 132.26, 130.14, 129.50, 129.25.

1*H*-Pyrrole-2-carbaldehyde (**S4**)^[104]



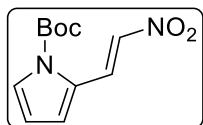
A 100 mL round bottom flask was charged with DMF (2.5 mL, 2.40 g, 32.8 mmol, 1.1 equiv), POCl₃ (2.9 mL, 4.94 g, 32.2 mmol, 1.1 equiv) was added dropwise and the reaction was stirred for 15 min at room temperature. DCE (10 mL) was added and the mixture cooled to 0 °C. A solution of pyrrole (2.1 mL, 2.00 g, 29.8 mmol, 1.0 equiv) in DCE (10 mL) was added dropwise and the reaction was heated to 85 °C for 15 min before cooling to room temperature. A solution of NaOAc (22.0 g, 268 mmol, 9.0 equiv) in H₂O (30 mL) was added and the biphasic mixture stirred at 100 °C for 15 min. The reaction was cooled to room temperature and the phases separated. The aqueous phase was extracted with Et₂O (3 × 30 mL). The combined organic layers were washed with NaHCO₃ (80 mL), dried over MgSO₄ and concentrated under reduced pressure to give **S4** (2.15 g, 22.6 mmol, 76%) as a colorless solid.

¹H-NMR (400 MHz, CDCl₃) δ 10.04 – 9.56 (m, 1H), 9.53 (s, 1H), 7.18 – 7.11 (m, 1H), 7.03 – 6.96 (m, 1H), 6.40 – 6.32 (m, 1H). ¹³C-NMR (101 MHz, CDCl₃) δ 179.43, 133.06, 126.41, 121.38, 111.50.

(E)-2-(2-Nitrovinyl)-1H-pyrrole (S5)^[105]

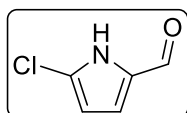
A flame dried 100 mL Schlenk flask was charged with **S4** (1.08 g, 11.3 mmol, 1.0 equiv) dissolved in anhydrous methanol (30 mL) and treated with nitromethane (1.2 mL, 1.31 g, 21.5 mmol, 1.9 equiv), NaOAc (928 mg, 11.3 mmol, 1.0 equiv), and methylamine hydrochloride (764 mg, 11.30 mmol, 1.0 equiv). Stirring at room temperature for 12 h afforded a yellow/brown mixture. The solvent was removed *in vacuo* without heating to give a brown oil. The oil was dissolved in EtOAc and passed through a pad of silica. The latter was washed with EtOAc until the washings were colorless. Evaporation of the solvent under reduced pressure without heating gave **S5** (900 mg, 6.52 mmol, 58%) as brown solid.

¹H-NMR (300 MHz, CDCl₃) δ 8.78 (bs, 1H), 7.95 (d, *J* = 13.4 Hz, 1H), 7.40 (d, *J* = 13.4 Hz, 1H), 7.14 – 7.08 (m, 1H), 6.83 – 6.78 (m, 1H), 6.43 – 6.36 (m, 1H). ¹³C-NMR (75 MHz, CDCl₃) δ 130.95, 129.76, 126.38, 124.01, 119.32, 112.78.

tert-Butyl (E)-2-(2-nitrovinyl)-1H-pyrrole-1-carboxylate (56b)^[106]

A 50 mL round bottom flask, equipped with a magnetic stirring bar, was charged with **S5** (400 mg, 2.90 mmol, 1.0 equiv) and was dissolved in THF (15 mL). Di-*tert*-butyl dicarbonate (758 mg, 3.48 mmol, 1.2 equiv) and NEt₃ (352 mg, 3.48 mmol, 1.2 equiv) were added subsequently. The reaction mixture was stirred for 16 h at room temperature, the solvent was removed under reduced pressure and the crude product was purified on silica (hexanes/EtOAc 6:1) to give **56b** (538 mg, 2.26 mmol, 78%) as a yellow solid.

¹H-NMR (300 MHz, CDCl₃) δ 8.76 (d, *J* = 13.5 Hz, 1H), 7.54 (dd, *J* = 3.2, 1.6 Hz, 1H), 7.48 (d, *J* = 13.5 Hz, 1H), 6.87 – 6.79 (m, 1H), 6.34 – 6.26 (m, 1H), 1.65 (s, 9H). ¹³C-NMR (101 MHz, CDCl₃) δ 148.59, 135.12, 129.99, 127.64, 126.25, 118.05, 112.32, 86.06, 28.09.

5-Chloro-1H-pyrrole-2-carbaldehyde (S6)^[107]

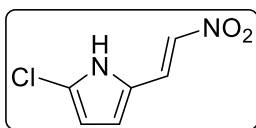
A flame dried 500 mL Schlenk flask was charged with pyrrole (2.00 g, 29.8 mmol, 1.0 equiv) in THF (130 mL) under N₂ atmosphere and was cooled to -78 °C. To the stirred pyrrole solution, a solution of NCS (3.98 g, 29.8 mmol, 1.0 equiv) in THF (130 mL) was added dropwise over 15 min. The resulting mixture was stirred for 30 min at -78 °C and placed in the freezer for 16 h. The solution was brought to 0 °C and was stirred for 6 h at this temperature. The acylation agent was added dropwise over 10 min and the resulting solution was stirred for 16 h at room temperature. An aq. solution of NaOAc

(8.56 g, 104.3 mmol, 3.5 equiv, 260 mL H₂O) was added and the mixture was heated to reflux for 30 min. The crude mixture was extracted with DEE (3 × 150 mL), washed with sat. NaHCO₃ (2 × 250 mL) and H₂O (2 × 400 mL). The organic layer was dried over MgSO₄, filtered and the solvent was removed under reduced pressure. The residue was purified on silica (CH₂Cl₂/EtOAc 9:1) to give **S6** (1.12 g, 8.65 mmol, 29%) as a colorless solid.

Acylating agent: A 100 mL round bottom flask was charged with POCl₃ (5.03 g, 32.8 mmol, 1.1 equiv) and cooled to 0 °C. DMF (2.40 g, 32.8 mmol, 1.1 equiv) was added dropwise and the resulting mixture was stirred at 0 °C until the corresponding salt was formed. The Vilsmeier reagent was dissolved in CH₂Cl₂ (70 mL) prior to addition.

¹H-NMR (400 MHz, CDCl₃) δ 10.97 (bs, 1H), 9.38 (s, 1H), 6.95 (dd, *J* = 3.9, 2.7 Hz, 1H), 6.22 (dd, *J* = 4.0, 2.4 Hz, 1H). ¹³C-NMR (101 MHz, CDCl₃) δ 178.43, 131.91, 126.24, 122.72, 110.16.

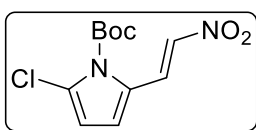
(*E*)-2-Chloro-5-(2-nitrovinyl)-1*H*-pyrrole (**S7**)



A 100 mL round bottom flask was charged with **S6** (500 mg, 3.86 mmol, 1.0 equiv) in anhydrous MeOH (10 mL). To this solution nitromethane (448 mg, 7.33 mmol, 1.9 equiv), NaOAc (317 mg, 3.86 mmol, 1.0 equiv) and methylamine hydrochloride (261 mg, 3.86 mmol, 1.0 equiv) was added and the resulting mixture was stirred at room temperature for 16 h. The solvent was removed under reduced pressure without heating, dissolved in EtOAc, passed through a pad of silica and washed with EtOAc until the washings were colorless. The solvent was removed under reduced pressure without heating to give **S7** (462 mg, 2.68 mmol, 69%) as a yellow solid.

¹H-NMR (400 MHz, CDCl₃) δ 9.24 (bs, 1H), 7.86 (d, *J* = 13.4 Hz, 1H), 7.45 (d, *J* = 13.4 Hz, 1H), 6.73 (dd, *J* = 4.0, 2.8 Hz, 1H), 6.23 (dd, *J* = 4.0, 2.3 Hz, 1H). ¹³C-NMR (101 MHz, CDCl₃) δ 131.11, 128.82, 124.05, 123.39, 120.72, 111.16. IR (neat): 3220, 1618, 1543, 1476, 1297, 1252, 1141, 1040, 980, 951, 813, 757 cm⁻¹. HRMS (EI) *m/z* calculated for C₆H₅N₂O₂Cl ([M]⁺) 172.00341, found 172.00357. Mp: 97 °C.

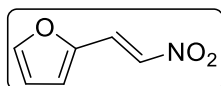
tert-Butyl (*E*)-2-chloro-5-(2-nitrovinyl)-1*H*-pyrrole-1-carboxylate (**56c**)



A round bottom flask was charged with **S7** (400 mg, 2.32 mmol, 1.0 equiv) in anhydrous THF (10 mL), di-*tert*-butyl dicarbonate (607 mg, 2.78 mmol, 1.2 equiv), NEt₃ (282 mg, 2.78 mmol, 1.2 equiv) and DMAP (28 mg, 0.23 mmol, 0.1 equiv). The resulting mixture was stirred at rt for 3 h. The solvent was removed under reduced pressure without heating and the crude product was purified on silica (hexanes/EtOAc 6:1) to give **56c** (348 mg, 1.28 mmol, 55%) as a yellow solid.

¹H-NMR (400 MHz, CDCl₃) δ 8.39 (d, *J* = 13.5 Hz, 1H), 7.41 (d, *J* = 13.4 Hz, 1H), 6.74 (dd, *J* = 4.0, 0.8 Hz, 1H), 6.27 (dd, *J* = 4.0, 0.5 Hz, 1H), 1.66 (s, 9H). **¹³C-NMR** (101 MHz, CDCl₃) δ 147.42, 134.68, 129.42, 126.34, 124.21, 116.11, 113.39, 87.56, 28.01. **IR** (neat): 3116, 2982, 2937, 1744, 1614, 1547, 1502, 1446, 1297, 1252, 1156, 1103, 1028, 962, 828, 787, 712 cm⁻¹. **HRMS** (ESI) *m/z* calculated for C₁₁H₁₄N₂O₄Cl ([M+H]⁺) 273.0637, found 273.0634. **Mp**: 105 °C.

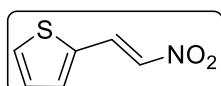
(*E*)-2-(2-Nitrovinyl)furan (56d)^[108]



A 500 mL round bottom flask equipped with a magnetic stirring bar was charged with nitromethane (7.98 g, 7.0 mL, 130 mmol, 2.5 equiv), 2-furfural (5.00 g, 52.0 mmol, 1.0 equiv) and methanol (10 mL) and the reaction mixture was cooled to 0 °C. Aqueous 1 M NaOH (5.21 g, 130 mL, 130 mmol, 2.5 equiv) was added *via* an addition funnel over 5 min then an ice/H₂O mixture (25 mL) was added and the mixture was stirred at 0 °C for 15 min. The mixture was then slowly added to aqueous 8 M HCl (50 mL) and allowed to stir for 24 h at room temperature. The mixture was extracted with CH₂Cl₂ (3 × 150 mL) and the combined organic layers were washed with brine (150 mL), dried over anhydrous MgSO₄, filtered and concentrated to give a brown residue. The product was purified on silica (hexanes/EtOAc 6:1) to give **56d** (5.85 g, 42.1 mmol, 81%) as a yellow solid.

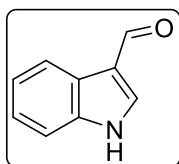
¹H-NMR (300 MHz, CDCl₃) δ 7.77 (d, *J* = 13.2 Hz, 1H), 7.63 – 7.57 (m, 1H), 7.52 (d, *J* = 13.2 Hz, 1H), 6.89 (d, *J* = 3.6 Hz, 1H), 6.57 (dd, *J* = 3.6, 1.8 Hz, 1H). **¹³C-NMR** (75 MHz, CDCl₃) δ 146.96, 146.74, 135.00, 125.56, 120.15, 113.47.

(*E*)-2-(2-Nitrovinyl)thiophene (56e)^[108]



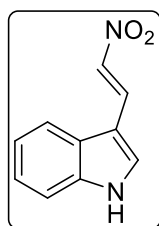
A 500 mL round bottom flask equipped with a magnetic stirring bar was charged with nitromethane (7.98 g, 7.00 mL, 130 mmol, 2.5 equiv), thiophen carbaldehyde (5.84 g, 52.0 mmol, 1.0 equiv) and methanol (10 mL) and the reaction mixture was cooled to 0 °C. Aqueous 1 M NaOH (130 mL, 130 mmol, 2.5 equiv) was added *via* an addition funnel over 5 min then an ice/H₂O mixture (25 mL) was added and the mixture was stirred at 0 °C for 15 min. The mixture was then slowly added to aqueous 8 M HCl (50 mL) and allowed to stir for 24 h. The mixture was extracted with CH₂Cl₂ (3 × 150 mL) and the combined organic layers were washed with brine (150 mL), dried over anhydrous MgSO₄, filtered and concentrated to give a brown residue. The product was purified on silica (hexanes/EtOAc 6:1) to give **56e** (7.12 g, 45.9 mmol, 88%) as a yellow solid.

¹H-NMR (300 MHz, CDCl₃) δ 8.14 (d, *J* = 13.4 Hz, 1H), 7.59 – 7.53 (m, 1H), 7.52 – 7.42 (m, 2H), 7.14 (dd, *J* = 5.1, 3.7 Hz, 1H). **¹³C-NMR** (75 MHz, CDCl₃) δ 135.39, 134.78, 133.82, 132.21, 131.76, 128.98.

1*H*-Indole-3-carbaldehyde (S8)^[109]

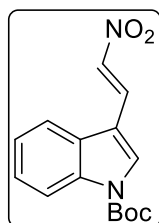
A 250 mL round bottom flask, equipped with a magnetic stirring bar, was charged with POCl₃ (38 mL, 62.8 g, 409 mmol, 6.0 equiv) and DMF (80 mL) and was cooled to 0 °C. To this stirred solution indole (8.00 g, 68.3 mmol, 1.0 equiv) in DMF (80 mL) was added. After stirring for 2 h at 0 °C the mixture was poured into 600 mL ice water. Then NaOH was added to adjust the pH to 9.0. The resulting mixture was filtered and washed with EtOAc. The filtrate was extracted with EtOAc (3 × 100 mL). The organic layers were dried over Na₂SO₄ and the solvent was removed under reduced pressure to give **S8** (8.96 g, 61.72 mmol, 90%) as a pale yellow solid.

¹H-NMR (400 MHz, DMSO) δ 12.13 (s, 1H), 9.94 (s, 1H), 8.28 (s, 1H), 8.17 – 8.02 (m, 1H), 7.60 – 7.44 (m, 1H), 7.35 – 7.11 (m, 2H). ¹³C-NMR (101 MHz, DMSO) δ 185.27, 138.64, 137.18, 124.22, 123.66, 122.33, 120.96, 118.30, 112.58.

(*E*)-3-(2-Nitrovinyl)-1*H*-indole (56m)^[110]

A 50 mL round bottom flask, equipped with a stir bar, was charged with **S8** (2.76 g, 19.0 mmol, 1.0 equiv), NH₄OAc (1.47 g, 19.0 mmol, 1.0 equiv) and AcOH (14.3 mL). Nitromethan (3.48 g, 3.05 mL, 57.0 mmol, 3.0 equiv) was added dropwise and the mixture was stirred at reflux for 4 h. After cooling to room temperature, the reaction mixture was extracted with EtOAc (2 × 250 mL) and the organic layers were washed with H₂O (3 × 200 mL) and dried over anhydrous Na₂SO₄. The solvent was removed under reduced pressure and the crude product was purified on silica (hexanes/EtOAc 9:1) and recrystallized from ethanol to give **56m** (1.85 g, 9.83 mmol, 52%) deep purple crystals.

¹H-NMR (300 MHz, DMSO) δ 12.26 (s, 1H), 8.41 (d, *J* = 13.4 Hz, 1H), 8.26 (d, *J* = 3.2 Hz, 1H), 8.01 (d, *J* = 13.4 Hz, 1H), 7.99 – 7.93 (m, 1H), 7.56 – 7.49 (m, 1H), 7.26 (pd, *J* = 7.2, 1.5 Hz, 2H). ¹³C-NMR (101 MHz, DMSO) δ 137.68, 136.36, 134.73, 131.11, 124.61, 123.35, 121.91, 120.52, 112.81, 108.24.

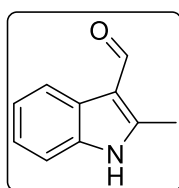
***tert*-Butyl (*E*)-3-(2-nitrovinyl)-1*H*-indole-1-carboxylate (56f)**

A 25 mL round bottom flask equipped with a stirring bar, was charged with **56m** (1.25 g, 6.64 mmol, 1.0 equiv) in anhydrous THF (10 mL), di-*tert*-butyl dicarbonate (1.74 g, 7.97 mmol, 1.2 equiv) and DMAP (81 mg, 664 μmol, 0.1 equiv). The reaction mixture was stirred for 2 h at room temperature until full conversion was observed judged by TLC. The solvent was removed under

reduced pressure and the crude product was purified on silica (hexanes/EtOAc 6:1) to give **56f** (650 mg, 2.25 mmol, 34%) as a pale green solid.

¹H-NMR (300 MHz, CDCl₃) δ 8.26 – 8.22 (m, 1H), 8.19 (d, *J* = 13.7 Hz, 1H), 8.04 (s, 1H), 7.79 (d, *J* = 13.7 Hz, 1H), 7.76 – 7.69 (m, 1H), 7.49 – 7.36 (m, 2H), 1.70 (s, 9H). **¹³C-NMR** (101 MHz, CDCl₃) δ 148.75, 136.52, 135.92, 132.32, 131.74, 126.98, 126.11, 124.40, 120.34, 116.06, 112.65, 85.71, 28.24. **IR** (neat): 3131, 3049, 2982, 2933, 1737, 1632, 1580, 1547, 1495, 1450, 1368, 1338, 1238, 1148, 969, 857, 749, 712 cm⁻¹. **HRMS** (ESI) *m/z* calculated for C₁₅H₁₆N₂NaO₄ ([M+Na]⁺) 311.1002, found 311.1007. **Mp**: 146 °C.

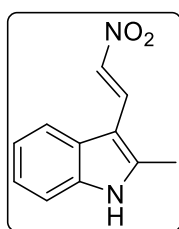
2-Methyl-1*H*-indole-3-carbaldehyde (**S9**)^[111]



A 250 mL three-necked round bottom flask, equipped with a stirring bar, a thermometer and a reflux condenser was charged with anhydrous DMF (12.9 mL, 12.3 g, 168 mmol, 4.4 equiv) under N₂ atmosphere and cooled to 0 °C. POCl₃ (3.83 mL, 6.43 g, 41.9 mmol, 1.1 equiv) was added dropwise and the mixture was stirred for 40 min at 0 °C. A solution of 2-methyl-1*H*-indole (5.00 g, 38.1 mmol, 1.0 equiv) in DMF (7 mL) was added dropwise, maintaining the temperature below 10 °C. The solution was stirred 40 min at 0 °C and then 40 min at 35 °C. Pilled ice was added and a solution of NaOH (16.9 g, 422 mmol, dissolved in 44 mL H₂O) was added *via* dropping funnel. The resulting mixture was heated to 100 °C for 30 min and cooled down to room temperature again. The brown precipitate was filtered off and washed with large amount of H₂O. The product was dried under reduced pressure to give **S9** (5.85 g, 36.8 mmol, 96%) as a brown solid.

¹H-NMR (300 MHz, DMSO) δ 11.99 (s, 1H), 10.05 (s, 1H), 8.12 – 7.97 (m, 1H), 7.47 – 7.31 (m, 1H), 7.25 – 7.07 (m, 2H), 2.68 (s, 3H). **¹³C-NMR** (101 MHz, DMSO) δ 184.23, 148.52, 135.33, 125.56, 122.61, 121.85, 119.96, 113.63, 111.37, 11.50.

(*E*)-2-Methyl-3-(2-nitrovinyl)-1*H*-indole (**56l**)^[112]

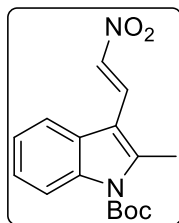


A 10 mL round bottom flask, equipped with a magnetic stirring bar, was charged with **S9** (2.50 g, 15.7 mmol, 1.0 equiv), NH₄OAc (1.82 g, 23.6 mmol, 1.5 equiv) and nitromethane (1.3 mL, 1.44 g, 23.6 mmol, 1.5 equiv) and refluxed for 3 h. The resulting mixture was poured over crushed ice (200 g), the formed precipitate was filtered, dried and purified on silica (hexanes/EtOAc 4:1) to give **56l** (2.00 g, 9.89 mmol, 63%) as a red solid.

¹H-NMR (300 MHz, DMSO) δ 12.26 (s, 1H), 8.32 (d, *J* = 13.2 Hz, 1H), 7.91 (d, *J* = 13.2 Hz, 1H), 7.88 – 7.81 (m, 1H), 7.47 – 7.37 (m, 1H), 7.28 – 7.13 (m, 2H), 2.61 (s, 3H).

$^{13}\text{C-NMR}$ (101 MHz, DMSO) δ 147.76, 136.40, 133.37, 129.69, 125.25, 122.89, 121.97, 120.19, 111.92, 105.19, 11.91.

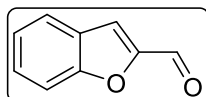
***tert*-Butyl (*E*)-2-methyl-3-(2-nitrovinyl)-1*H*-indole-1-carboxylate (**56g**)**



A 25 mL round bottom flask equipped with a magnetic stirring bar, was charged with **56I** (1.05 g, 5.19 mmol, 1.0 equiv) in anhydrous THF (10 mL), di-*tert*-butyl dicarbonate (1.36 g, 6.23 mmol, 1.2 equiv) and DMAP (63 mg, 519 μmol , 0.1 equiv). The reaction mixture was stirred for 2 h at room temperature until full conversion was observed judged by TLC. The solvent was removed under reduced pressure and the crude product was purified on silica (hexanes/EtOAc 6:1) to give **56g** (550 mg, 1.82 mmol, 35%) as a pale yellow solid.

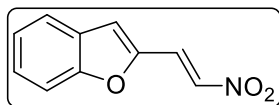
$^1\text{H-NMR}$ (300 MHz, CDCl_3) δ 8.33 (d, $J = 13.6$ Hz, 1H), 8.20 – 8.11 (m, 1H), 7.82 (d, $J = 13.6$ Hz, 1H), 7.71 – 7.63 (m, 1H), 7.41 – 7.32 (m, 2H), 2.78 (s, 3H), 1.72 (s, 9H). $^{13}\text{C-NMR}$ (101 MHz, CDCl_3) δ 149.80, 145.26, 136.60, 135.36, 131.43, 126.13, 125.16, 124.32, 119.60, 115.99, 111.02, 85.85, 28.32, 14.71. **IR** (neat): 3131, 2978, 2933, 1733, 1618, 1543, 1495, 1457, 1372, 1305, 1219, 1118, 1055, 977, 857, 805, 746 cm^{-1} . **HRMS** (ESI) m/z calculated for $\text{C}_{16}\text{H}_{18}\text{N}_2\text{NaO}_4$ ($[\text{M}+\text{Na}]^+$) 325.1159, found 325.1162. **Mp**: 125 $^\circ\text{C}$.

Benzofuran-2-carbaldehyde (S10**)^[113]**



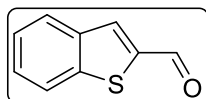
A 100 mL flame dried Schlenk flask equipped with a magnetic stirring bar was charged with a solution of benzofuran (0.50 g, 4.23 mmol, 1.0 equiv) in anhydrous THF (20 mL) and cooled to -78 $^\circ\text{C}$. To this solution *n*-BuLi (2.9 mL, 1.6 M in hexane, 4.66 mmol) was added dropwise. After stirring for 1 h DMF (0.7 mL, 8.47 mmol, 2.0 equiv) was added dropwise. After 2.5 h at -78 $^\circ\text{C}$ the reaction mixture was quenched by addition of saturated aqueous NH_4Cl solution (25 mL). The aqueous phase was extracted with EtOAc (3 \times 50 mL) and the organic layer was washed with brine (50 mL), dried over MgSO_4 and concentrated. The crude product was purified on silica (hexanes/EtOAc 95:5) to give **S10** (547 mg, 3.74 mmol, 88%) as a yellow oil.

$^1\text{H-NMR}$ (300 MHz, CDCl_3) δ 9.88 (s, 1H), 7.79 – 7.73 (m, 1H), 7.66 – 7.49 (m, 3H), 7.39 – 7.31 (m, 1H). $^{13}\text{C-NMR}$ (75 MHz, CDCl_3) δ 179.91, 156.41, 152.83, 129.38, 126.79, 124.36, 123.81, 117.94, 112.89.

(E)-2-(2-Nitrovinyl)benzofuran (56h)^[113]

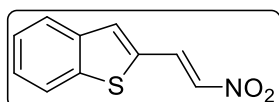
A 25 mL round bottom flask was charged with a solution of **S10** (500 mg, 3.42 mmol, 1.0 equiv) in nitromethane (6.5 mL). To this solution NH₄OAc (396 mg, 5.13 mmol, 1.5 equiv) was added and the resulting mixture was stirred for 3 h at reflux before quenching with H₂O (9 mL). The aqueous layer was extracted with EtOAc (3 × 50 mL) and the combined organic extracts were dried over MgSO₄, filtered and concentrated. The crude product was purified on silica (hexanes/EtOAc 95:5 to 85:15) to give **56h** (265 mg, 1.40 mmol, 41%) as a yellow solid.

¹H-NMR (300 MHz, CDCl₃) δ 7.86 (d, *J* = 13.2 Hz, 1H), 7.72 – 7.60 (m, 2H), 7.54 – 7.40 (m, 2H), 7.34 – 7.26 (m, 1H), 7.19 (s, 1H). ¹³C-NMR (75 MHz, CDCl₃) δ 156.24, 148.15, 137.08, 128.23, 128.13, 126.00, 124.08, 122.39, 116.37, 111.84.

Benzo[b]thiophene-2-carbaldehyde (S11)^[114]

A 250 mL flame dried Schlenk flask equipped with a magnetic stirring bar was charged with a solution of benzothiophene (2.00 g, 14.9 mmol, 1.0 equiv) in anhydrous THF (75 mL) and cooled to -78 °C. To this solution *n*-BuLi (10.3 mL, 1.6 M in hexane, 16.4 mmol, 1.1 equiv) was added dropwise. After stirring for 1 h DMF (1.7 mL, 22.4 mmol, 1.5 equiv) was added dropwise. After 2.5 h at -78 °C the reaction mixture was warmed slowly to room temperature and quenched by addition of sat. NH₄Cl solution (50 mL). The aqueous phase was extracted with EtOAc (3 × 150 mL) and the organic phase was washed with brine (150 mL), dried over MgSO₄ and concentrated. The crude product was purified on silica (hexanes/EtOAc 95:5) to give **S11** (2.20 g, 13.6 mmol, 91%).

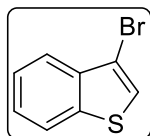
¹H-NMR (300 MHz, CDCl₃) δ 10.11 (s, 1H), 8.03 (s, 1H), 7.99 – 7.86 (m, 2H), 7.56 – 7.39 (m, 2H). ¹³C-NMR (101 MHz, CDCl₃) δ 184.71, 143.35, 142.67, 138.58, 134.56, 128.21, 126.32, 125.30, 123.30.

(E)-2-(2-Nitrovinyl)benzo[b]thiophene (56i)^[113]

A 100 mL round bottom flask was charged with a solution of **S11** (2.03 g, 12.51 mmol, 1.0 equiv) in nitromethane (27 mL) and NH₄OAc (1.45 g, 18.77 mmol, 1.5 equiv). The resulting mixture was stirred during 1 h at reflux before quenching with H₂O. The aqueous layer was extracted with EtOAc (3 × 30 mL) and the combined organic extracts were dried over MgSO₄, filtered and concentrated. The crude product was purified on silica (hexanes/EtOAc 92:2 to 95:5) to give **56i** (1.08 g, 5.26 mmol, 42%) as a yellow solid.

¹H-NMR (400 MHz, CDCl₃) δ 8.22 (d, *J* = 13.3 Hz, 1H), 7.87 – 7.79 (m, 2H), 7.68 (s, 1H), 7.49 (d, *J* = 13.4 Hz, 3H). **¹³C-NMR** (101 MHz, CDCl₃) δ 141.20, 139.29, 137.15, 133.82, 133.12, 132.79, 127.71, 125.53, 125.15, 122.75.

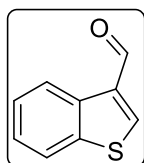
3-Bromobenzo[b]thiophene (**S12**)^[115]



A 250 mL round bottom flask was charged with a solution of benzo[b]thiophene (5.09 g, 37.9 mmol, 1.0 equiv) in CHCl₃ (37.5 mL) and AcOH (37.5 mL). *N*-bromosuccinimide (8.43 g, 47.4 mmol, 1.3 equiv) was added stepwise for 4 h at 0 °C and then allowed to stir at room temperature for 24 h. Then CHCl₃ (15 mL) was added and the resulting mixture was successively washed with sat. Na₂S₂O₃ solution (100 mL), sat. Na₂CO₃ solution (100 mL) and H₂O (75 mL). The combined organic layers were then dried over MgSO₄, filtered and the solvent was removed under reduced pressure. The resulting red liquid was then filtered through of a pad of silica, eluting with cyclohexane to give **S12** (7.00 g, 32.9 mmol, 87%) as a yellow oil.

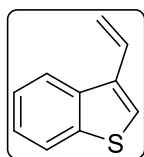
¹H-NMR (300 MHz, CDCl₃) δ 7.90 – 7.81 (m, 2H), 7.53 – 7.37 (m, 3H). **¹³C-NMR** (101 MHz, CDCl₃) δ 138.57, 137.51, 125.30, 125.03, 123.48, 123.06, 122.74, 107.69.

Benzo[b]thiophene-3-carbaldehyde (**S13**)^[116]



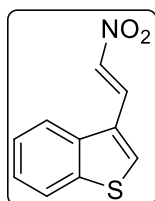
A 250 mL round bottom flask equipped with a magnetic stirring bar was charged with a *n*-BuLi solution (10.3 mL, 1.6 M, 16.4 mmol, 1.0 equiv) and Et₂O (45 mL). A **S12** (3.50 g, 16.4 mmol, 1.0 equiv) solution in anhydrous Et₂O (45 mL) was added over 5 min to the stirred *n*-BuLi solution. The mixture was stirred at -78 °C for further 30 min to give an ethereal suspension of 3-benzo[b]thienyllithium. A solution of DMF (1.53 mL, 19.7 mmol, 1.5 equiv) in Et₂O (1.50 mL) was added dropwise to the stirred suspension of 3-benzo[b]thienyllithium at -78 °C and the mixture was stirred for 4 h. The mixture was then allowed to warm slowly to -5 °C and was stirred for 15 min. An excess of 2 M HCl was added, the organic layer was separated, and the aqueous layer was extracted with Et₂O (2 × 40 mL). The organic layers were combined, washed with H₂O (50 mL), dried over MgSO₄, filtered and concentrated. The residue was purified on silica (CH₂Cl₂/hexanes 3:7) to give **S13** (1.36 g, 8.38 mmol, 51%) as a colorless solid.

¹H-NMR (400 MHz, CDCl₃) δ 10.16 (s, 1H), 8.73 – 8.65 (m, 1H), 8.33 (s, 1H), 7.94 – 7.86 (m, 1H), 7.57 – 7.43 (m, 2H). **¹³C-NMR** (101 MHz, CDCl₃) δ 185.56, 143.32, 140.62, 136.67, 135.32, 126.32, 126.27, 124.97, 122.57.

3-Vinylbenzo[b]thiophene (S14)^[117]

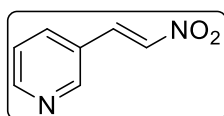
A flame dried 100 mL Schlenk flask equipped with a magnetic stirring bar was charged with methyltriphenylphosphonium iodide (2.96 g, 7.32 mmol, 1.1 equiv) and anhydrous THF (30 mL). To this suspension *n*-BuLi (2.71 mL, 2.7 M in toluene, 7.32 mmol, 1.1 equiv) was added dropwise at 0 °C under N₂ atmosphere. The mixture was further stirred for 30 min and the ylide can be visibly observed by its persistent yellow color. **S13** (1.08 g, 6.66 mmol, 1.0 equiv) was dissolved in dry THF (8 mL) and added dropwise at 0 °C. The resulting mixture was stirred for another 20 min and allowed to warm to room temperature for further reaction. After 4 h, the reaction was quenched by saturated NH₄Cl solution. CH₂Cl₂ (20 mL) was added and the aqueous phase was extracted with CH₂Cl₂ (3 × 30 mL). The organic layers were combined, dried over Na₂SO₄ and the solvent was removed under reduced pressure. The crude reaction mixture was purified on silica (hexanes) to give **S14** (881 mg, 5.50 mmol, 83%) as a colorless oil.

¹H-NMR (400 MHz, CDCl₃) δ 7.93 (d, *J* = 8.0 Hz, 1H), 7.87 (d, *J* = 7.6 Hz, 1H), 7.47 (s, 1H), 7.44 – 7.34 (m, 2H), 6.99 (dd, *J* = 17.6, 11.1 Hz, 1H), 5.81 (dd, *J* = 17.6, 1.4 Hz, 1H), 5.39 (dd, *J* = 11.1, 1.1 Hz, 1H). **¹³C-NMR** (101 MHz, CDCl₃) δ 140.63, 137.79, 134.72, 129.39, 124.59, 124.41, 123.03, 122.41, 122.10, 115.73.

(E)-3-(2-Nitrovinyl)benzo[b]thiophene (56j)^[118]

A flame dried 50 mL round bottom flask was equipped with a magnetic stirring bar and a reflux condenser and was charged with **S14** (1.04 g, 6.49 mmol, 1.0 equiv), TEMPO (406 mg, 2.60 mmol, 0.4 equiv) and *t*BuONO (1.34 g, 13.0 mmol, 2.0 equiv) in 1,4-dioxane (24 mL). The reaction mixture was then stirred for 16 h at 90 °C. The crude mixture was concentrated and purified on silica (hexanes/EtOAc 99:1) to give **56j** (440 mg, 2.14 mmol, 33%) as a yellow solid.

¹H-NMR (400 MHz, CDCl₃) δ 8.30 (d, *J* = 14.1 Hz, 1H), 8.00 – 7.91 (m, 3H), 7.76 (d, *J* = 13.7 Hz, 1H), 7.58 – 7.45 (m, 2H). **¹³C-NMR** (101 MHz, CDCl₃) δ 140.66, 136.86, 136.54, 132.98, 131.22, 127.24, 125.86, 125.83, 123.47, 122.16.

(E)-3-(2-Nitrovinyl)pyridine (56k)^[119]

A 25 mL round bottom flask equipped with a magnetic stirring bar was charged with methanol (4 mL) and nitromethane (6.3 mL, 117 mmol, 2.5 equiv). With stirring methylamine hydrochloride (189 mg, 2.80 mmol, 0.06 equiv), NaHCO₃ (78 mg, 934 μmol, 0.02 equiv) and nicotinaldehyde (5.00 g, 46.7 mmol,

1.0 equiv) were added. The resulting mixture was stirred for 72 h at room temperature and the precipitate was filtered off and washed with a small amount of cold methanol. The solvent was removed under reduced pressure to give **56k** (3.17 g, 21.1 mmol, 45%) as a pale yellow solid. **¹H-NMR** (400 MHz, CDCl₃) δ 8.78 (d, *J* = 2.5 Hz, 1H), 8.70 (dd, *J* = 4.8, 1.7 Hz, 1H), 7.99 (d, *J* = 13.8 Hz, 1H), 7.87 (dt, *J* = 8.1, 2.1 Hz, 1H), 7.62 (d, *J* = 13.8 Hz, 1H), 7.40 (dd, *J* = 8.0, 4.8 Hz, 1H). **¹³C-NMR** (101 MHz, CDCl₃) δ 152.73, 150.47, 138.52, 135.56, 135.27, 126.27, 124.20.

5.2.3 General Procedure for High Pressure/ambient Pressure Reactions

A

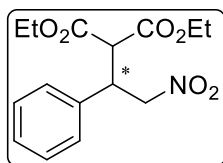
Ambient pressure reactions were conducted in 5 mL round bottom flasks. The appropriate nitroolefin **56** (0.40 mmol, 1.0 equiv) and the thiourea catalyst **57** (1 mol%) were weighed into the flask and anhydrous solvent (0.8 mL) was added subsequently. Diethyl malonate (**45**, 0.80 mmol, 2.0 equiv) was added to the flask and the reaction mixture was stirred for the indicated time. After that the solvent was removed under reduced pressure. The crude reaction mixture was analyzed by NMR-spectroscopy and the product was purified on silica.

B

High-pressure reactions were conducted in self-made PTFE tubes. A PTFE tube was sealed through melting off one side using crucible tongs and a brazing torch. The appropriate nitroolefin **56** (0.40 mmol, 1.0 equiv) and the thiourea catalyst **57** (1 mol%) were weighed into the tube. Anhydrous solvent (0.8 mL) was added subsequently. Diethyl malonate (**45**, 0.80 mmol, 2.0 equiv) was added to the PTFE tube. After that the PTFE tube was sealed immediately, shaken and inserted into the high pressure reactor. The reactor was filled with the pressurizing medium, inserted into the apparatus and pressure was applied. After pressurizing for the indicated reaction time, the reaction mixture was filled into a round bottom flask and the solvent was removed under reduced pressure. The crude reaction mixture was analyzed by NMR-spectroscopy and the product was purified on silica.

5.2.4 Michael Addition Products

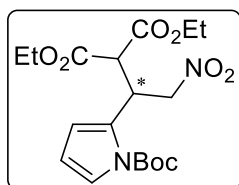
Diethyl 2-(2-nitro-1-phenylethyl)malonate (**58a**)^[65]



Product **58a** was prepared by following the general procedure A/B: Nitroolefin **56a** (1.0 equiv), diethyl malonate (**45**, 2.0 equiv), solvent (0.5 M with respect to nitroolefin), **57** (1 mol%). The product was purified on flash silica (hexanes/EtOAc 6:1) to give **58a** as a colorless solid.

¹H-NMR (300 MHz, CDCl₃) δ 7.35 – 7.20 (m, 5H), 4.97 – 4.80 (m, 2H), 4.29 – 4.16 (m, 3H), 4.00 (q, *J* = 7.1 Hz, 2H), 3.82 (d, *J* = 9.3 Hz, 1H), 1.26 (t, *J* = 7.1 Hz, 3H), 1.04 (t, *J* = 7.1 Hz, 3H). **¹³C-NMR** (75 MHz, CDCl₃) δ 167.57, 166.92, 136.31, 129.03, 128.45, 128.13, 77.76, 62.28, 62.00, 55.07, 43.07, 14.08, 13.85.

Diethyl-2-(1-(1-(*tert*-butyloxycarbonyl)-1*H*-pyrrol-2-yl)-2-nitroethyl)malonate (**58b**)

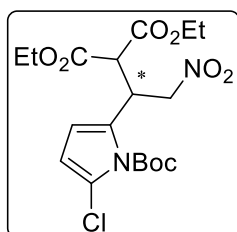


Product **58b** was prepared by following the general procedure A/B: Nitroolefin **56b**, diethyl malonate (**45**, 2.0 equiv), solvent (0.5 M with respect to nitroolefin), **57** (1 mol%). The product was purified on flash silica (hexanes/EtOAc 4:1) to give **58b** as a colorless oil (156 mg,

392 μmol, 99%).

¹H-NMR (300 MHz, CDCl₃): δ 7.20 (dd, *J* = 3.4, 1.7 Hz, 1H), 6.13 (dd, *J* = 3.4, 1.8 Hz, 1H), 6.05 (t, *J* = 3.4 Hz, 1H), 4.86 – 5.09 (m, 3H), 4.04 – 4.25 (m, 5H), 1.61 (s, 9H), 1.24 (t, *J* = 7.1 Hz, 3H), 1.16 (t, *J* = 7.1 Hz, 3H). **¹³C-NMR** (101 MHz, CDCl₃) δ 167.76, 167.43, 149.29, 129.56, 122.87, 113.90, 110.26, 84.71, 76.41, 62.00, 61.92, 53.47, 36.07, 28.08, 14.10, 14.00. **IR** (neat): 2982, 2937, 1729, 1554, 1479, 1416, 1371, 1323, 1244, 1155, 1125, 1069, 1025, 846, 771, 730, 664 cm⁻¹. **HRMS** (ESI) *m/z* calculated for C₁₈H₂₆N₂O₈Na ([M+Na]⁺) 421.1571, found 421.1587. **Chiral HPLC** (Phenomenex Lux Cellulose-1 4.6 × 250 mm, 5 μm, *n*-heptan/*i*-PrOH = 99:1, 1.0 mL/min, λ = 215 nm): *t*_R(major) = 22.99 min, *t*_R(minor) = 9.87 min, 95% ee. **Specific rotation** [α]²⁰₅₈₉ = +8.36° (c = 1.0, CH₂Cl₂).

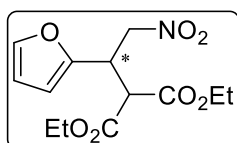
Diethyl 2-(1-(1-(*tert*-butoxycarbonyl)-5-chloro-1*H*-pyrrol-2-yl)-2-nitroethyl)malonate (58c)



Product **58c** was prepared by following the general procedure A/B: Nitroolefin **56c**, diethyl malonate (**45**, 2.0 equiv), solvent (0.5 M with respect to nitroolefin), **57** (1 mol%). The product was purified on flash silica (hexanes/EtOAc 4:1) to give **58c** as a colorless oil (72 mg, 231 μmol , 50%).

$^1\text{H-NMR}$ (400 MHz, CDCl_3) δ 6.04 (q, $J = 3.9$ Hz, 2H), 5.05 – 4.85 (m, 2H), 4.75 (td, $J = 8.2$, 4.3 Hz, 1H), 4.26 – 4.06 (m, 5H), 1.64 (s, 9H), 1.25 (t, $J = 7.1$ Hz, 3H), 1.17 (t, $J = 7.2$ Hz, 3H). **$^{13}\text{C-NMR}$** (101 MHz, CDCl_3) δ 167.67, 167.26, 148.54, 130.23, 118.03, 111.72, 111.27, 86.37, 76.45, 62.15, 62.13, 36.24, 28.02, 14.13, 14.03. **IR** (neat): 2986, 2937, 1733, 1558, 1480, 1372, 1308, 1252, 1215, 1156, 1096, 1021, 850, 783, 667 cm^{-1} . **HRMS** (ESI) m/z calculated for $\text{C}_{18}\text{H}_{25}\text{ClN}_2\text{O}_8\text{Na}$ ($[\text{M}+\text{Na}]^+$) 455.1192, found 455.1203.

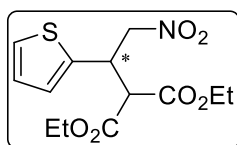
Diethyl 2-(1-(furan-2-yl)-2-nitroethyl)malonate (58d)^[120]



Product **58d** was prepared by following the general procedure A/B: Nitroolefin **56d**, diethyl malonate (**45**, 2.0 equiv), solvent (0.5 M with respect to nitroolefin), **57** (1 mol%). The product was purified on flash silica (hexanes/EtOAc 4:1) to give **58d** as a colorless oil (107 mg, 356 μmol , 93%).

$^1\text{H-NMR}$ (300 MHz, CDCl_3) δ 7.34 (dd, $J = 1.9$, 0.8 Hz, 1H), 6.28 (dd, $J = 3.3$, 1.9 Hz, 1H), 6.21 (dt, $J = 3.3$, 0.7 Hz, 1H), 4.97 – 4.82 (m, 2H), 4.37 (td, $J = 7.9$, 5.4 Hz, 1H), 4.26 – 4.09 (m, 4H), 3.90 (d, $J = 7.9$ Hz, 1H), 1.25 (t, $J = 7.1$ Hz, 3H), 1.19 (t, $J = 7.1$ Hz, 3H). **$^{13}\text{C-NMR}$** (75 MHz, CDCl_3) δ 167.24, 166.94, 149.66, 142.85, 110.65, 108.57, 75.55, 62.27, 53.11, 36.94, 14.08, 14.03. **Chiral HPLC** (Phenomenex Lux Cellulose-2, 4.6 \times 250 mm, 5 μm , *n*-heptan/*i*-PrOH = 99:1, 1.0 mL/min, $\lambda = 215$ nm): t_{R} (major) = 38.58 min, t_{R} (minor) = 30.88 min, 93% ee.

Diethyl 2-(2-nitro-1-(thiophen-2-yl)ethyl)malonate (58e)^[65]

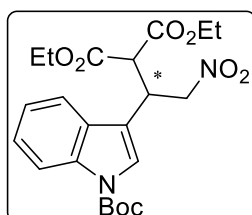


Product **58e** was prepared by following the general procedure A/B: Nitroolefin **56e**, diethyl malonate (**45**, 2.0 equiv), solvent (0.5 M with respect to nitroolefin), **57** (1 mol%). The product was purified on flash silica (hexanes/EtOAc 4:1) to give **58e** as a colorless oil (109 mg, 312 μmol , 67%).

$^1\text{H-NMR}$ (300 MHz, CDCl_3) δ 7.22 (dd, $J = 5.0$, 1.4 Hz, 1H), 6.99 – 6.87 (m, 2H), 4.98 – 4.83 (m, 2H), 4.55 (td, $J = 8.0$, 5.5 Hz, 1H), 4.22 (qd, $J = 7.1$, 2.5 Hz, 2H), 4.11 (q, $J = 7.1$ Hz, 2H),

3.86 (d, $J = 8.1$ Hz, 1H), 1.26 (t, $J = 7.1$ Hz, 3H), 1.15 (t, $J = 7.1$ Hz, 3H). $^{13}\text{C-NMR}$ (75 MHz, CDCl_3) δ 167.30, 166.81, 138.63, 127.11, 126.90, 125.66, 78.16, 62.35, 62.25, 55.66, 38.49, 14.07, 13.95. **Chiral HPLC** (Phenomenex Lux Cellulose-2, 4.6 \times 250 mm, 5 μm , *n*-heptan/*i*-PrOH = 90:10, 0.5 mL/min, $\lambda = 215$ nm): t_{R} (major) = 24.88 min, t_{R} (minor) = 21.87 min, 91% ee.

Diethyl-2-(1-(1-(*tert*-butyloxycarbonyl)-1*H*-indol-3-yl)-2-nitroethyl)malonat (**58f**)

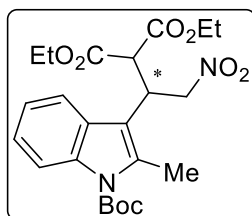


Product **58f** was prepared by following the general procedure A/B: Nitroolefin **56f**, diethyl malonate (**45**, 2.0 equiv), solvent (0.5 M with respect to nitroolefin), **57** (1 mol%). The product was purified on flash silica (hexanes/EtOAc 4:1) to give **58f** as a colorless oil (153 mg, 340 μmol , 79%).

$^1\text{H-NMR}$ (400 MHz, CDCl_3): δ 8.12 (d, $J = 8.0$ Hz, 1H), 7.58 (d, $J = 7.7$ Hz, 1H), 7.52 (s, 1H), 7.33 (td, $J = 7.7, 1.2$ Hz, 1H), 7.27 (td, $J = 7.5, 1.2$ Hz, 1H), 5.01 (dd, $J = 13.3, 8.0$ Hz, 1H), 4.97 (dd, $J = 13.3, 5.3$ Hz, 1H), 4.54 (td, $J = 8.0, 5.4$ Hz, 1H), 4.14 – 4.27 (m, 2H), 4.03 – 4.14 (m, 2H), 4.01 (d, $J = 8.4$ Hz, 1H), 1.66 (s, 9H), 1.24 (t, $J = 7.1$ Hz, 3H), 1.09 (t, $J = 7.1$ Hz, 3H). $^{13}\text{C-NMR}$ (101 MHz, CDCl_3) δ 167.58, 167.15, 149.36, 135.38, 128.78, 125.10, 124.23, 122.99, 118.63, 115.98, 115.56, 84.28, 76.76, 62.22, 62.12, 54.00, 34.25, 28.24, 14.04, 13.86.

IR (neat): 3123, 2981, 2937, 1729, 1610, 1554, 1453, 1367, 1308, 1256, 1151, 1095, 1021, 857, 745 cm^{-1} . **HRMS** (ESI) m/z calculated for $\text{C}_{22}\text{H}_{32}\text{N}_3\text{O}_8$ ($[\text{M}+\text{NH}_4]^+$) 466.2184, found 466.2190. **Chiral HPLC** (Phenomenex Lux Cellulose-2 4.6 \times 250 mm, 5 μm , *n*-heptan/*i*-PrOH = 95:5, 1.0 mL/min, $\lambda = 215$ nm): t_{R} (major) = 15.25 min, t_{R} (minor) = 11.68 min, 91% ee. **Specific rotation** $[\alpha]_{589}^{20} = -4.52^\circ$ ($c = 1.0, \text{CH}_2\text{Cl}_2$).

Diethyl-2-(1-(1-(*tert*-butyloxycarbonyl)-2-methyl-1*H*-indol-3-yl)-2-nitroethyl)malonat (**58g**)

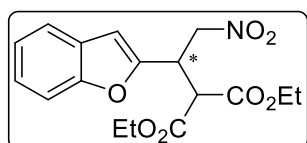


Product **58g** was prepared by following the general procedure A/B: Nitroolefin **56g**, diethyl malonate (**45**, 2.0 equiv), solvent (0.5 M with respect to nitroolefin), **57** (1 mol%). The product was purified on flash silica (hexanes/EtOAc 6:1) to give **58g** as a colorless oil (160 mg, 350 μmol , 80%).

$^1\text{H-NMR}$ (300 MHz, CDCl_3): δ 8.08 – 8.17 (m, 1H), 7.40 – 7.49 (m, 1H), 7.16 – 7.28 (m, 2H), 4.90 – 5.02 (m, 2H), 4.66 (ddd, $J = 11.2, 8.8, 6.1$ Hz, 1H), 4.18 – 4.36 (m, 2H), 4.10 (d, $J = 11.2$ Hz, 1H), 3.80 – 3.99 (m, 2H), 2.60 (s, 3H), 1.66 (d, $J = 7.1$ Hz, 9H), 1.30 (t, $J = 7.1$ Hz, 3H), 0.88 (t, $J = 7.2$ Hz, 3H). $^{13}\text{C-NMR}$ (75 MHz, CDCl_3) δ 167.70, 166.72, 150.34, 136.99,

136.10, 126.92, 123.71, 122.74, 117.93, 115.93, 112.04, 84.34, 76.22, 62.44, 61.77, 53.16, 34.88, 28.29, 14.09, 13.55. **IR** (neat): 2981, 2937, 1729, 1606, 1558, 1457, 1367, 1319, 1256, 1226, 1159, 1028, 976, 913, 853, 745 cm^{-1} . **HRMS** (ESI) m/z calculated for $\text{C}_{23}\text{H}_{30}\text{N}_2\text{O}_8\text{Na}$ ($[\text{M}+\text{Na}]^+$) 485.1894, found 485.1896. **Chiral HPLC** (Phenomenex Lux Cellulose-1 4.6 \times 250 mm, 5 μm , *n*-heptan/*i*-PrOH = 70:30, 0.5 mL/min, λ = 215 nm): $t_{\text{R}}(\text{major})$ = 9.90 min, $t_{\text{R}}(\text{minor})$ = 11.77 min, 85% ee. **Specific rotation** $[\alpha]_{589}^{20} = +1.28^\circ$ (c = 1.00, CH_2Cl_2).

Diethyl 2-(1-(benzofuran-2-yl)-2-nitroethyl)malonate (**58h**)



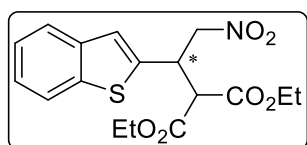
Product **58h** was prepared by following the general procedure A/B: Nitroolefin **56h**, diethyl malonate (**45**, 2.0 equiv), solvent (0.5 M with respect to nitroolefin), **57** (1 mol%). The product was purified on

flash silica (hexanes/EtOAc 4:1) to give **58h** as a colorless oil (109 mg, 312 μmol , 83%).

$^1\text{H-NMR}$ (300 MHz, CDCl_3) δ 7.56 – 7.46 (m, 1H), 7.46 – 7.37 (m, 1H), 7.32 – 7.16 (m, 2H), 6.63 (s, 1H), 5.12 – 4.93 (m, 2H), 4.53 (td, J = 8.1, 4.3 Hz, 1H), 4.30 – 4.19 (m, 2H), 4.14 (q, J = 7.1 Hz, 2H), 4.03 (d, J = 7.7 Hz, 1H), 1.25 (t, J = 7.1 Hz, 3H), 1.14 (t, J = 7.1 Hz, 3H).

$^{13}\text{C-NMR}$ (75 MHz, CDCl_3) δ 167.15, 166.88, 154.94, 152.51, 127.89, 124.74, 123.21, 121.31, 111.24, 105.64, 75.11, 62.43, 62.41, 52.88, 37.32, 14.08, 13.97. **IR** (neat): 2986, 2941, 1730, 1558, 1454, 1371, 1252, 1219, 1178, 1156, 1096, 1025, 932, 857, 813, 753, 678 cm^{-1} . **HRMS** (ESI) m/z calculated for $\text{C}_{17}\text{H}_{19}\text{NO}_7\text{Na}$ ($[\text{M}+\text{Na}]^+$) 372.1054, found 372.1064. **Chiral HPLC** (Phenomenex Lux Cellulose-1, 4.6 \times 250 mm, 5 μm , *n*-heptan/*i*-PrOH = 50:50, 0.5 mL/min, λ = 215 nm): $t_{\text{R}}(\text{major})$ = 19.08 min, $t_{\text{R}}(\text{minor})$ = 13.87 min, 90% ee. **Specific rotation** $[\alpha]_{589}^{20} = +7.41^\circ$ (c = 1.0, CH_2Cl_2).

Diethyl 2-(1-(benzo[b]thiophen-2-yl)-2-nitroethyl)malonate (**58i**)



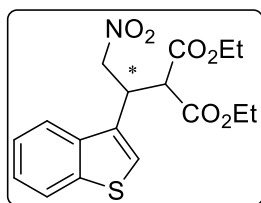
Product **58i** was prepared by following the general procedure A/B: Nitroolefin **56i**, diethyl malonate (**45**, 2.0 equiv), solvent (0.5 M with respect to nitroolefin), **57** (1 mol%). The product was purified on

flash silica (hexanes/EtOAc 6:1) to give **58i** as a colorless solid (42 mg, 116 μmol , 32%).

$^1\text{H-NMR}$ (300 MHz, CDCl_3) δ 7.81 – 7.65 (m, 2H), 7.38 – 7.27 (m, 2H), 7.20 (s, 1H), 5.10 – 4.93 (m, 2H), 4.68 – 4.56 (m, 1H), 4.32 – 4.18 (m, 2H), 4.13 (q, J = 7.1 Hz, 2H), 3.96 (d, J = 8.0 Hz, 1H), 1.26 (t, J = 7.1 Hz, 3H), 1.14 (t, J = 7.1 Hz, 3H). **$^{13}\text{C-NMR}$** (75 MHz, CDCl_3) δ 167.26, 166.77, 139.62, 139.44, 139.25, 124.89, 124.73, 123.90, 123.84, 122.39, 62.48, 62.42, 55.33, 39.21, 14.10, 13.98. **IR** (neat): 3053, 2982, 2930, 1730, 1554, 1439, 1368, 1290, 1238, 1178, 1088, 1059, 1029, 861, 809, 753, 708 cm^{-1} . **HRMS** (ESI) m/z calculated for $\text{C}_{17}\text{H}_{19}\text{NO}_6\text{SNa}$ ($[\text{M}+\text{Na}]^+$) 388.0825, found 388.0827. **Chiral HPLC** (Phenomenex Lux

Cellulose-1, 4.6 × 250 mm, 5 μm, *n*-heptan/*i*-PrOH = 50:50, 0.5 mL/min, λ = 215 nm): $t_R(\text{major}) = 18.17$ min, $t_R(\text{minor}) = 23.81$ min, 90% ee. **Mp:** 95 °C. **Specific rotation** $[\alpha]_{589}^{20} = +4.94^\circ$ (c = 0.5, CH₂Cl₂).

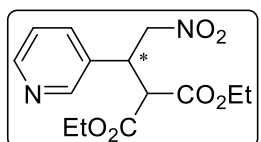
Diethyl 2-(1-(benzo[*b*]thiophen-3-yl)-2-nitroethyl)malonate (**58j**)



Product **58j** was prepared by following the general procedure A/B: Nitroolefin **56j**, diethyl malonate (**45**, 2.0 equiv), solvent (0.5 M with respect to nitroolefin), **57** (1 mol%). The product was purified on flash silica (hexanes/EtOAc 4:1) to give **58j** as a colorless oil (72 mg, 231 μmol, 67%).

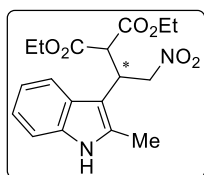
¹H-NMR (300 MHz, CDCl₃) δ 7.89 – 7.81 (m, 2H), 7.49 – 7.34 (m, 3H), 5.17 – 4.93 (m, 2H), 4.74 (td, *J* = 8.1, 4.8 Hz, 1H), 4.19 (qd, *J* = 7.1, 2.5 Hz, 2H), 4.10 – 4.00 (m, 3H), 1.21 (t, *J* = 7.1 Hz, 3H), 1.04 (t, *J* = 7.1 Hz, 3H). **¹³C-NMR** (75 MHz, CDCl₃) δ 167.57, 167.13, 140.38, 137.54, 131.15, 125.07, 124.68, 124.51, 123.11, 121.22, 76.64, 62.26, 62.23, 54.08, 36.06, 14.05, 13.85. **IR** (neat): 3079, 2982, 1726, 1554, 1461, 1431, 1372, 1297, 1245, 1178, 1096, 1025, 850, 760, 731 cm⁻¹. **HRMS** (ESI) *m/z* calculated for C₁₇H₁₉NO₆SNa ([M+Na]⁺) 388.0825, found 388.0832. **Chiral HPLC** (Phenomenex Lux Cellulose-1 4.6 × 250 mm, 5 μm, *n*-heptan/*i*-PrOH = 50:50, 0.5 mL/min, λ = 215 nm): $t_R(\text{major}) = 21.66$ min, $t_R(\text{minor}) = 16.54$ min, 87% ee. **Specific rotation** $[\alpha]_{589}^{20} = +6.12^\circ$ (c = 1.0, CH₂Cl₂).

Diethyl 2-(2-nitro-1-(pyridin-3-yl)ethyl)malonate (**58k**)



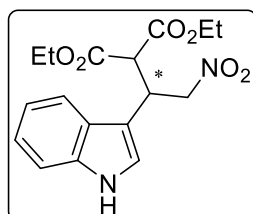
Product **58k** was prepared by following the general procedure A/B: Nitroolefin **56k**, diethyl malonate (**45**, 2.0 equiv), solvent (0.5 M with respect to nitroolefin), **57** (1 mol%). The product was purified on flash silica (hexanes/EtOAc 4:1) to give **58k** as a colorless oil (72 mg, 231 μmol, 60%).

¹H-NMR (300 MHz, CDCl₃): δ 8.55 (s, 2H), 7.63 (ddd, *J* = 8.0, 2.1, 1.4 Hz, 1H), 7.33 – 7.27 (m, 1H), 5.01 – 4.84 (m, 2H), 4.32 – 4.15 (m, 3H), 4.05 (q, *J* = 7.1 Hz, 2H), 3.83 (d, *J* = 9.0 Hz, 1H), 1.26 (t, *J* = 7.1 Hz, 3H), 1.08 (t, *J* = 7.1 Hz, 3H). **¹³C-NMR** (75 MHz, CDCl₃): δ 167.19, 166.62, 149.69, 135.90, 132.38, 123.85, 77.07, 62.58, 62.37, 54.57, 40.70, 14.11, 13.93. **IR** (neat): 2986, 2941, 1730, 1554, 1476, 1431, 1372, 1297, 1260, 1234, 1178, 1025, 857, 809, 716 cm⁻¹. **HRMS** (APCI) *m/z* calculated for C₁₄H₁₉N₂O₆ ([M+H]⁺) 311.1238, found 311.1241. **Chiral HPLC** (Phenomenex Lux Cellulose-1 4.6 × 250 mm, 5 μm, *n*-heptan/*i*-PrOH = 70:30, 0.5 mL/min, λ = 215 nm): $t_R(\text{major}) = 19.32$ min, $t_R(\text{minor}) = 22.67$ min, 60% ee. **Specific rotation** $[\alpha]_{589}^{20} = +1.08^\circ$ (c = 0.25, CH₂Cl₂).

Diethyl-2-(1-(2-methyl-1*H*-indol-3-yl)-2-nitroethyl)malonat (58l)

Product **58l** was prepared by following the general procedure A/B: Nitroolefin **56l**, diethyl malonate (**45**, 2.0 equiv), solvent (0.5 M with respect to nitroolefin), **57** (1 mol%). The product was purified on flash silica (hexanes/EtOAc 4:1) to give **58l** as a colorless solid (122 mg, 336 μmol , 92%).

¹H-NMR (300 MHz, CDCl_3): δ 7.93 (bs, 1H), 7.43 – 7.53 (m, 1H), 7.16 – 7.25 (m, 1H), 7.02 – 7.14 (m, 2H), 4.89 – 5.04 (m, 2H), 4.49 – 4.62 (m, 1H), 4.19 – 4.36 (m, 2H), 4.12 (d, $J = 11.2$ Hz, 1H), 3.75 – 3.93 (m, 2H), 2.35 (s, 3H, signal doubling due to rotamers), 1.30 (t, $J = 7.2$ Hz, 3H), 0.80 (t, $J = 7.2$ Hz, 3H). **¹³C-NMR** (75 MHz, CDCl_3) δ 167.97, 167.12, 135.36, 134.40, 126.10, 121.25, 119.73, 117.90, 110.86, 105.35, 105.32, 62.24, 61.51, 53.63, 35.33+35.25 (signal doubling due to rotamers), 14.05, 13.42, 11.74. **IR** (neat): 3395, 2981, 2937, 1722, 1621, 1546, 1461, 1371, 1300, 1244, 1177, 1155, 1017, 890, 857, 741, 670 cm^{-1} . **HRMS** (ESI) m/z calculated for $\text{C}_{18}\text{H}_{23}\text{N}_2\text{O}_6$ ($[\text{M}+\text{H}]^+$) 363.1551, found 363.1555. **Chiral HPLC** (Chiralpak AS-H, 4.6 \times 250 mm, 10 μm , *n*-heptan/*i*-PrOH = 90:10, 1.0 mL/min, $\lambda = 215$ nm): t_{R} (major) = 25.27 min, t_{R} (minor) = 21.67 min, 70% ee. **Mp**: 107 $^\circ\text{C}$. **Specific rotation** $[\alpha]_{589}^{20} = +7.21^\circ$ ($c = 1.0$, CH_2Cl_2).

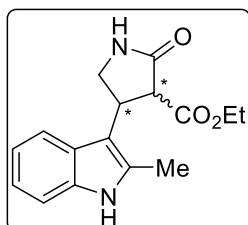
Diethyl-2-(2-(1-(1*H*-indol-3-yl)-2-nitroethyl)malonat (58m)

Product **58m** was prepared by following the general procedure A/B: Nitroolefin **56m**, diethyl malonate (**45**, 2.0 equiv), solvent (0.5 M with respect to nitroolefin), **57** (1 mol%). The product was purified on flash silica (hexanes/EtOAc 4:1) to give **58m** as a colorless oil (111 mg, 320 μmol , 84%).

¹H-NMR (400 MHz, CDCl_3): δ 8.23 (bs, 1H), 7.62 (d, $J = 7.9$ Hz, 1H), 7.32 (d, $J = 7.9$ Hz, 1H), 7.20 (td, $J = 7.5, 1.3$ Hz, 1H), 7.15 (td, $J = 7.5, 1.2$ Hz, 1H), 7.10 (d, $J = 2.5$ Hz, 1H), 5.03 (dd, $J = 12.8, 8.1$ Hz, 1H), 4.96 (dd, $J = 12.8, 5.2$ Hz, 1H), 4.55 – 4.64 (m, 1H), 4.11 – 4.27 (m, 2H), 4.08 (dd, $J = 8.7, 1.6$ Hz), 4.01 (qd, $J = 7.1, 2.7$ Hz, 2H), 1.22 (t, $J = 7.1$ Hz, 3H), 1.01 (t, $J = 7.1$ Hz, 3H). **¹³C-NMR** (101 MHz, CDCl_3) δ 167.98, 167.54, 136.09, 126.05, 123.12, 122.68, 120.14, 118.42, 111.60, 110.85, 110.83, 62.11, 61.95, 54.57, 34.96, 14.05, 13.79. **IR** (neat): 3407, 3123, 3060, 2981, 1722, 1621, 1550, 1461, 1423, 1371, 1233, 1177, 1155, 109.6, 1062, 1025, 909, 857, 823, 678 cm^{-1} . **HRMS** (ESI) m/z calculated for $\text{C}_{17}\text{H}_{20}\text{N}_2\text{O}_6\text{Na}$ ($[\text{M}+\text{Na}]^+$) 371.1214, found 371.1215. **Chiral HPLC** (Chiralpak AS-H, 4.6 \times 250 mm, 10 μm , *n*-heptan/*i*-PrOH = 70:30, 0.5 mL/min, $\lambda = 215$ nm): t_{R} (major) = 18.66 min, t_{R} (minor) = 15.71 min, 69% ee. **Specific rotation** $[\alpha]_{589}^{20} = +3.74^\circ$ ($c = 0.5$, CH_2Cl_2).

5.2.5 Synthesis of γ -amino acid 4-amino-3-(2-methyl-1*H*-indol-3-yl)butanoic acid

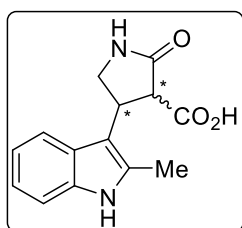
Rac. Ethyl 4-(2-methyl-1*H*-indol-3-yl)-2-oxopyrrolidine-3-carboxylate (**61**)



A 100 mL round bottom flask, equipped with a stir bar, was charged with racemic **58I** (230 mg, 635 μ mol, 1.0 equiv), NiCl₂·6 H₂O (151 mg, 635 μ mol, 1.0 equiv) and MeOH (3.3 mL). The suspension was cooled to 0 °C and NaBH₄ (288 mg, 7.62 mmol, 12.0 equiv) was added. After stirring for 6 h at room temperature the reaction mixture was quenched with sat. NH₄Cl solution and diluted with CHCl₃ (20 mL). The organic layer was separated and dried over MgSO₄, filtrated and the solvent was removed under reduced pressure. **61** was obtained as a beige solid (159 mg, 555 μ mol, 87%).

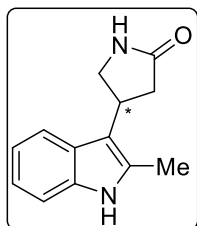
¹H-NMR (400 MHz, CDCl₃) δ 7.90 (s, 1H), 7.49 (d, *J* = 7.8 Hz, 1H), 7.35 – 7.29 (m, 1H), 7.19 – 7.05 (m, 2H), 6.37 (s, 1H), 4.46 – 4.34 (m, 1H), 4.28 – 4.09 (m, 2H), 3.90 (d, *J* = 10.3 Hz, 1H), 3.82 (t, *J* = 9.3 Hz, 1H), 3.66 (t, *J* = 9.4 Hz, 1H), 2.44 (s, 3H), 1.24 (t, *J* = 7.2 Hz, 3H). **¹³C-NMR** (101 MHz, CDCl₃) δ 172.95, 169.76, 135.74, 132.68, 126.46, 121.55, 119.79, 118.36, 110.99, 110.11, 109.02, 61.85, 53.42, 45.59, 36.04, 14.27, 11.91. **IR** (neat): 3384, 3228, 2919, 1674, 1491, 1461, 1439, 1349, 1301, 1267, 1156, 1103, 1077, 1040, 854, 742, 686 cm⁻¹. **HRMS** (ESI) *m/z* calculated for C₁₆H₁₉N₂O₃ ([M+H]⁺) 287.1390, found 287.1395. **Mp**: 119 °C.

Rac. 4-(2-methyl-1*H*-indol-3-yl)-2-oxopyrrolidine-3-carboxylic acid (**62**)



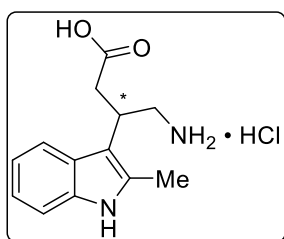
A 10 mL round bottom flask, equipped with a magnetic stirring bar, was charged with **61** (118 mg, 412 μ mol, 1.0 equiv) and was dissolved in EtOH (1.7 mL). 1 M NaOH solution (0.5 mL) was added and the reaction mixture was stirred for 24 h at room temperature. The resulting mixture was diluted with H₂O (2 mL) and 1 M HCl was added to adjust a pH of 5. The solvents were removed under reduced pressure and the residue was dissolved in EtOH, filtrated and the solvent was removed under reduced pressure to give **62** (94.0 mg, 365 μ mol, 93%) as a beige solid.

¹H-NMR (400 MHz, CD₃OD) δ 7.39 (d, *J* = 7.8 Hz, 1H), 7.24 (d, *J* = 8.0 Hz, 1H), 7.07 – 6.80 (m, 2H), 4.25 (s, 1H), 3.90 – 3.50 (m, 3H), 2.35 (s, 3H). **¹³C-NMR** (101 MHz, CD₃OD) δ 175.58, 173.35, 137.49, 134.05, 127.50, 121.61, 119.77, 118.68, 111.98, 109.04, 55.50, 47.03, 37.95, 11.43. **IR** (neat): 3396, 3280, 2363, 1685, 1487, 1439, 1353, 1327, 1226, 1021, 1096, 1055, 921, 753, 682 cm⁻¹. **HRMS** (ESI) *m/z* calculated for C₁₄H₁₅N₂O₃ ([M+H]⁺) 259.1077, found 259.1081. **Mp**: 192 °C.

Rac. 4-(2-methyl-1H-indol-3-yl)pyrrolidin-2-one (63)

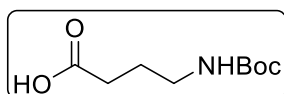
A 10 mL round bottom flask was charged with **62** (84.0 mg, 325 μmol , 1.0 equiv) and was heated with a heat gun for 60 seconds (heat gun temperature 290 $^{\circ}\text{C}$). No further purification was needed. **63** was obtained as a light brown solid (67.0 mg, 313 μmol , 96%).

$^1\text{H-NMR}$ (400 MHz, CDCl_3) δ 8.29 (s, 1H), 7.53 (d, $J = 7.8$ Hz, 1H), 7.30 (d, $J = 7.9$ Hz, 1H), 7.17 – 7.11 (m, 1H), 7.11 – 7.05 (m, 1H), 6.93 (s, 1H), 3.97 – 3.85 (m, 1H), 3.76 – 3.69 (m, 1H), 3.68 – 3.62 (m, 1H), 2.86 (dd, $J = 17.3, 9.5$ Hz, 1H), 2.65 (dd, $J = 17.3, 9.7$ Hz, 1H), 2.39 (s, 3H). **$^{13}\text{C-NMR}$** (101 MHz, CDCl_3) δ 178.88, 135.69, 131.51, 126.50, 121.25, 119.41, 118.48, 111.02, 110.89, 48.11, 36.70, 31.66, 11.97. **IR** (neat): 3396, 3280, 2363, 1685, 1487, 1439, 1353, 1327, 1226, 1021, 1096, 1055, 921, 753, 682 cm^{-1} . **HRMS** (ESI) m/z calculated for $\text{C}_{13}\text{H}_{15}\text{N}_2\text{O}$ ($[\text{M}+\text{H}]^+$) 215.1179, found 215.1182. **Mp**: 90 $^{\circ}\text{C}$.

Rac. 4-amino-3-(2-methyl-1H-indol-3-yl)butanoic acid hydrochloride (64)

A 5 mL round bottom flask, equipped with a magnetic stirring bar, was charged with **63** (21.0 mg, 98.0 μmol , 1.0 equiv) and 6 M HCl (0.5 mL). The reaction mixture was stirred for 24 h at room temperature, the solvent was removed under reduced pressure and **64** was obtained as a brown solid (16 mg, 60.0 μmol , 62%).

$^1\text{H-NMR}$ (300 MHz, CD_3OD) δ 7.57 – 7.49 (m, 1H), 7.28 – 7.20 (m, 1H), 7.03 – 6.87 (m, 2H), 3.58 – 3.45 (m, 1H), 3.28 – 3.10 (m, 2H), 2.83 (dd, $J = 14.8, 9.1$ Hz, 1H), 2.59 (dd, $J = 14.8, 5.7$ Hz, 1H), 2.43 (s, 3H). **$^{13}\text{C-NMR}$** (75 MHz, CD_3OD) δ 179.63, 136.14, 132.62, 126.68, 119.94, 118.11, 118.06, 110.25, 109.43, 44.21, 41.96, 35.40, 10.50. **IR** (neat): 3392, 3213, 3053, 2919, 1558, 1461, 1394, 1304, 1245, 1156, 1129, 1100, 1018, 947, 850, 742, 686 cm^{-1} . **HRMS** (ESI) m/z calculated for $\text{C}_{13}\text{H}_{17}\text{N}_2\text{O}_2$ ($[\text{M}+\text{H}]^+$) 233.1285, found 233.1290. **Mp**: 169 $^{\circ}\text{C}$.

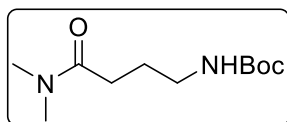
5.2.6 Amide Synthesis**4-((*tert*-Butoxycarbonyl)amino)butanoic acid (69)^[93]**

A 250 mL round bottom flask was charged with γ -aminobutyric acid (5.00 g, 48.5 mmol, 1.0 equiv) and was dissolved in H_2O (60 mL) and dioxane (120 mL). Subsequently K_2CO_3 (13.4 g, 97.0 mmol, 2.0 equiv) was added, the resulting solution was cooled to 0 $^{\circ}\text{C}$ in an ice bath and di-*tert*-butyl dicarbonate (11.6 g, 53.3 mmol, 1.1 equiv) was added. The reaction mixture was warmed to

room temperature and was stirred for 3 h. The solvent was removed under reduced pressure, the crude mixture dissolved in H₂O (140 mL) and washed with EtOAc (2 × 250 mL). The aqueous layer was again cooled to 0 °C and acidified by 1 M HCl (approx. 190 mL) to pH 3. The aqueous phase was extracted with EtOAc (5 × 250 mL), the combined organic layers were dried over MgSO₄, filtered and the solvent was removed under reduced pressure to give **69** (9.79 g, 48.2 mmol, 99%) as a colorless oil.

¹H-NMR (400 MHz, CDCl₃) δ 8.75 (bs, 1H), 6.04 (bs, 0.34H), 4.80 (bs, 0.64H), 3.10 (s, 2H), 2.31 (t, *J* = 7.3 Hz, 2H), 1.37 (s, 9H). **¹³C-NMR** (101 MHz, CDCl₃) δ 178.16, 156.34, 79.56, 39.89, 31.35, 28.43, 25.17.

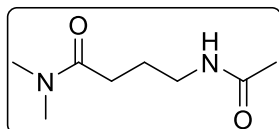
tert-Butyl (4-(dimethylamino)-4-oxobutyl)carbamate (70)^[93]



A 500 mL round bottom flask was charged with **69** in DMF (200 mL), NHS (4.25 g, 36.9 mmol, 1.5 equiv) and DCC (6.35 g, 30.8 mmol, 1.25 equiv) were added subsequently and the mixture was stirred under N₂ atmosphere for 1 h. Thereafter, dimethylamine hydrochloride (6.02 g, 73.8 mmol, 3.0 equiv) and NEt₃ (13 mL) were added and the mixture was stirred for 20 h under N₂ atmosphere. The formed precipitate was filtered off and the solvent of the filtrate was removed under reduced pressure. The residue was purified by three columns on flash silica (first column: CHCl₃/MeOH 96:4, second column: EtOAc followed by CHCl₃/MeOH 97:3, third column: EtOAc) to give **70** (3.95 g, 17.2 mmol, 70%) as a colorless oil.

¹H-NMR (400 MHz, CDCl₃) δ 4.62 (bs, 1H), 3.17 (t, *J* = 6.7 Hz, 2H), 3.01 – 2.93 (m, 6H), 2.36 (t, *J* = 7.2 Hz, 2H), 1.83 (p, *J* = 7.0 Hz, 2H), 1.43 (s, 9H). **¹³C-NMR** (101 MHz, CDCl₃) δ 172.73, 156.27, 79.25, 40.61, 30.72, 28.56, 25.36.

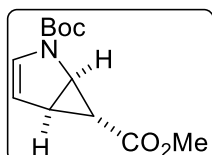
***N*-Acetyl-γ-aminobutyric acid *N,N'*-dimethylamide / 4-Acetamido-*N,N*-dimethylbutanamide (68)^[93]**



A 100 mL round bottom flask was charged with **70** (1.19 g, 5.17 mmol, 1.0 equiv), 4.2 M HCl in dioxane (35 mL) was added and the resulting mixture was stirred for 1 h under N₂ atmosphere. The solvent was removed under reduced pressure, the resulting precipitate was dissolved in dioxane (35 mL) and NEt₃ (2.09 g, 2.9 mL, 20.7 mmol, 4.0 equiv) was added. The reaction mixture was cooled to 0 °C in an ice bath and acetyl chloride (1.08 g, 981 μL, 13.7 mmol, 2.7 equiv) was added dropwise under N₂ atmosphere. The mixture was allowed to warm to room temperature and was stirred for 20 h under N₂ atmosphere. The formed precipitate was filtered off and the solvent of the filtrate was removed under reduced pressure. The residue was purified by four

columns on flash silica (first and second columns: CHCl₃/MeOH 95:5, third and fourth columns: EtOAc followed by CHCl₃/MeOH 95:5) to give **68** (399 mg, 2.32 mmol, 45%) as a colorless oil. ¹H-NMR (400 MHz, CDCl₃) δ 6.60 (bs, 1H), 3.27 (t, *J* = 6.6 Hz, 2H), 3.00 (s, 3H), 2.94 (s, 3H), 2.39 (t, *J* = 6.6 Hz, 2H), 1.95 (s, 3H), 1.86 (p, *J* = 6.6 Hz, 2H). ¹³C-NMR (101 MHz, CDCl₃) δ 173.09, 170.57, 39.96, 37.45, 35.72, 31.36, 24.07, 23.32.

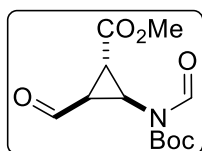
2-(*tert*-Butyl) 6-methyl-2-azabicyclo[3.1.0]hex-3-ene-2,6-dicarboxylate (**72**)^[26]



A flame dried Schlenk tube was charged with Cu(OTf)₂ (637 mg, 1.76 mmol, 0.02 equiv) in anhydrous CH₂Cl₂ (10 mL) and stirred for 30 min under N₂ atmosphere at room temperature. Another flame dried 500 mL Schlenk flask was charged with *N*-Boc-pyrrole (14.7 g, 88.0 mmol, 1.0 equiv) in anhydrous CH₂Cl₂ (100 mL) under N₂ atmosphere. The Cu(OTf)₂ solution was added in one portion and PhNHNH₂ (190 mg, 1.76 mmol, 0.02 equiv) was added dropwise. A solution of methyl diazoacetate (10.6 g, 106 mmol, 1.2 equiv) in CH₂Cl₂ (80 mL) was added slowly by an electronically controlled dropping system for 5 d. The resulting mixture was filtered through basic alumina and washed with CH₂Cl₂ (800 mL). The solvent was removed under reduced pressure and the crude mixture was purified on flash silica (hexanes/EtOAc 50:1) to give **72** (7.09 g, 29.6 mmol, 34%) as a colorless oil.

¹H-NMR (300 MHz, CDCl₃) δ 6.66 – 6.35 (m, 1H), 5.47 – 5.27 (m, 1H), 4.52 – 4.22 (m, 1H), 3.75 – 3.60 (m, 3H), 2.87 – 2.74 (m, 1H), 1.50 (s, 9H), 1.00 – 0.95 (m, 1H) (signal broadening and doubling due to rotamers).

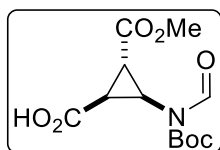
Methyl-2-(*N*-(*tert*-butoxycarbonyl)formamido)-3-formylcyclopropane-1-carboxylate (**73**)^[26]



A 250 mL round bottom flask was charged with **72** (1.50 g, 6.27 mmol, 1.0 equiv) in CH₂Cl₂ (170 mL) and the solution was treated with ozone at -78 °C until the solution maintained a deep blue color. The excess of ozone was removed by passing oxygen through the solution, dimethyl sulfide (1.95 g, 31.4 mmol, 5.0 equiv) was added and the resulting mixture was stirred for 16 h at room temperature. The solvent was removed under reduced pressure and the crude product was purified on flash silica (hexanes/EtOAc 5:1) to give **73** (1.51 g, 5.58 mmol, 89%) as a colorless solid.

¹H-NMR (400 MHz, CDCl₃) δ 9.53 (s, 1H), 9.07 (s, 1H), 3.75 (s, 3H), 3.24 – 3.16 (m, 1H), 3.00 – 2.91 (m, 1H), 2.80 – 2.70 (m, 1H), 1.52 (s, 9H). ¹³C-NMR (101 MHz, CDCl₃) δ 193.19, 170.10, 163.50, 152.01, 85.50, 52.72, 36.78, 35.06, 27.99, 27.89.

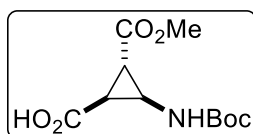
2-(*N*-(*tert*-Butoxycarbonyl)formamido)-3-(methoxycarbonyl)cyclopropane-1-carboxylic acid (74**)^[26]**



A 100 mL round bottom flask was charged with **73** (1.00 g, 3.69 mmol, 1.0 equiv) in CH₃CN and cooled to 0 °C. A solution of KH₂PO₄ (301 mg, 2.21 mmol, 0.6 equiv in 2.3 mL H₂O) and H₂O₂ (35%, 1.1 mL) were added. NaClO₂ (733 mg, 8.11 mmol, 2.2 equiv in 6.8 mL H₂O) was added and the mixture was stirred for 2 h at room temperature. Then Na₂SO₃ (372 mg, 2.95 mmol, 0.8 equiv) was added and stirred for 1 h. After addition of 1 M KHSO₄ (8 mL) the solution was extracted with EtOAc (3 × 30 mL). The combined organic layers were dried over Na₂SO₄, filtered and the solvent was removed under reduced pressure to give **74** (1.06, 3.69 mmol, 100%) as a colorless oil.

¹H-NMR (400 MHz, CDCl₃) δ 9.13 (s, 1H), 3.78 (s, 3H), 3.23 (dd, *J* = 7.7, 5.0 Hz, 1H), 2.70 – 2.64 (m, 1H), 2.64 – 2.58 (m, 1H), 1.52 (s, 9H). ¹³C-NMR (101 MHz, CDCl₃) δ 173.16, 170.04, 163.45, 152.05, 85.35, 52.86, 36.03, 29.71, 27.94, 27.91.

2-((*tert*-Butoxycarbonyl)amino)-3-(methoxycarbonyl)cyclopropane-1-carboxylic acid (75**)^[26]**

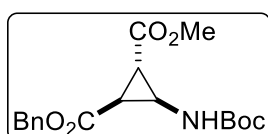


A 25 mL round bottom flask was charged with **74** (1.06 g, 3.69 mmol, 1.0 equiv) in MeCN (12 mL) and DEAEA (879 mg, 7.56 mmol, 2.1 equiv). The resulting mixture was stirred for 24 h at room temperature, the solvent was removed under reduced pressure, EtOAc was added and the solution was adjusted to pH 2 with 1 M KHSO₄. The aqueous layer was extracted with EtOAc (4 × 30 mL) and the combined organic layers were dried over Na₂SO₄, filtered and the solvent was removed under reduced pressure to give **75** (794 mg, 3.06 mmol, 83%) as a colorless solid.

¹H-NMR (400 MHz, CDCl₃) δ 10.09 (bs, 1H), 6.76 (s, 0.65H), 5.51 (s, 0.35H), 3.89 (s, 0.36H), 3.72 (s, 3H), 3.44 (s, 0.64H), 2.50 – 2.38 (m, 1H), 2.31 (t, *J* = 5.0 Hz, 1H), 1.47 (s, 9H).

¹³C-NMR (101 MHz, CDCl₃) δ 172.16, 170.61, 158.41, 82.54, 52.48, 37.65, 29.61, 28.35, 26.97.

1-Benzyl 2-methyl-3-((*tert*-butoxycarbonyl)amino)cyclopropane-1,2-dicarboxylate (76**)^[26]**

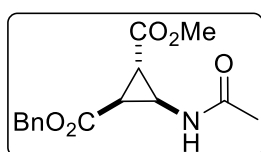


A 50 mL round bottom flask was charged with **75** (749 mg, 2.89 mmol, 1.0 equiv) in DMF (11 mL), NaHCO₃ (485 mg, 5.78 mmol, 2.0 equiv) and BnBr (544 mg, 3.18 mmol, 1.1 equiv) were added and the mixture was stirred at room temperature for 48 h. EtOAc (15 mL) and H₂O (15 mL) were added, the

phases separated and the aqueous layer was extracted with EtOAc (3 × 30 mL). The combined organic layers were washed with H₂O, dried over Na₂SO₄, filtered and the solvent was removed under reduced pressure. The crude mixture was purified on flash silica (hexanes/EtOAc 5:1) to give **76** (1.01 g, 2.89 mmol, 100%) as a colorless solid.

¹H-NMR (400 MHz, CDCl₃) δ 7.44 – 7.29 (m, 5H), 5.52 (s, 1H), 5.21 (d, *J* = 12.2 Hz, 1H), 5.13 (d, *J* = 12.3 Hz, 1H), 3.86 (s, 1H), 3.69 (s, 3H), 2.52 (dd, *J* = 8.4, 5.3 Hz, 1H), 2.32 – 2.25 (m, 1H), 1.44 (s, 9H). **¹³C-NMR** (101 MHz, CDCl₃) δ 169.90, 155.18, 134.91, 128.48, 128.36, 128.16, 80.16, 67.16, 52.16, 37.40, 28.63, 28.09, 26.06, 23.65.

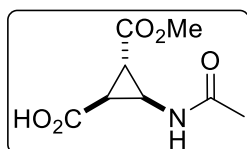
1-Benzyl 2-methyl-3-acetamidocyclopropane-1,2-dicarboxylate (**77**)^[94]



A 25 mL round bottom flask was charged with **76** (500 mg, 1.43 mmol, 1.0 equiv), 3 M HCl (4.3 mL in EtOAc) and was stirred at 0 °C for 3 h. The solvent was removed under reduced pressure and the salt was resuspended in CH₂Cl₂ (25 mL). Then, acetyl chloride (202 mg, 2.58 mmol, 1.8 equiv) was added, cooled to 0 °C and NEt₃ (463 mg, 4.58 mmol, 3.2 equiv) was added dropwise. The resulting mixture was stirred at room temperature for 16 h. The solvent was removed under reduced pressure and the crude product was purified on flash silica (CHCl₃/MeOH 60:1) to give **77** (315 mg, 1.08 mmol, 76%) as colorless solid.

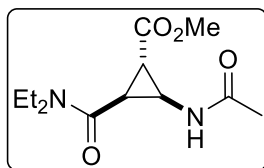
¹H-NMR (400 MHz, CDCl₃) δ 7.44 – 7.31 (m, 5H), 6.48 (d, *J* = 8.0 Hz, 1H), 5.22 (d, *J* = 12.2 Hz, 1H), 5.14 (d, *J* = 12.3 Hz, 1H), 4.16 (td, *J* = 8.3, 4.8 Hz, 1H), 3.70 (s, 3H), 2.56 (dd, *J* = 8.3, 5.1 Hz, 1H), 2.27 (t, *J* = 5.0 Hz, 1H), 1.96 (s, 3H). **¹³C-NMR** (101 MHz, CDCl₃) δ 170.61, 170.51, 169.93, 135.10, 128.86, 128.80, 128.51, 67.66, 52.59, 36.37, 29.00, 26.08, 23.43.

2-Acetamido-3-(methoxycarbonyl)cyclopropane-1-carboxylic acid (**78**)^[94]



A flame dried 25 mL Schlenk flask was charged with **77** (385 mg, 1.32 mmol, 1.0 equiv) in anhydrous MeOH (10 mL), 1,4-cyclohexadiene (106 mg, 1.32 mmol, 1.0 equiv) and Pd/C (10wt%, 80 mg) under N₂ atmosphere. The reaction mixture was stirred at room temperature for 16 h, then filtered through a pad of celite, washed with MeOH (15 mL) and the solvent was removed under reduced pressure to give **78** (220 mg, 1.09 mmol, 83%) as a colorless solid.

¹H-NMR (400 MHz, CD₃OD) δ 3.72 (s, 3H), 3.63 – 3.45 (m, 1H), 2.48 – 2.32 (m, 2H), 1.94 (s, 3H). **¹³C-NMR** (101 MHz, CD₃OD) δ 174.52, 174.41, 172.07, 52.92, 36.88, 28.75, 28.00, 22.39.

Methyl-2-acetamido-3-(diethylcarbamoyl)cyclopropane-1-carboxylate (79)^[94]

A 100 mL round bottom flask was charged with **78** (132 mg, 654 μmol , 1.0 equiv) in CH_2Cl_2 (40 mL) and DMF (2 mL). To this solution EDC hydrochloride (125 mg, 0.654 mmol, 1.0 equiv) and HOBt (88 mg, 654 μmol , 1.0 equiv) were added. The mixture was cooled in an ice bath and diethylamine (72 mg, 981 μmol , 1.5 equiv) was added and stirred at room temperature for 16 h. The solvent was removed under reduced pressure and the crude product was purified on flash silica ($\text{CHCl}_3/\text{MeOH}$ 50:1) to give **79** (143 mg, 558 μmol , 85%) as a colorless solid.

¹H-NMR (400 MHz, CDCl_3) δ 7.33 (d, $J = 8.1$ Hz, 1H), 4.01 (td, $J = 8.2, 4.4$ Hz, 1H), 3.66 (s, 3H), 3.48 (dq, $J = 14.4, 7.2$ Hz, 1H), 3.41 – 3.24 (m, 3H), 2.50 (dd, $J = 8.4, 5.3$ Hz, 1H), 2.29 (dd, $J = 5.2, 4.4$ Hz, 1H), 1.91 (s, 3H), 1.19 (t, $J = 7.2$ Hz, 3H), 1.08 (t, $J = 7.1$ Hz, 3H).

¹³C-NMR (101 MHz, CDCl_3) δ 171.03, 170.69, 167.21, 52.08, 42.46, 40.91, 36.39, 27.04, 25.12, 22.93, 14.45, 12.79.

5.3 NMR Spectra

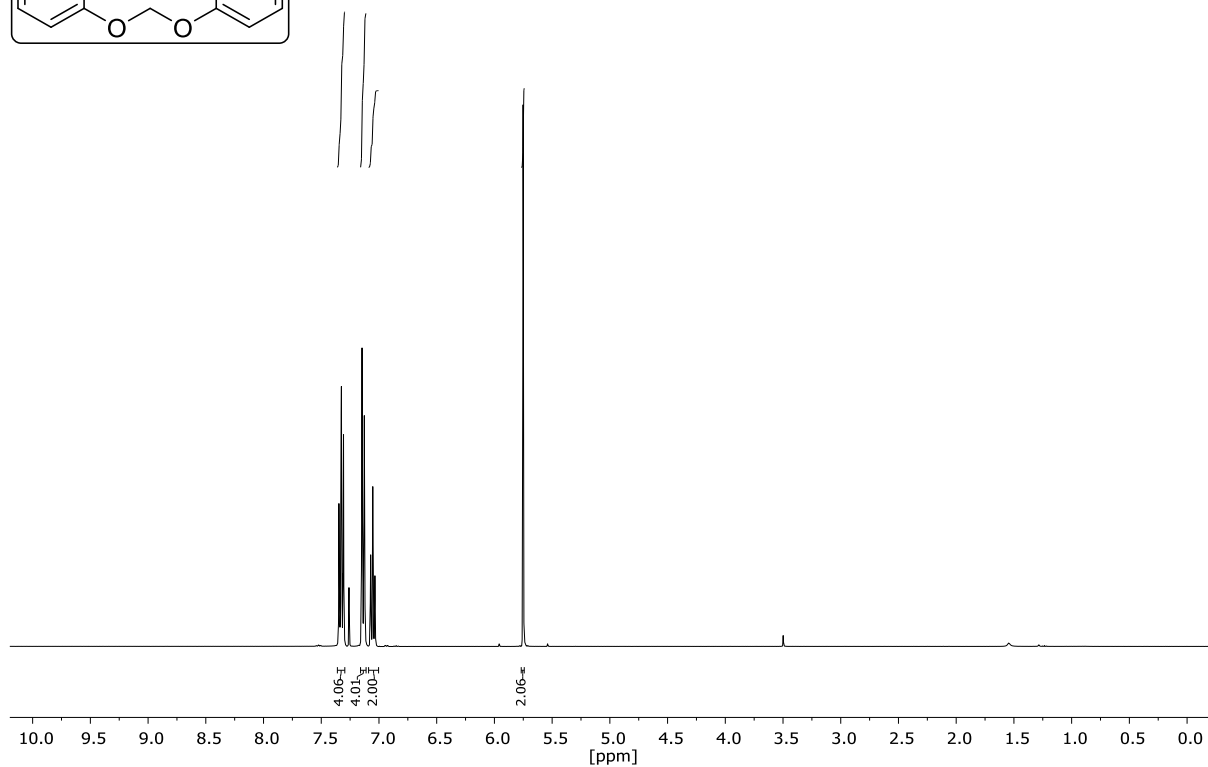
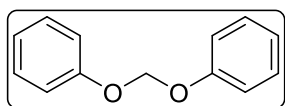
^1H -NMR

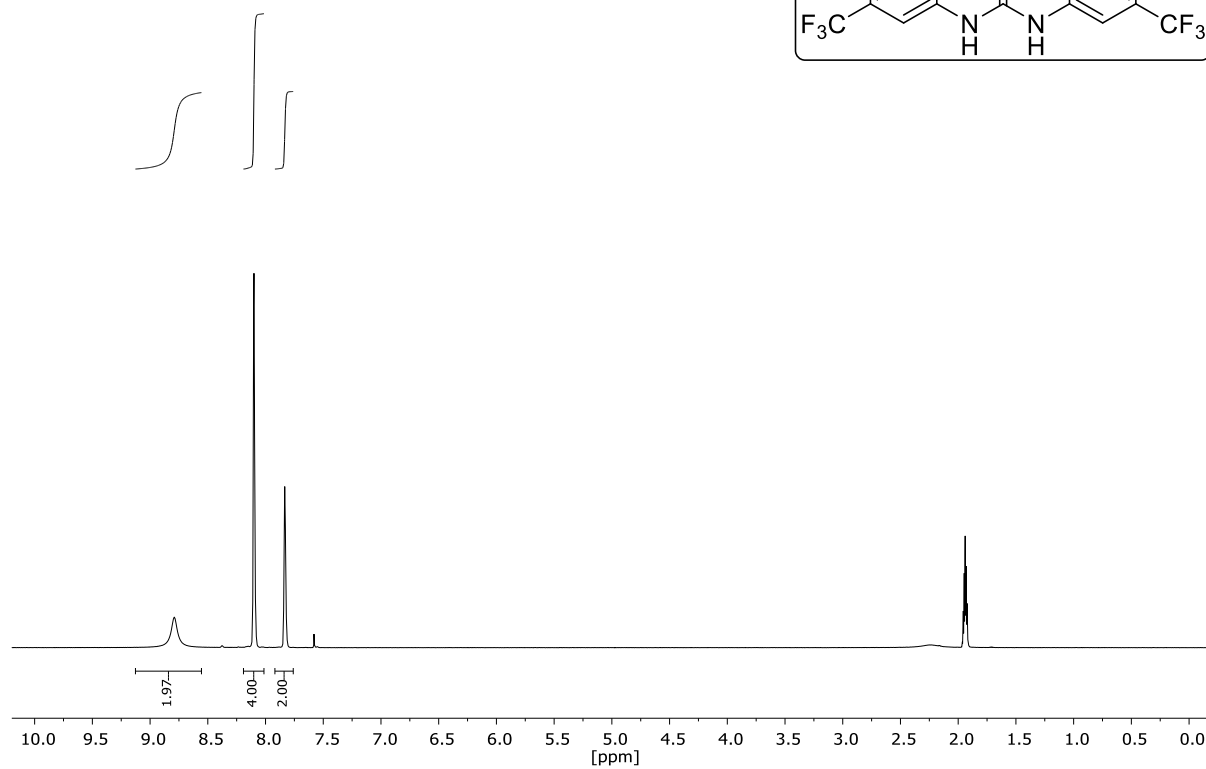
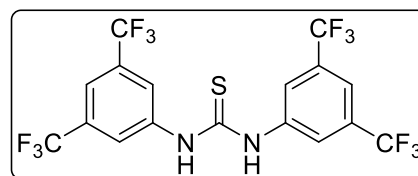
first image

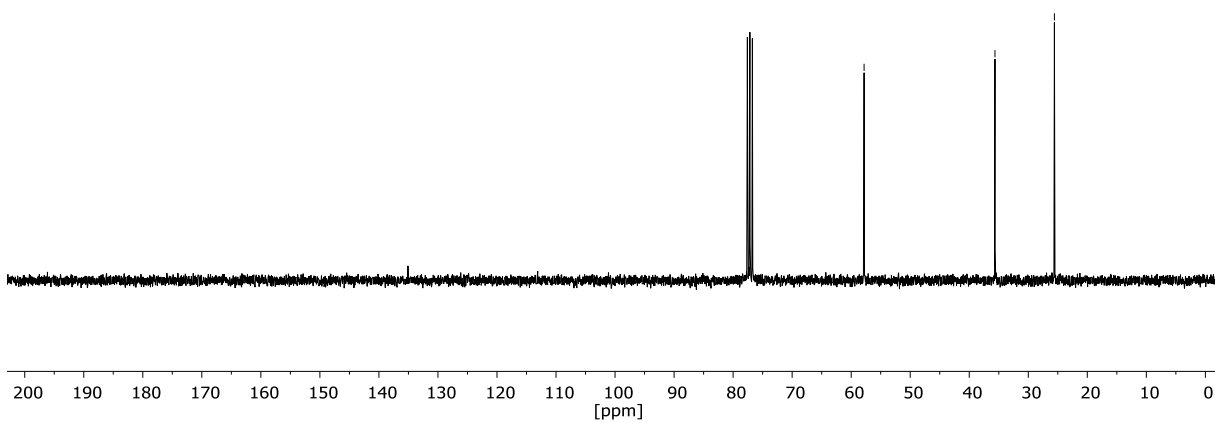
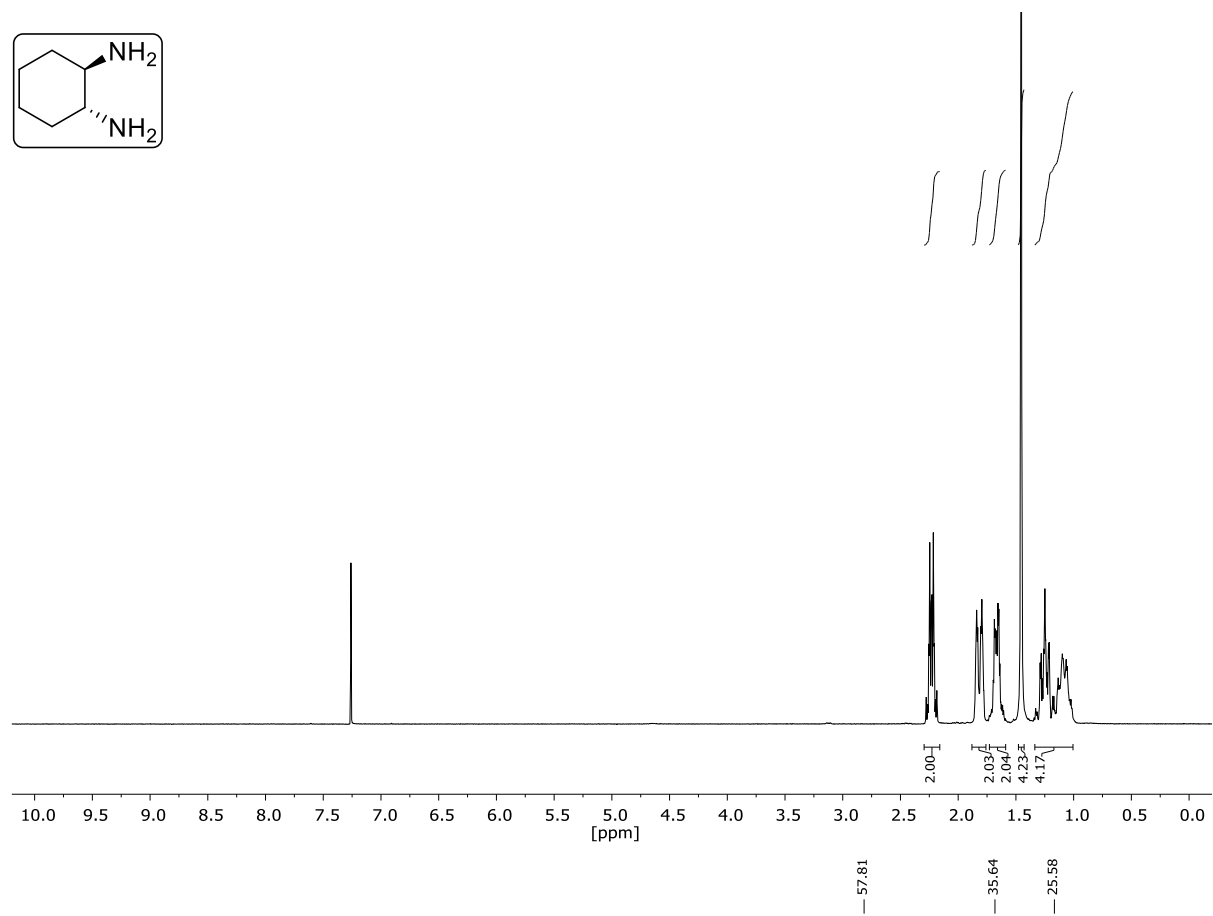
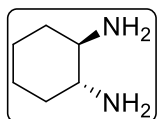
^{13}C -NMR

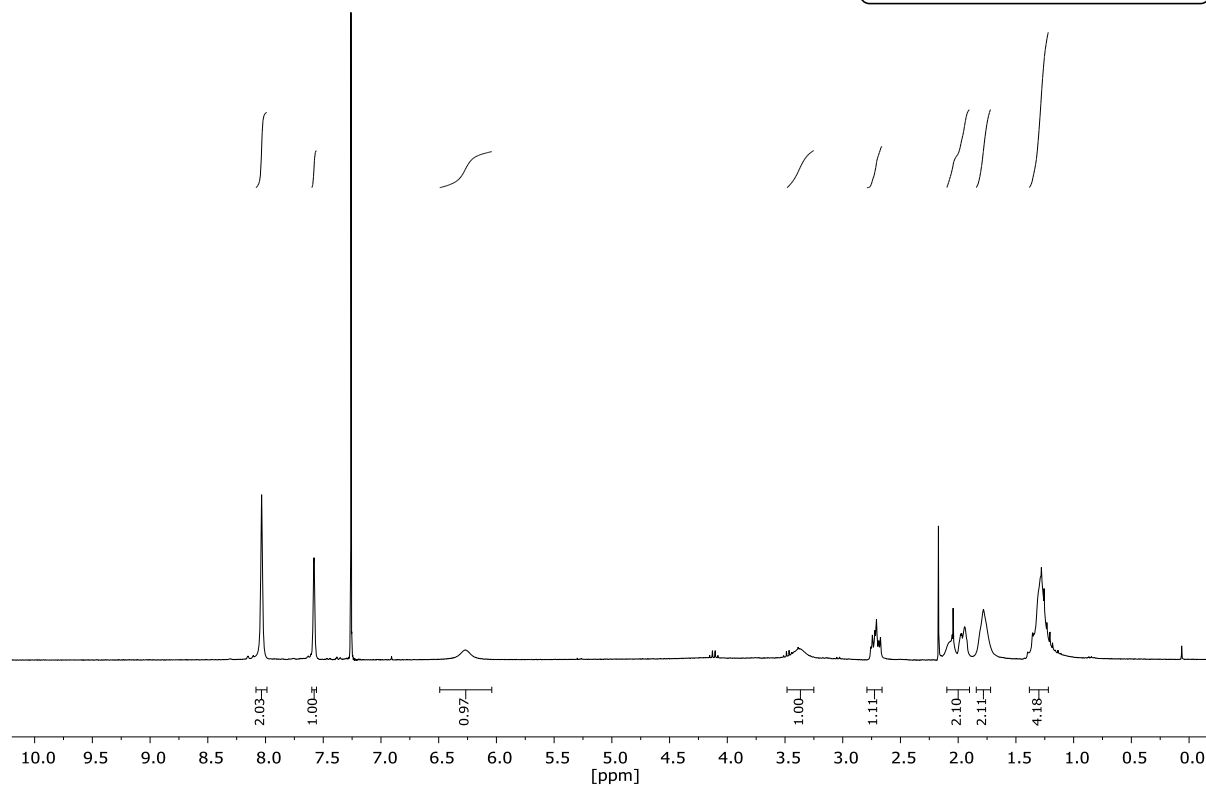
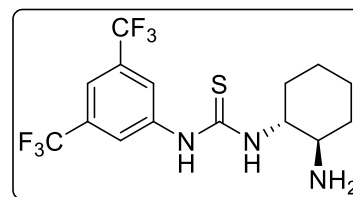
second image

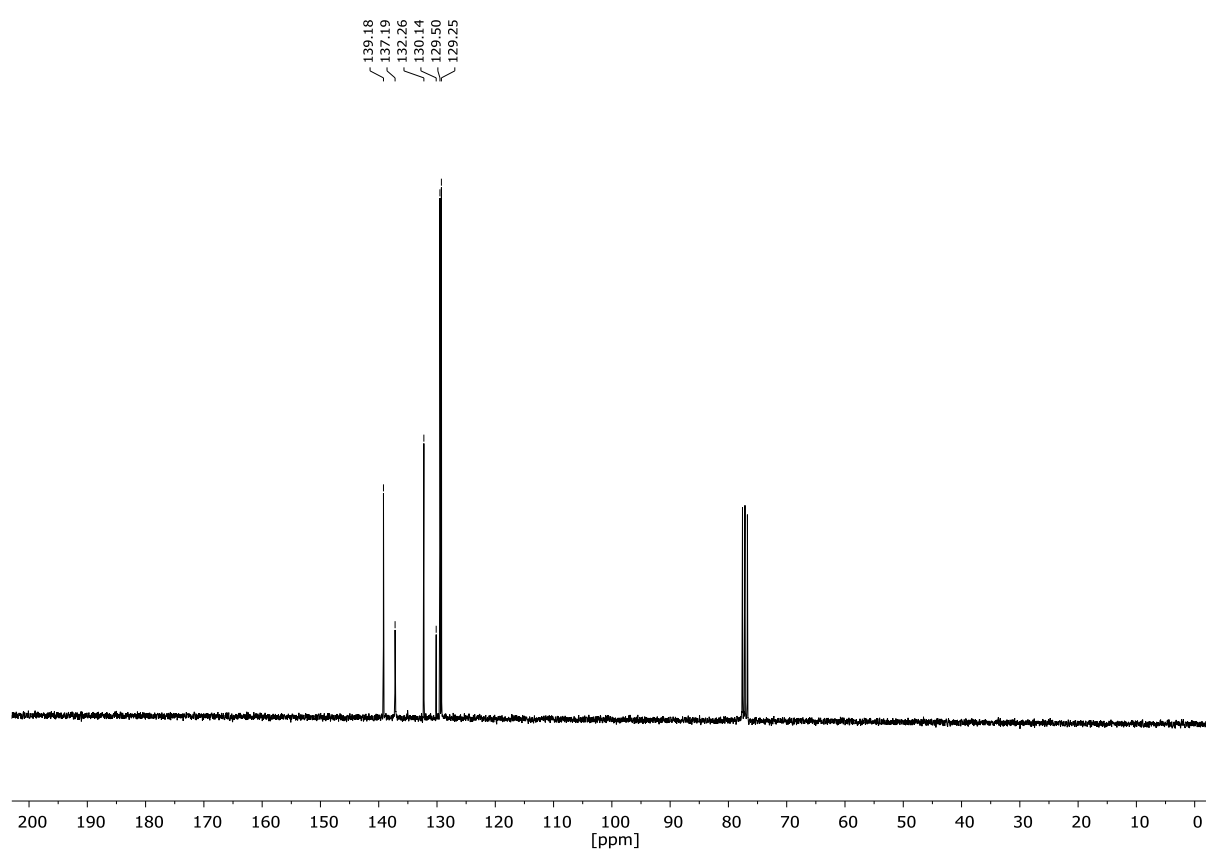
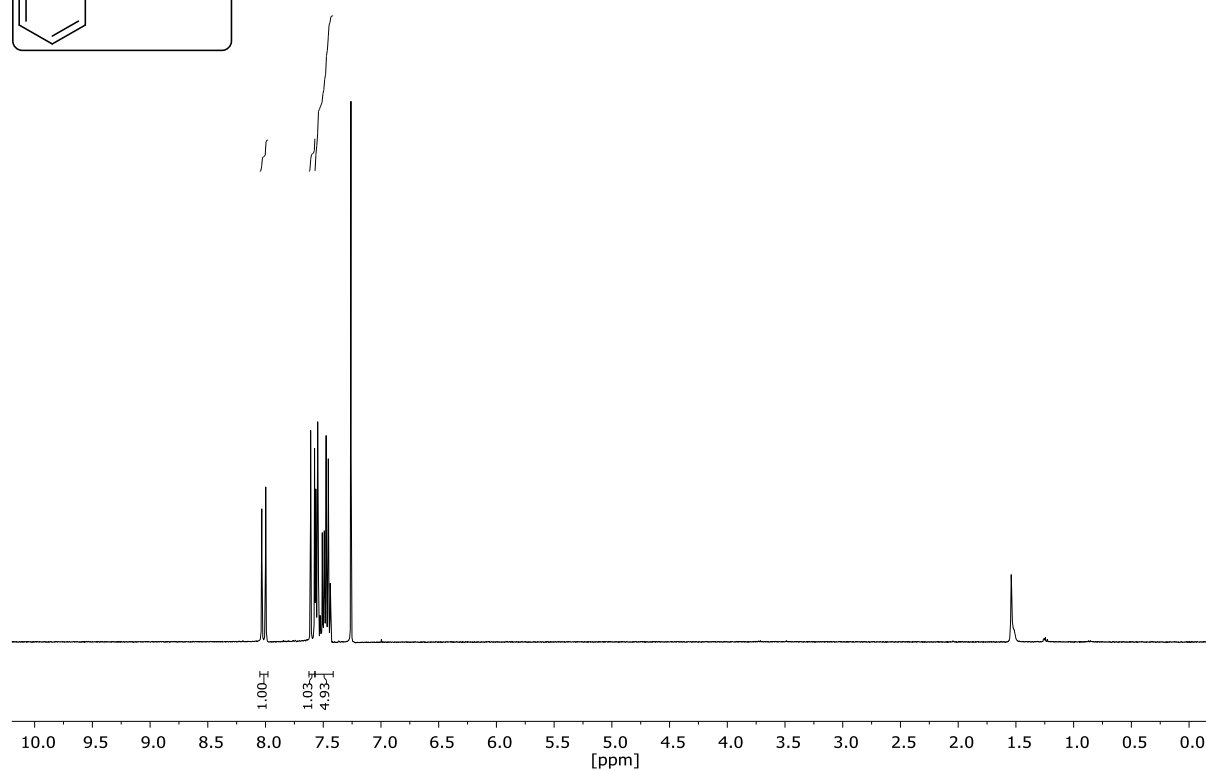
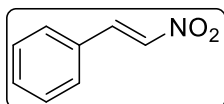
Diphenoxymethane (S1)

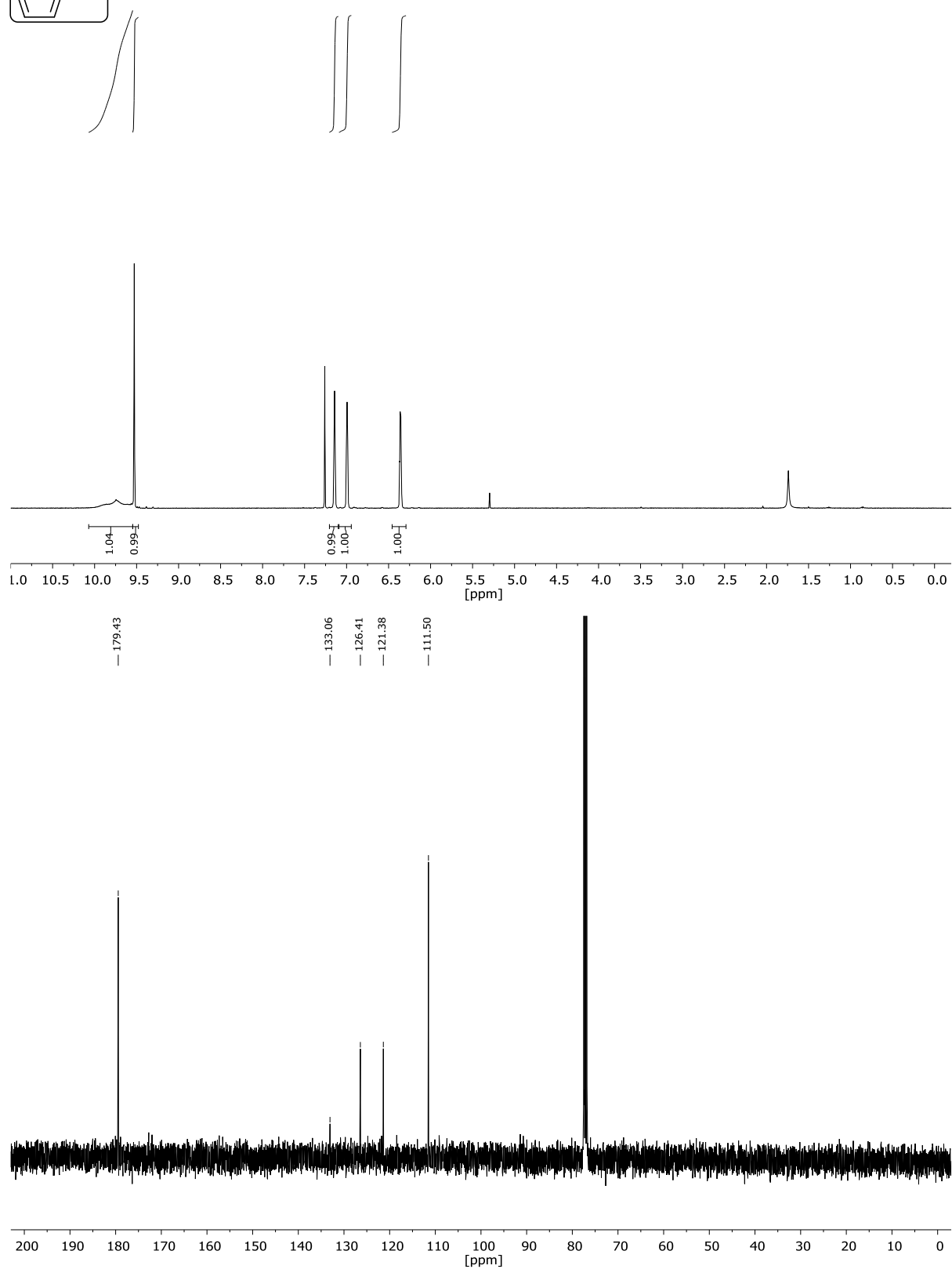
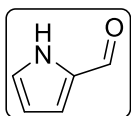
NMR-Solvent: CDCl₃

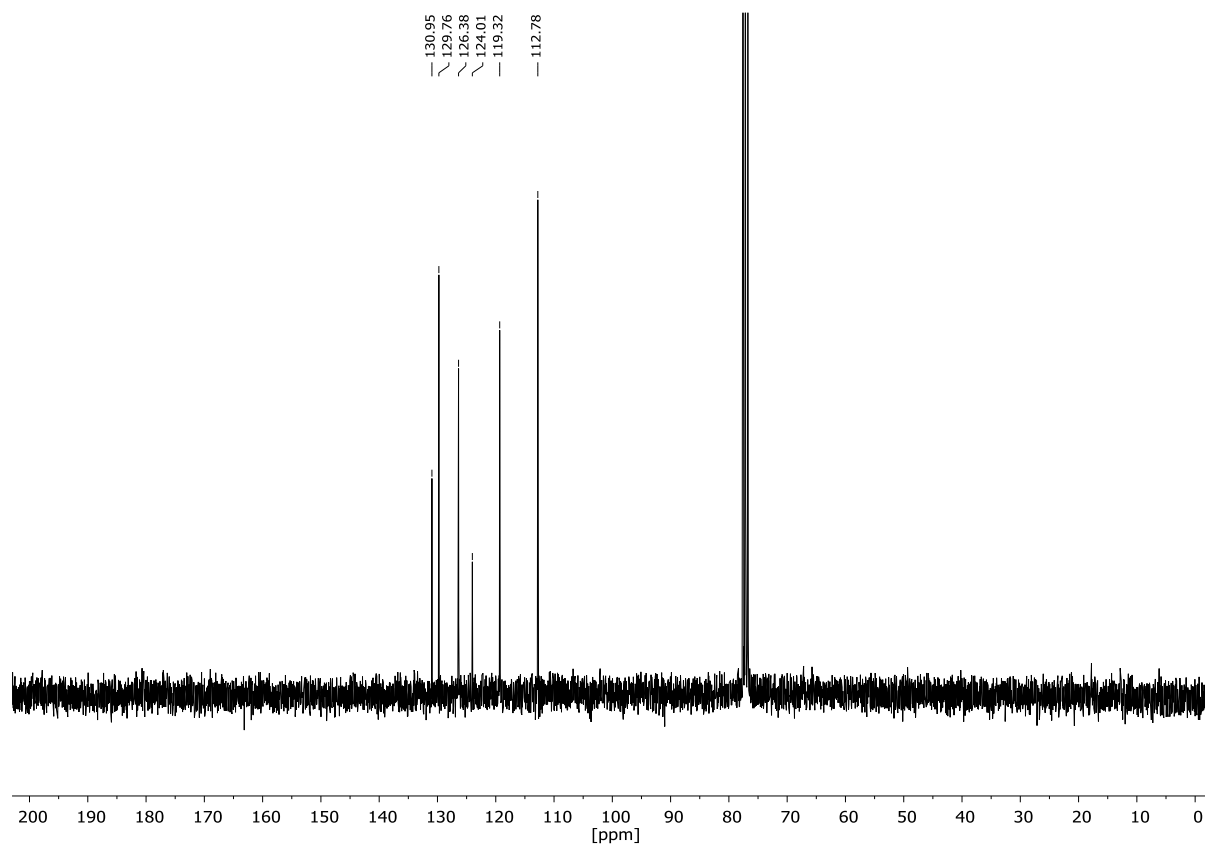
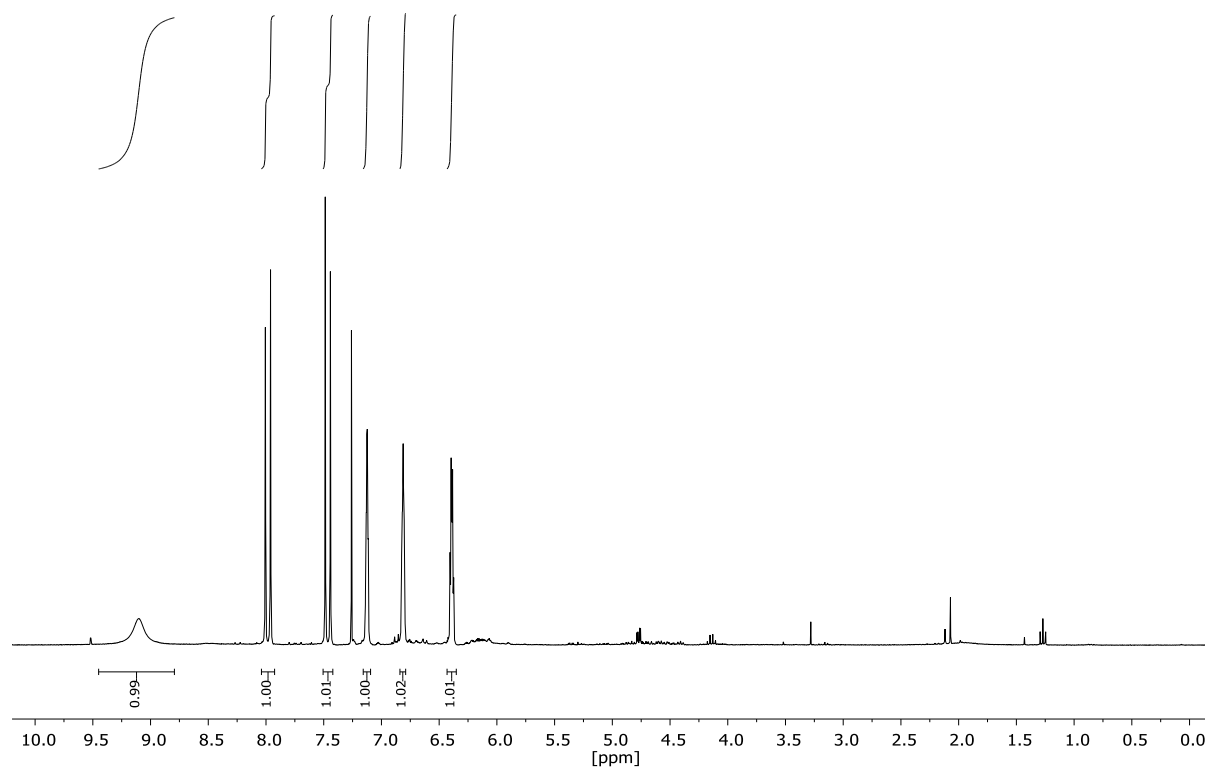
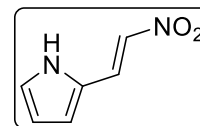
1,3-bis(3,5-bis(trifluoromethyl)phenyl)thiourea (42)NMR-Solvent: CD₃CN

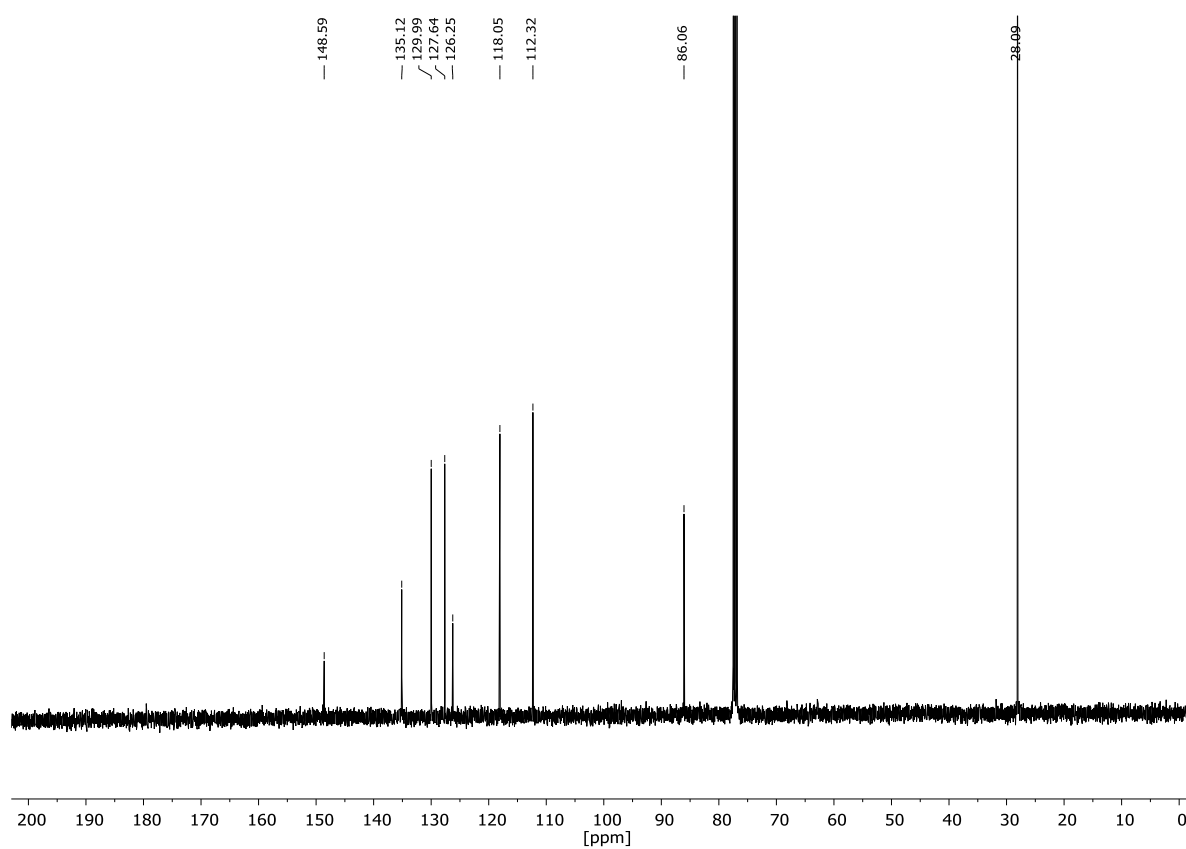
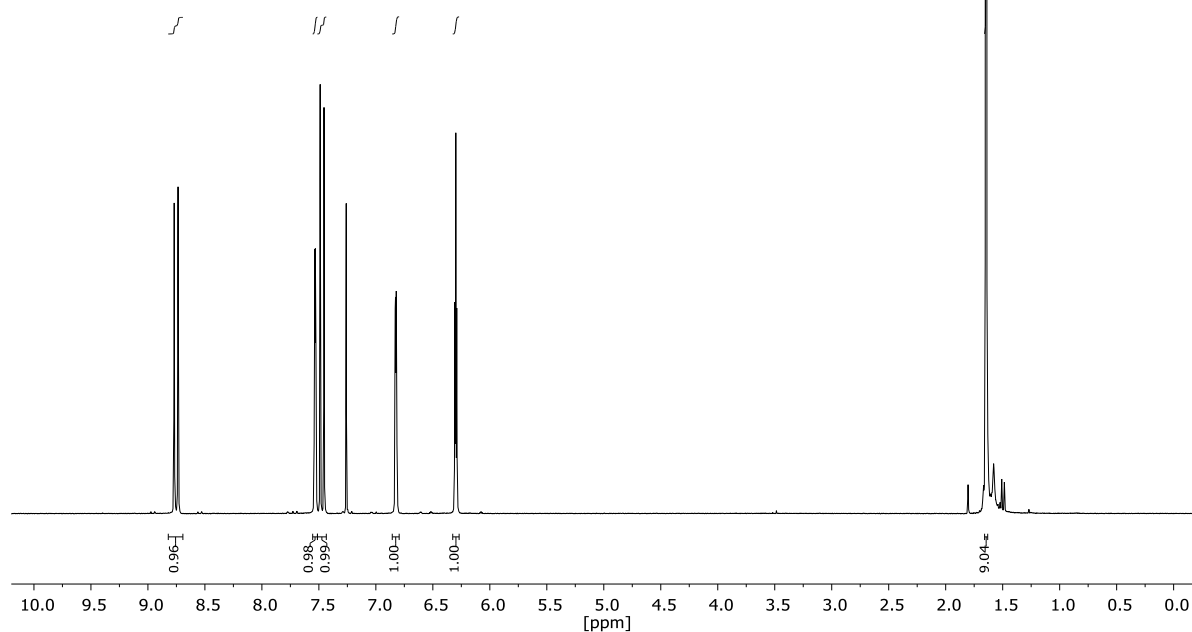
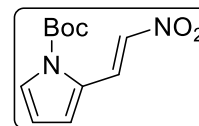
(1*R*,2*R*)-Cyclohexane-1,2-diamine (S3)NMR-Solvent: CDCl₃

1-((1*R*,2*R*)-2-Aminocyclohexyl)-3-(3,5-bis(trifluoromethyl)phenyl)thiourea (46)NMR-Solvent: CDCl₃

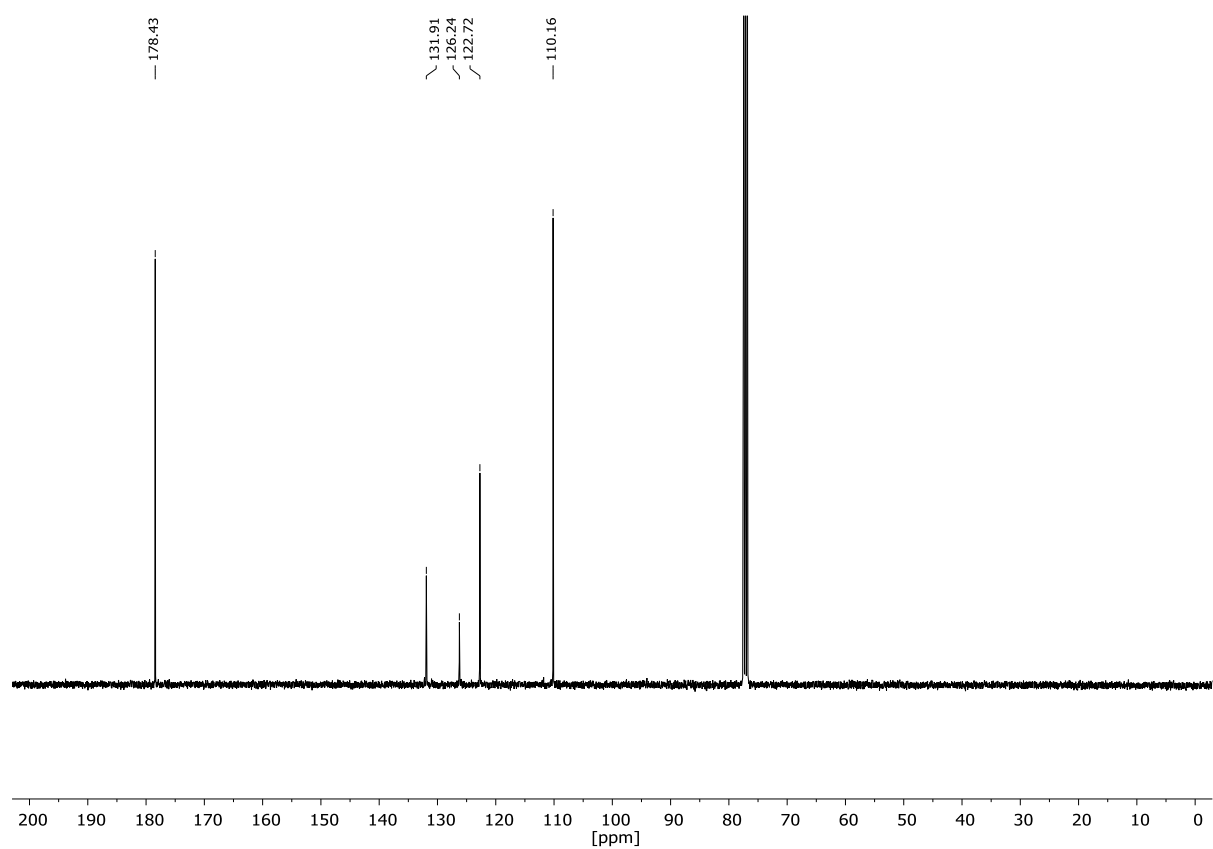
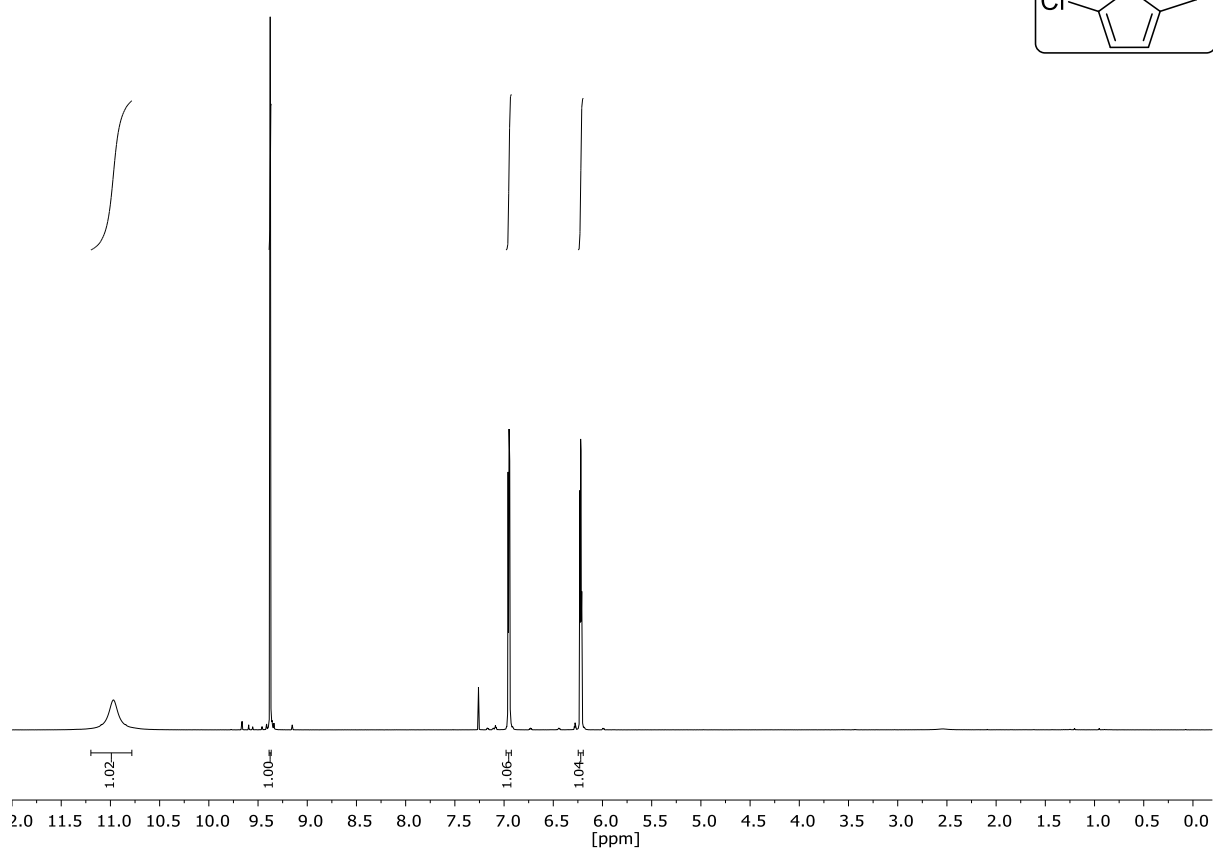
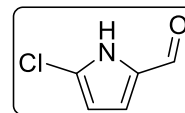
(E)-(2-Nitrovinyl)benzene (56a)NMR-Solvent: CDCl₃

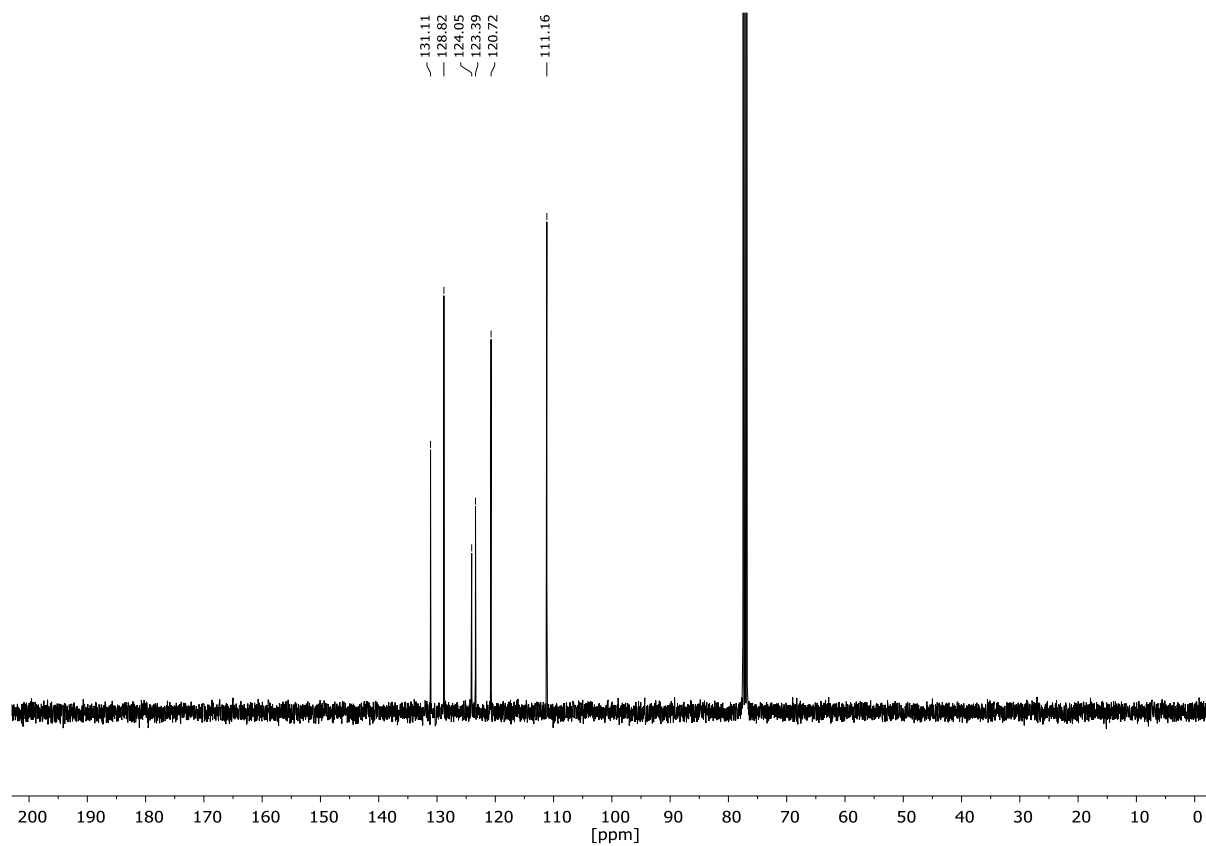
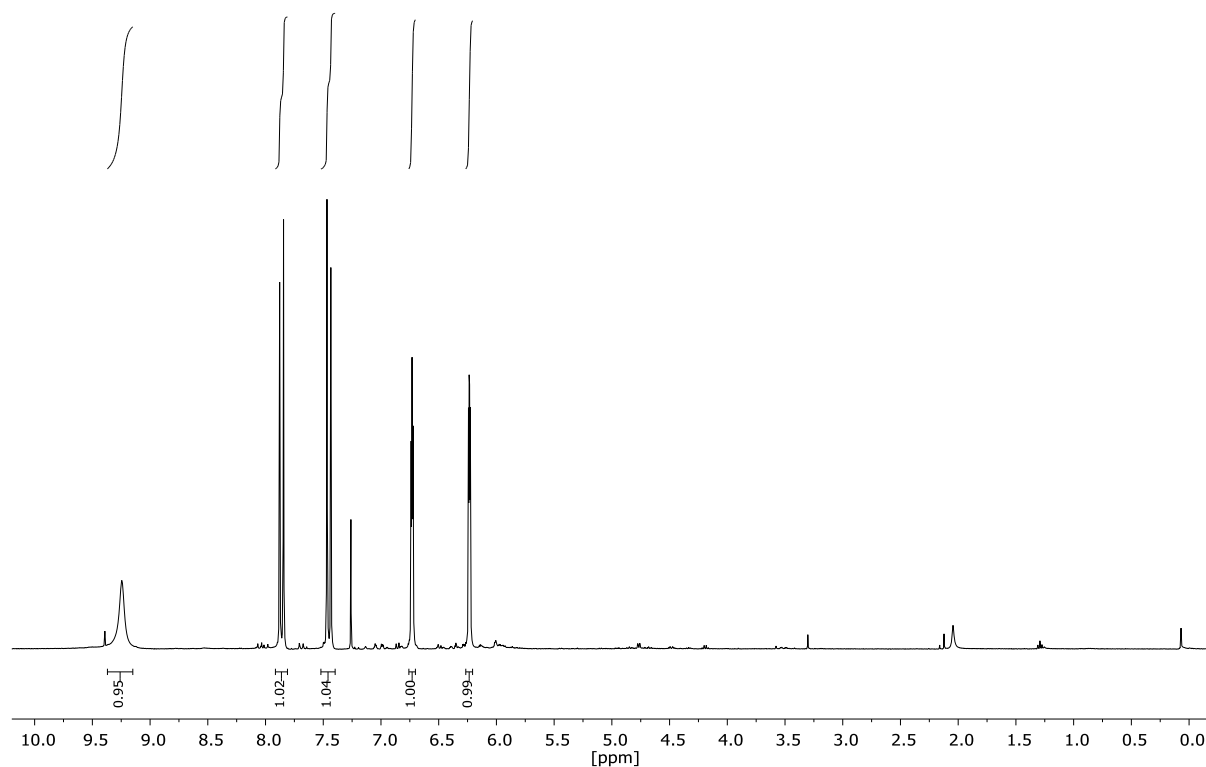
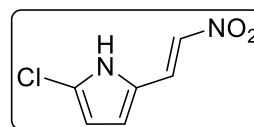
1H-Pyrrole-2-carbaldehyde (S4)NMR-Solvent: CDCl₃

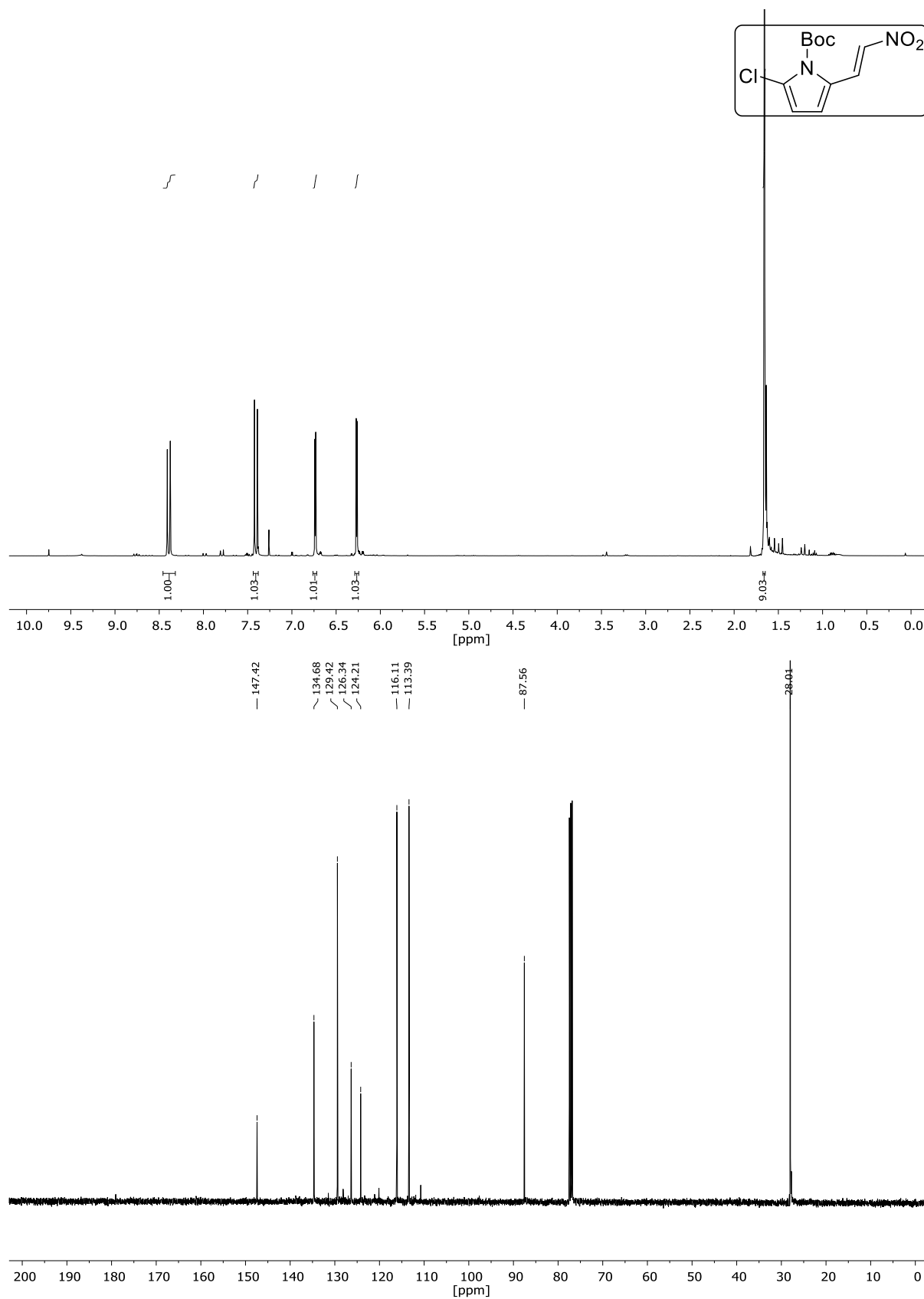
(E)-2-(2-Nitrovinyl)-1H-pyrrole (S5)NMR-Solvent: CDCl₃

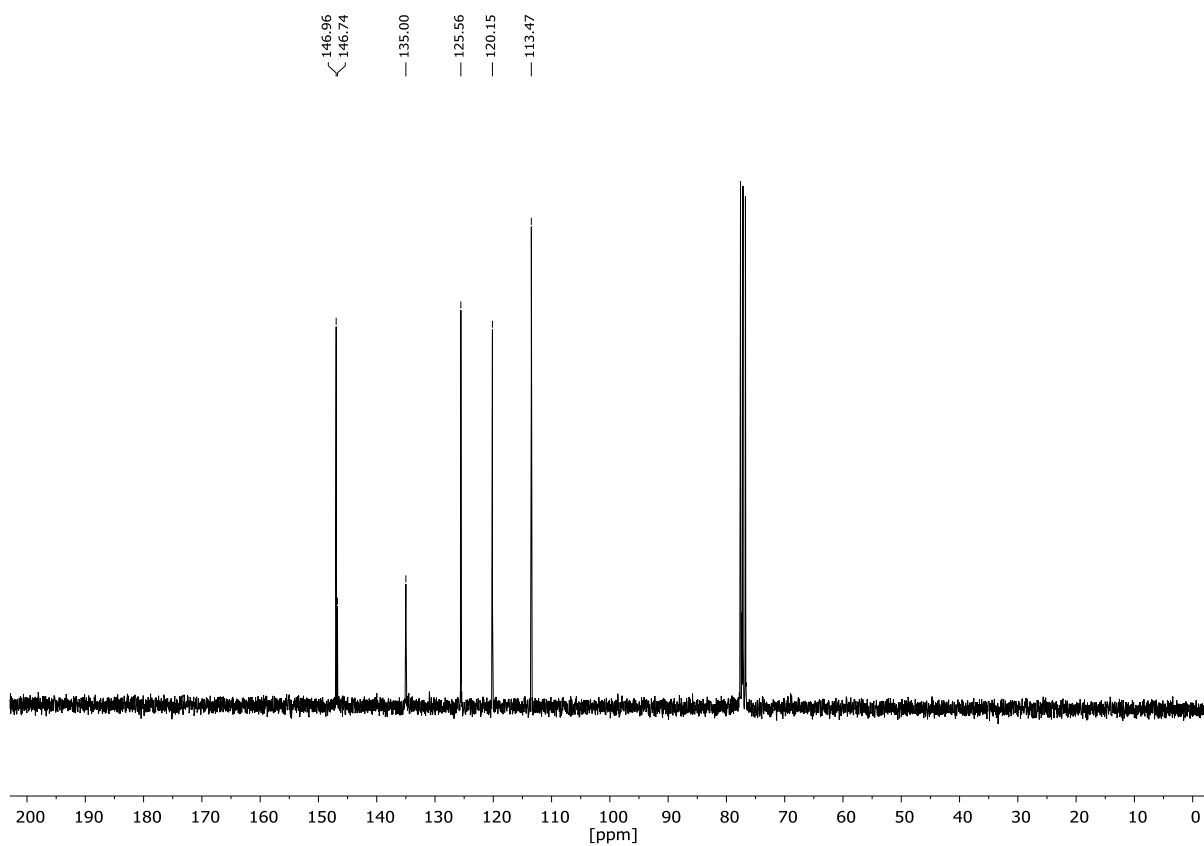
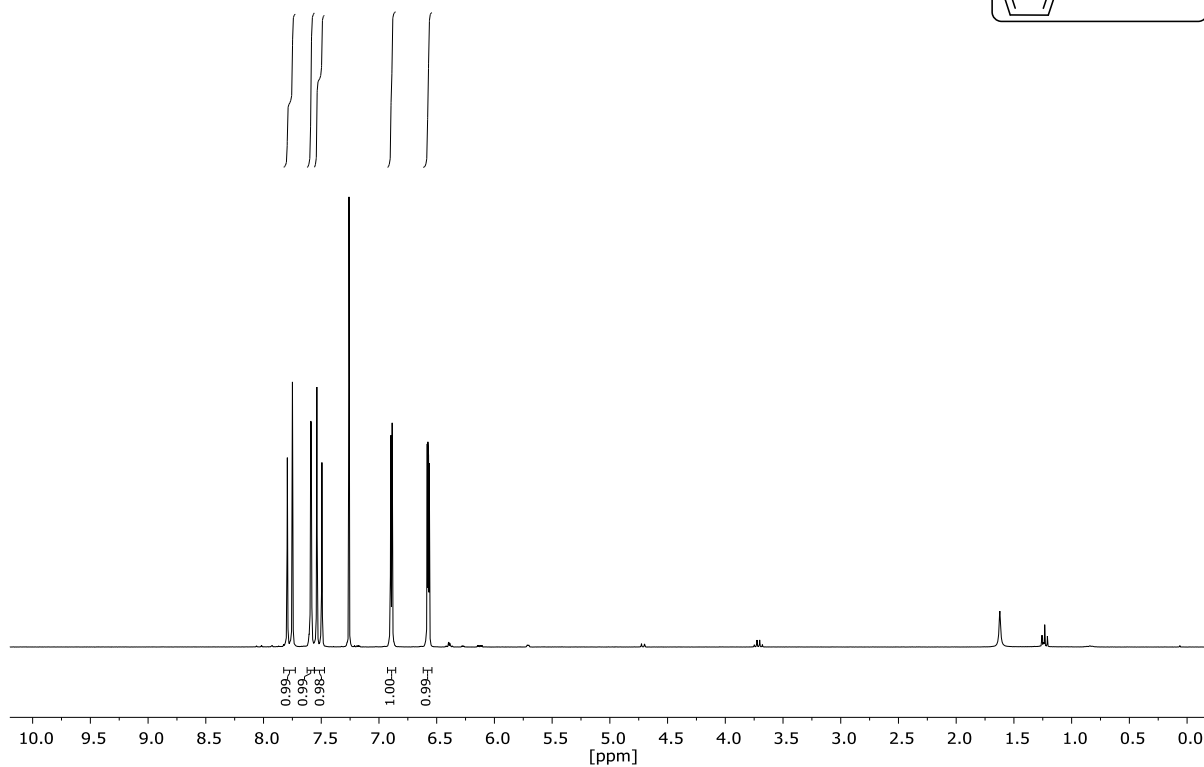
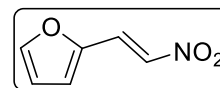
***tert*-Butyl (*E*)-2-(2-nitrovinyl)-1*H*-pyrrole-1-carboxylate (56b)**NMR-Solvent: CDCl₃

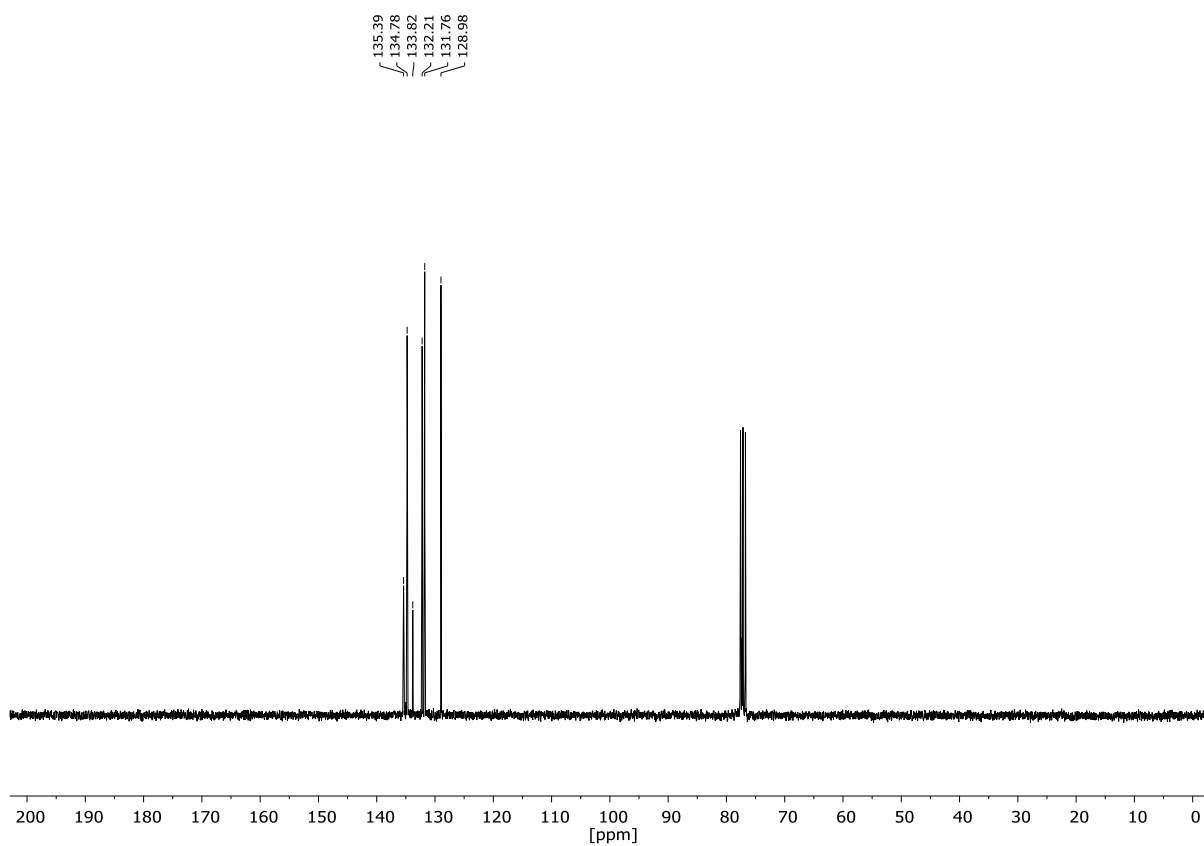
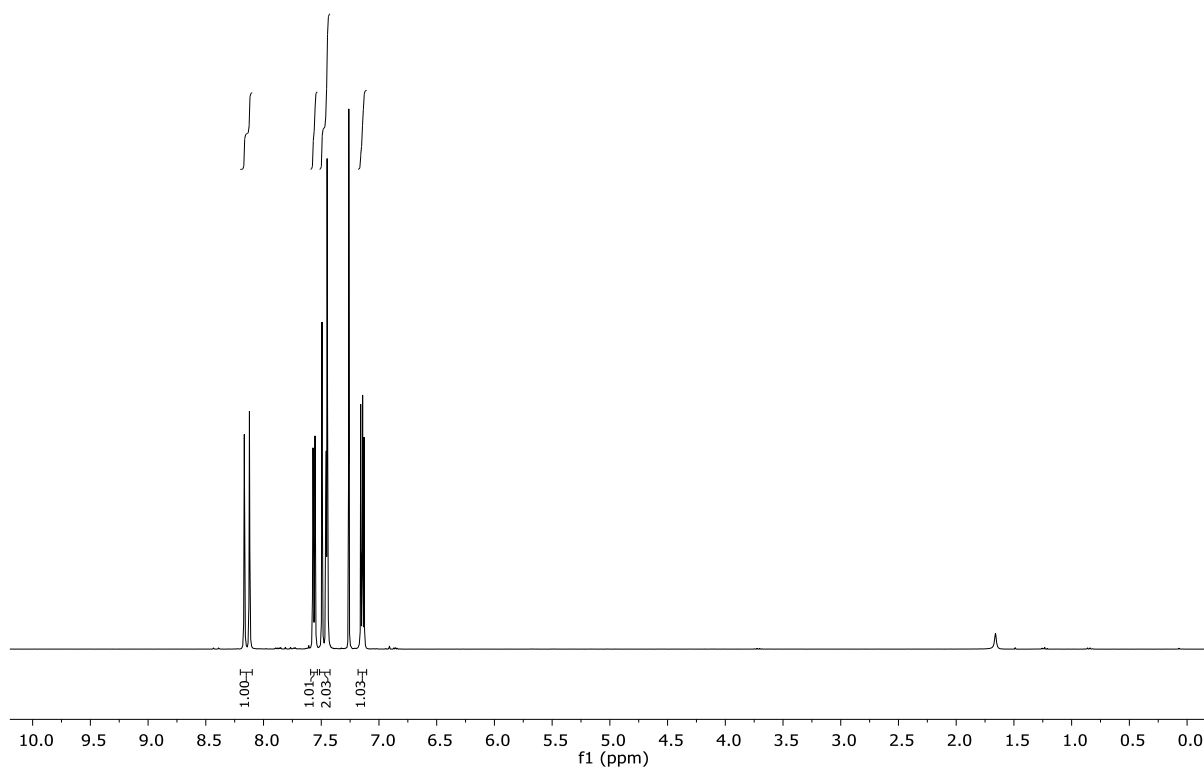
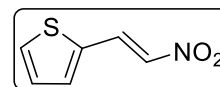
5-Chloro-1H-pyrrole-2-carbaldehyde (S6)

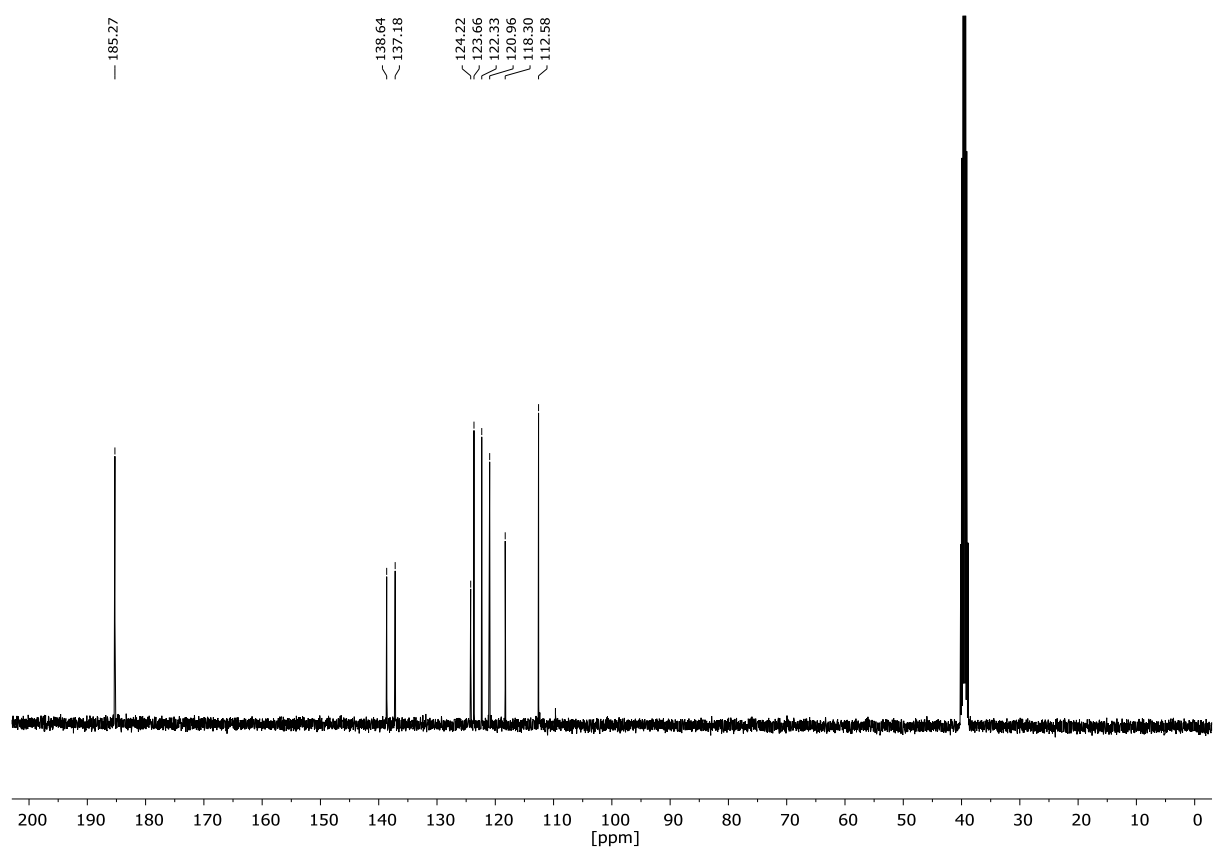
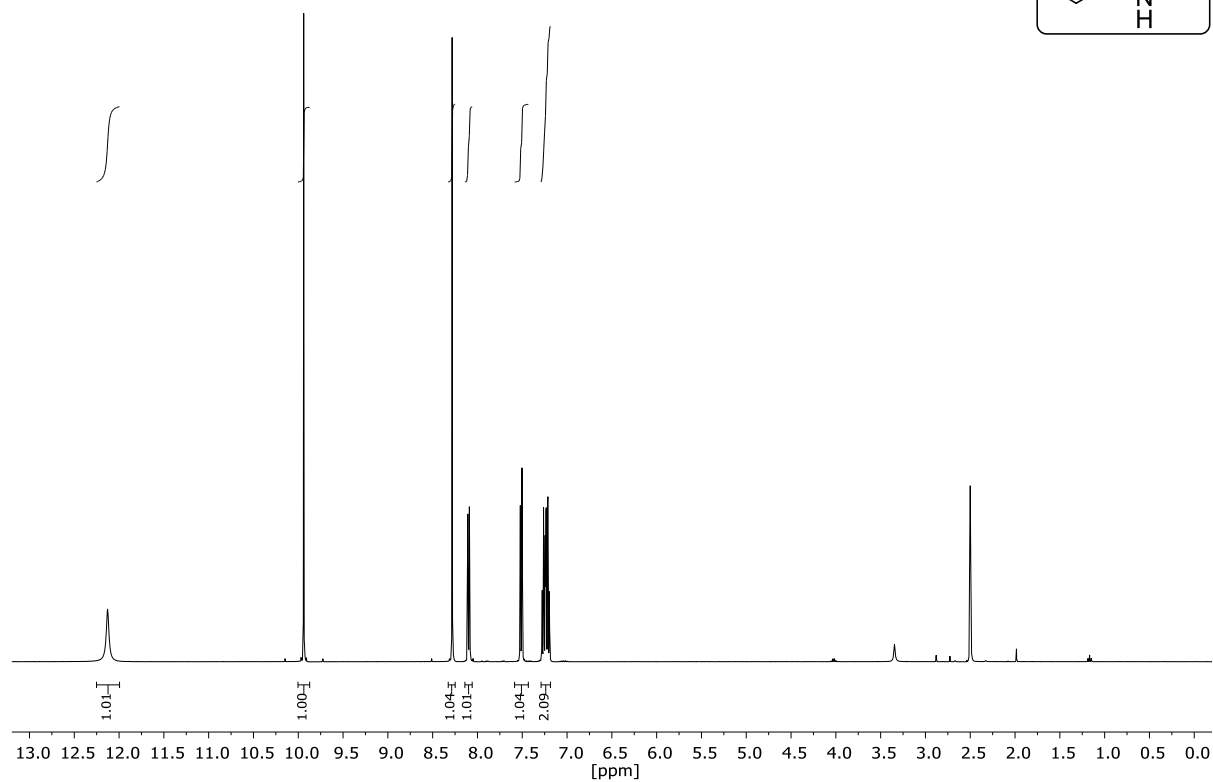
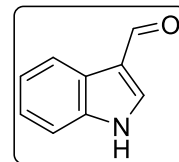
NMR-Solvent: CDCl₃

(E)-2-Chloro-5-(2-nitrovinyl)-1H-pyrrole (S7)NMR-Solvent: CDCl₃

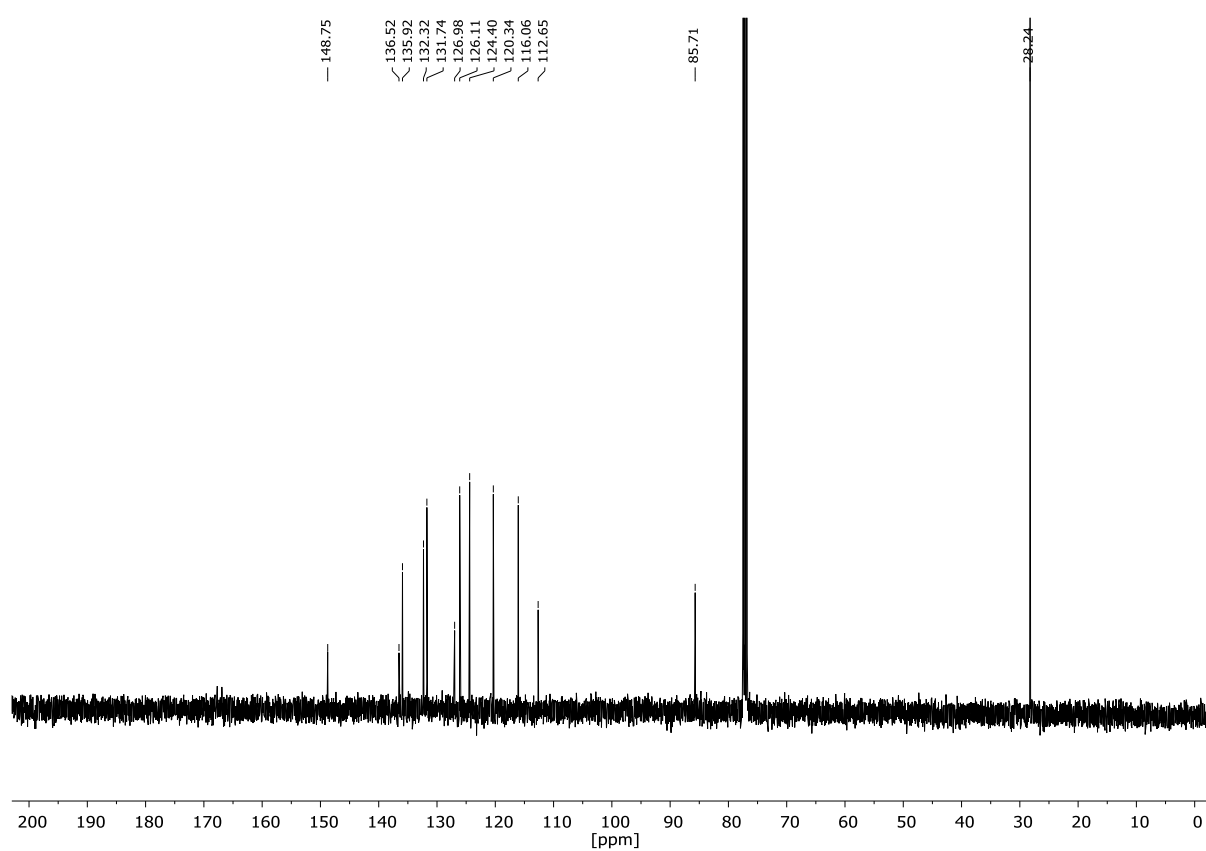
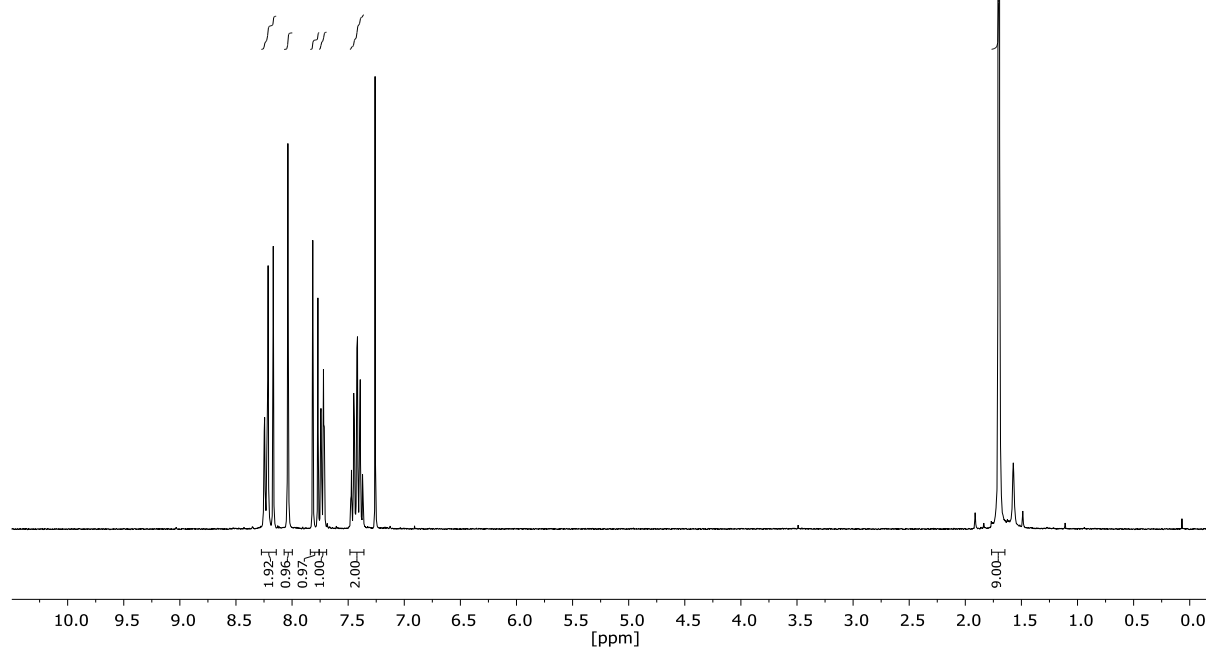
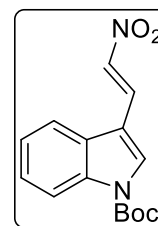
***tert*-Butyl (*E*)-2-chloro-5-(2-nitrovinyl)-1*H*-pyrrole-1-carboxylate (56c)**NMR-Solvent: CDCl₃

(E)-2-(2-Nitrovinyl)furan (56d)NMR-Solvent: CDCl_3

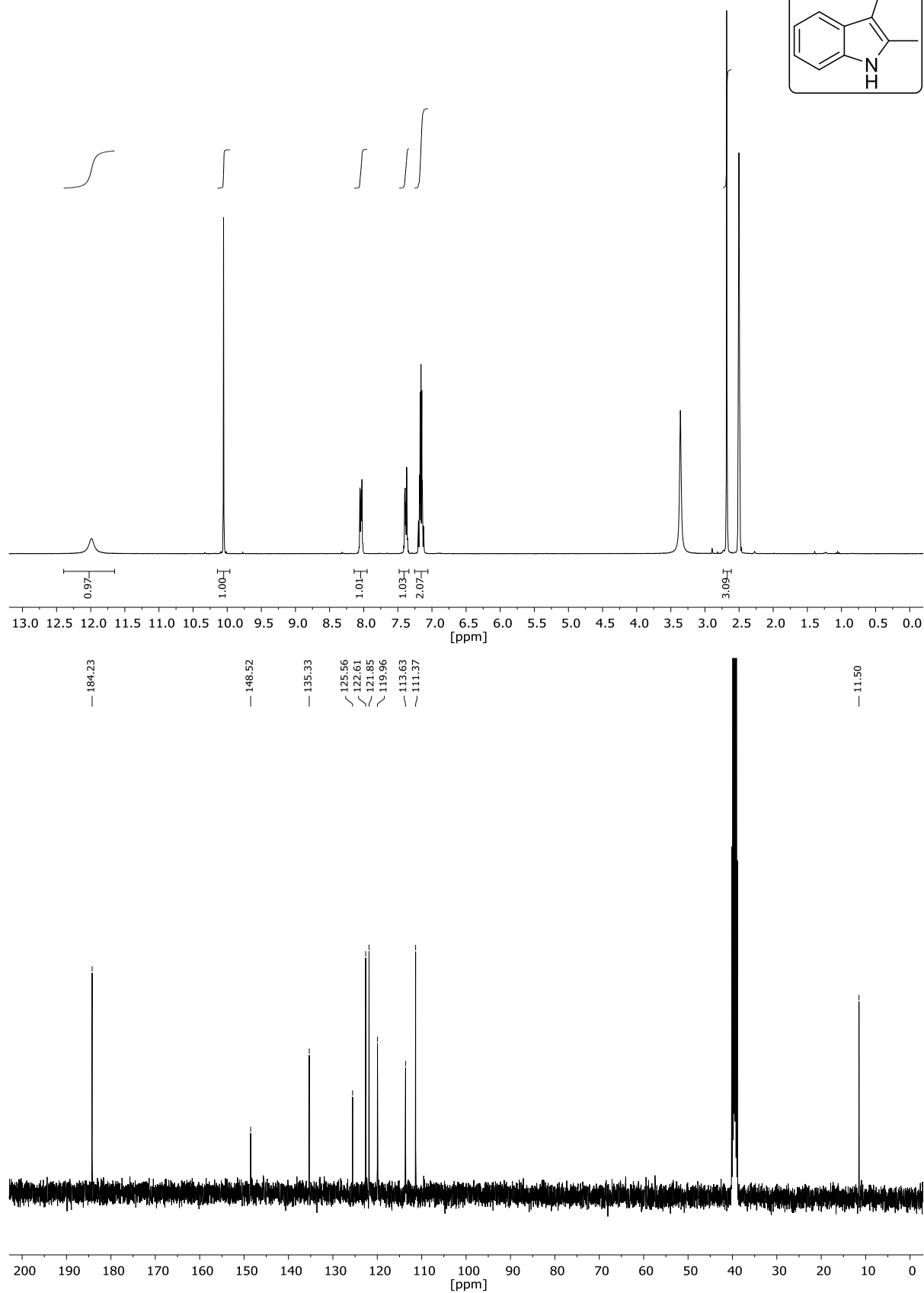
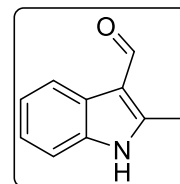
(E)-2-(2-Nitrovinyl)thiophene (56e)NMR-Solvent: CDCl₃

1H-Indole-3-carbaldehyde (S8)

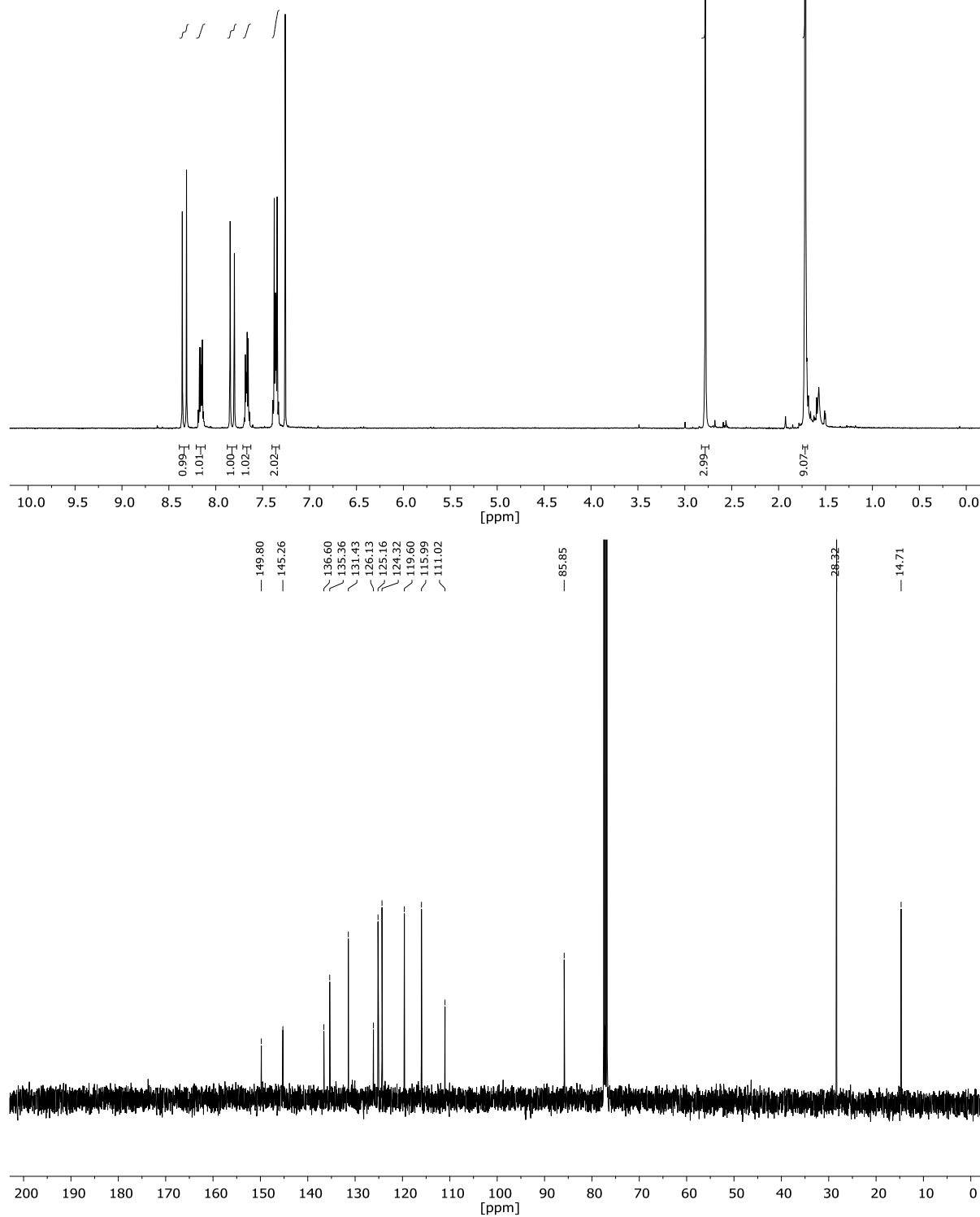
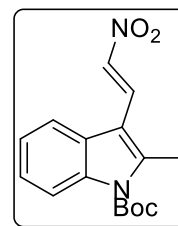
NMR-Solvent: DMSO

***tert*-Butyl (*E*)-3-(2-nitrovinyl)-1*H*-indole-1-carboxylate (56f)**NMR-Solvent: CDCl_3

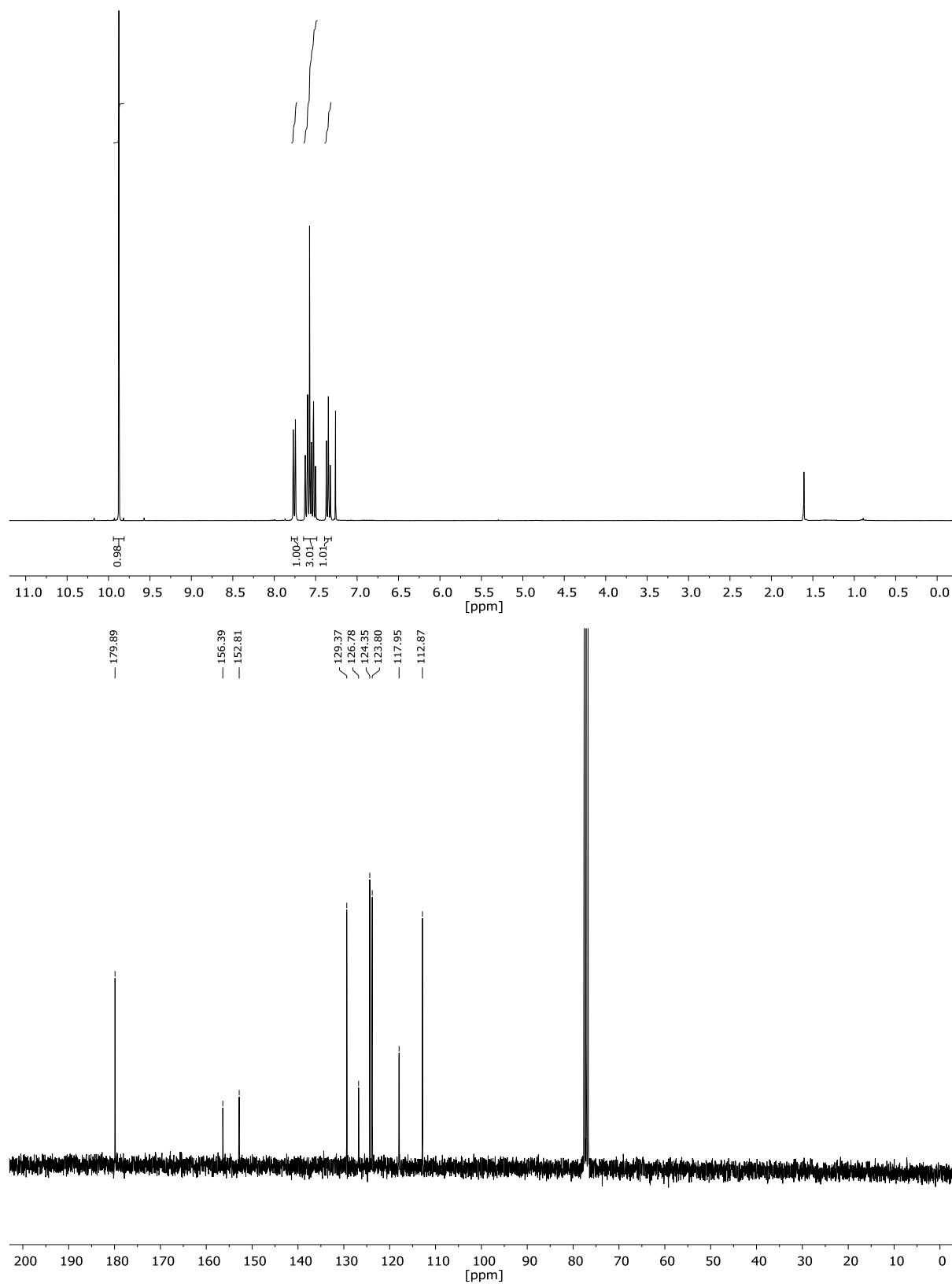
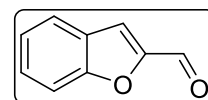
2-Methyl-1H-indole-3-carbaldehyde (S9)

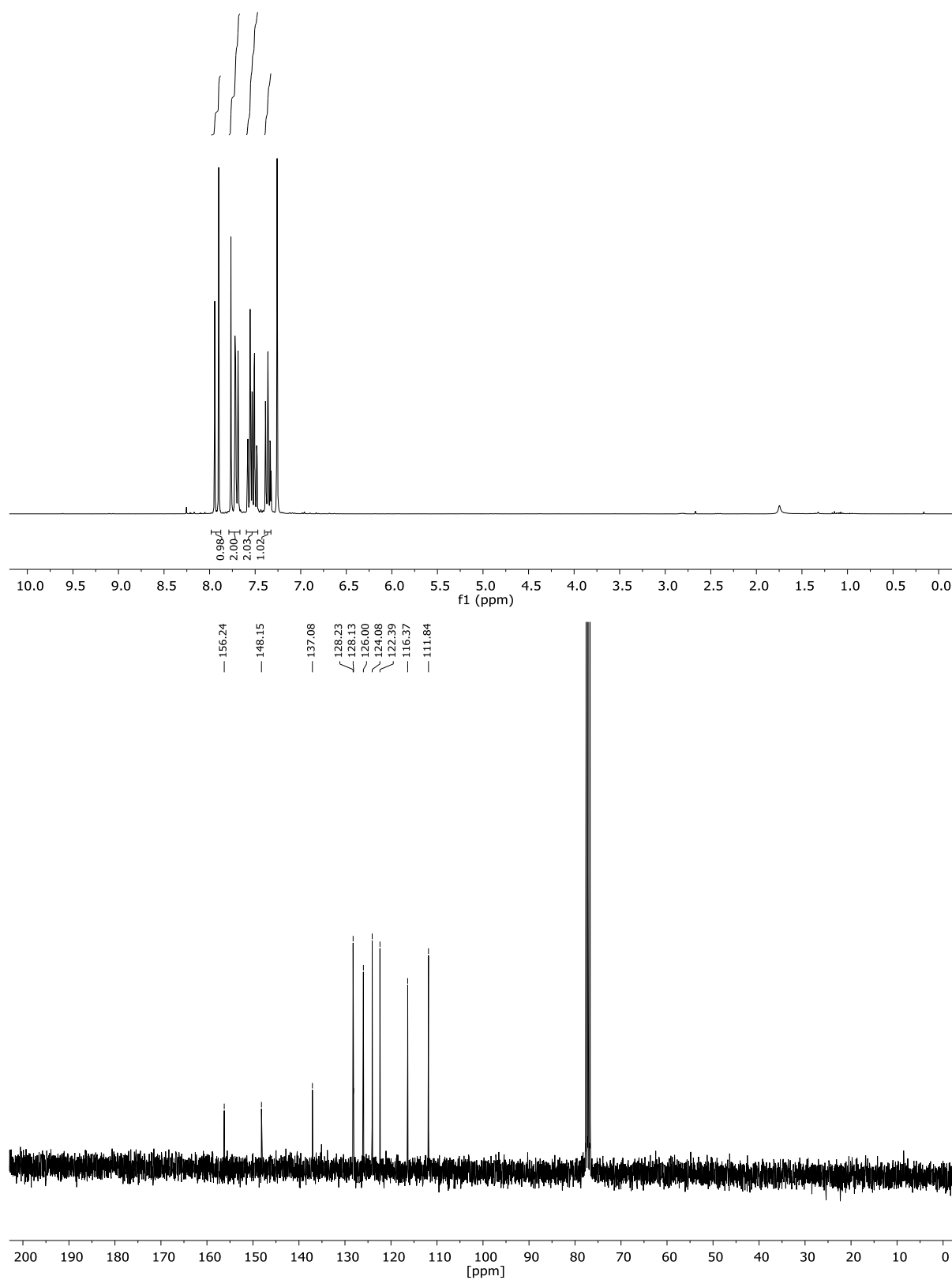
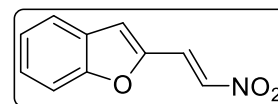


NMR-Solvent: DMSO

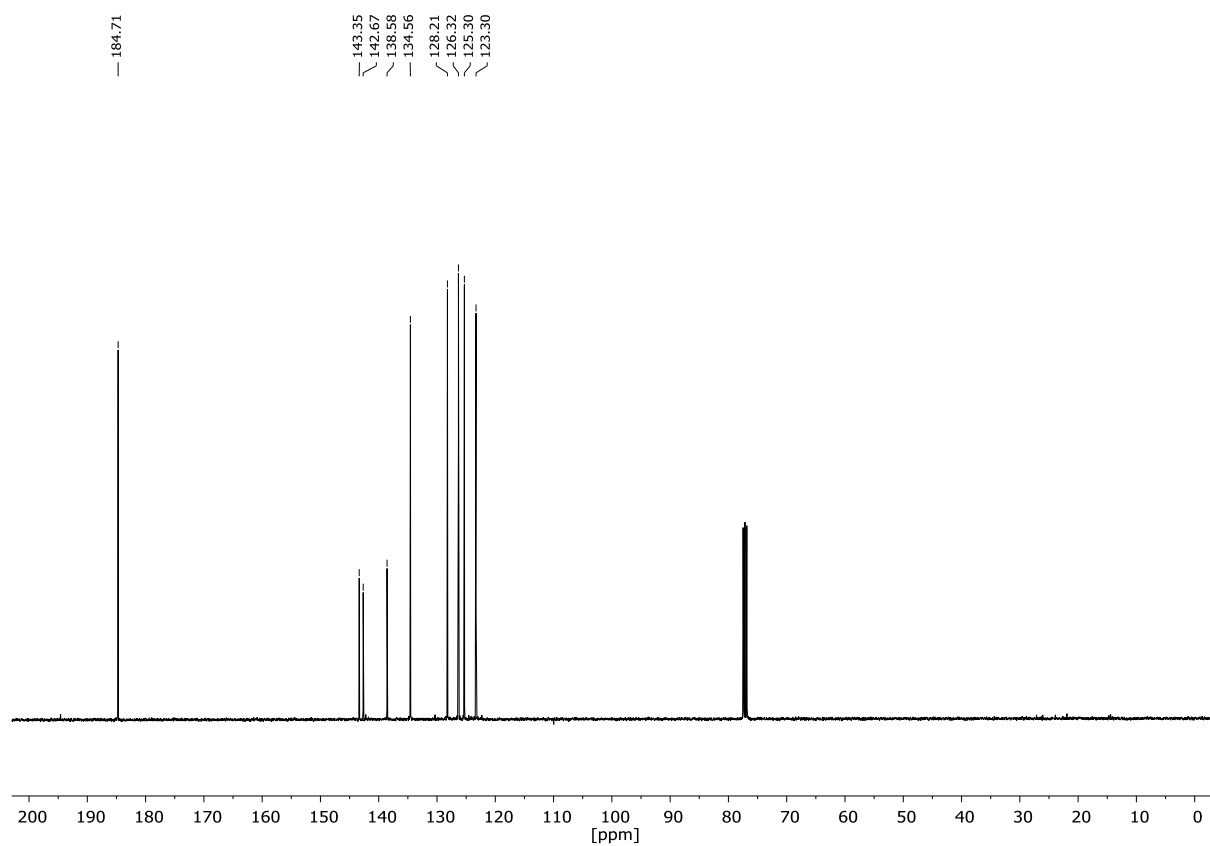
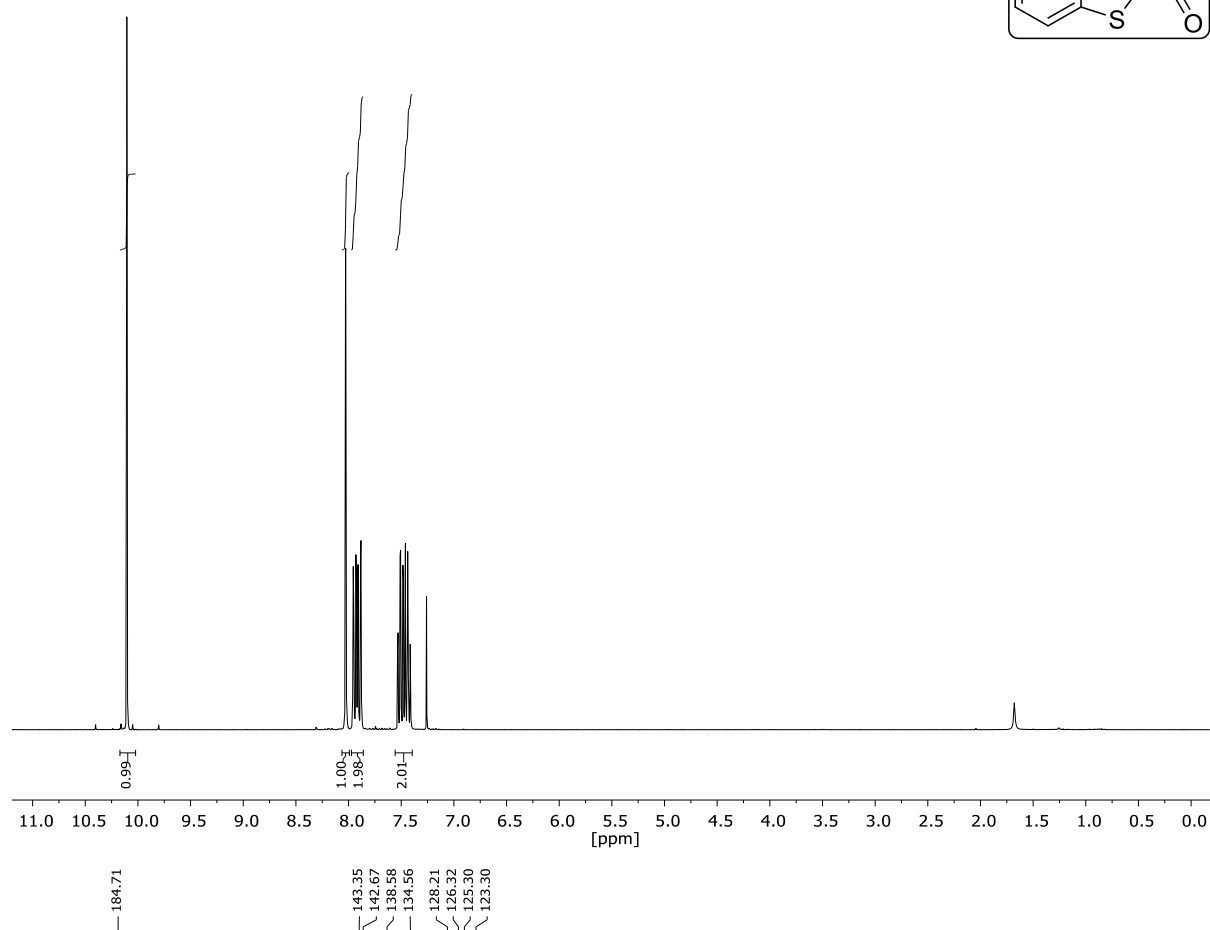
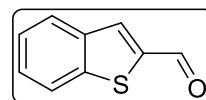
***tert*-Butyl (*E*)-2-methyl-3-(2-nitrovinyl)-1*H*-indole-1-carboxylate (56g)**NMR-Solvent: CDCl₃

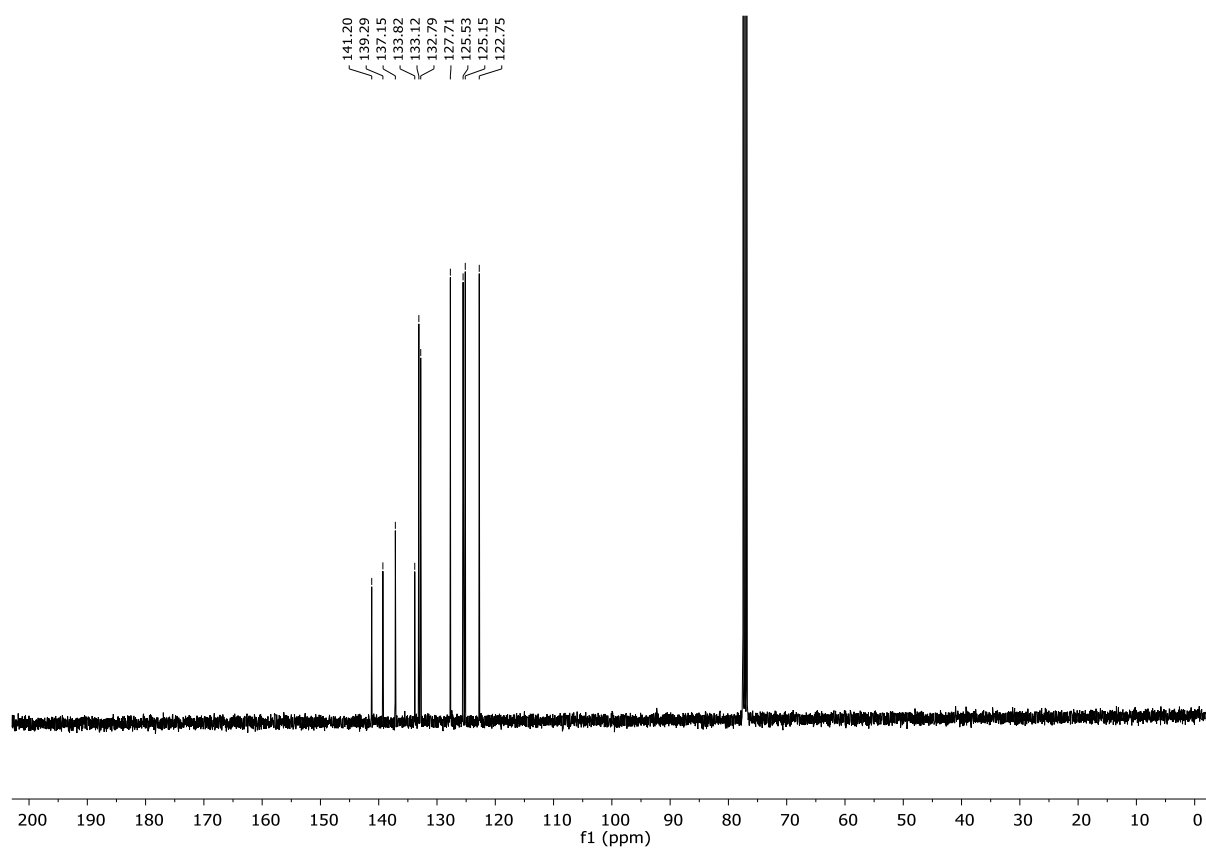
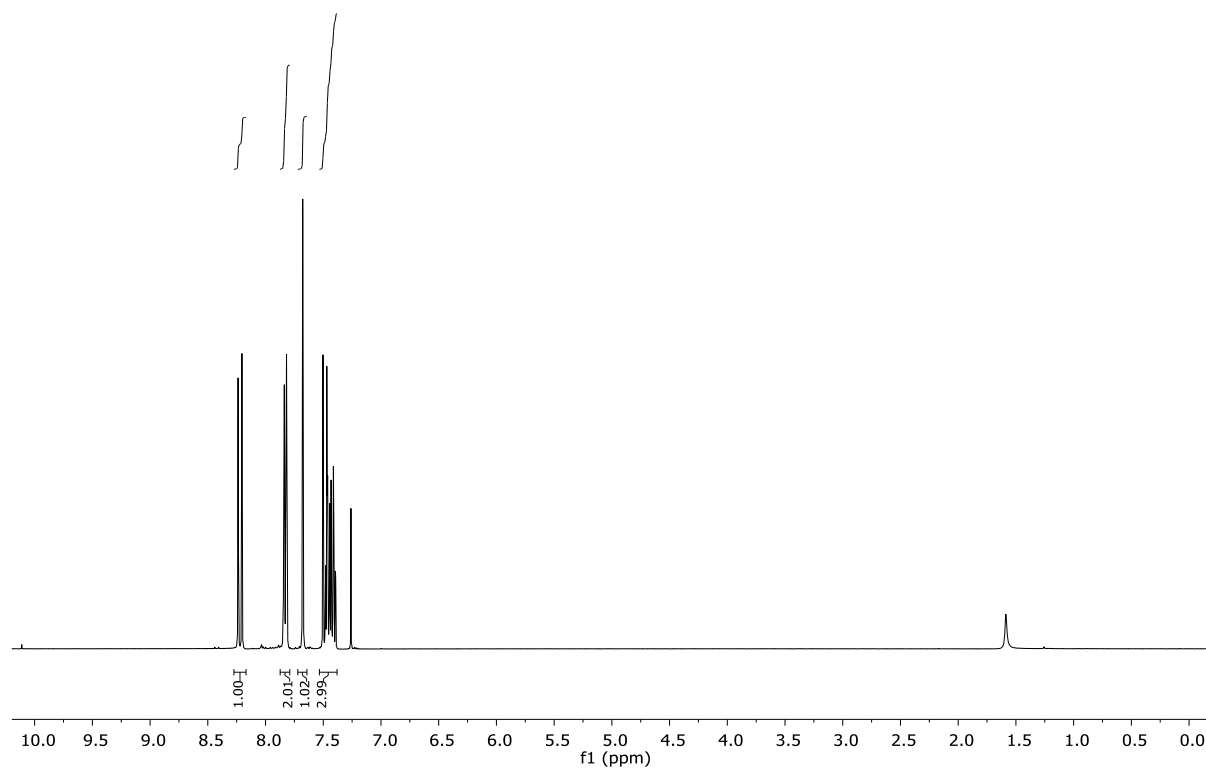
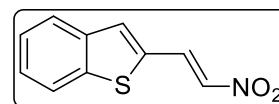
Benzofuran-2-carbaldehyde (S10)

NMR-Solvent: CDCl₃

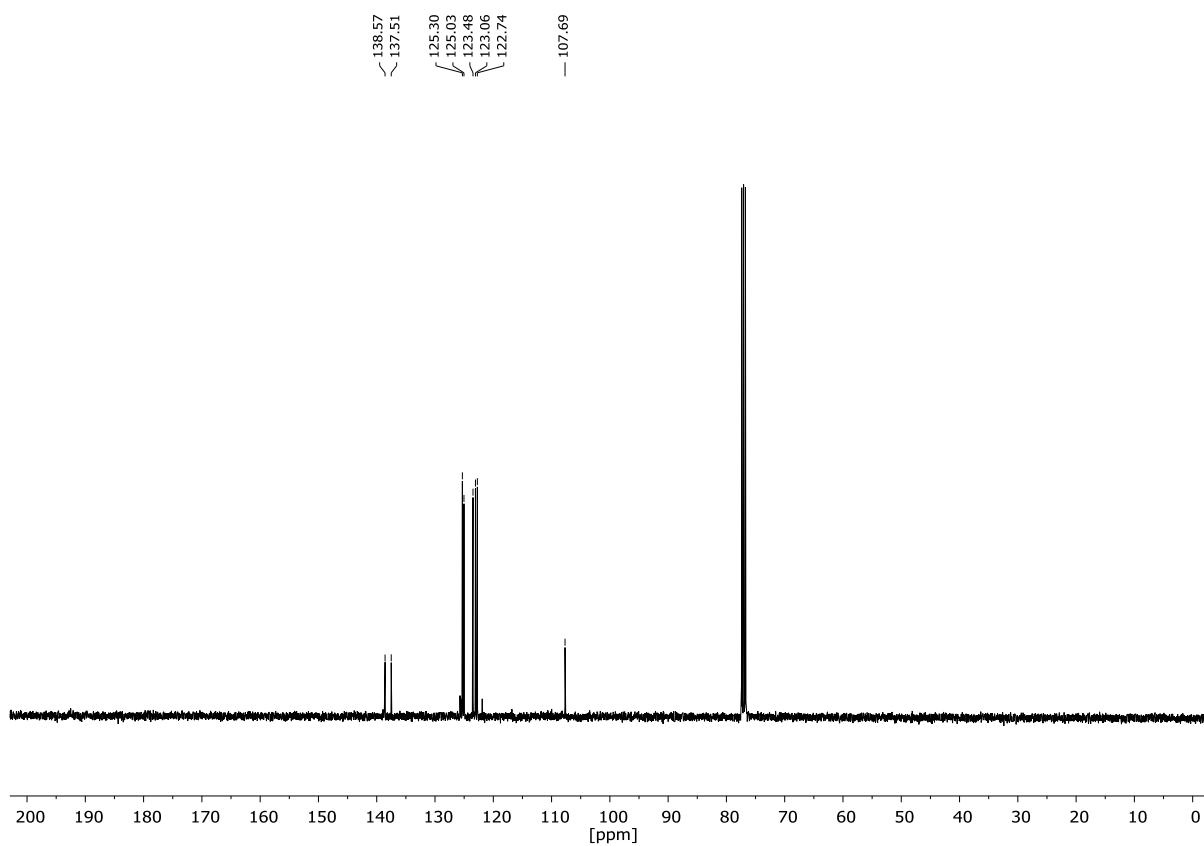
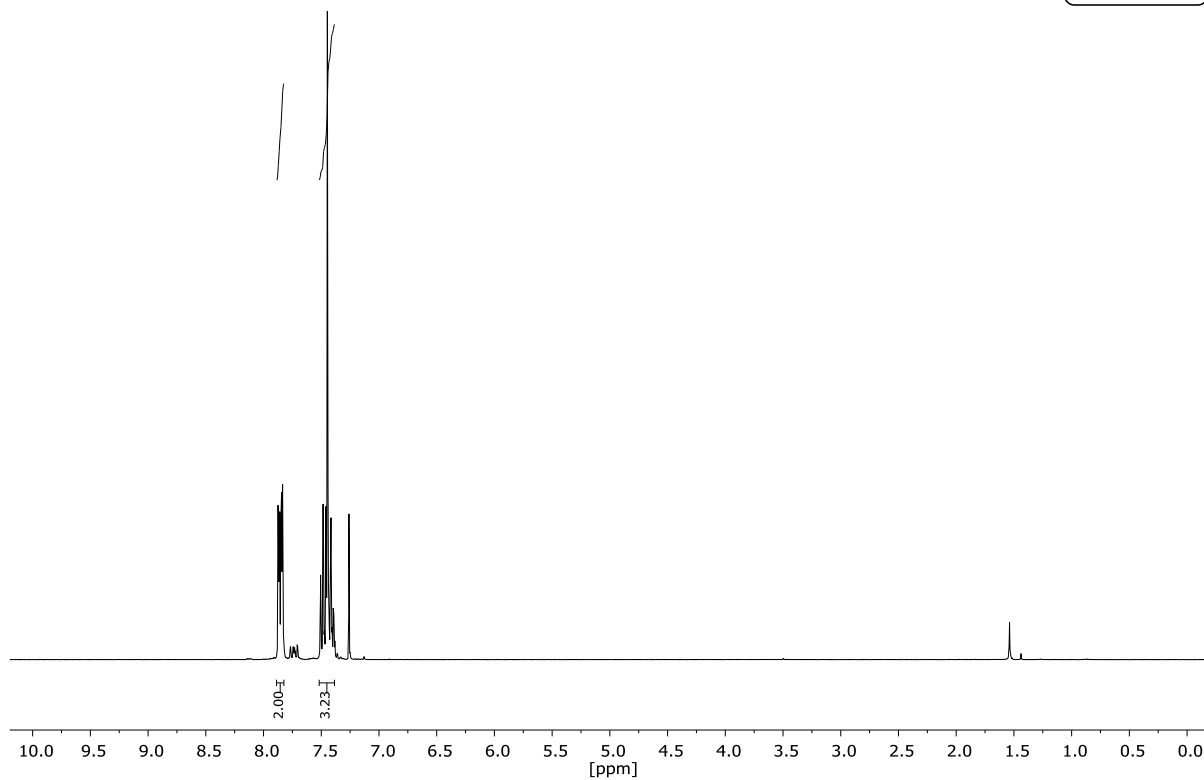
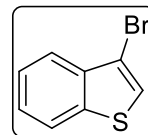
(E)-2-(2-Nitrovinyl)benzofuran (56h)NMR-Solvent: CDCl₃

Benzo[b]thiophene-2-carbaldehyde (S11)

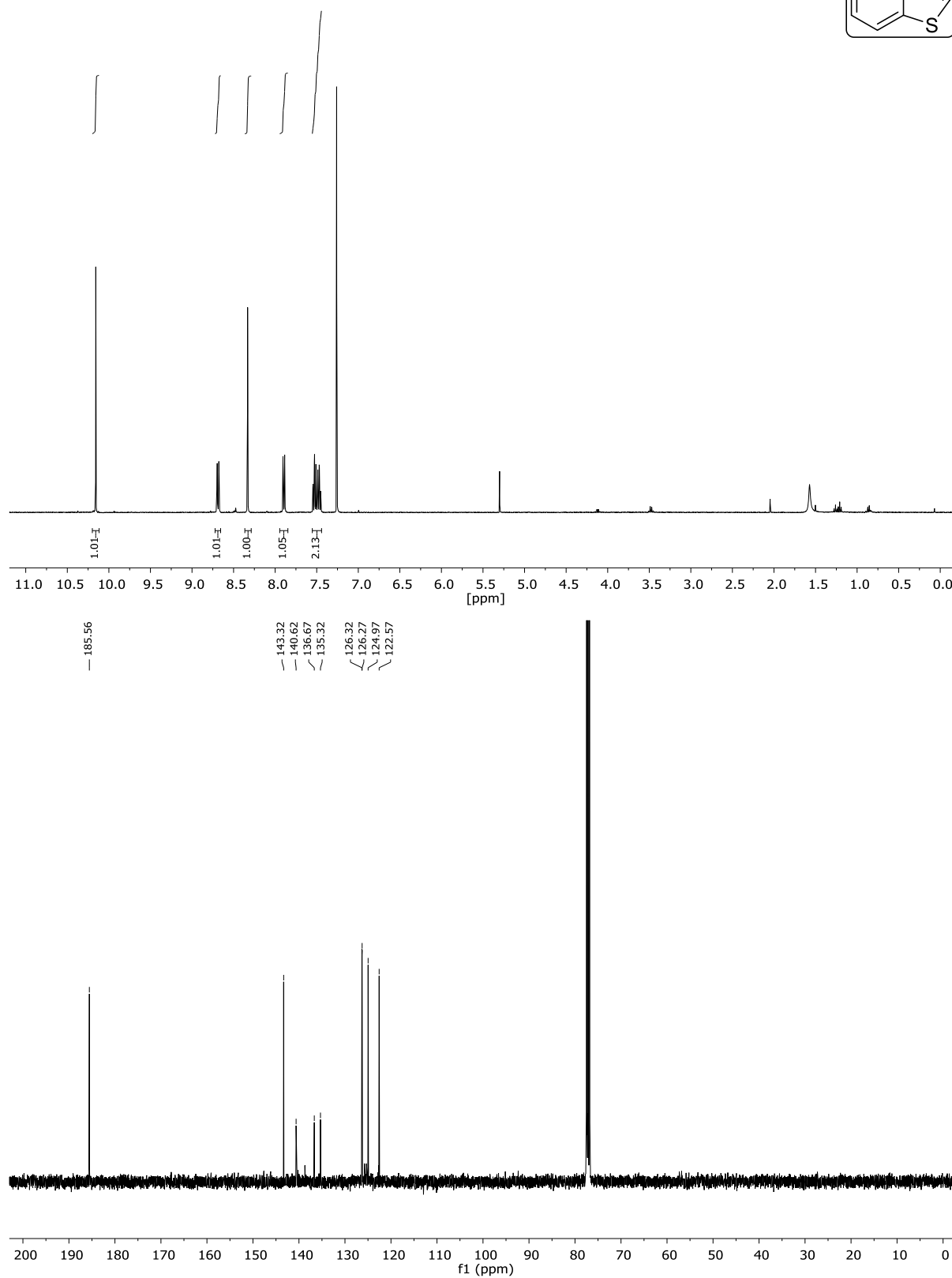
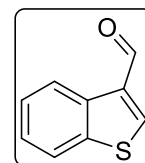
NMR-Solvent: CDCl₃

(E)-2-(2-Nitrovinyl)benzo[b]thiophene (56i)NMR-Solvent: CDCl₃

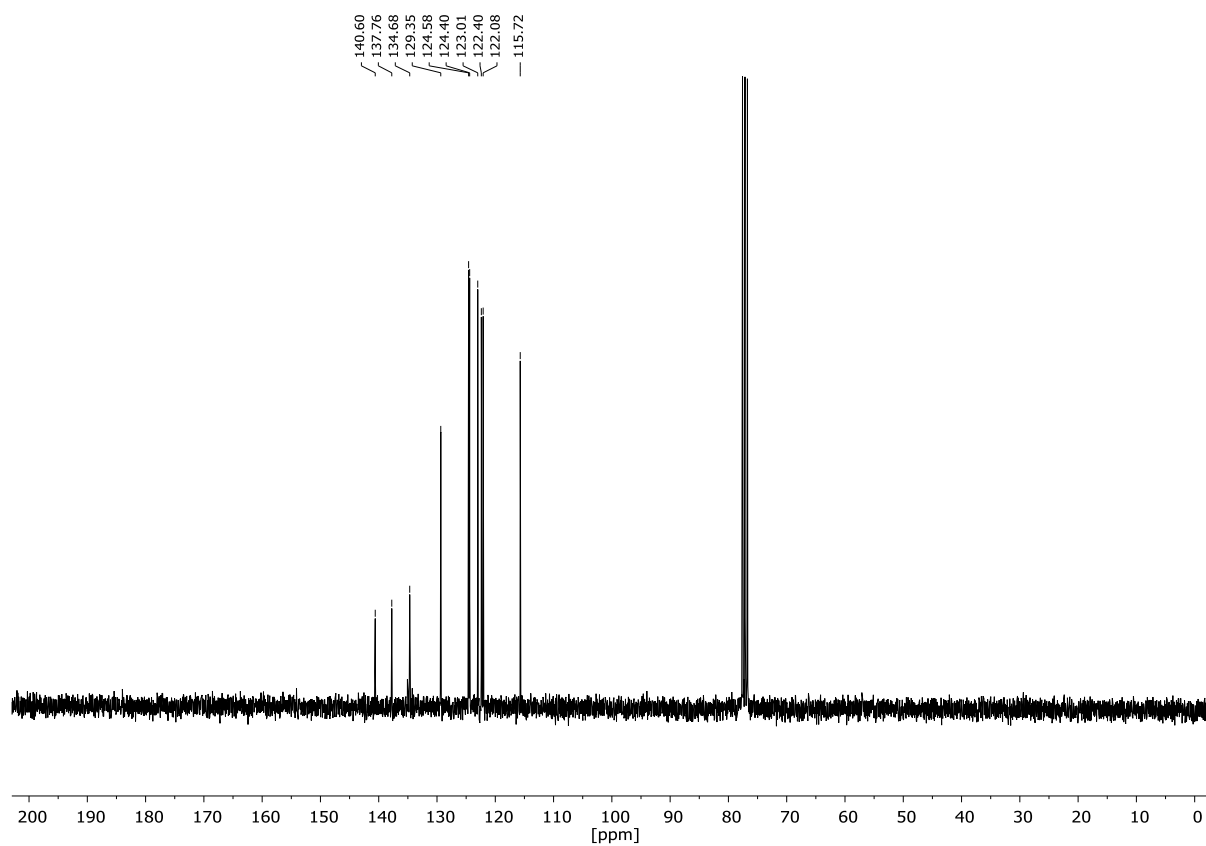
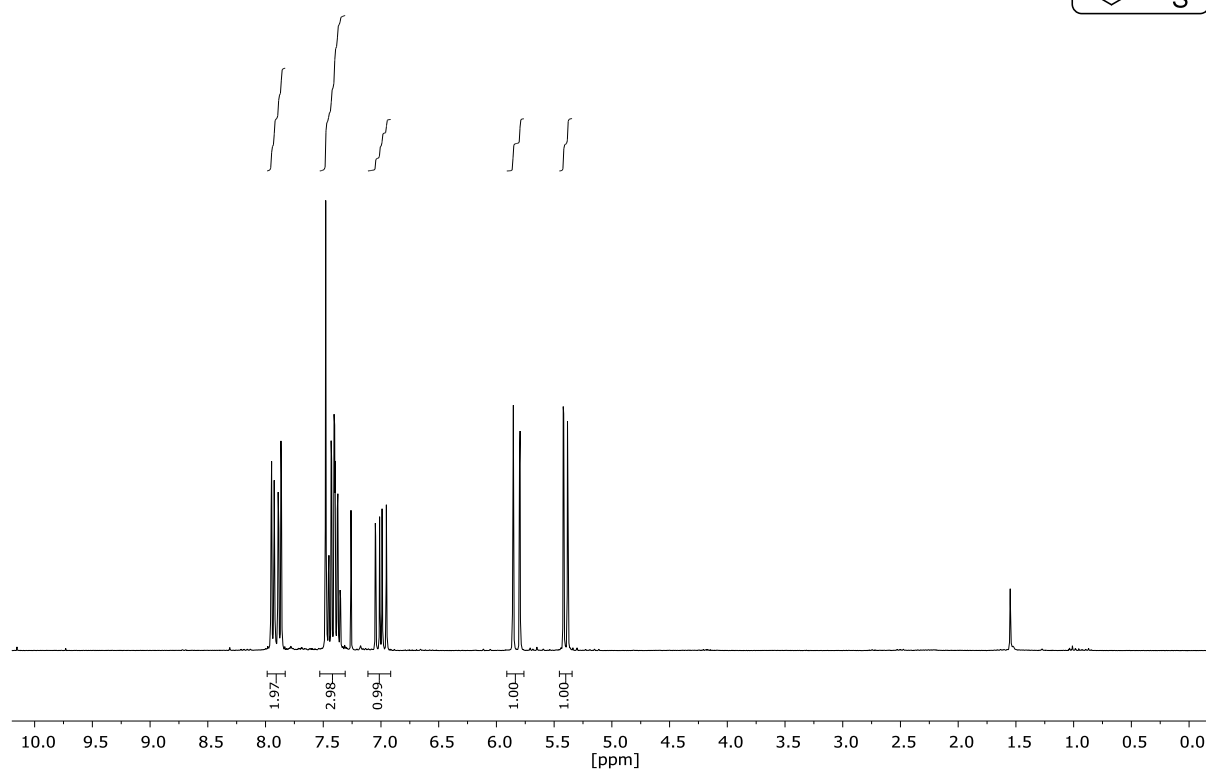
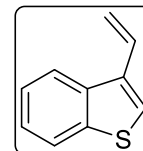
3-Bromobenzo[b]thiophene (S12)

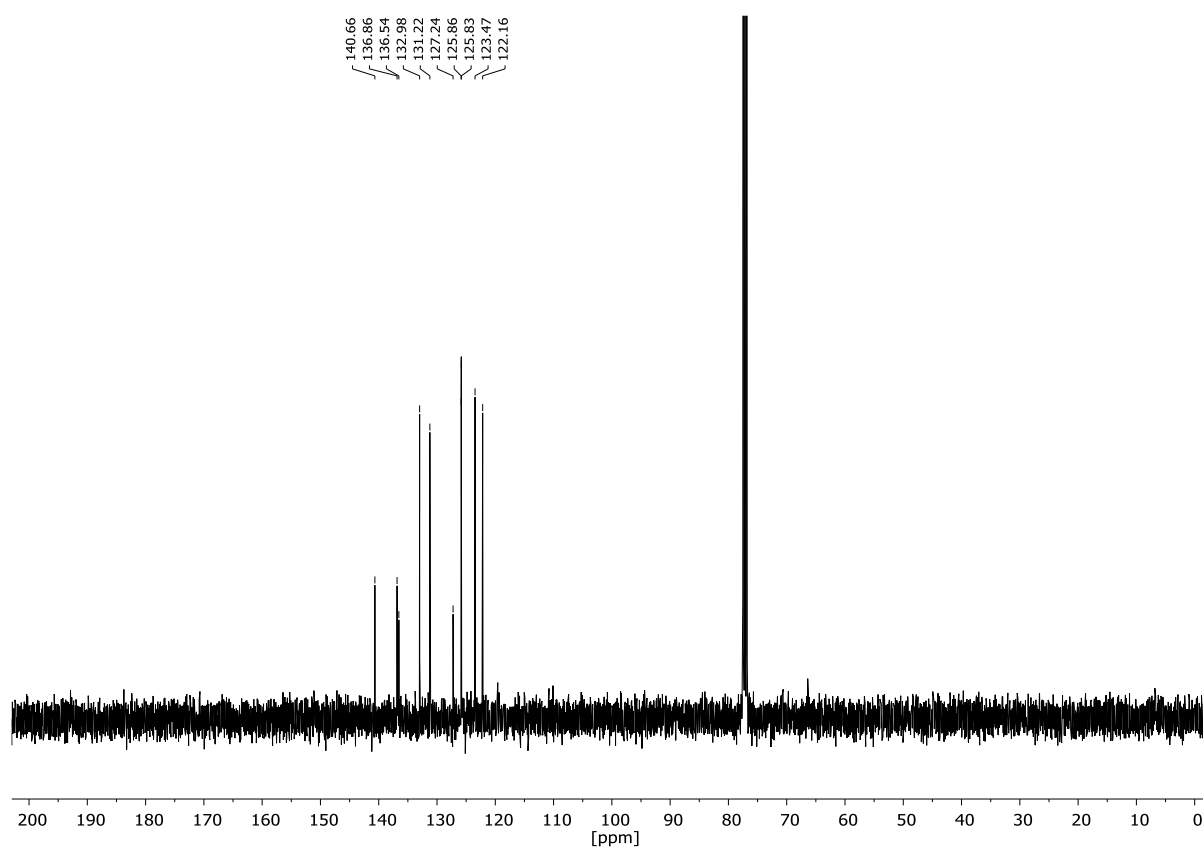
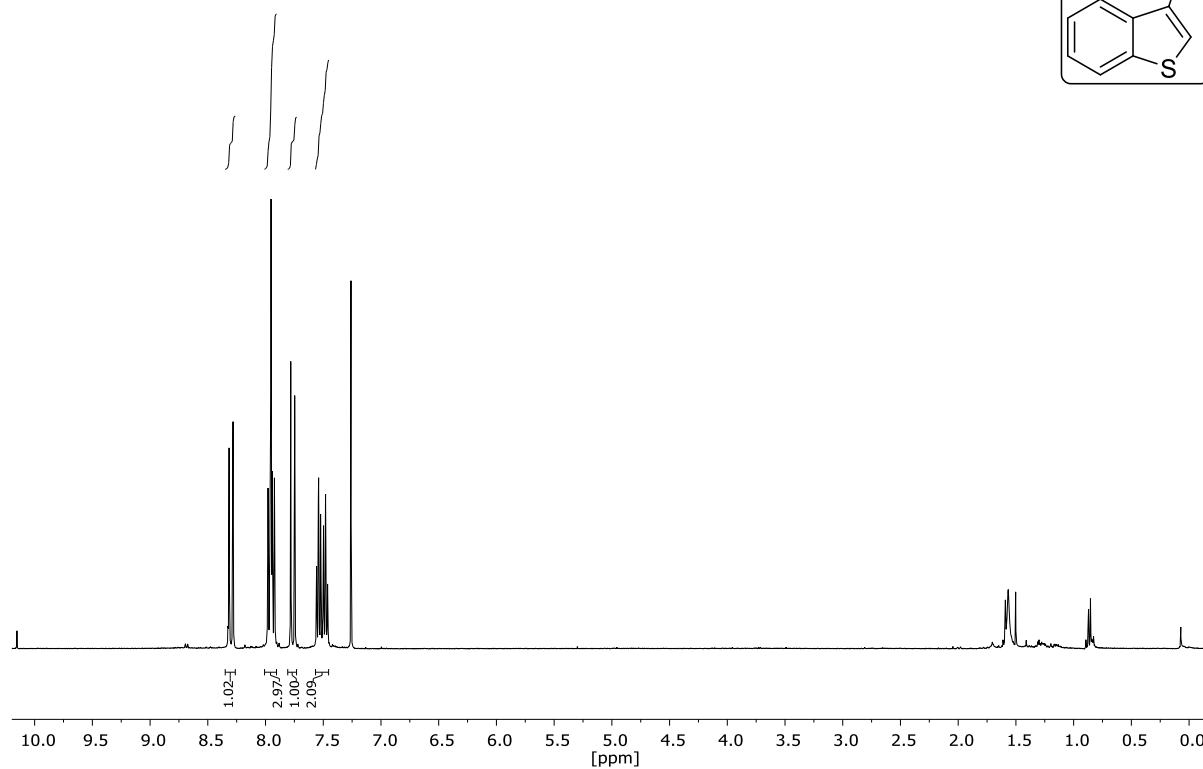
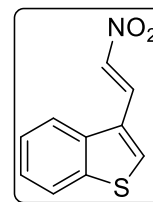
NMR-Solvent: CDCl_3

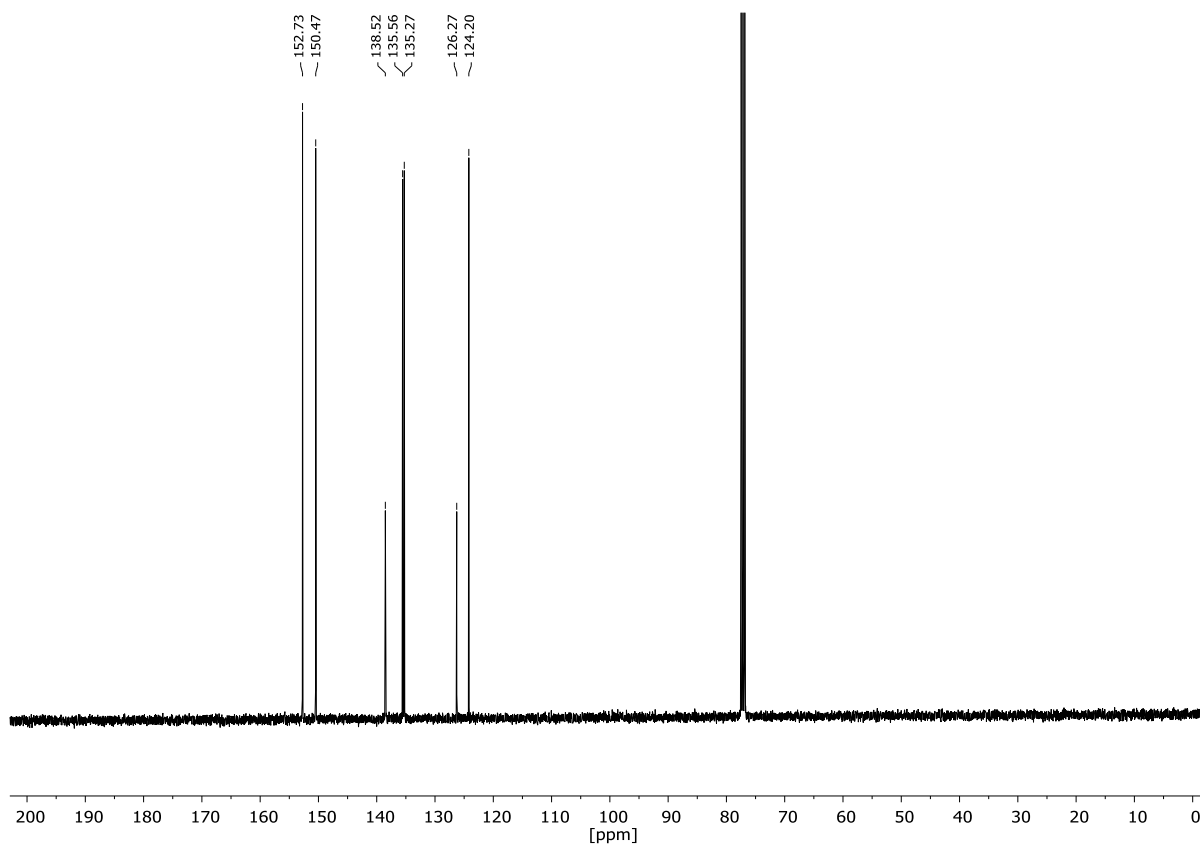
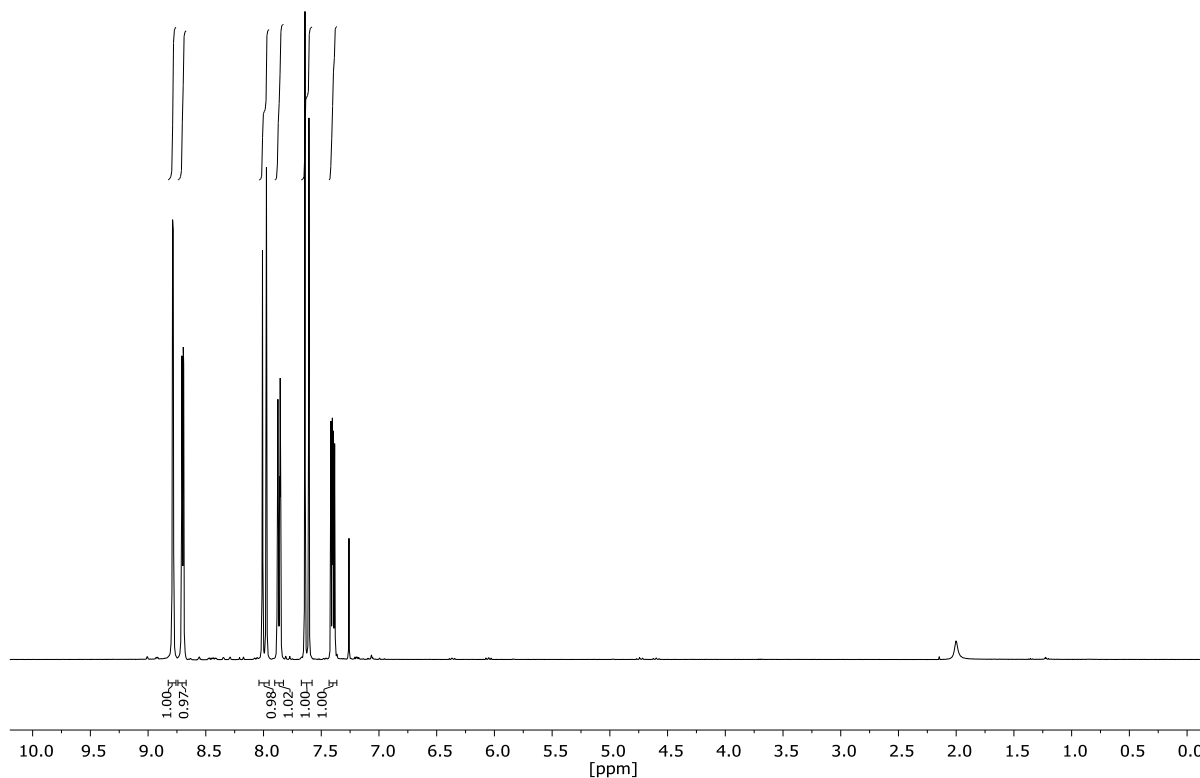
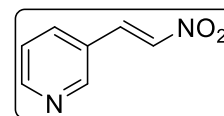
Benzo[b]thiophene-3-carbaldehyde (S13)

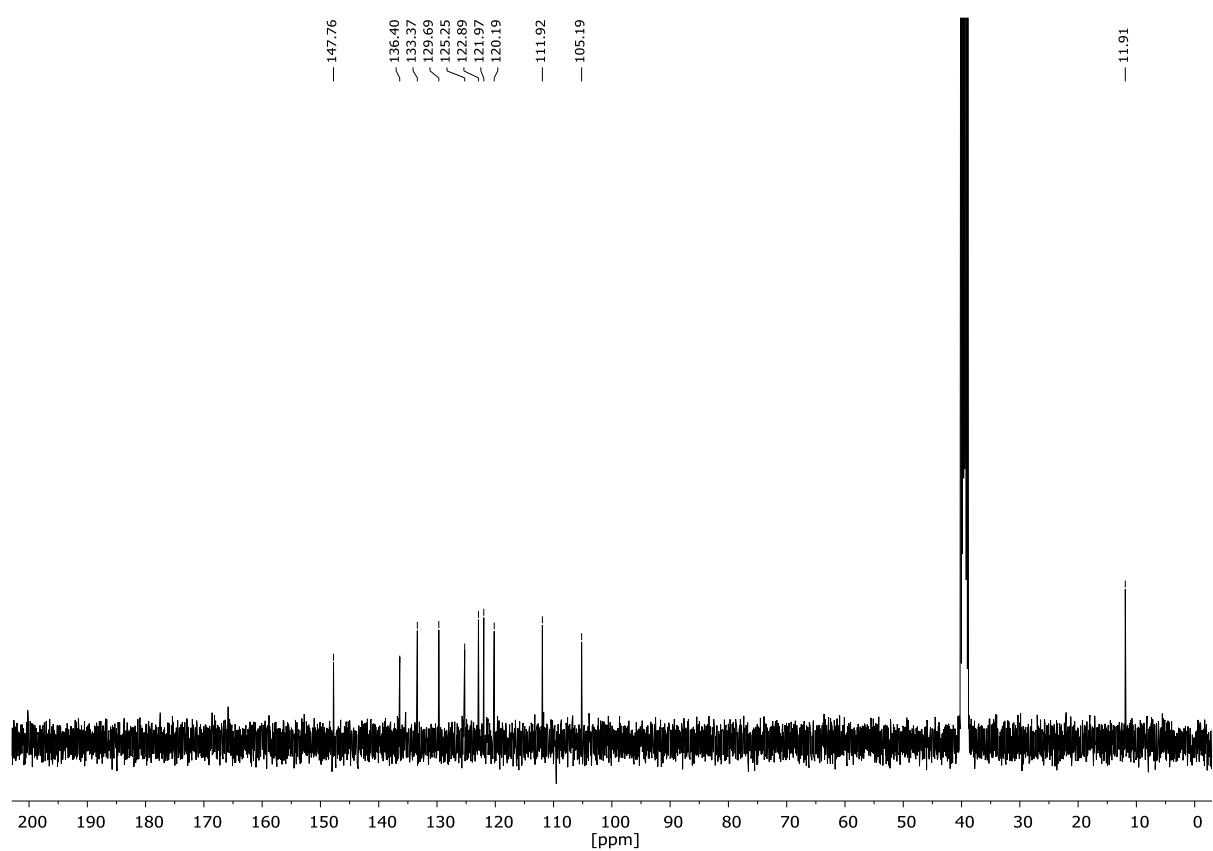
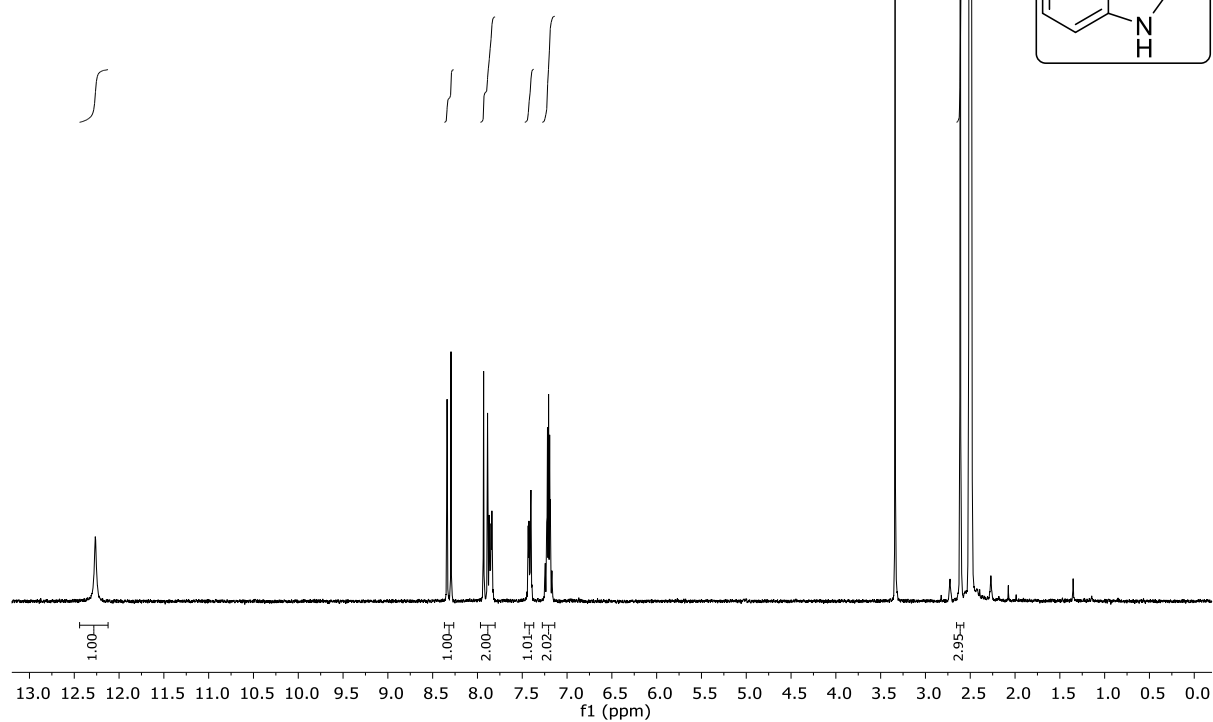
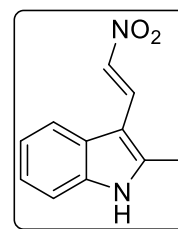
NMR-Solvent: CDCl₃

3-Vinylbenzo[b]thiophene (S14)

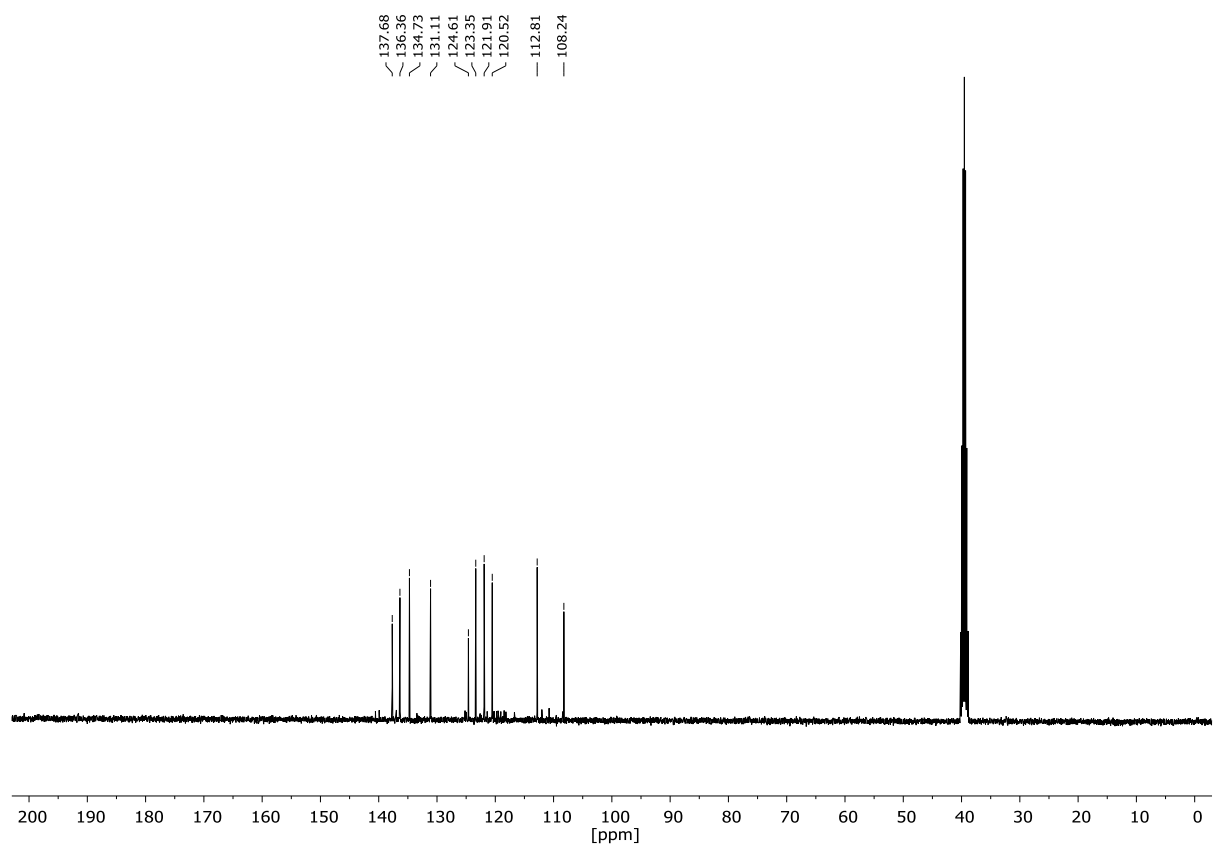
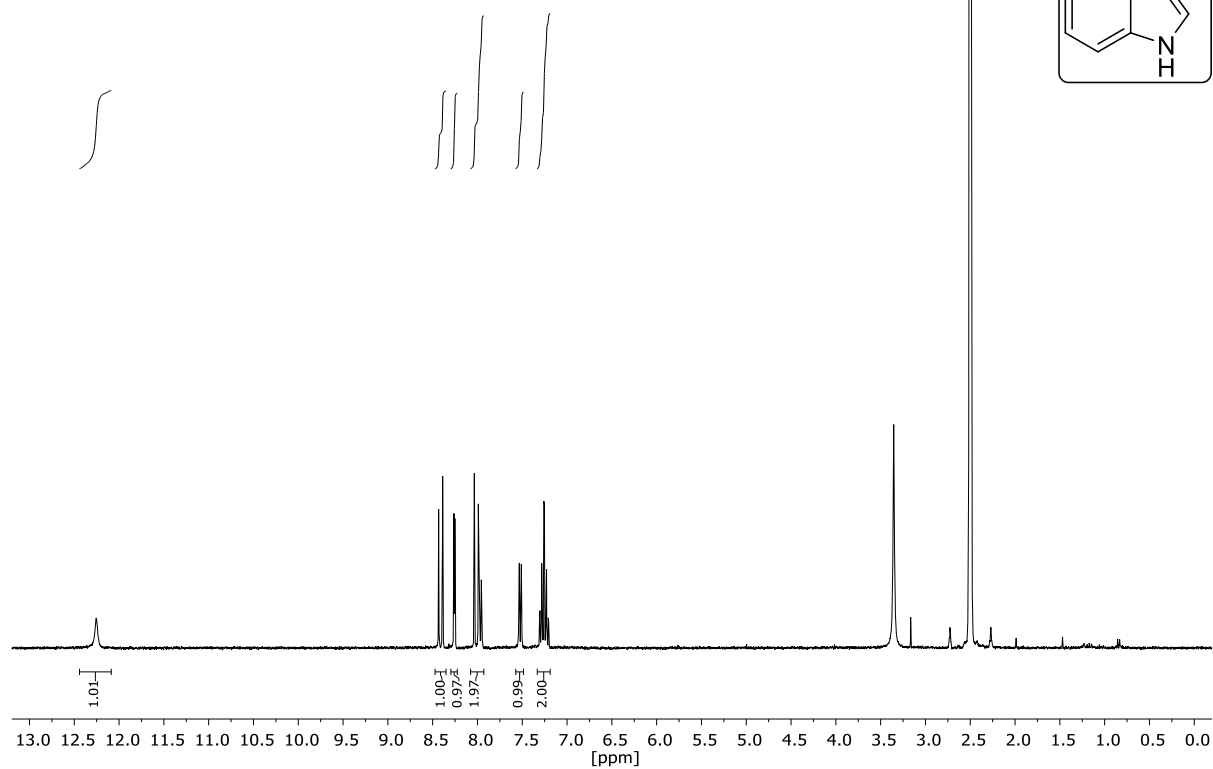
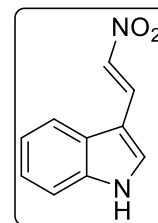
NMR-Solvent: CDCl₃

(E)-3-(2-Nitrovinyl)benzo[b]thiophene (56j)NMR-Solvent: CDCl_3

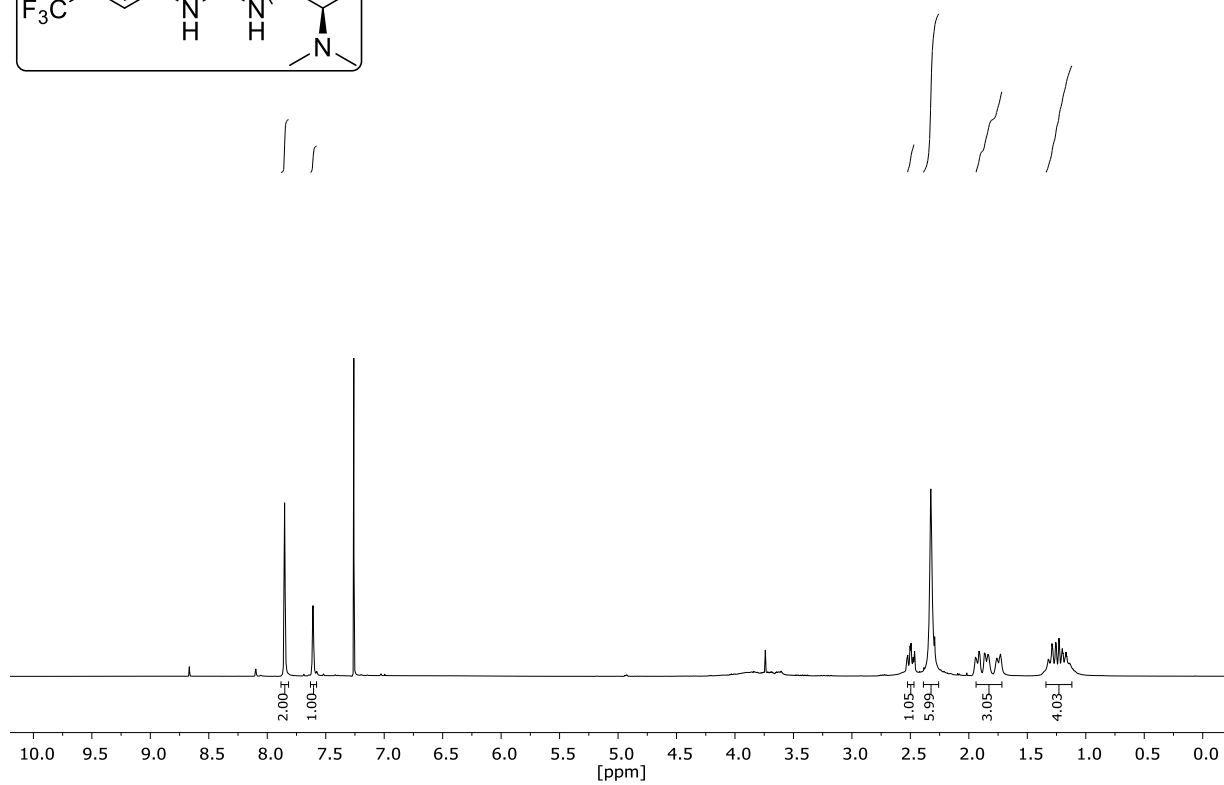
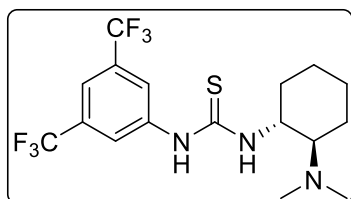
(E)-3-(2-Nitrovinyl)pyridine (56k)NMR-Solvent: CDCl₃

(E)-2-Methyl-3-(2-nitrovinyl)-1H-indole (56l)

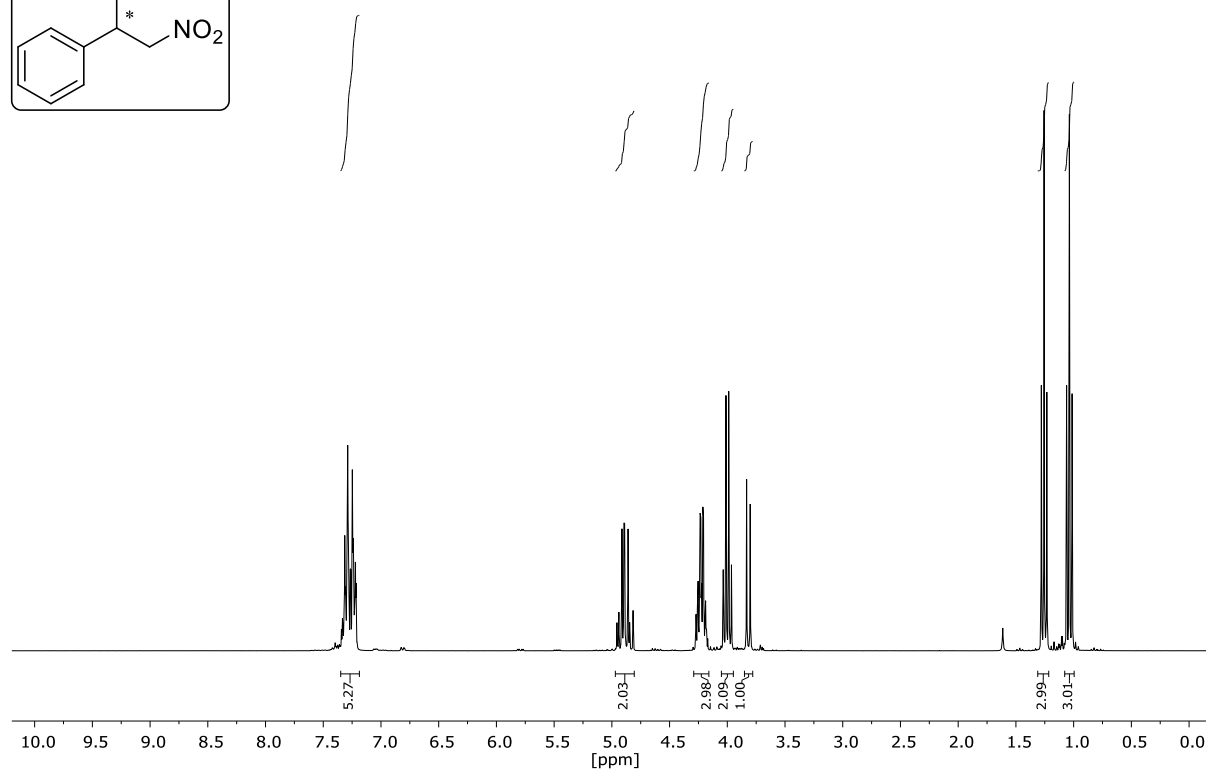
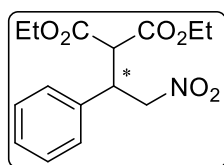
NMR-Solvent: DMSO

(E)-3-(2-Nitrovinyl)-1H-indole (56m)

NMR-Solvent: DMSO

**1-(3,5-bis(Trifluoromethyl)phenyl)-3-((1*R*,2*R*)-2-(dimethylamino)cyclohexyl)thiourea
(57)**NMR-Solvent: CDCl₃

Diethyl 2-(2-nitro-1-phenylethyl)malonate (58a)



167.57
166.92

136.31
129.03
128.45
128.13

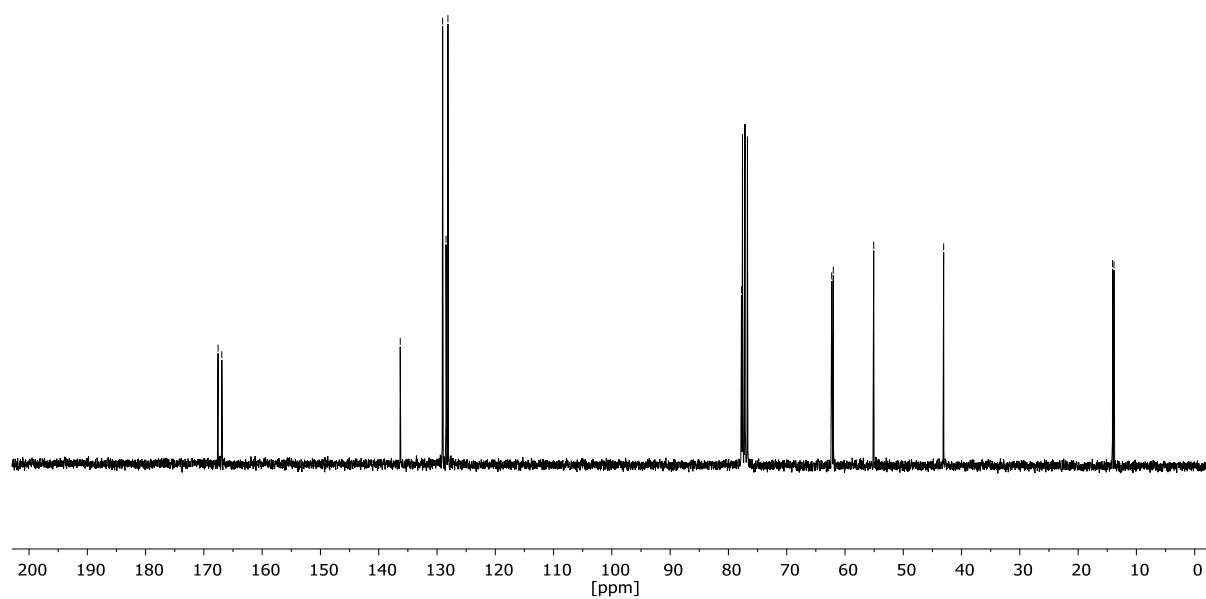
77.76

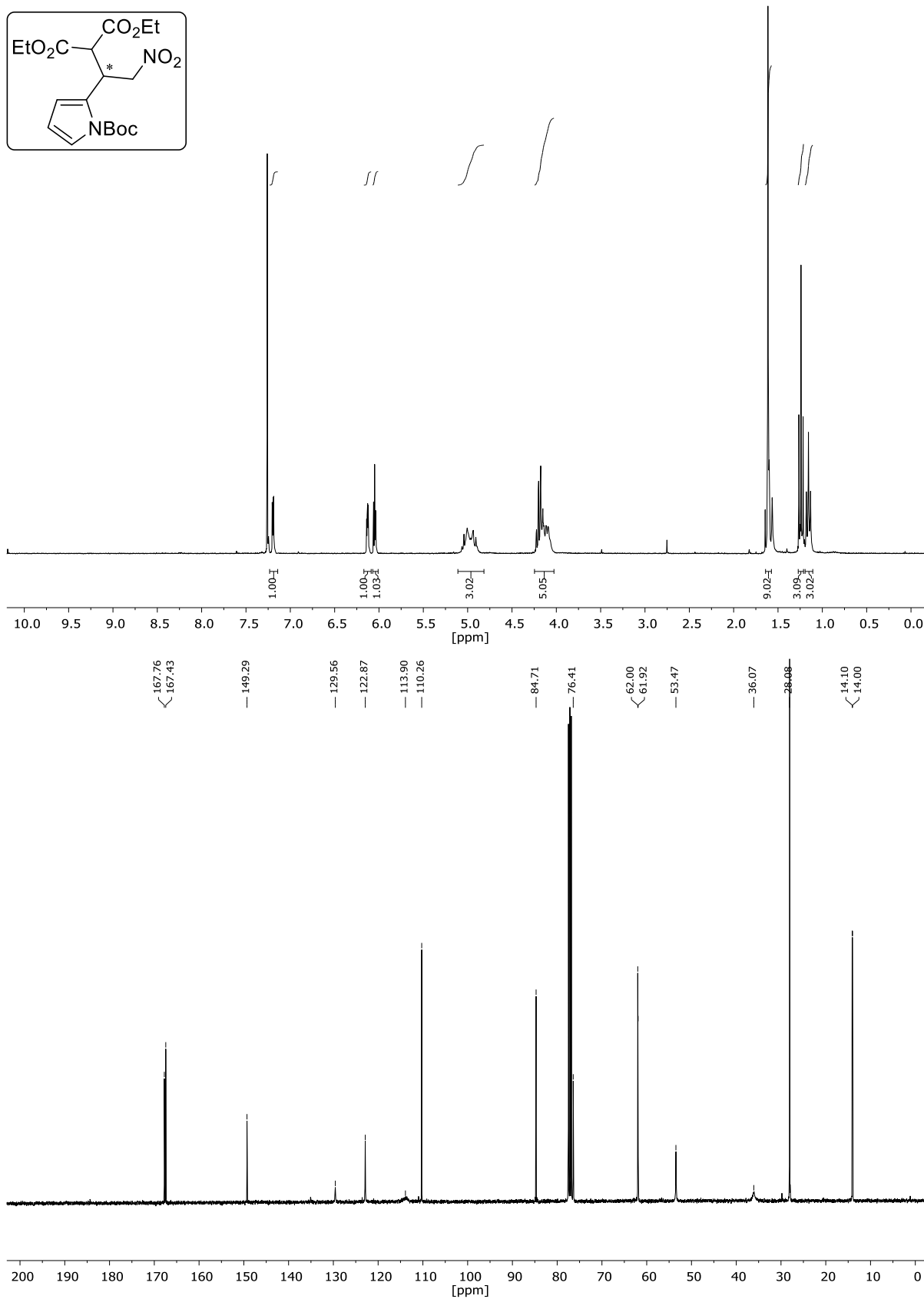
62.28
62.00

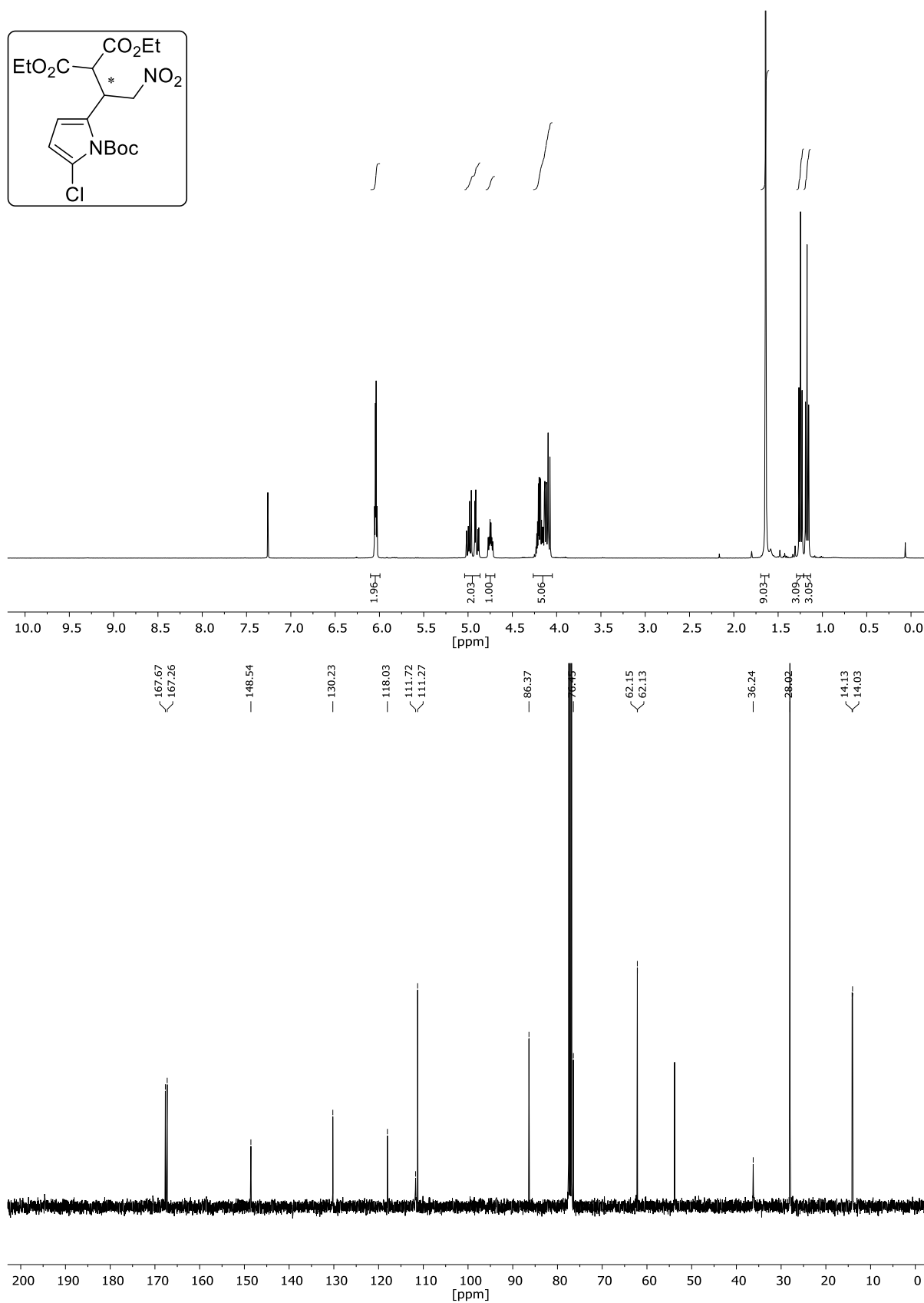
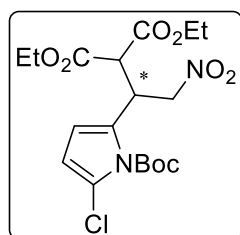
55.07

43.07

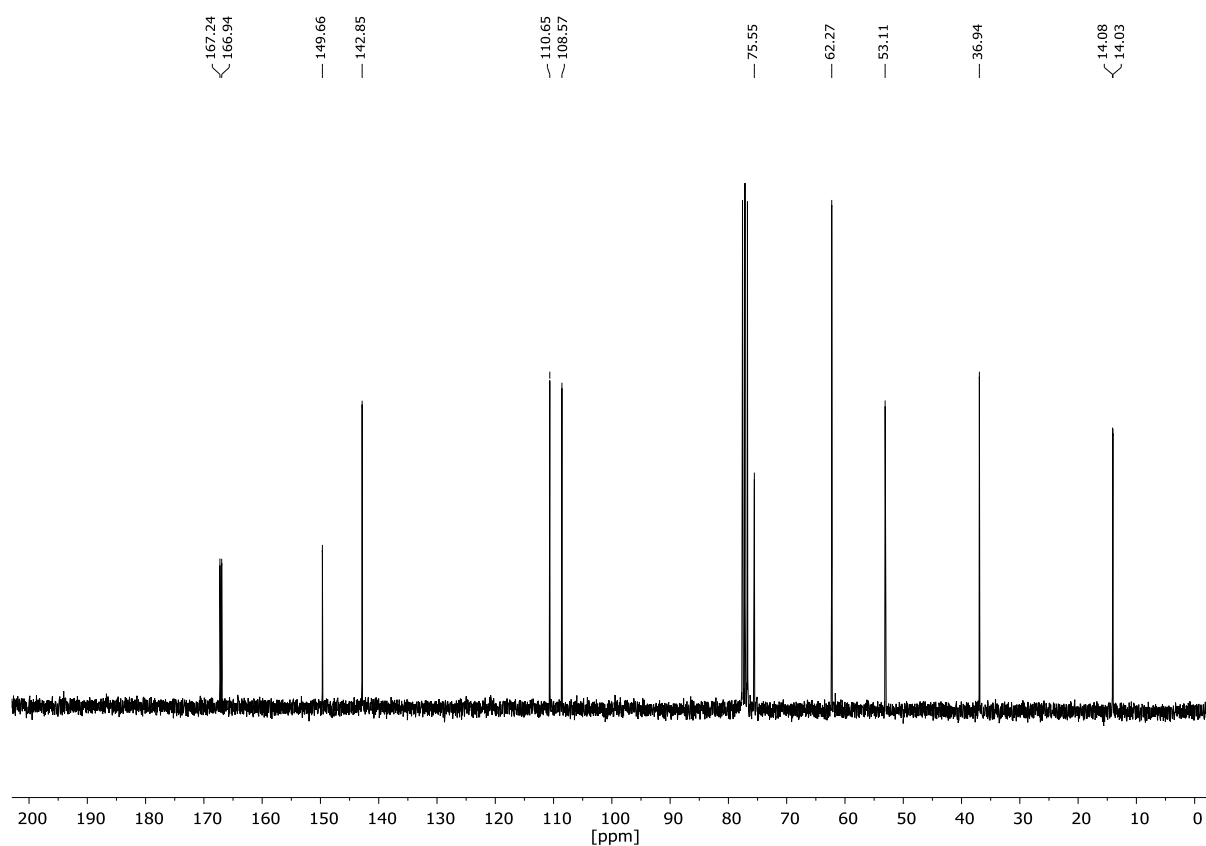
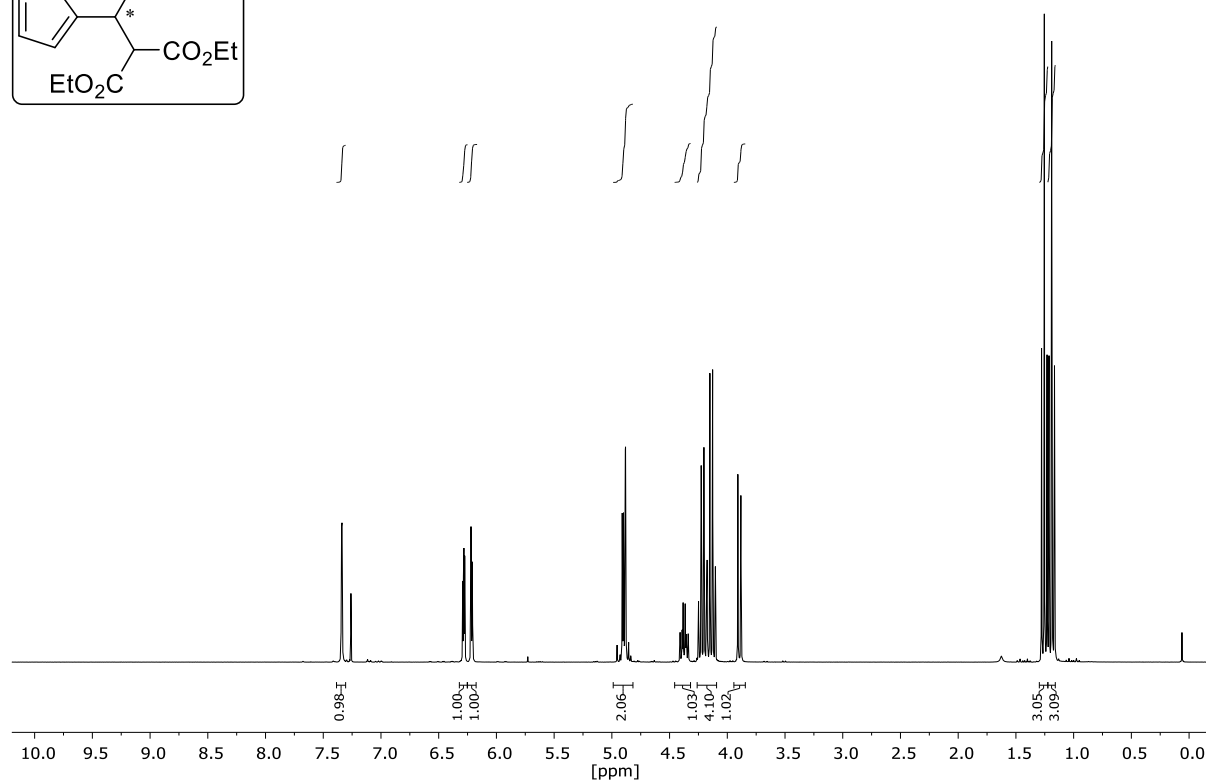
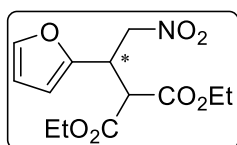
14.08
13.85

NMR-Solvent: CDCl₃

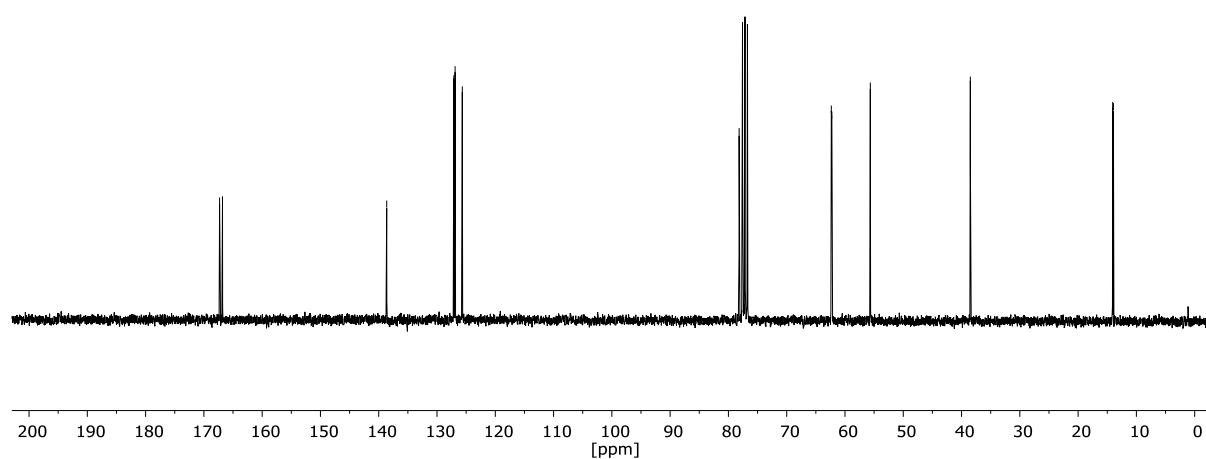
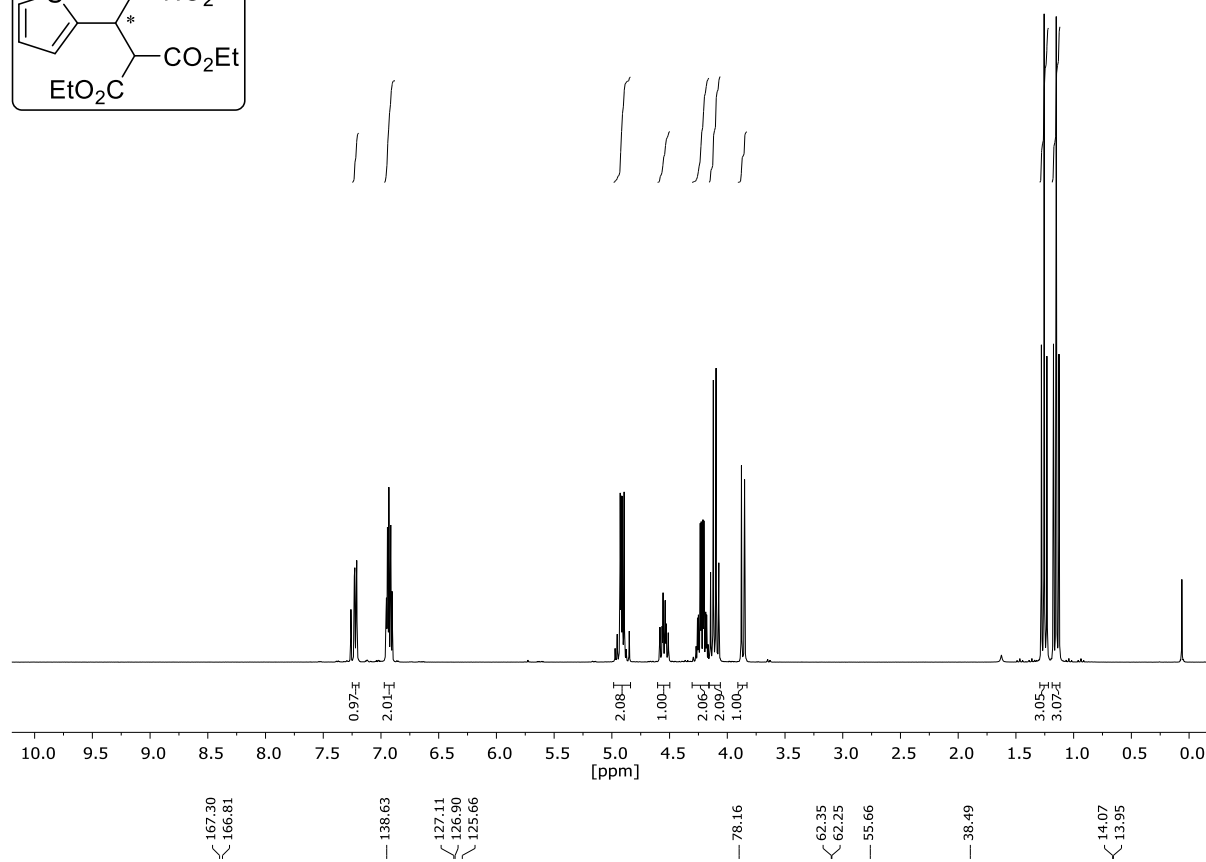
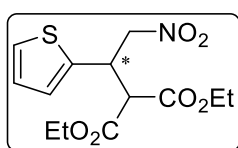
Diethyl-2-(1-(1-(*tert*-butyloxycarbonyl)-1*H*-pyrrol-2-yl)-2-nitroethyl)malonate (58b)NMR-Solvent: CDCl₃

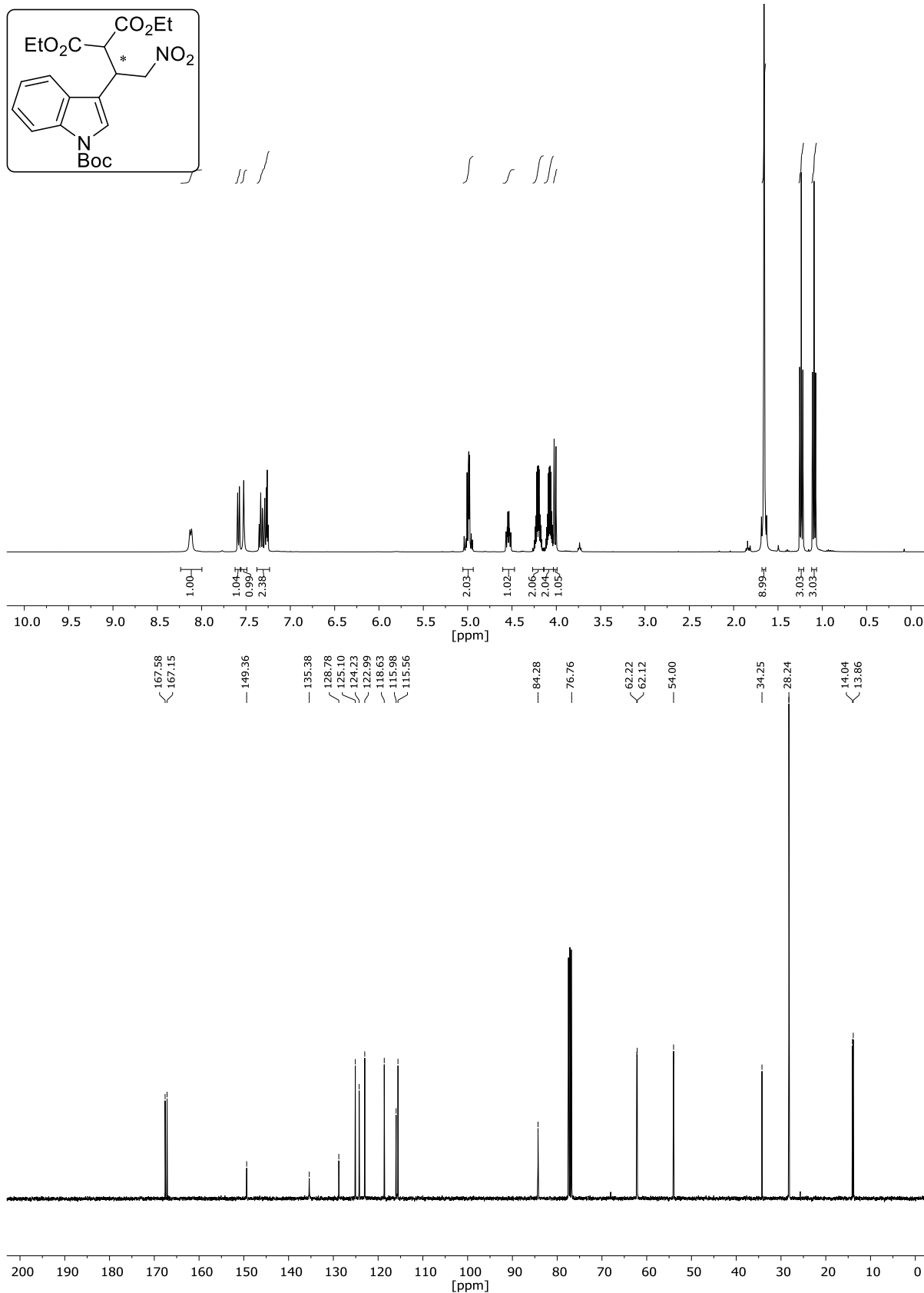
Diethyl 2-(1-(1-(*tert*-butoxycarbonyl)-5-chloro-1*H*-pyrrol-2-yl)-2-nitroethyl)malonate (58c)NMR-Solvent: CDCl₃

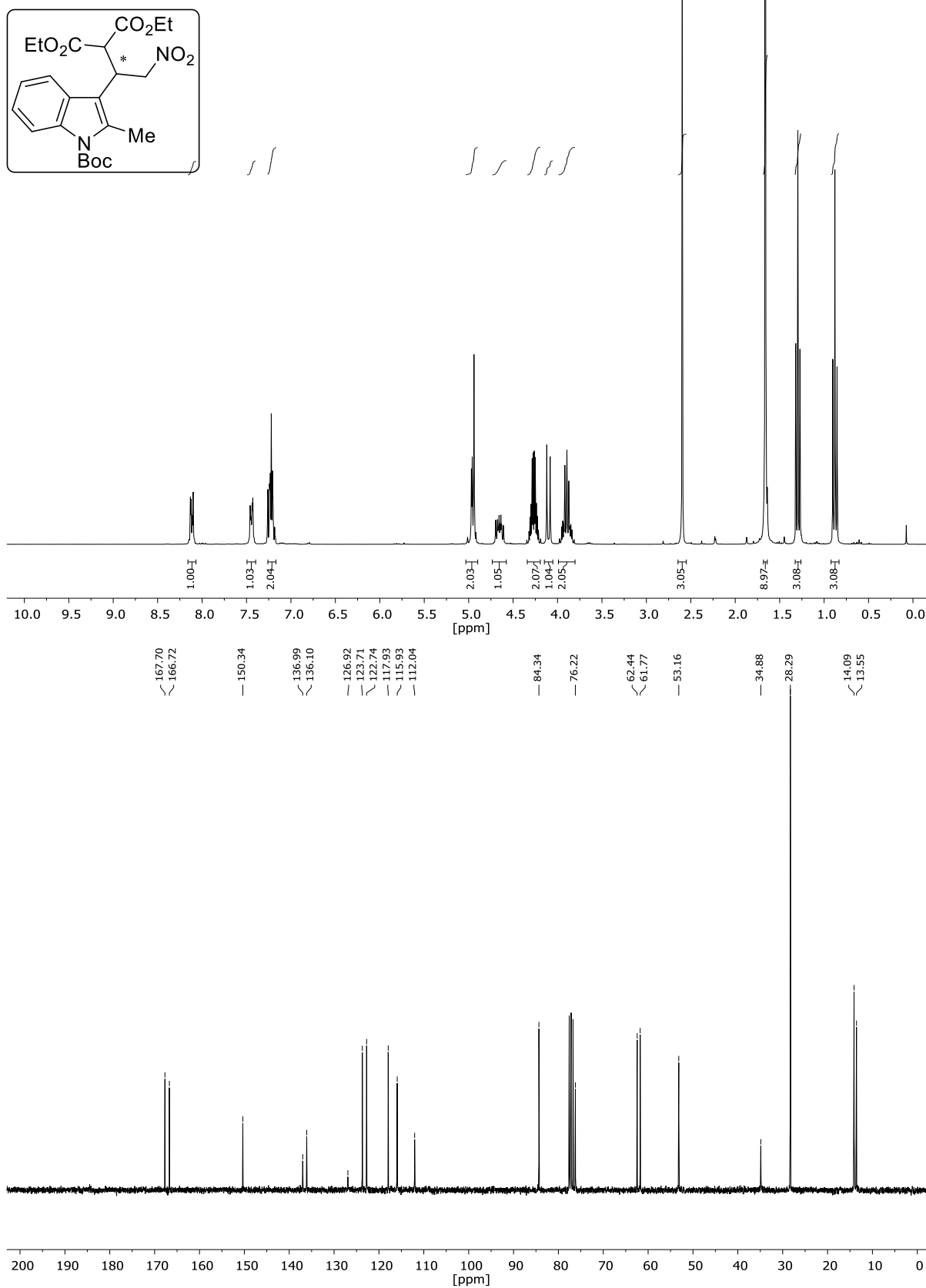
Diethyl 2-(1-(furan-2-yl)-2-nitroethyl)malonate (58d)

NMR-Solvent: CDCl₃

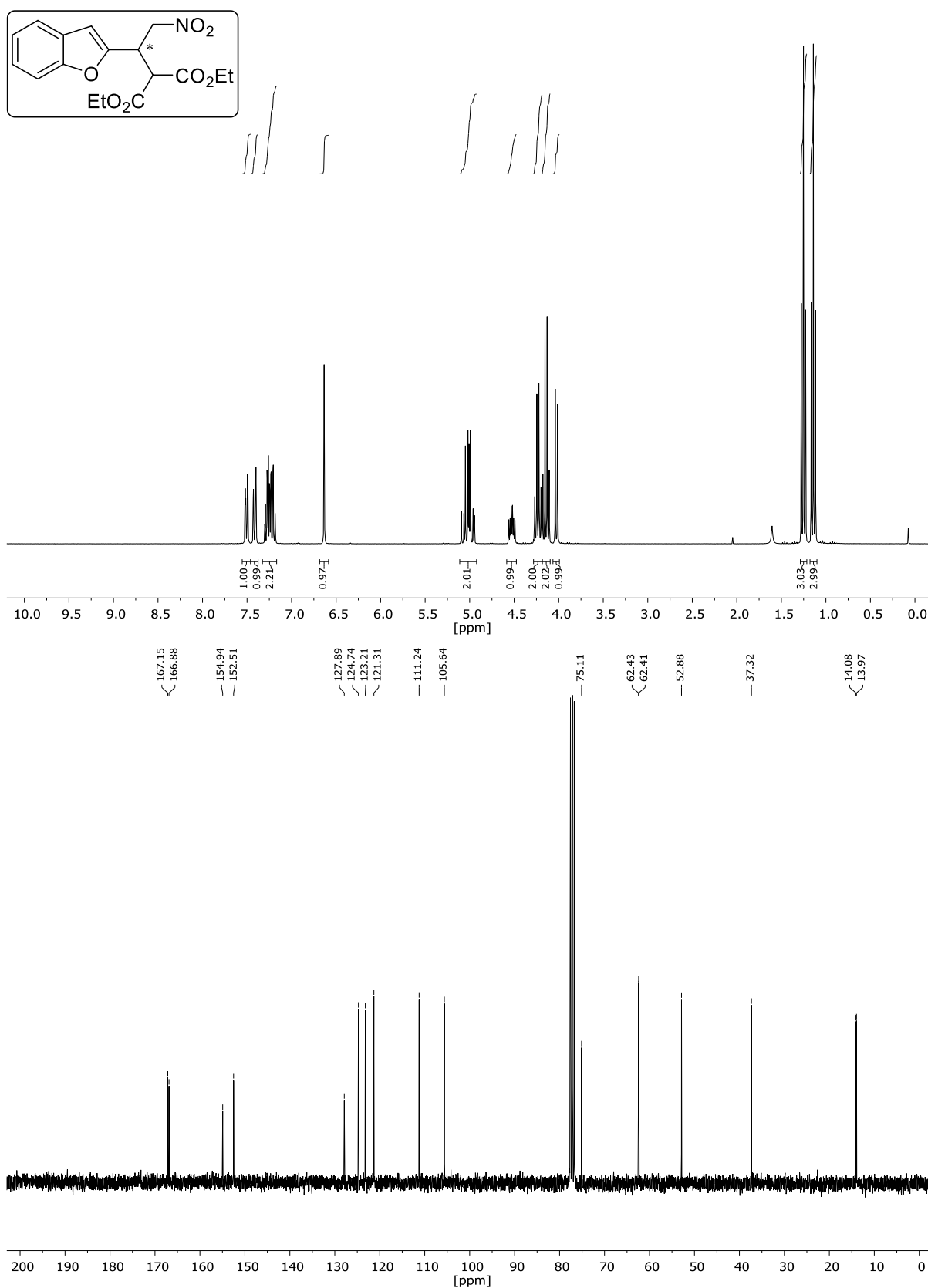
Diethyl 2-(2-nitro-1-(thiophen-2-yl)ethyl)malonate (58e)

NMR-Solvent: CDCl₃

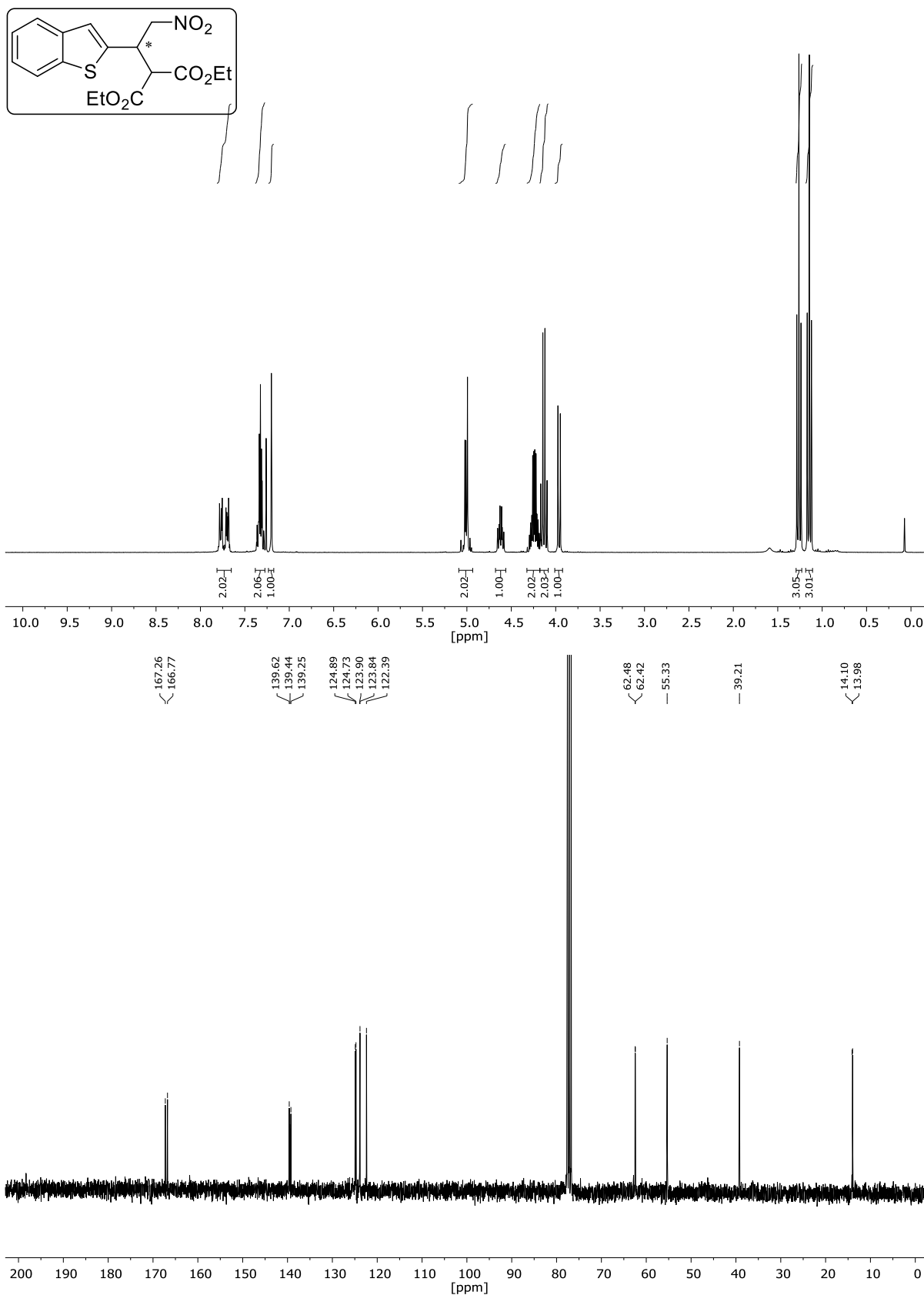
Diethyl-2-(1-(1-(*tert*-butyloxycarbonyl)-1*H*-indol-3-yl)-2-nitroethyl)malonat (58f)NMR-Solvent: CDCl₃

Diethyl-2-(1-(1-(*tert*-butyloxycarbonyl)-2-methyl-1*H*-indol-3-yl)-2-nitroethyl)malonat (58g)NMR-Solvent: CDCl₃

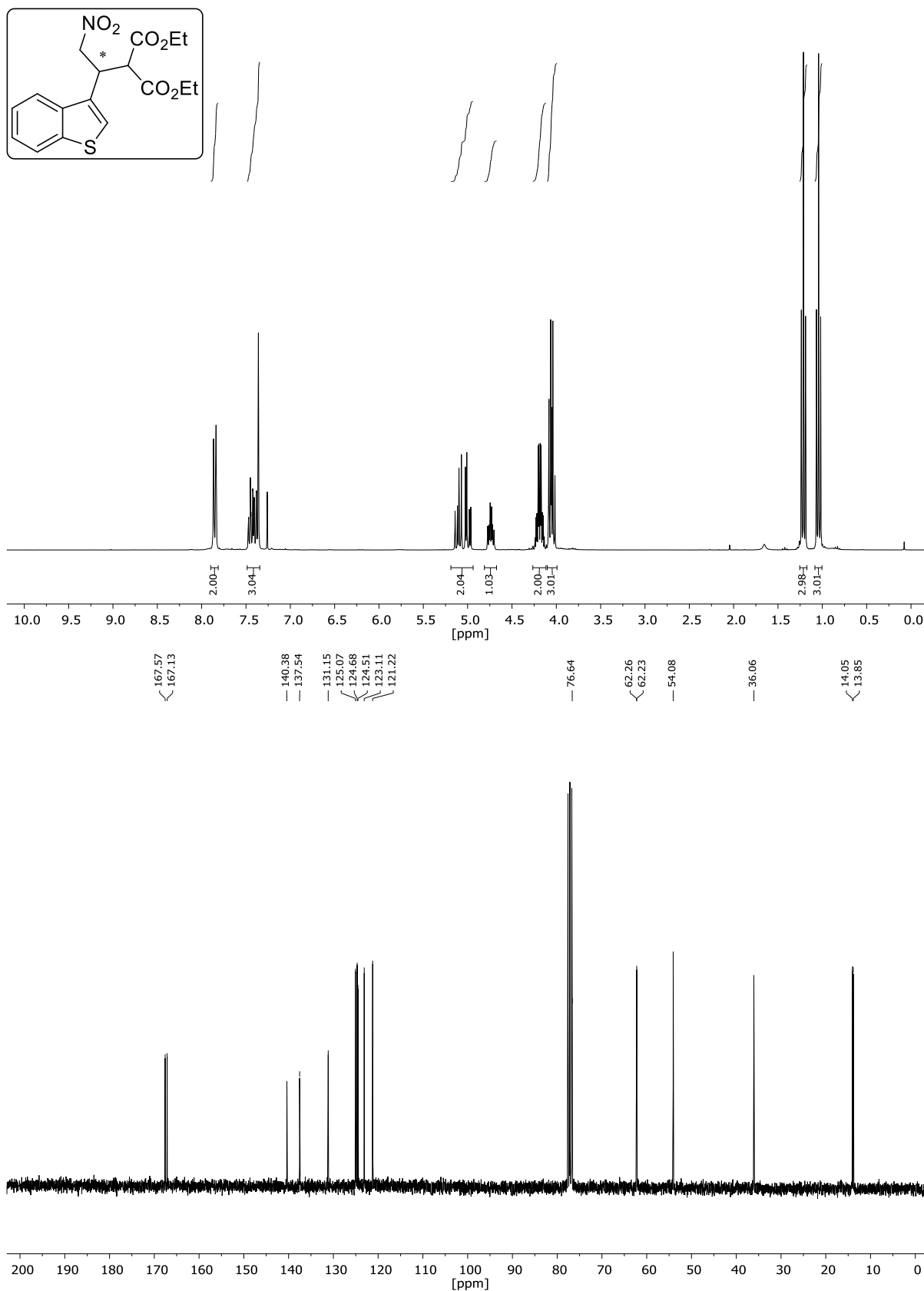
Diethyl 2-(1-(benzofuran-2-yl)-2-nitroethyl)malonate (58h)

NMR-Solvent: CDCl₃

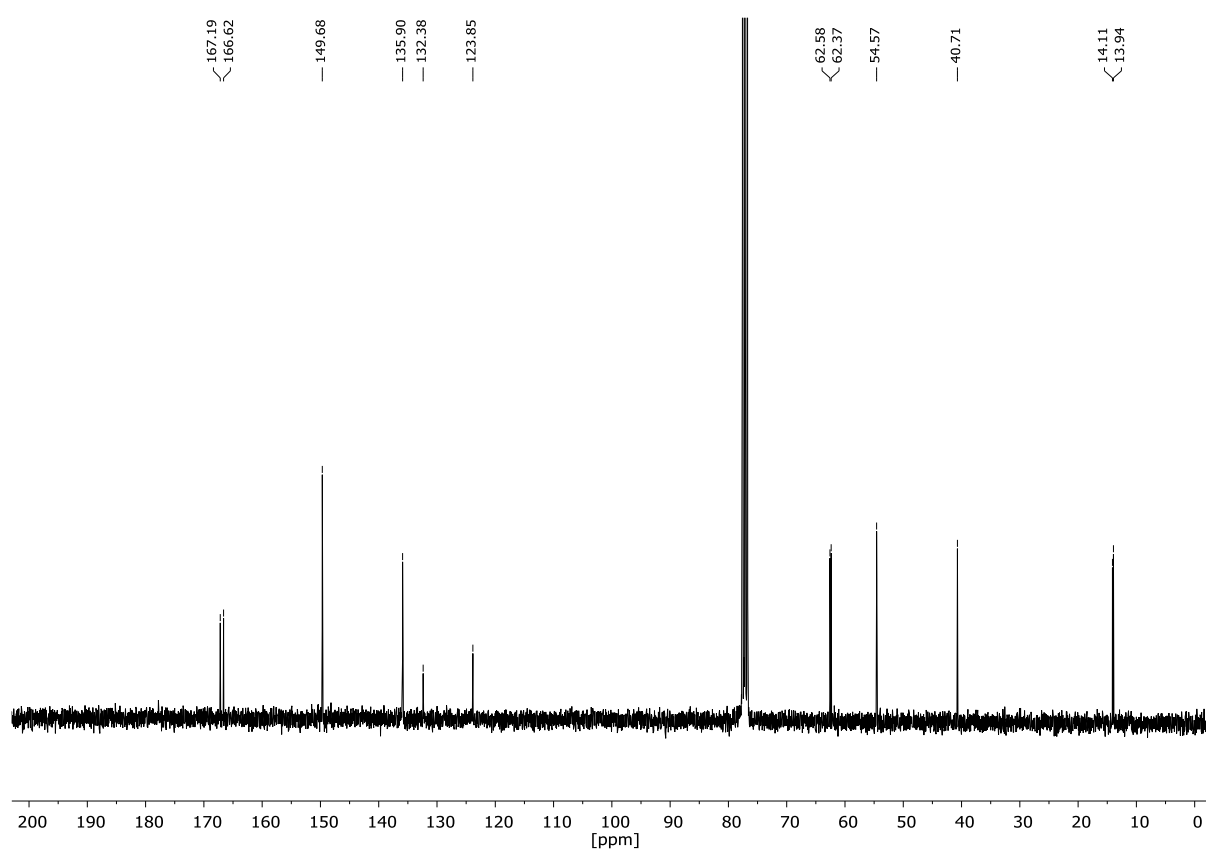
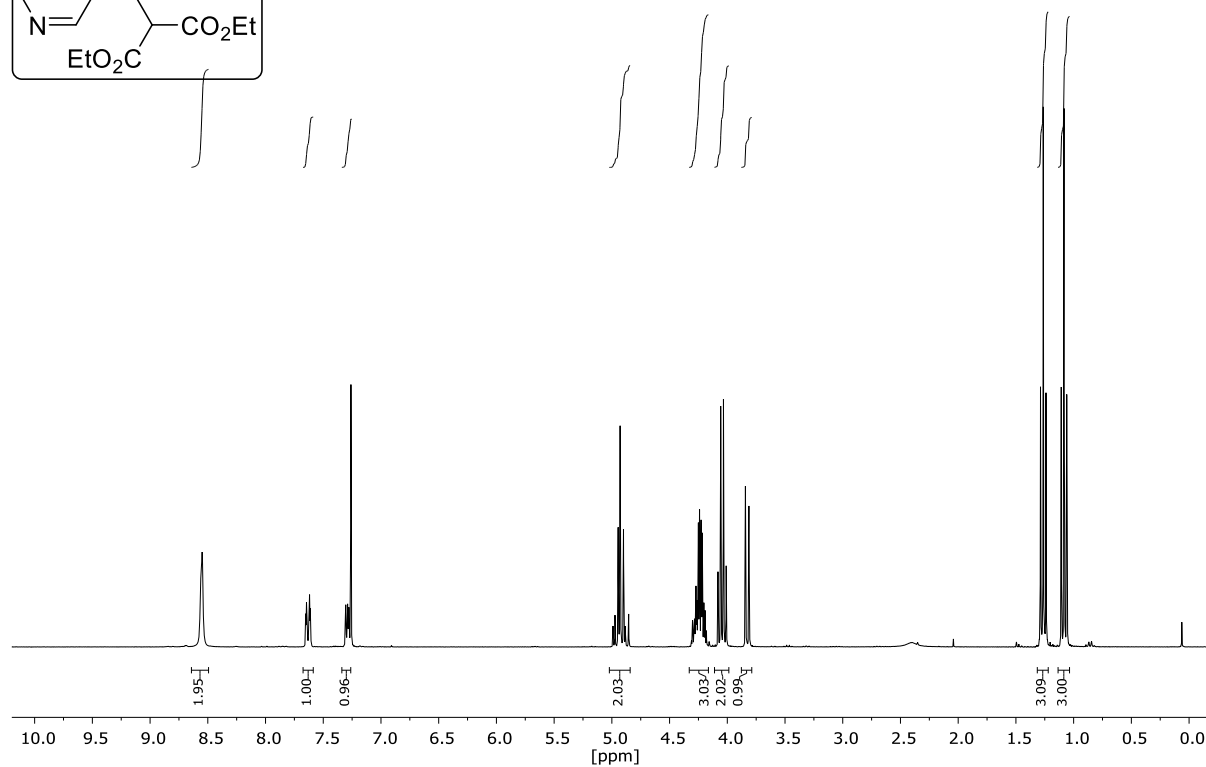
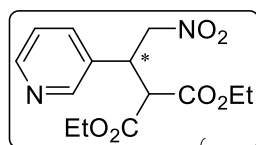
Diethyl 2-(1-(benzo[b]thiophen-2-yl)-2-nitroethyl)malonate (58i)

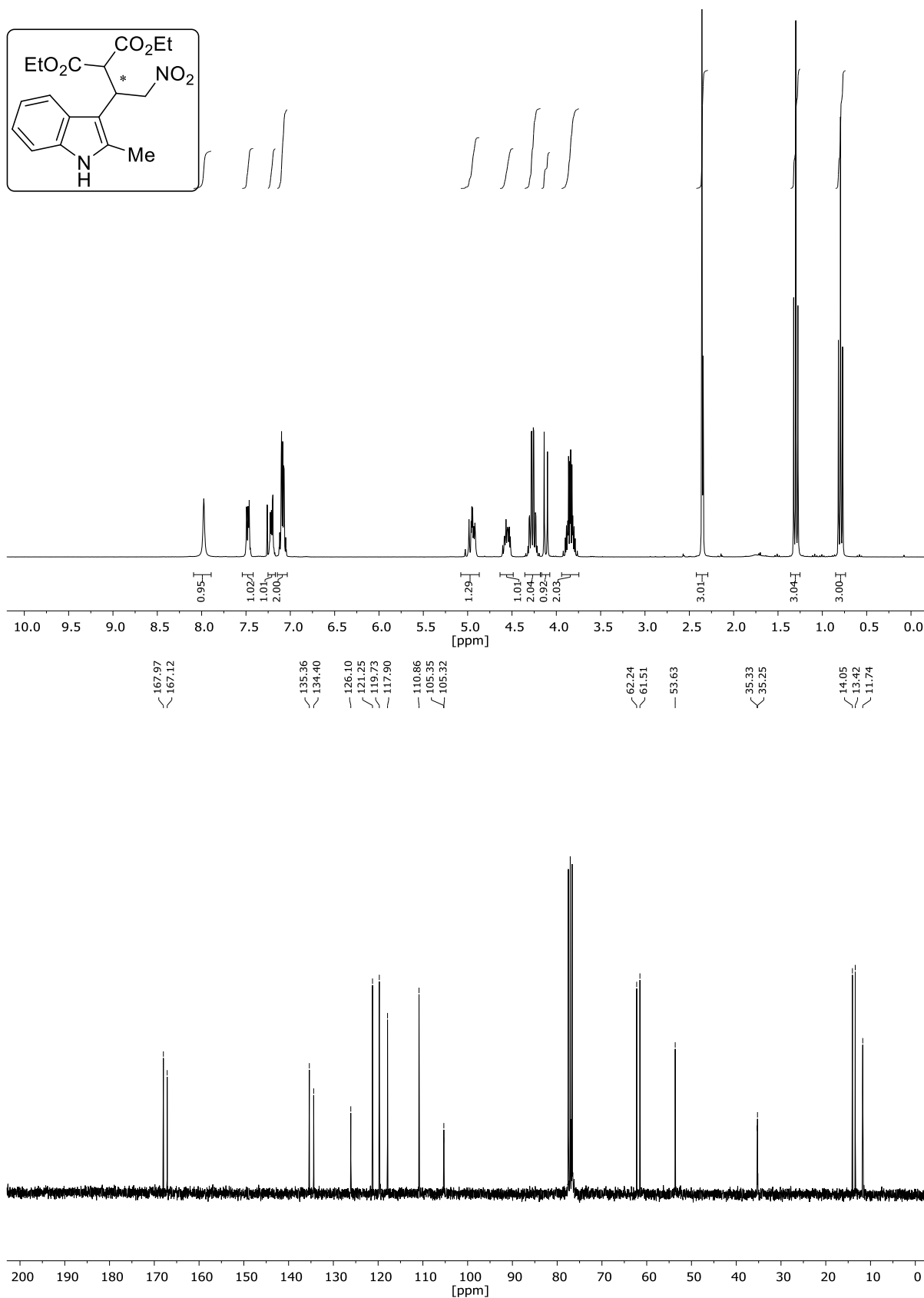
NMR-Solvent: CDCl₃

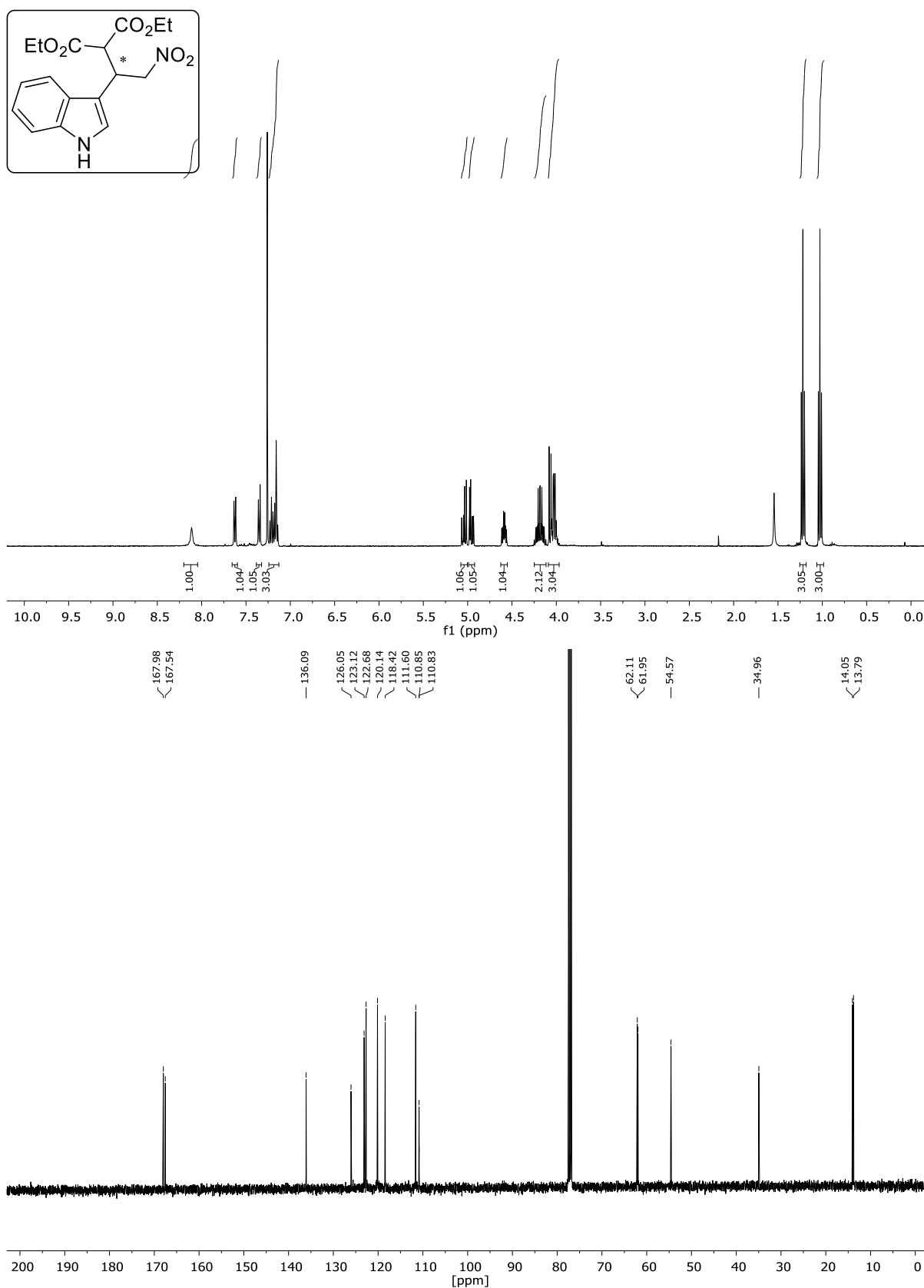
Diethyl 2-(1-(benzo[b]thiophen-3-yl)-2-nitroethyl)malonate (58j)

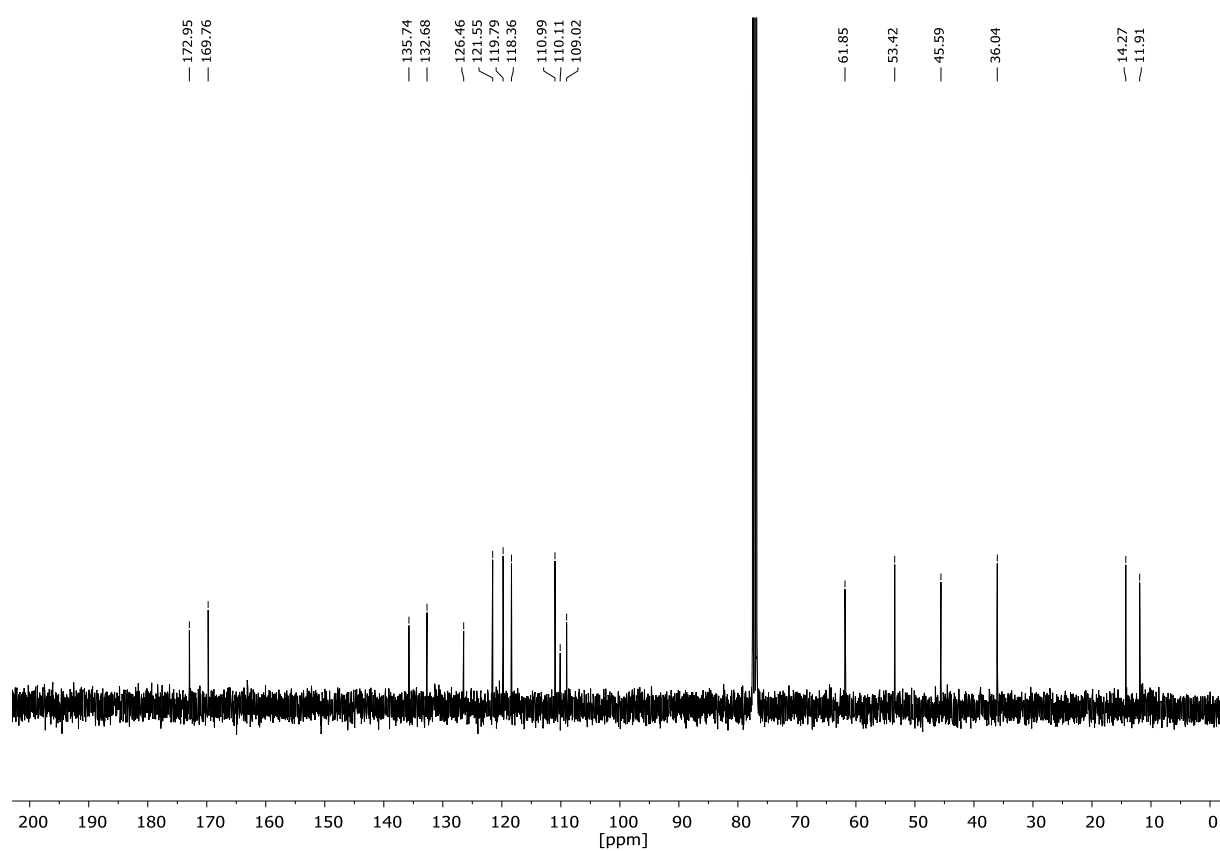
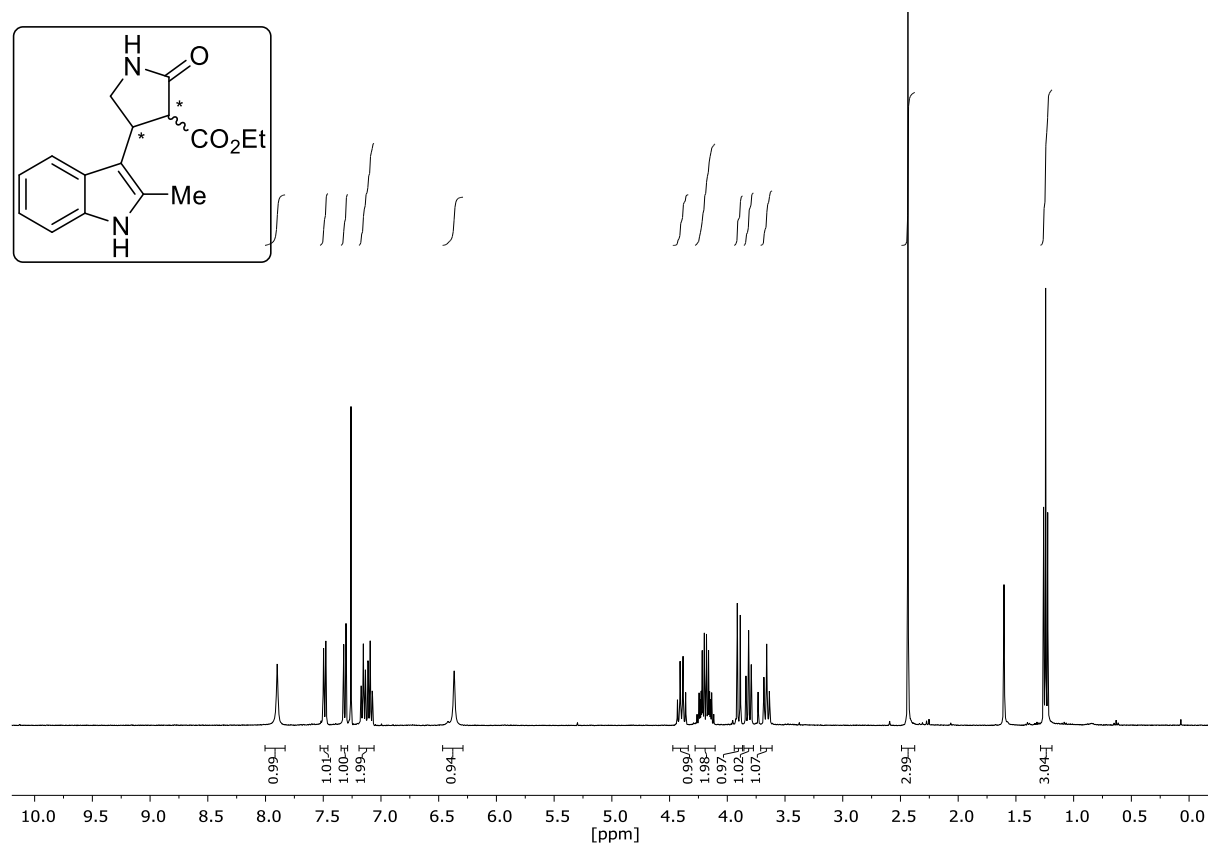
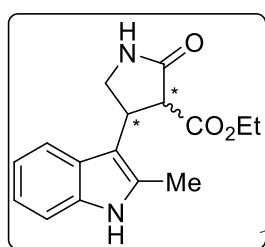
NMR-Solvent: CDCl₃

Diethyl 2-(2-nitro-1-(pyridin-3-yl)ethyl)malonate (58k)

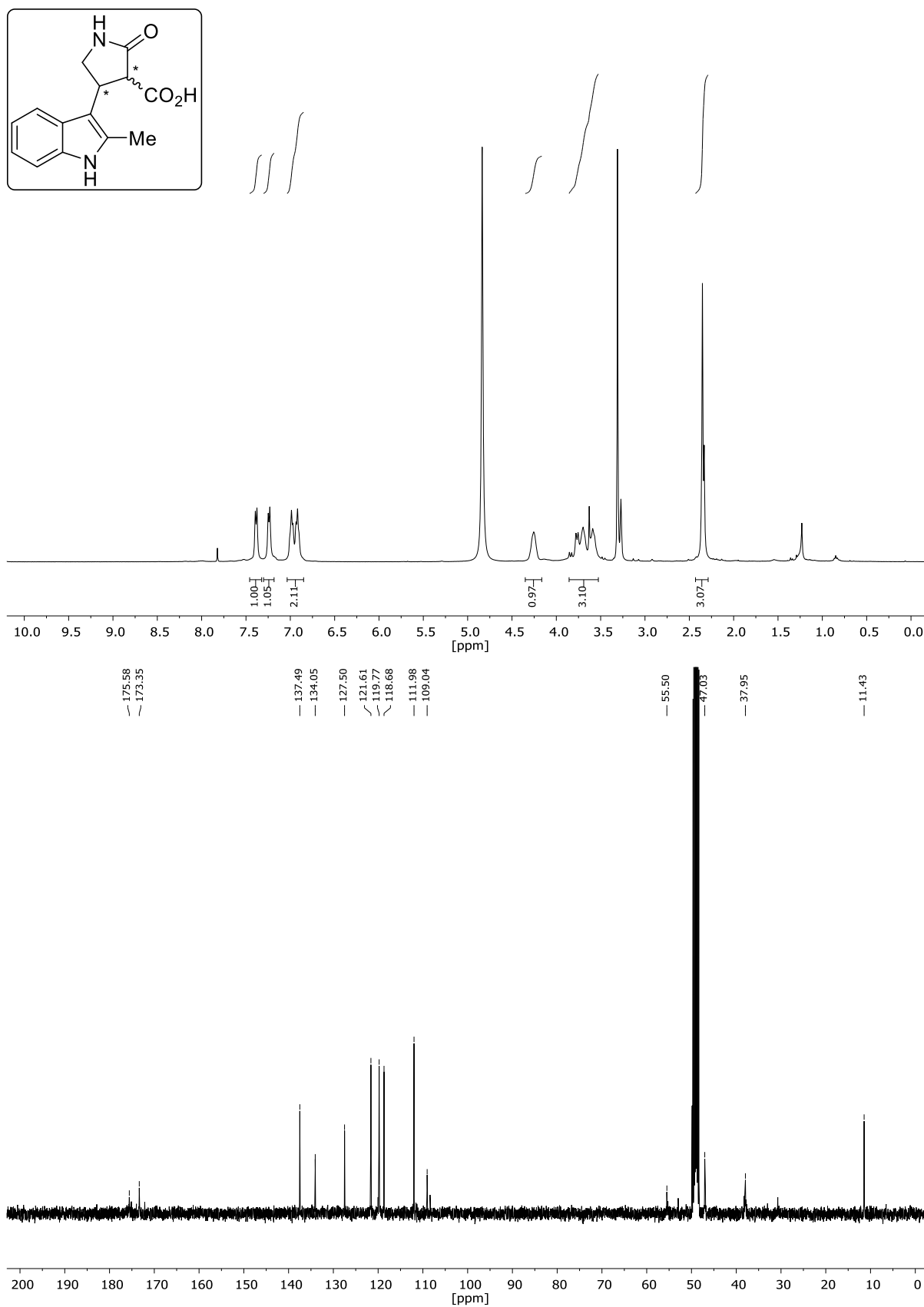
NMR-Solvent: CDCl_3

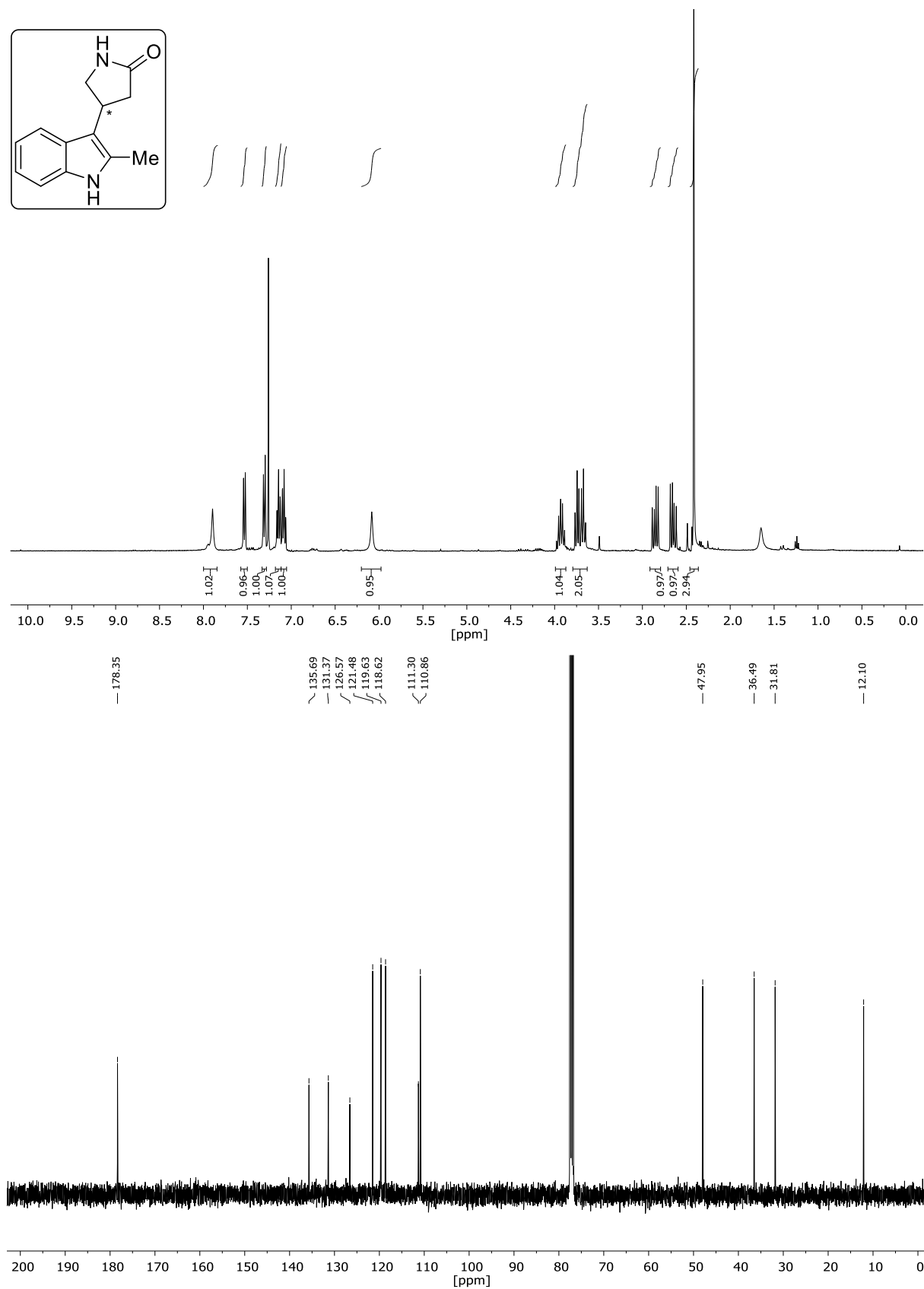
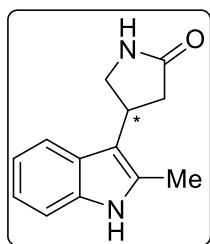
Diethyl-2-(1-(2-methyl-1*H*-indol-3-yl)-2-nitroethyl)malonat (58l)NMR-Solvent: CDCl₃

Diethyl-2-(2-(1*H*-indol-3-yl)-2-nitroethyl)malonat (58m)NMR-Solvent: CDCl₃

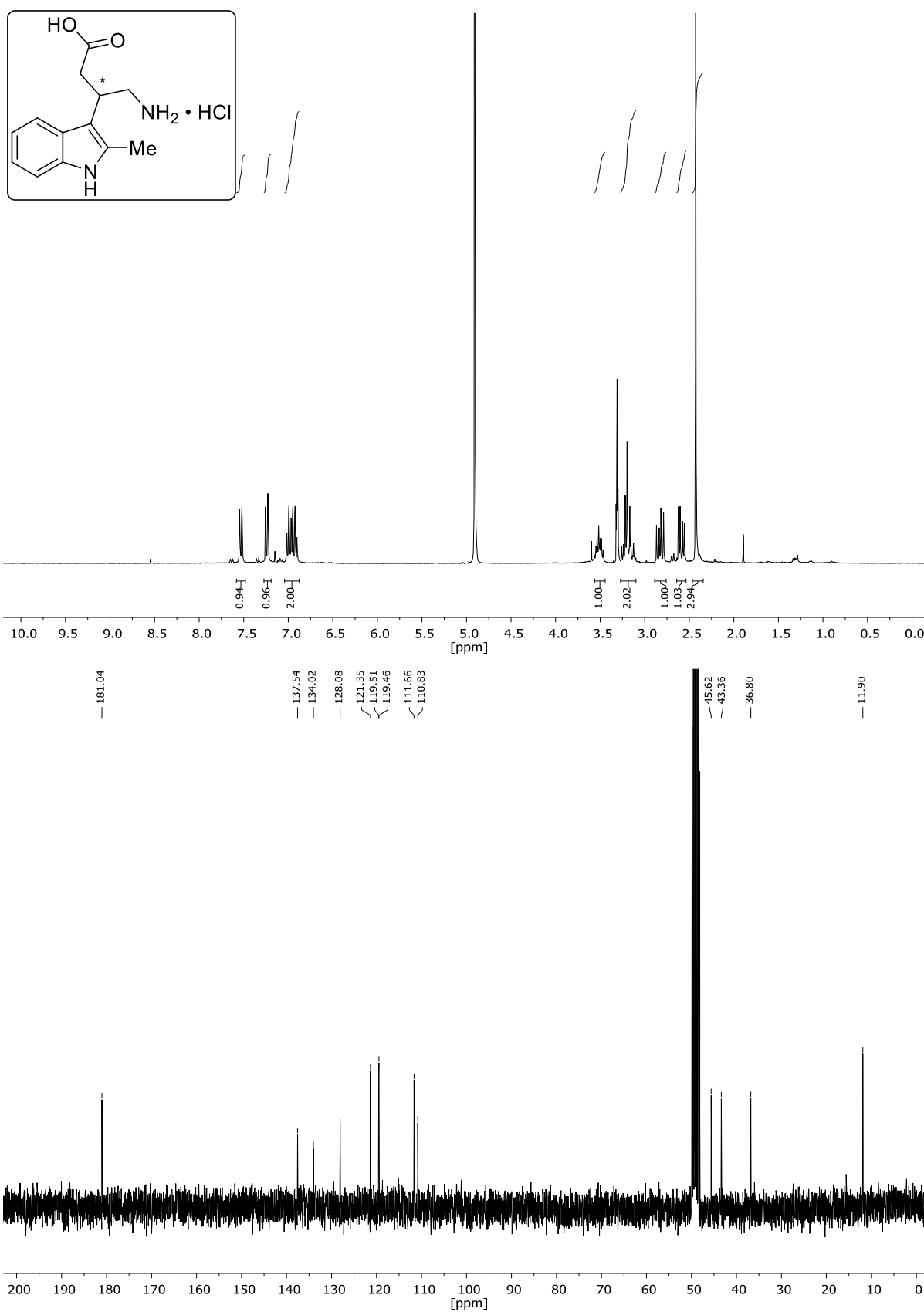
Rac. Ethyl 4-(2-methyl-1H-indol-3-yl)-2-oxopyrrolidine-3-carboxylate (61)NMR-Solvent: CDCl_3

Rac. 4-(2-methyl-1H-indol-3-yl)-2-oxopyrrolidine-3-carboxylic acid (62)

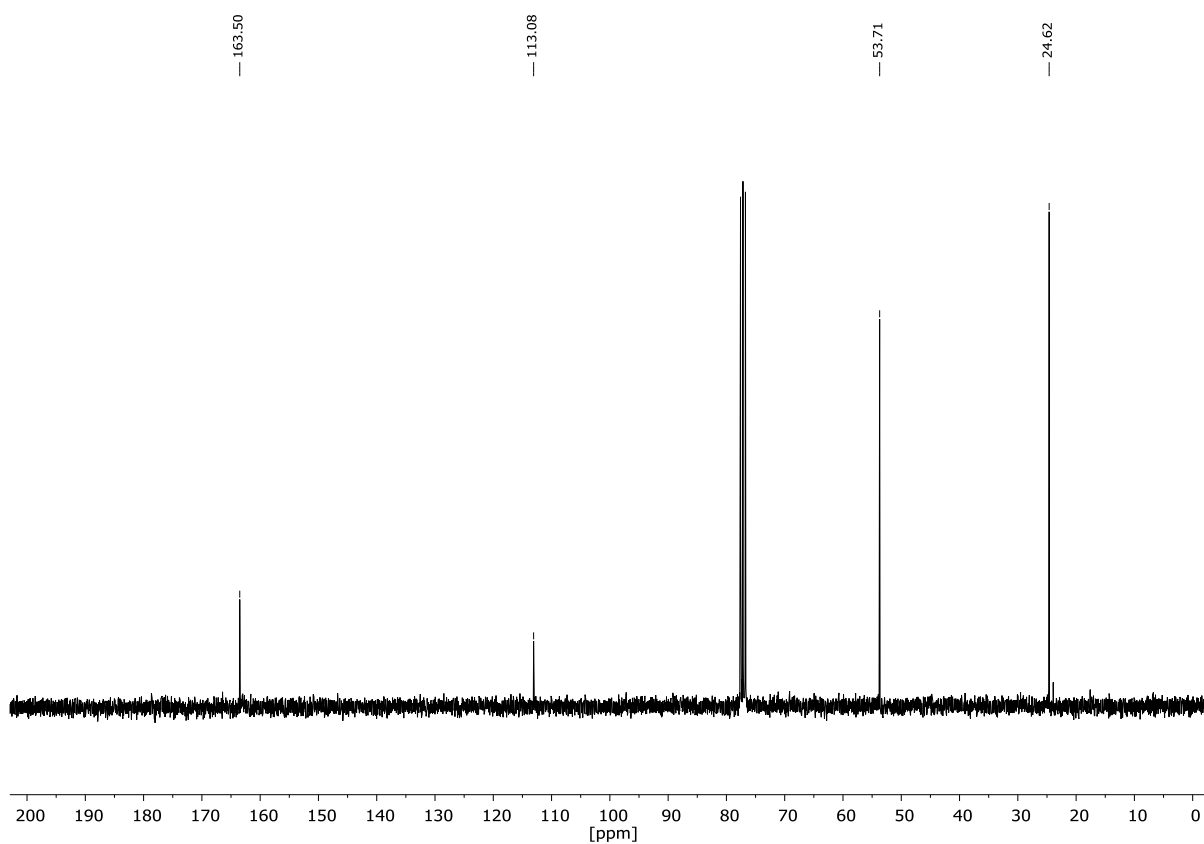
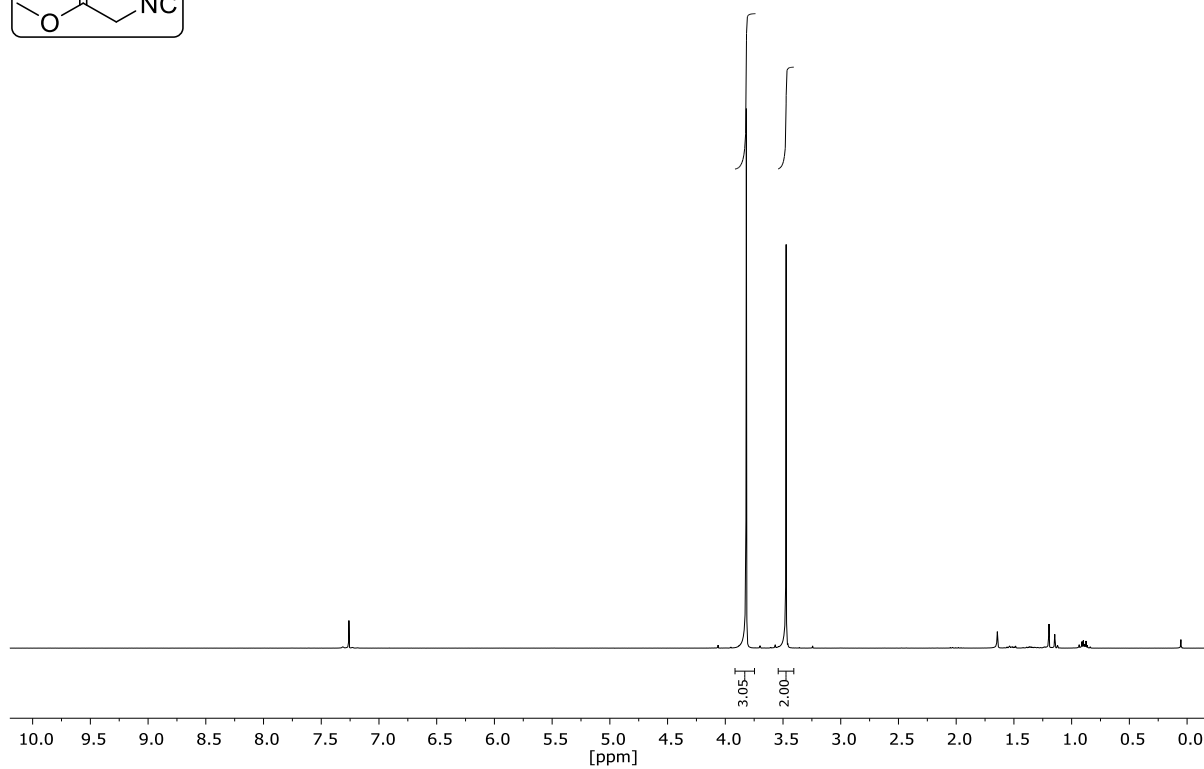
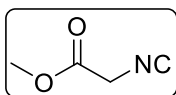
NMR-Solvent: CD₃OD

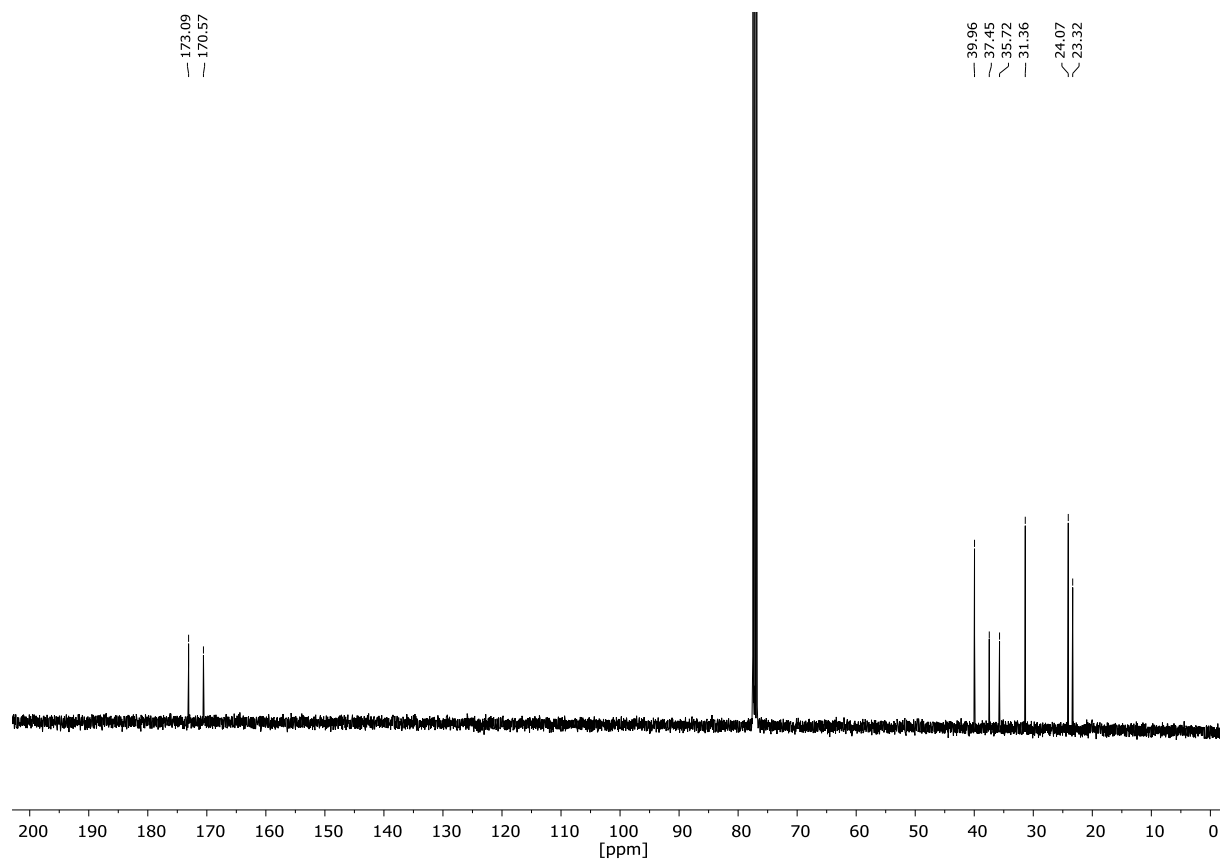
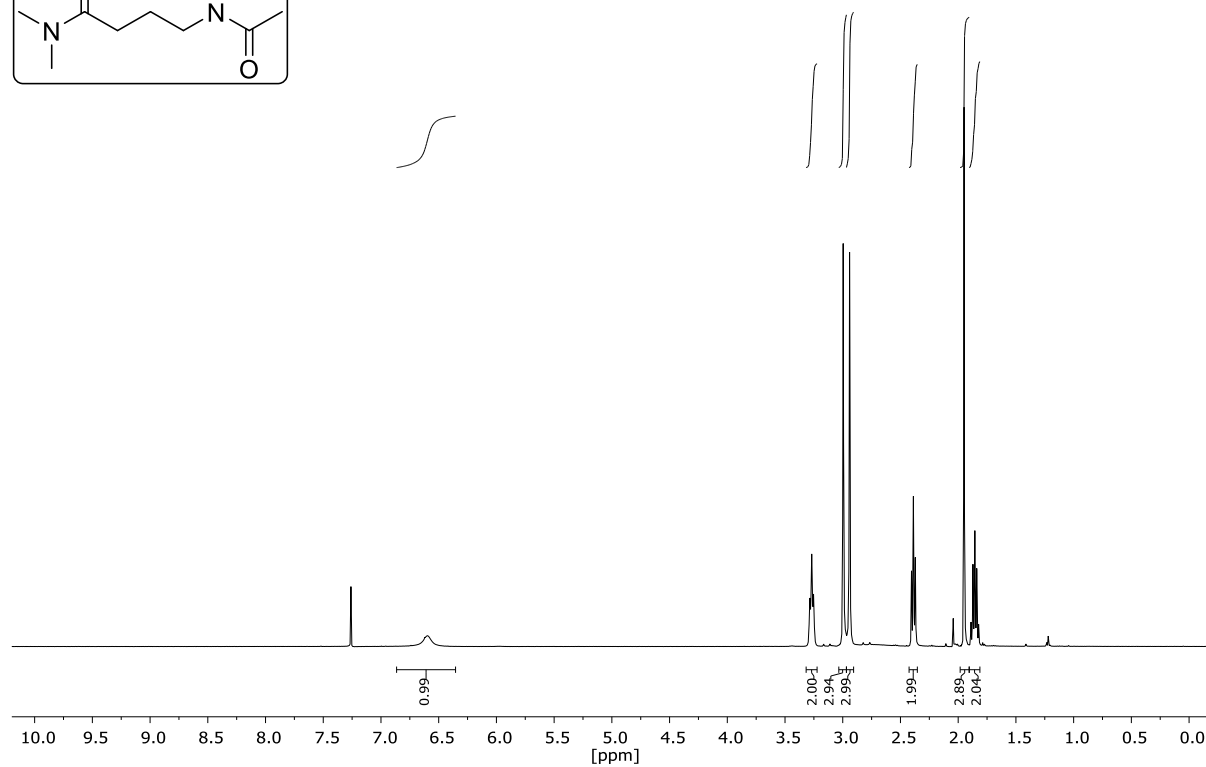
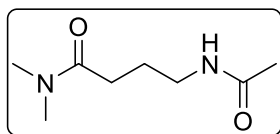
Rac. 4-(2-methyl-1*H*-indol-3-yl)pyrrolidin-2-one (63)NMR-Solvent: CDCl₃

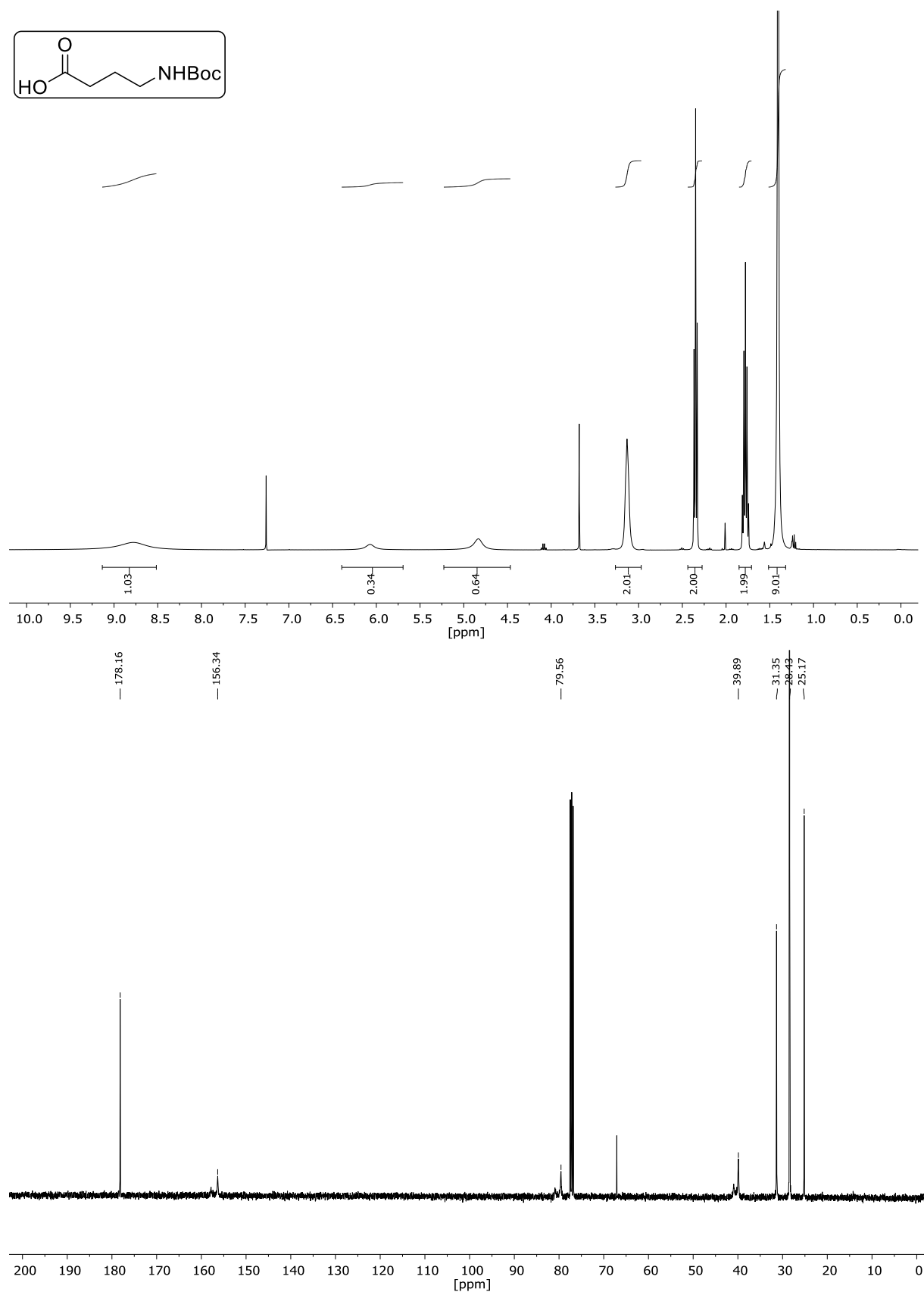
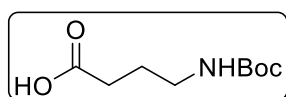
Rac. 4-amino-3-(2-methyl-1H-indol-3-yl)butanoic acid hydrochloride (64)

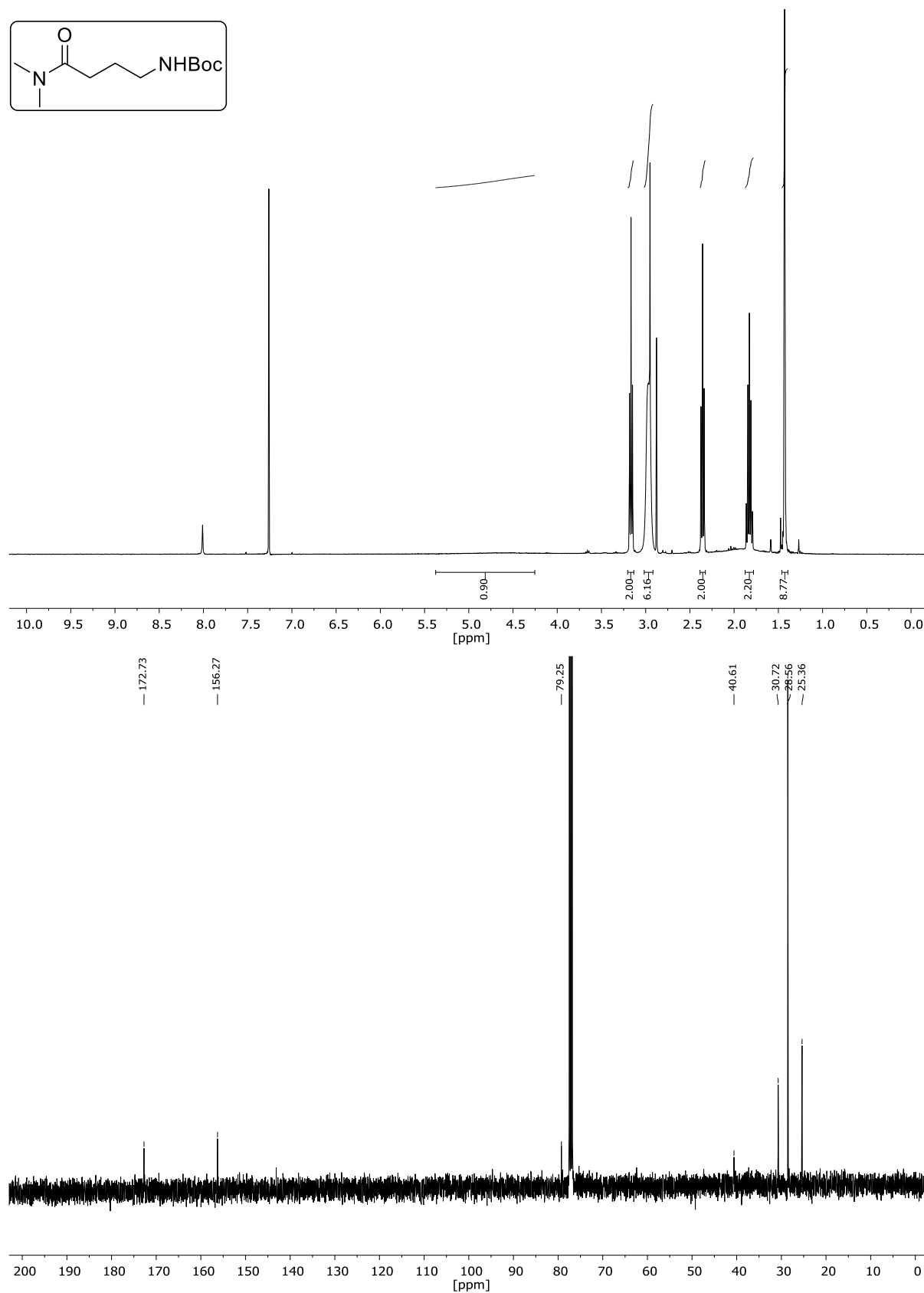
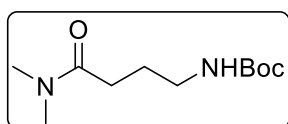
NMR-Solvent: CD₃OD

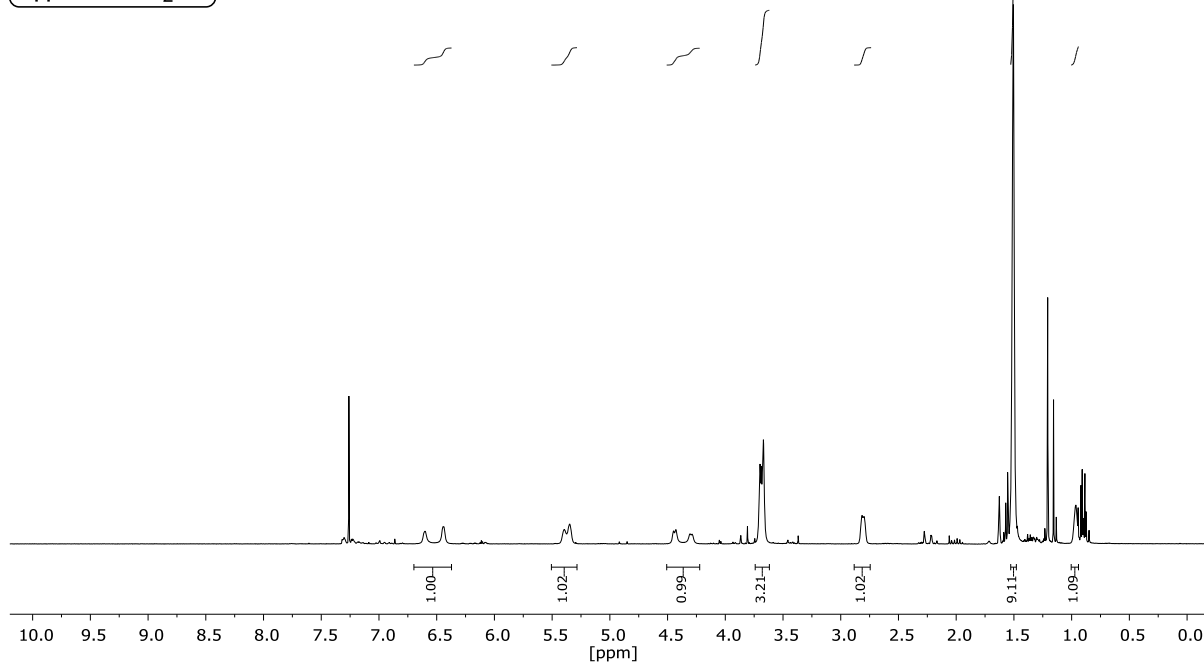
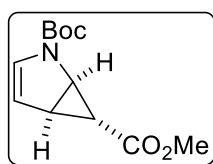
Methyl 2-isocyanoacetate (66)

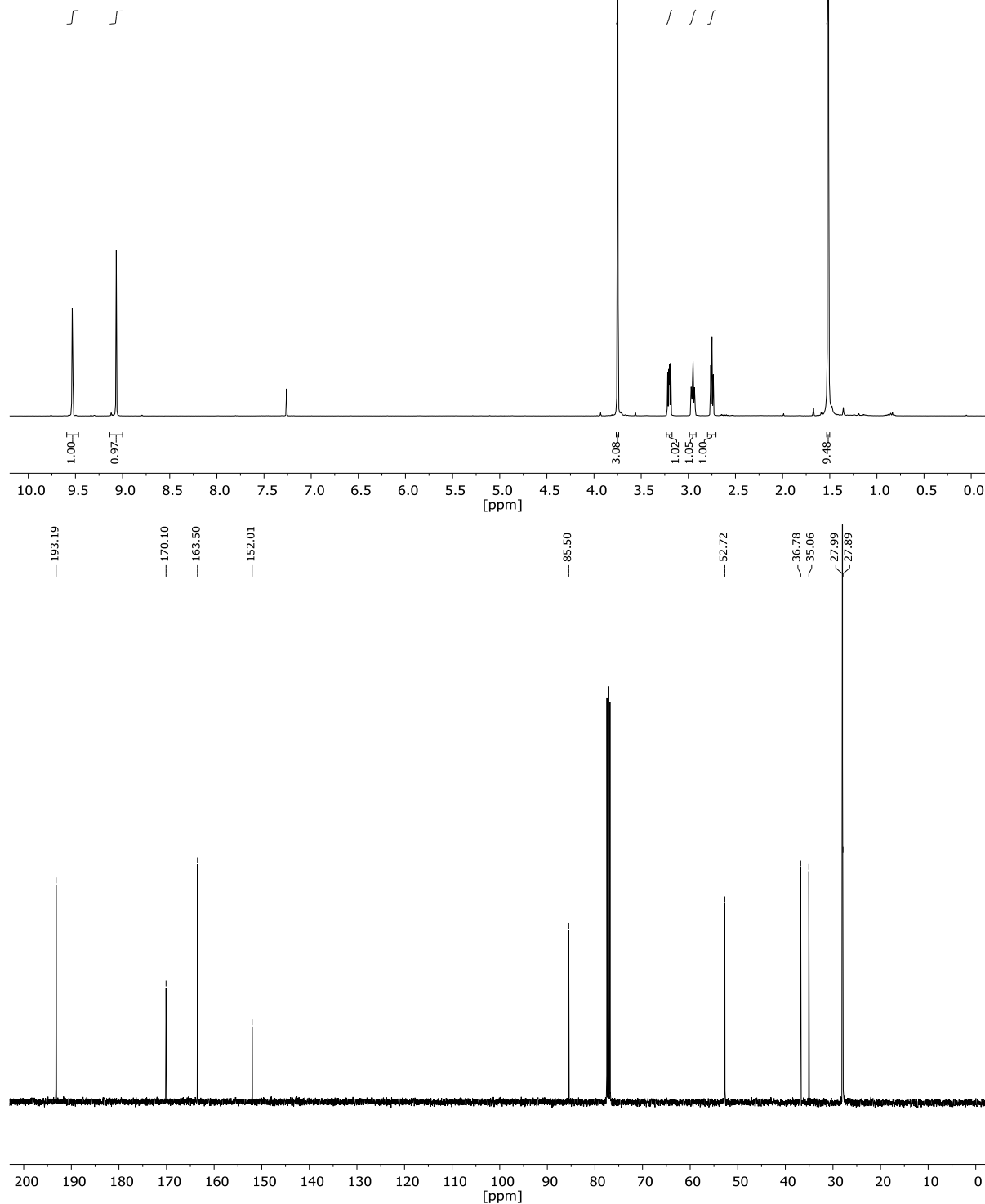
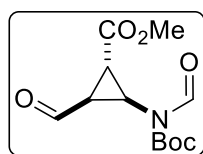
NMR-Solvent: CDCl₃

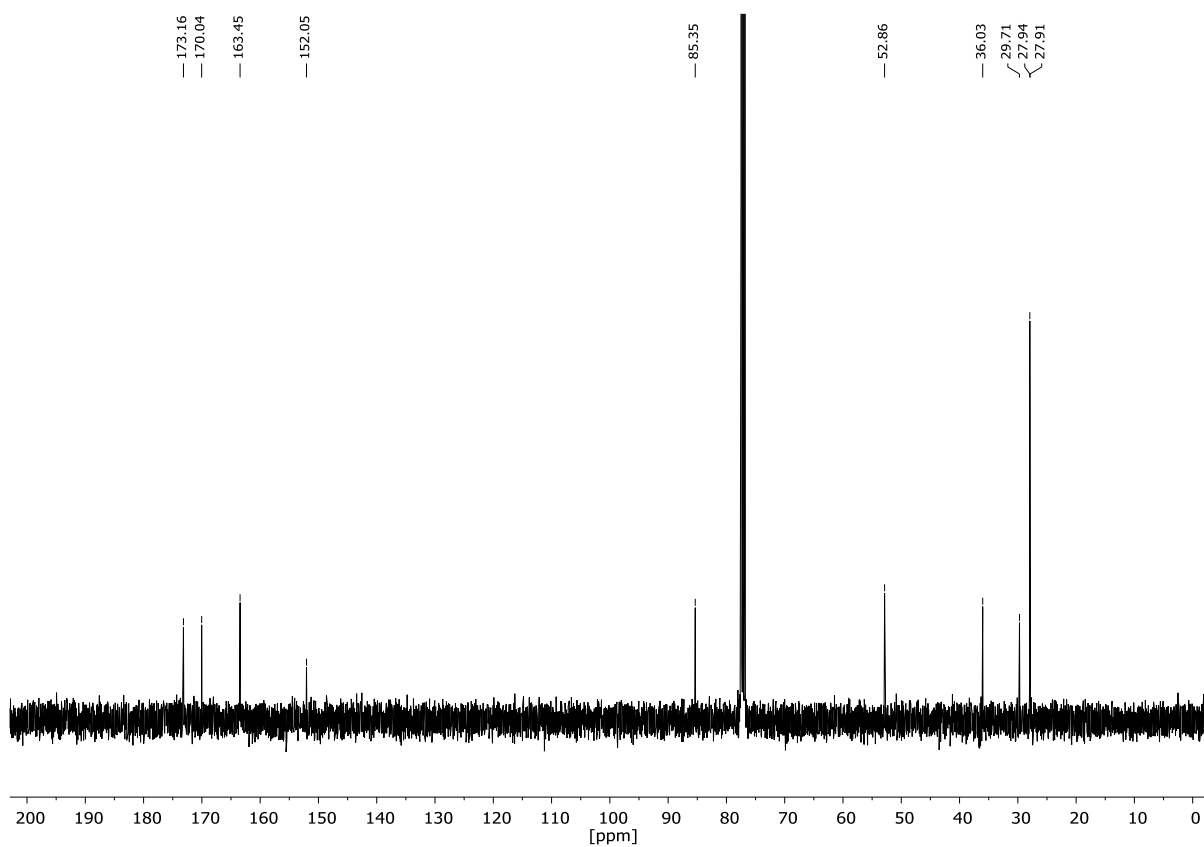
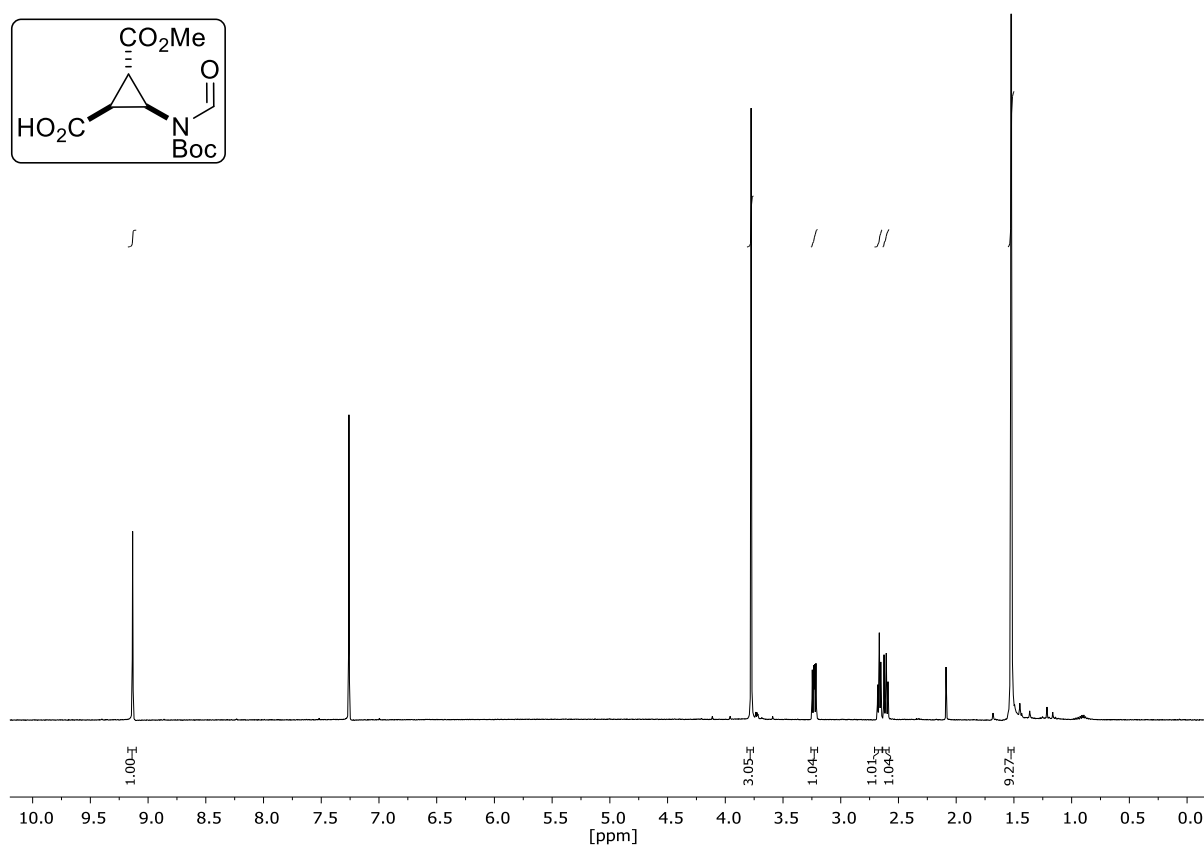
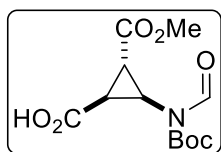
***N*-Acetyl- γ -aminobutyric acid *N,N'*-dimethylamide / 4-Acetamido-*N,N'*-dimethylbutanamide (68)**NMR-Solvent: CDCl₃

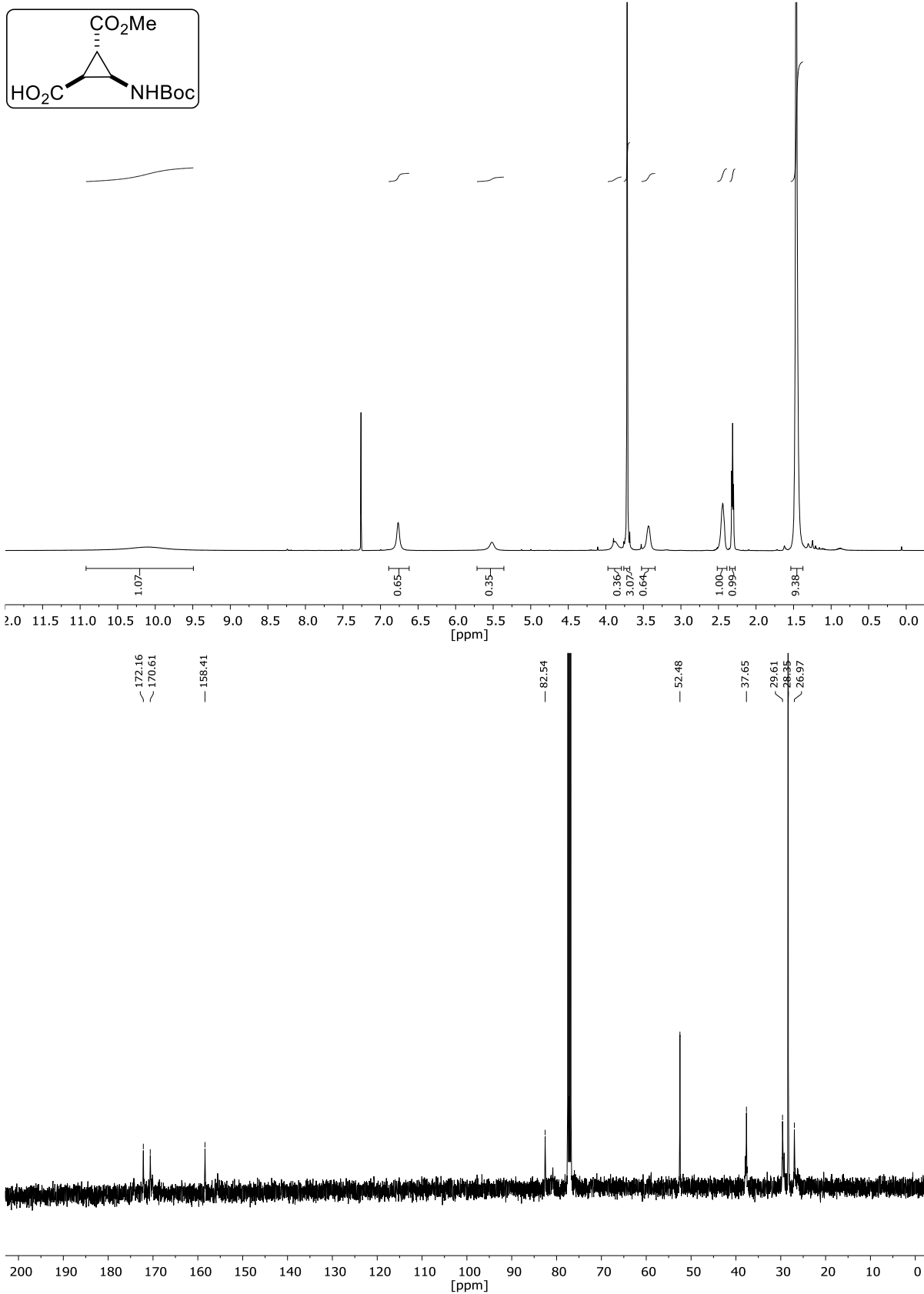
4-((*tert*-Butoxycarbonyl)amino)butanoic acid (69)NMR-Solvent: CDCl₃

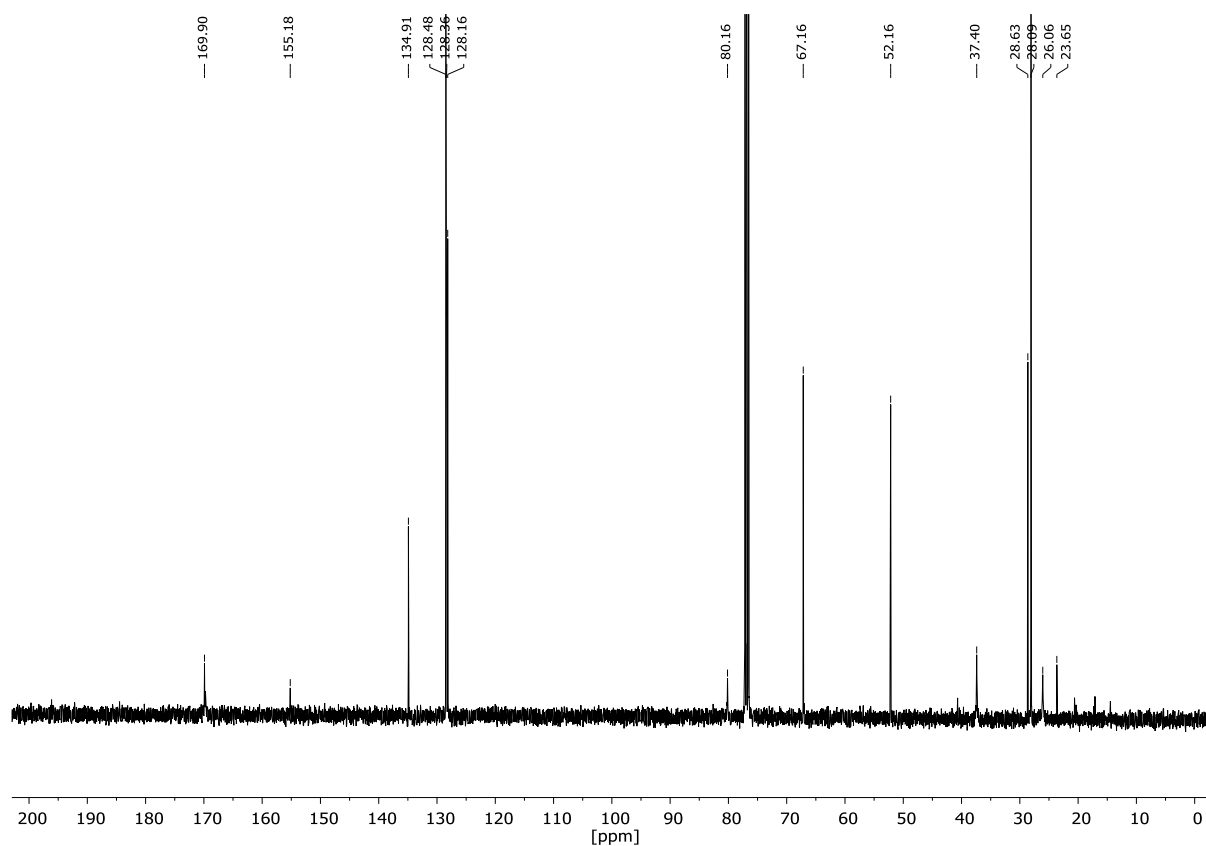
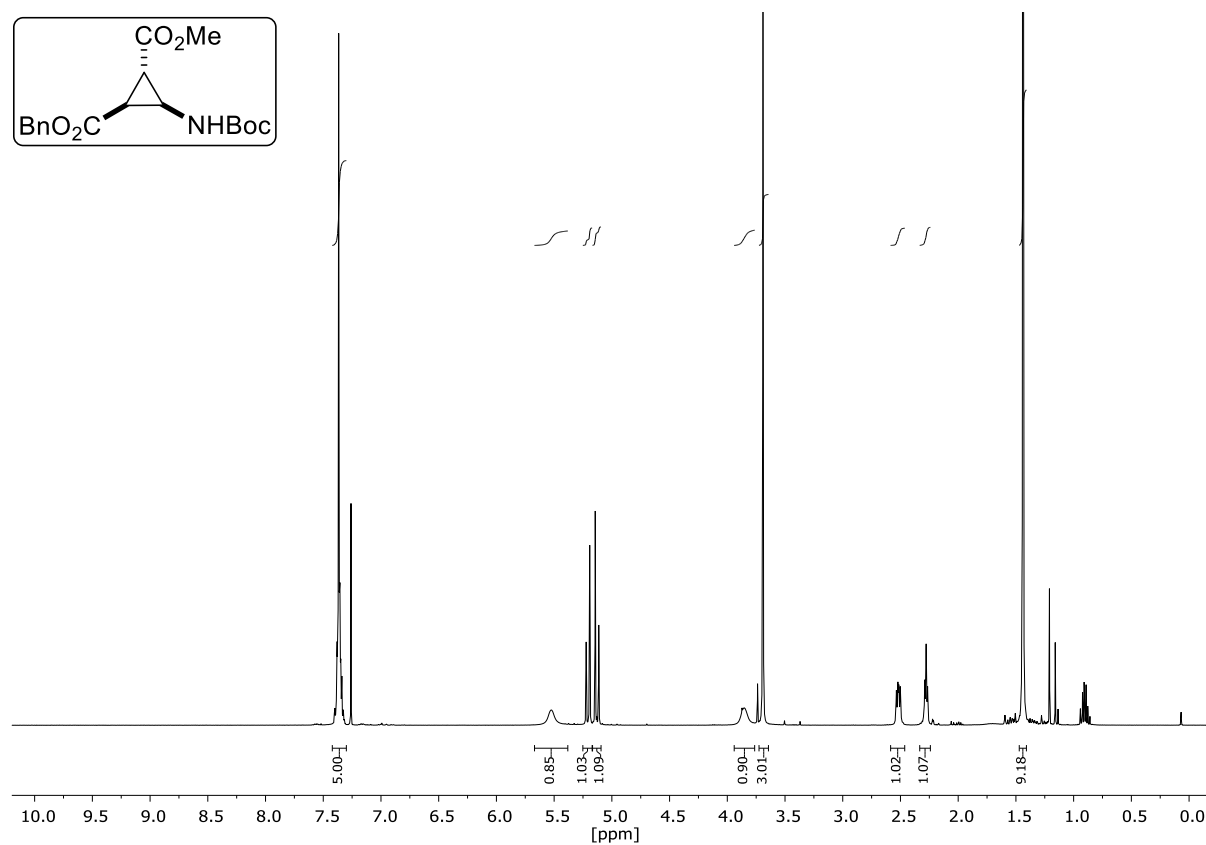
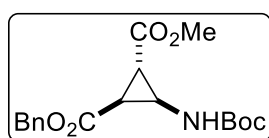
***tert*-Butyl (4-(dimethylamino)-4-oxobutyl)carbamate (70)**NMR-Solvent: CDCl_3

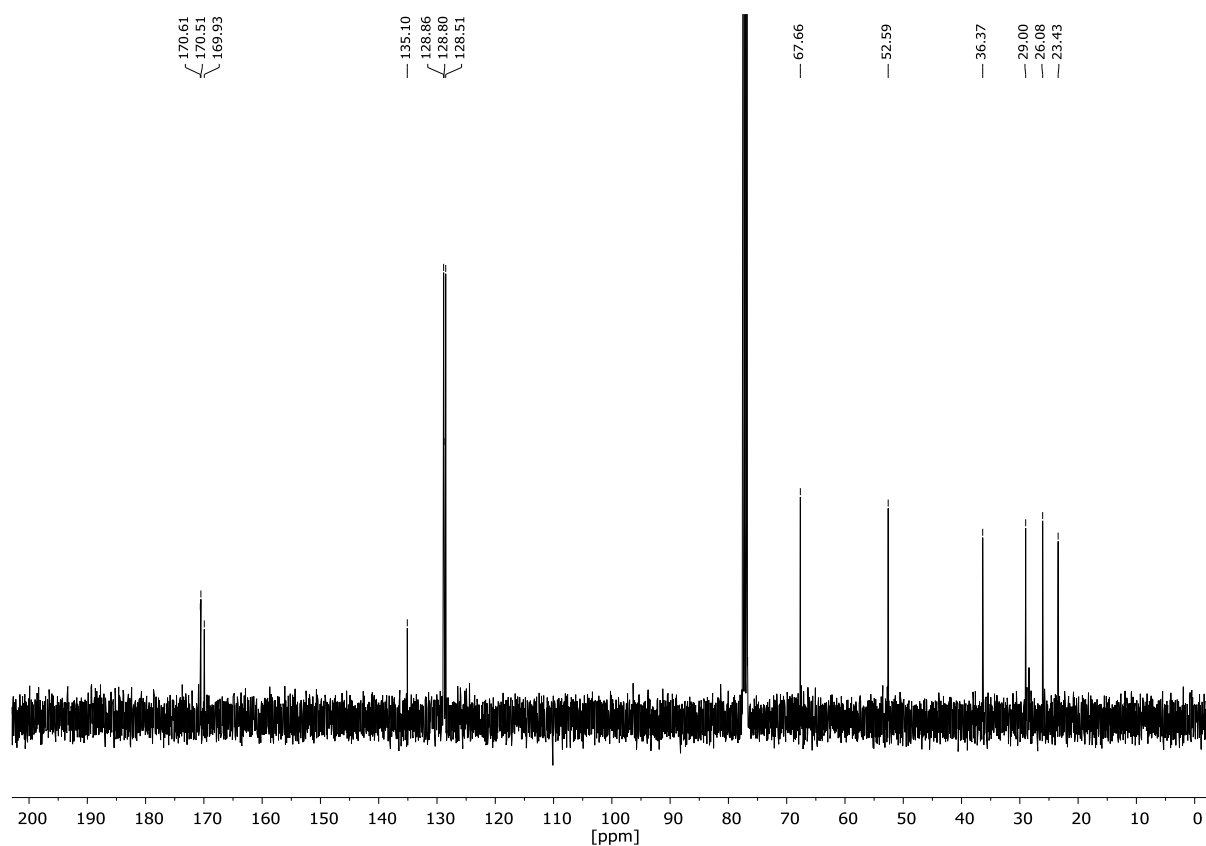
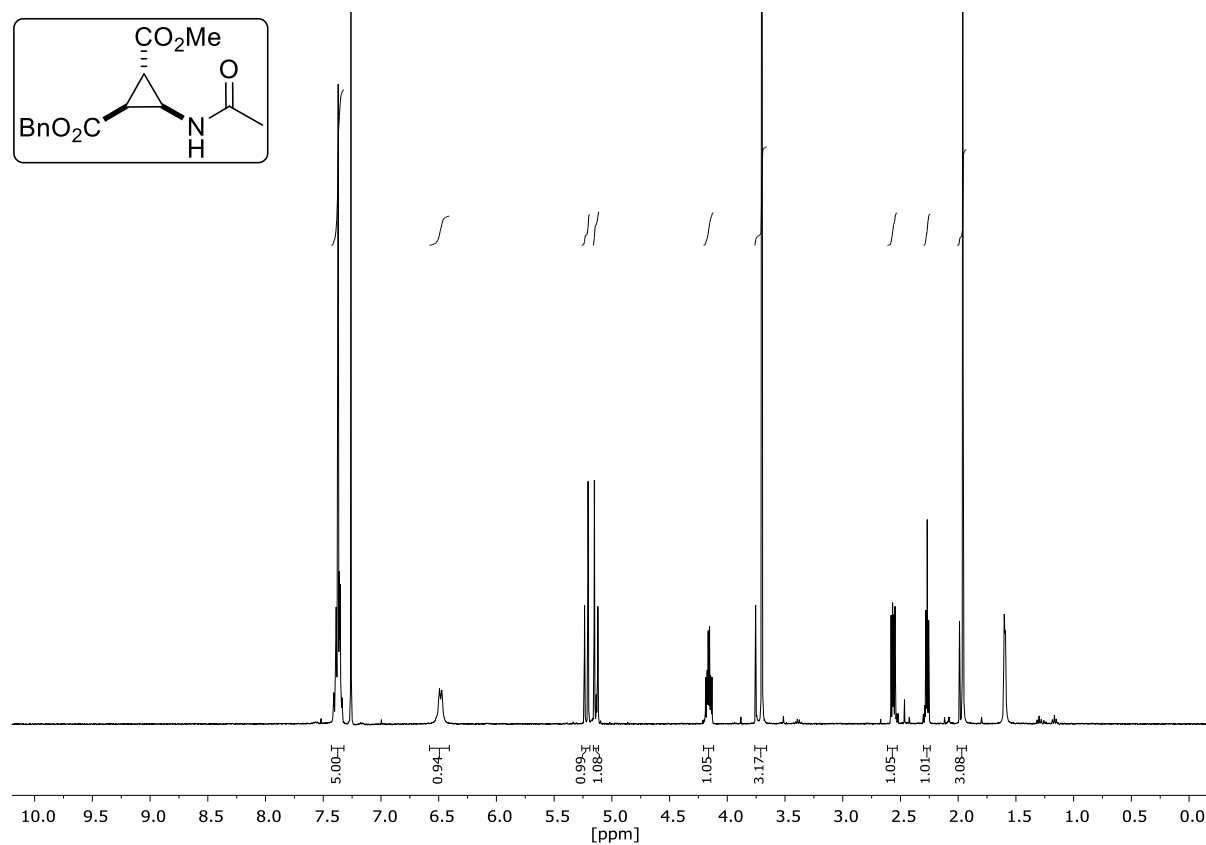
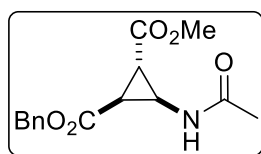
2-(*tert*-Butyl) 6-methyl-2-azabicyclo[3.1.0]hex-3-ene-2,6-dicarboxylate (72)NMR-Solvent: CDCl₃

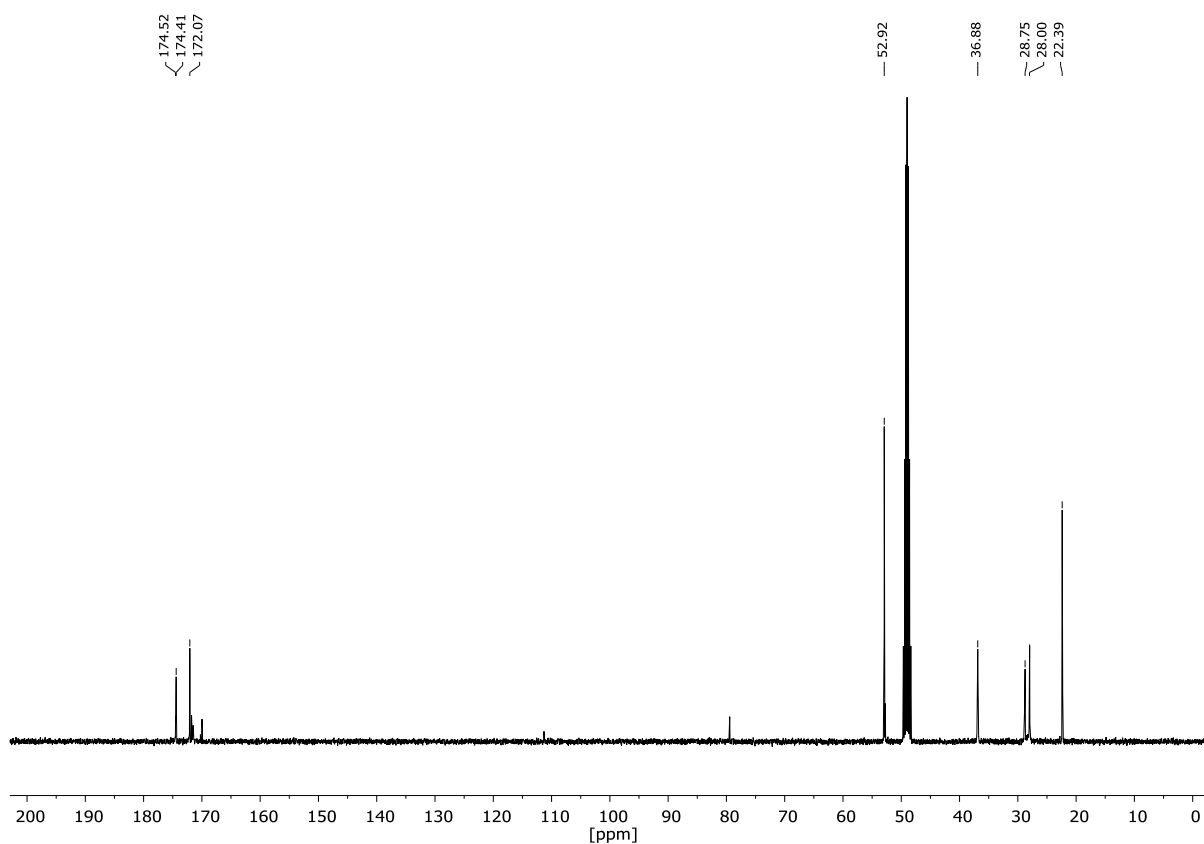
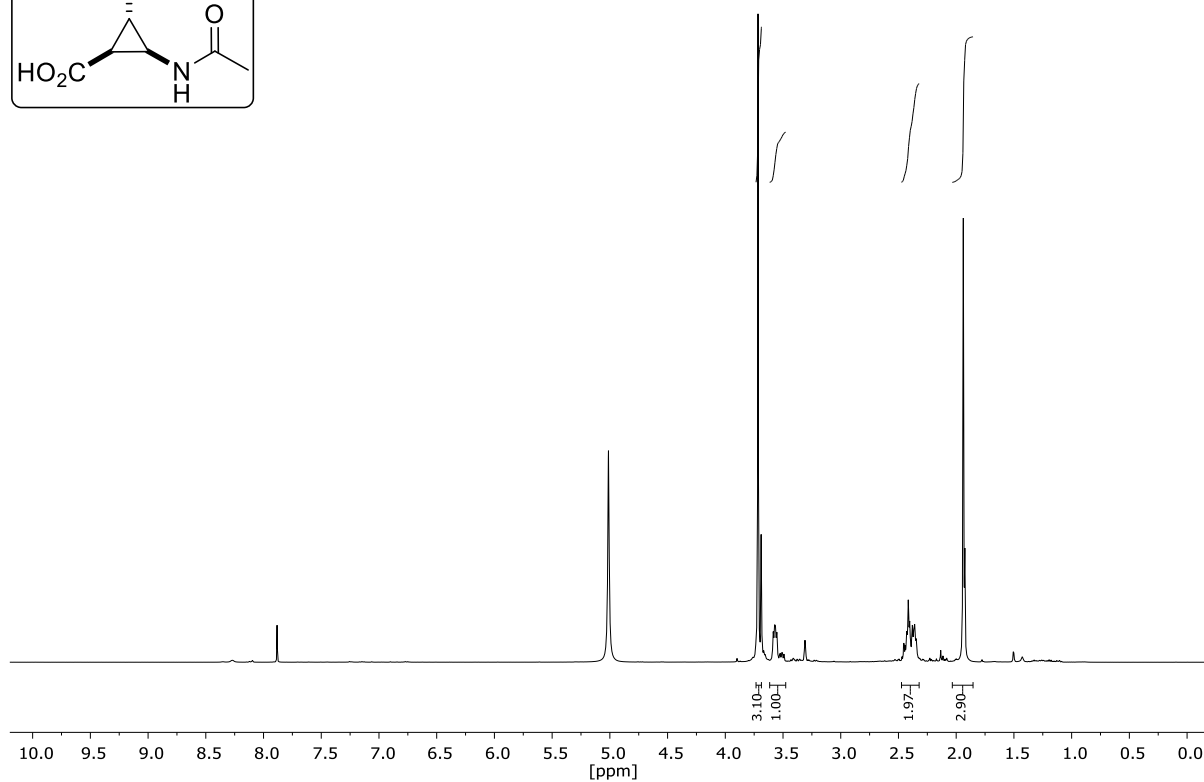
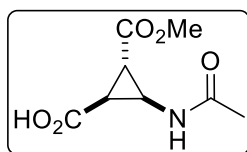
Methyl-2-(*N*-(*tert*-butoxycarbonyl)formamido)-3-formylcyclopropane-1-carboxylate (73)NMR-Solvent: CDCl₃

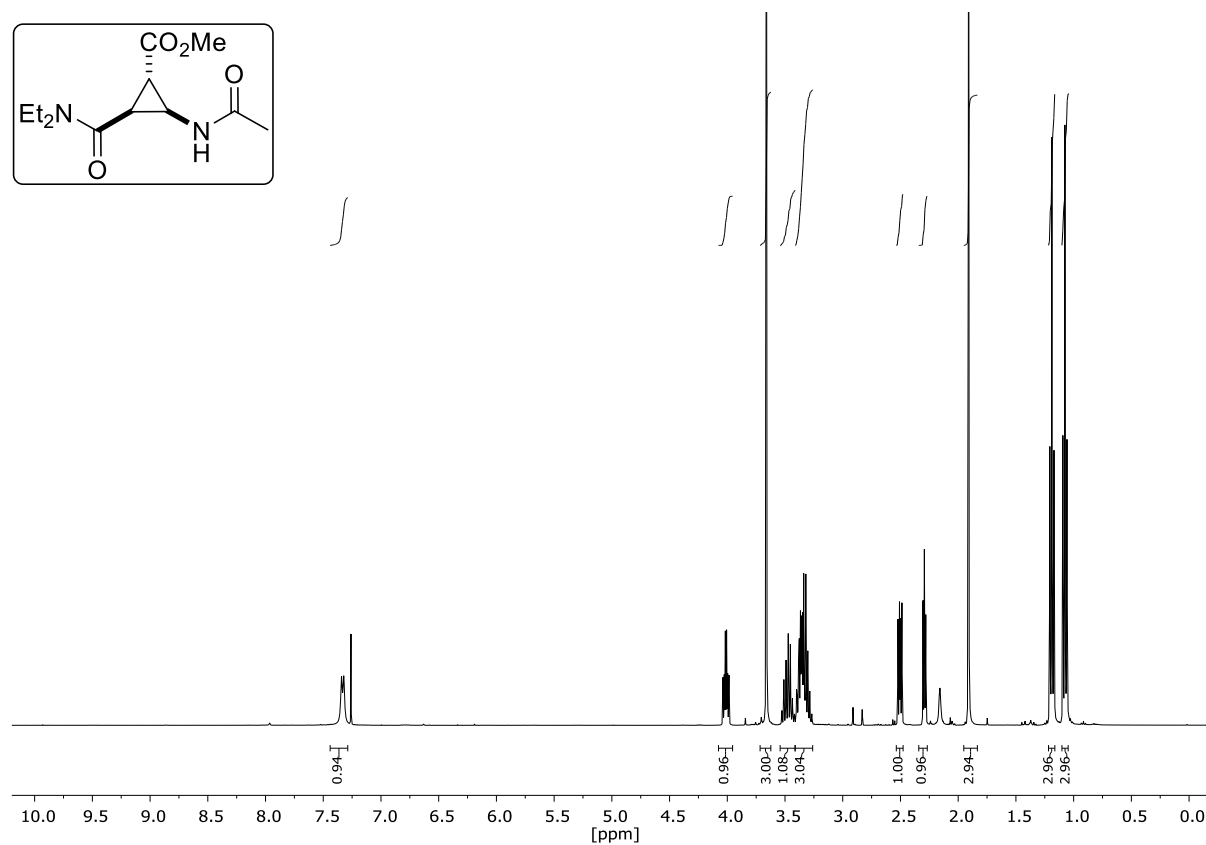
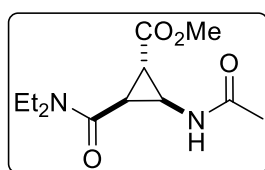
2-(*N*-(*tert*-Butoxycarbonyl)formamido)-3-(methoxycarbonyl)cyclopropane-1-carboxylic acid (74)NMR-Solvent: CDCl_3

2-((*tert*-Butoxycarbonyl)amino)-3-(methoxycarbonyl)cyclopropane-1-carboxylic acid (75)NMR-Solvent: CDCl₃

1-Benzyl 2-methyl-3-((*tert*-butoxycarbonyl)amino)cyclopropane-1,2-dicarboxylate (76)NMR-Solvent: CDCl₃

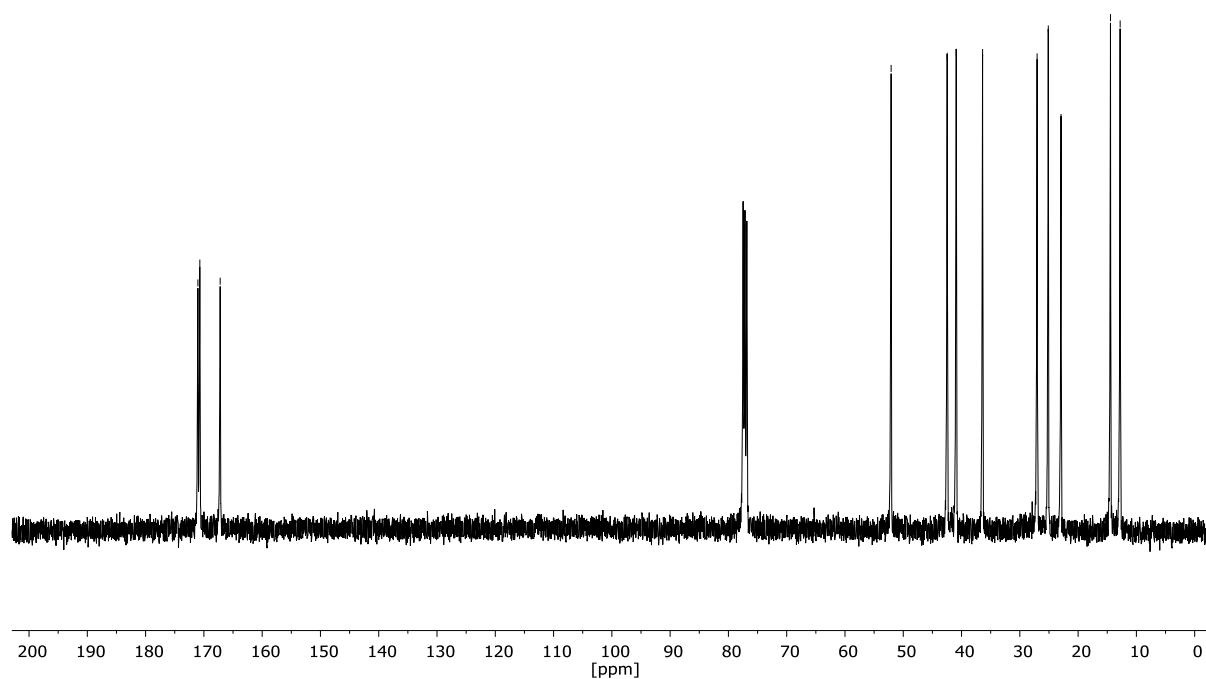
1-Benzyl 2-methyl-3-acetamidocyclopropane-1,2-dicarboxylate (77)NMR-Solvent: CDCl₃

2-Acetamido-3-(methoxycarbonyl)cyclopropane-1-carboxylic acid (78)NMR-Solvent: CD₃OD

Methyl-2-acetamido-3-(diethylcarbamoyl)cyclopropane-1-carboxylate (79)

171.03
170.69
167.21

52.08
42.46
40.91
36.39
27.04
25.12
22.93
14.45
12.79

NMR-Solvent: CDCl₃

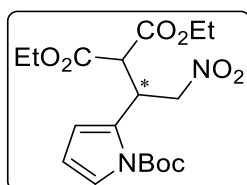
5.4 HPLC Chromatograms

Racemic Chromatogram

first image

Enantiomeric enriched Chromatogram

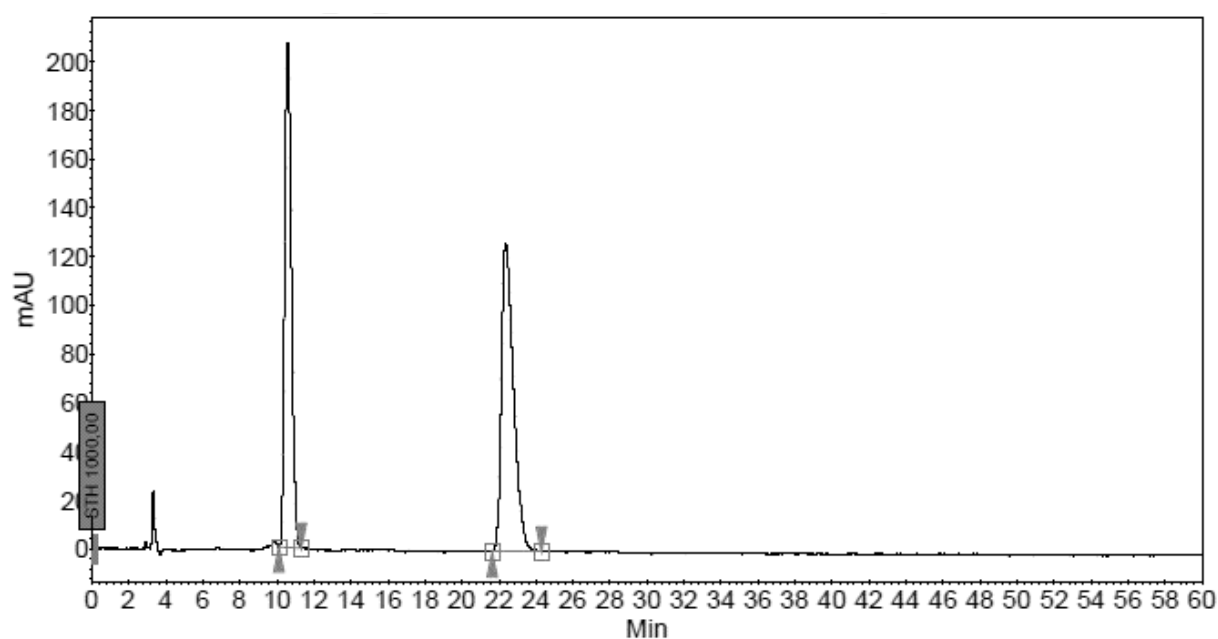
second image

Diethyl-2-(1-(1-(*tert*-butyloxycarbonyl)-1*H*-pyrrol-2-yl)-2-nitroethyl)malonat (58b)

Vial : 116
Method : Phex-Cel1_99-1
Run time : 60,00 min
Inj. vol. : 10,000 µl

Column : Phenomenex Lux Cellulose-1,
4.6 x 250 mm, 5 µm
Eluents : A = n-Heptane
B = i-Propanol
Flow : 1.0 ml/min

λ : 215 nm

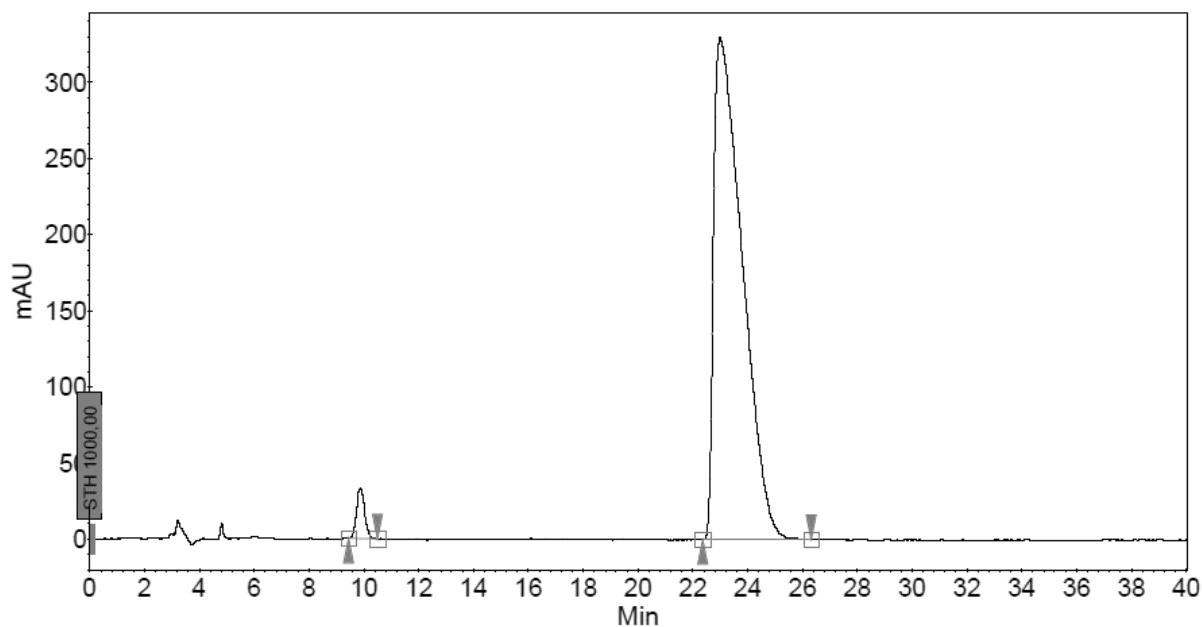
**Peak Results :**

Index	Name	Time [Min]	Quantity [% Area]	Height [mAU]	Area [mAU.Min]	Area % [%]
1	UNKNOWN	10.59	47.73	206.9	88.4	47.728
2	UNKNOWN	22.36	52.27	126.9	96.8	52.272
Total			100.00	333.8	185.2	100.000

Vial : 122
 Method : Phex-Cel1_99-1
 Run time : 40,00 min
 Inj. vol. : 10,000 µl

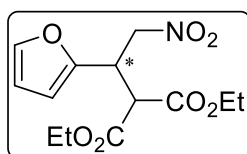
Column : Phenomenex Lux Cellulose-1,
 4.6 x 250 mm, 5 µm
 Eluents : A = n-Heptane
 B = i-Propanol
 Flow : 1.0 ml/min

λ : 215 nm



Peak Results :

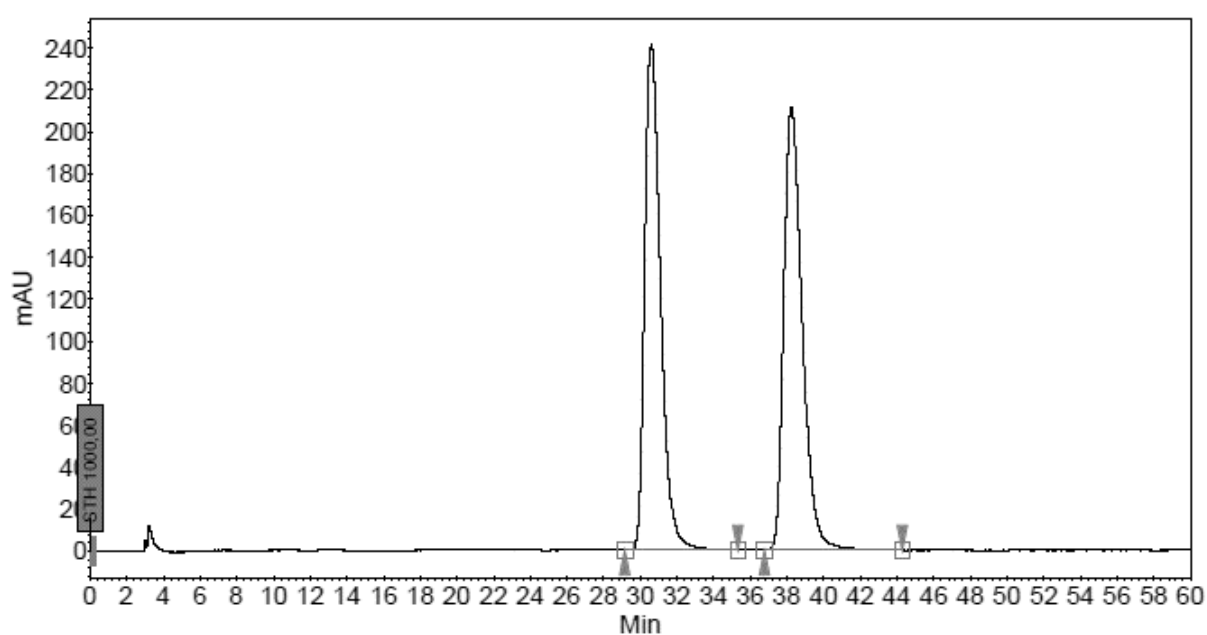
Index	Name	Time [Min]	Quantity [% Area]	Height [mAU]	Area [mAU.Min]	Area % [%]
1	UNKNOWN	9.87	2.77	32.9	11.4	2.775
2	UNKNOWN	22.99	97.23	329.6	398.4	97.225
Total			100.00	362.6	409.7	100.000

Diethyl 2-(1-(furan-2-yl)-2-nitroethyl)malonate (58d)

Vial : 80
Method : Phex-Cel2_99-1
Run time : 60,00 min
Inj. vol. : 10,000 µl

Column : Phenomenex Lux Cellulose-2,
4.6 x 250 mm, 5 µm
Eluents : A = n-Heptane
B = i-Propanol
Flow : 1.0 ml/min

λ : 215 nm

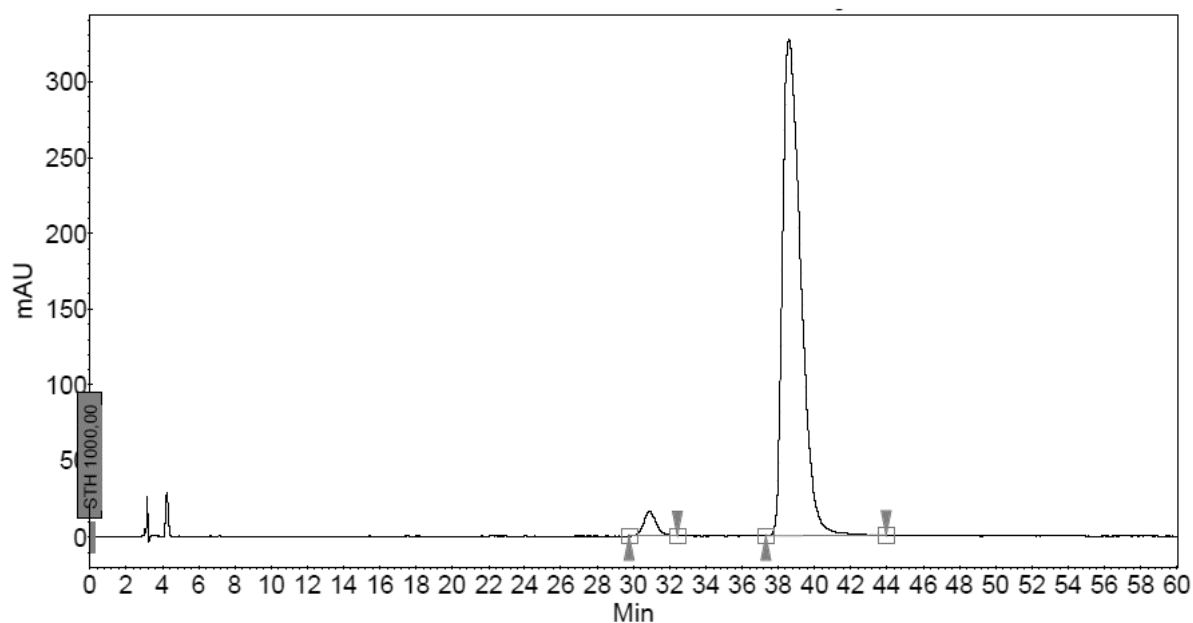
**Peak Results :**

Index	Name	Time [Min]	Quantity [% Area]	Height [mAU]	Area [mAU.Min]	Area % [%]
1	UNKNOWN	30.60	49.48	241.3	240.9	49.476
2	UNKNOWN	38.23	50.52	211.6	246.0	50.524
Total			100.00	452.9	487.0	100.000

Vial : 147
 Method : Phex-Cel2_99-1
 Run time : 60,00 min
 Inj. vol. : 10,000 µl

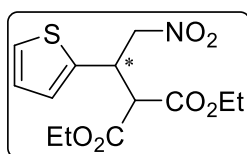
Column : Phenomenex Lux Cellulose-2,
 4.6 x 250 mm, 5 µm
 Eluents : A = n-Heptane
 B = i-Propanol
 Flow : 1.0 ml/min

λ : 215 nm



Peak Results :

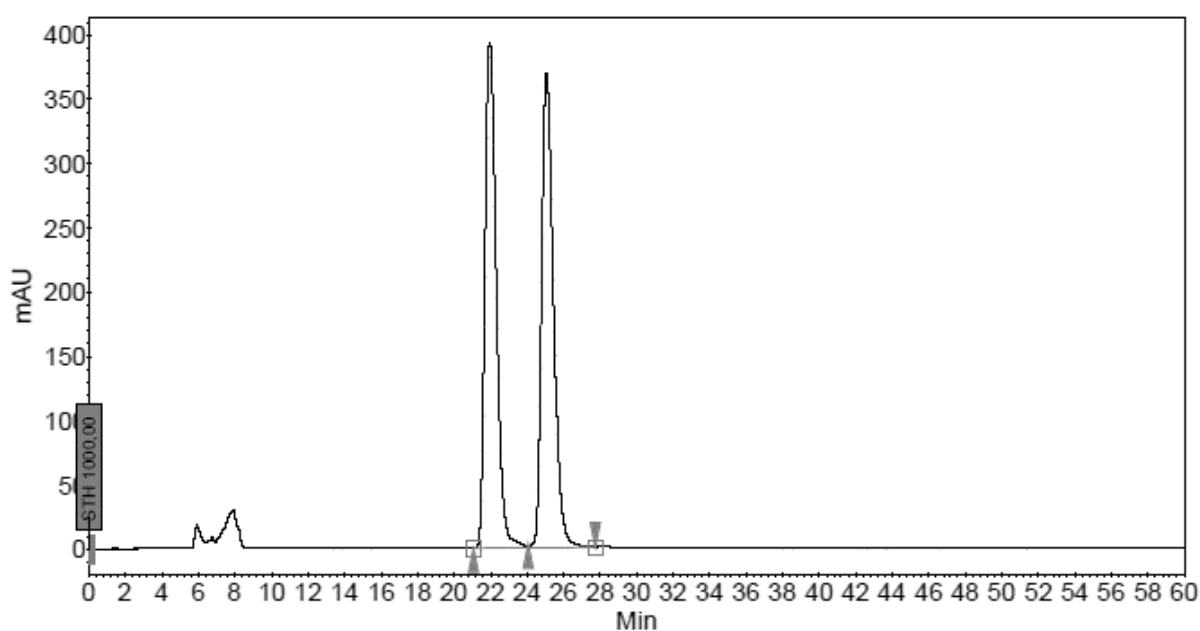
Index	Name	Time [Min]	Quantity [% Area]	Height [mAU]	Area [mAU.Min]	Area % [%]
1	UNKNOWN	30,88	3,29	15,8	13,0	3,294
2	UNKNOWN	38,58	96,71	326,8	381,8	96,706
Total			100,00	342,6	394,8	100,000

Diethyl 2-(2-nitro-1-(thiophen-2-yl)ethyl)malonate (58e)

Vial : 56
Method : Phex-Cel2_90-10_0.5
Run time : 60,00 min
Inj. vol. : 10,000 μ l

Column : Phenomenex Lux Cellulose-2,
4.6 x 250 mm, 5 μ m
Eluents : A = n-Heptane
B = i-Propanol
Flow : 0.5 ml/min

λ : 215 nm

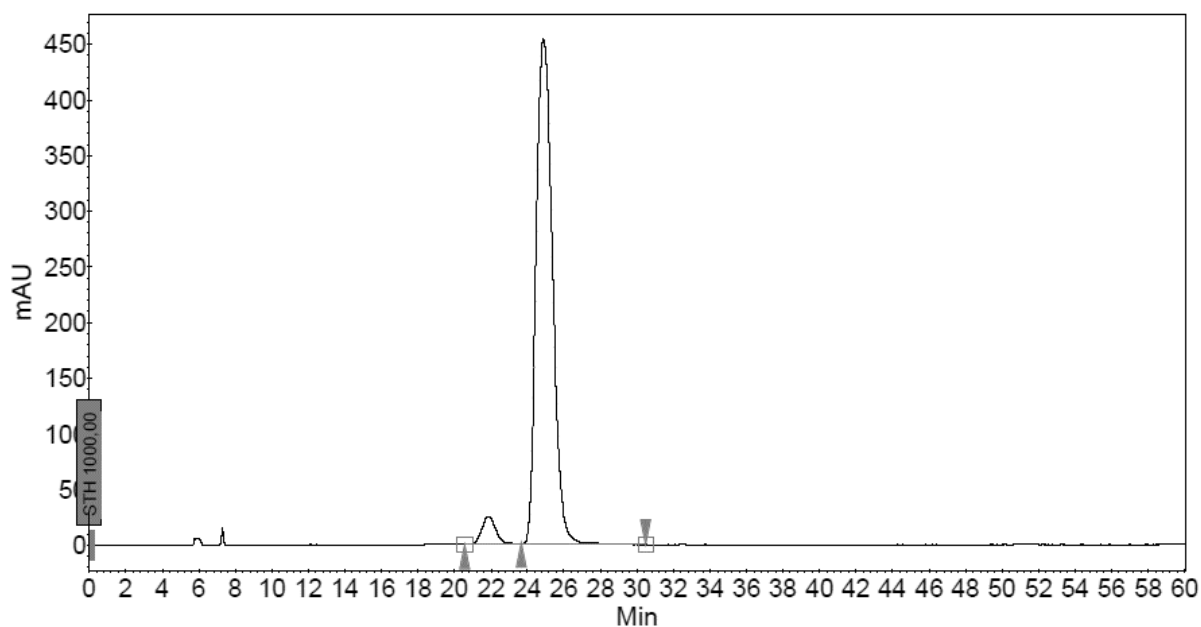
**Peak Results :**

Index	Name	Time [Min]	Quantity [% Area]	Height [mAU]	Area [mAU.Min]	Area % [%]
1	UNKNOWN	21.96	49.73	393.2	278.5	49.733
2	UNKNOWN	25.07	50.27	369.5	281.5	50.267
Total			100.00	762.7	560.1	100.000

Vial : 88
Method : Phex-Cel2_90-10_0.5
Run time : 60,00 min
Inj. vol. : 10,000 µl

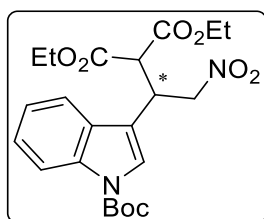
Column : Phenomenex Lux Cellulose-2,
4.6 x 250 mm, 5 µm
Eluents : A = n-Heptane
B = i-Propanol
Flow : 0.5 ml/min

λ : 215 nm



Peak Results :

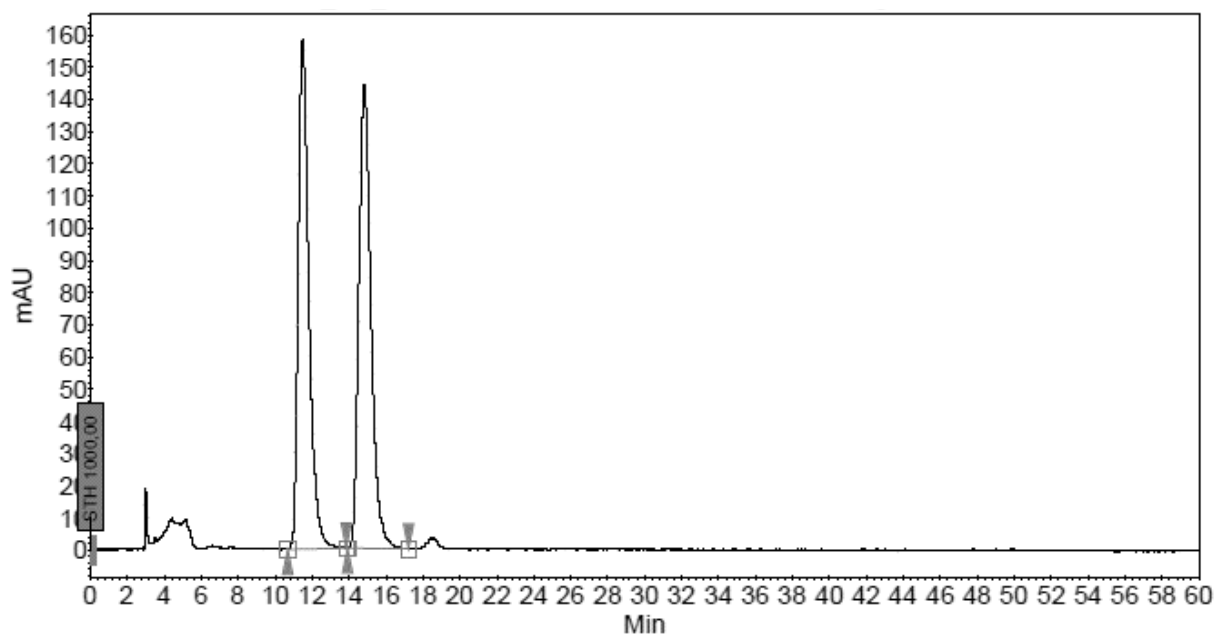
Index	Name	Time [Min]	Quantity [% Area]	Height [mAU]	Area [mAU.Min]	Area % [%]
1	UNKNOWN	21.87	4.62	25.3	22.9	4.618
2	UNKNOWN	24.88	95.38	454.1	472.9	95.382
Total			100.00	479.4	495.8	100.000

Diethyl-2-(1-(1-(*tert*-butyloxycarbonyl)-1*H*-indol-3-yl)-2-nitroethyl)malonat (58f)

Vial : 199
Method : Phex-Cel2_95-5
Run time : 60,00 min
Inj. vol. : 10,000 µl

Column : Phenomenex Lux Cellulose-2,
4.6 x 250 mm, 5 µm
Eluents : A = n-Heptane
B = i-Propanol
Flow : 1.0 ml/min

λ : 215 nm

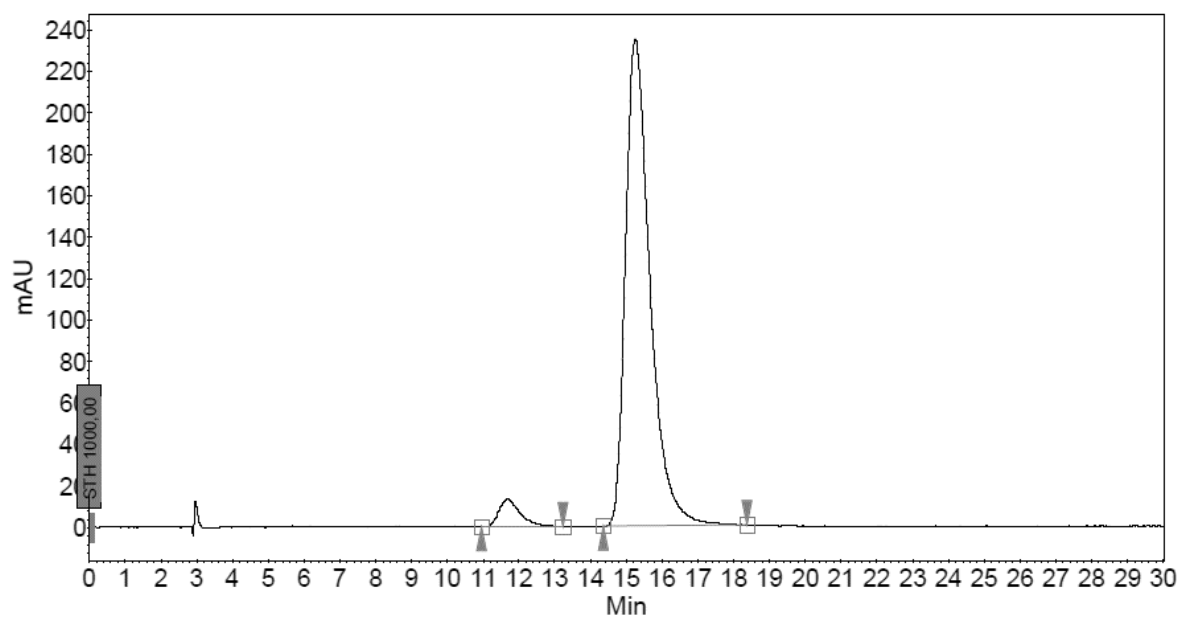
**Peak Results :**

Index	Name	Time [Min]	Quantity [% Area]	Height [mAU]	Area [mAU.Min]	Area % [%]
1	UNKNOWN	11.49	49.55	158.2	107.2	49.552
2	UNKNOWN	14.82	50.45	143.9	109.1	50.448
Total			100.00	302.1	216.3	100.000

Vial : 21
Method : Phex-Cel2_95-5
Run time : 30,00 min
Inj. vol. : 10,000 µl

Column : Phenomenex Lux Cellulose-2,
4.6 x 250 mm, 5 µm
Eluents : A = n-Heptane
B = i-Propanol
Flow : 1.0 ml/min

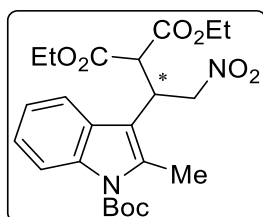
λ : 215 nm



Peak Results :

Index	Name	Time [Min]	Quantity [% Area]	Height [mAU]	Area [mAU.Min]	Area % [%]
1	UNKNOWN	11,68	4,70	13,1	9,2	4,702
2	UNKNOWN	15,25	95,30	234,8	186,6	95,298
Total			100,00	247,8	195,8	100,000

**Diethyl-2-(1-(1-(*tert*-butyloxycarbonyl)-2-methyl-1*H*-indol-3-yl)-2-nitroethyl)malonat
(58g)**



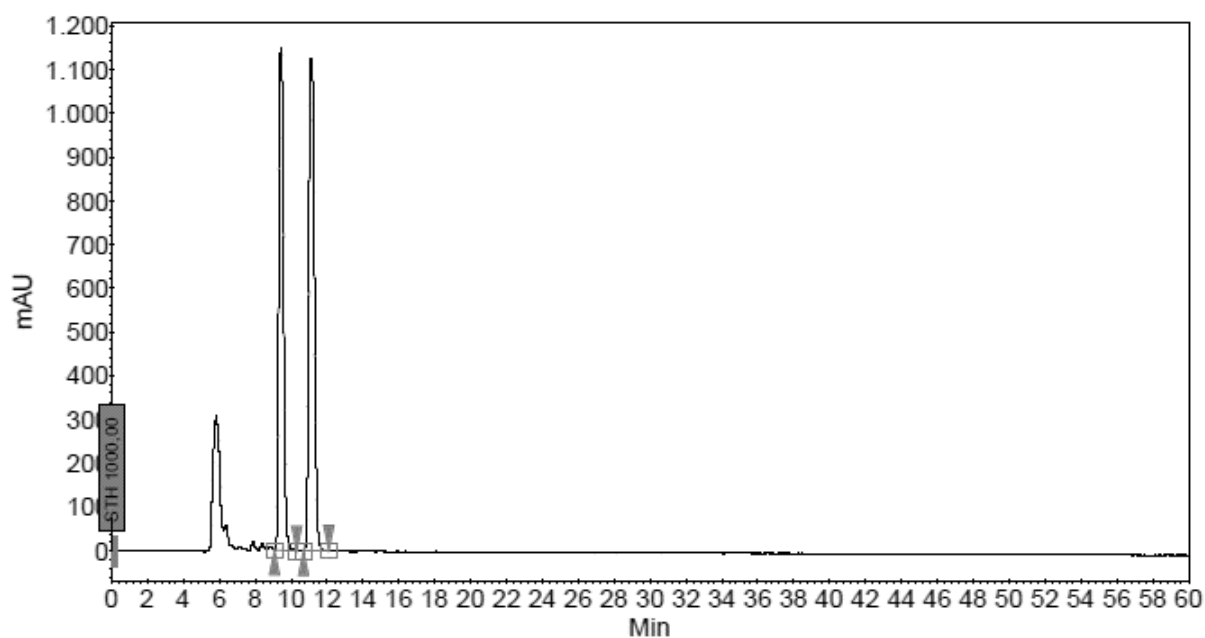
Vial : 141
Method : Phex-Cel1_70-30_0.5
Run time : 60,00 min
Inj. vol. : 10,000 μ l

Column : Phenomenex Lux Cellulose-1,
4.6 x 250 mm, 5 μ m

Eluents : A = n-Heptane
B = i-Propanol

Flow : 0.5 ml/min

λ : 215 nm



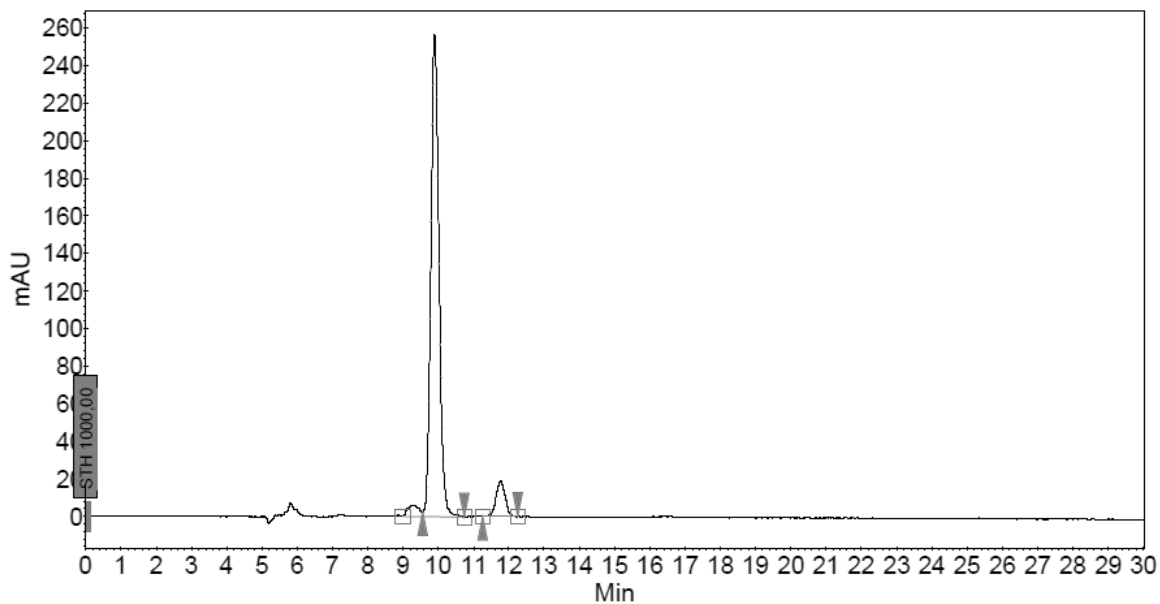
Peak Results :

Index	Name	Time [Min]	Quantity [% Area]	Height [mAU]	Area [mAU.Min]	Area % [%]
1	UNKNOWN	9.44	48.22	1147.7	356.9	48.219
2	UNKNOWN	11.13	51.78	1125.0	383.3	51.781
Total			100.00	2272.7	740.2	100.000

Vial : 185
 Method : Phex-Cel1_70-30_0.5
 Run time : 30,00 min
 Inj. vol. : 10,000 µl

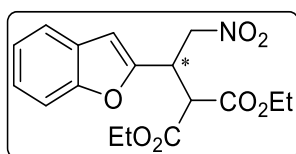
Column : Phenomenex Lux Cellulose-1,
 4.6 x 250 mm, 5 µm
 Eluents : A = n-Heptane
 B = i-Propanol
 Flow : 0.5 ml/min

λ : 215 nm



Peak Results :

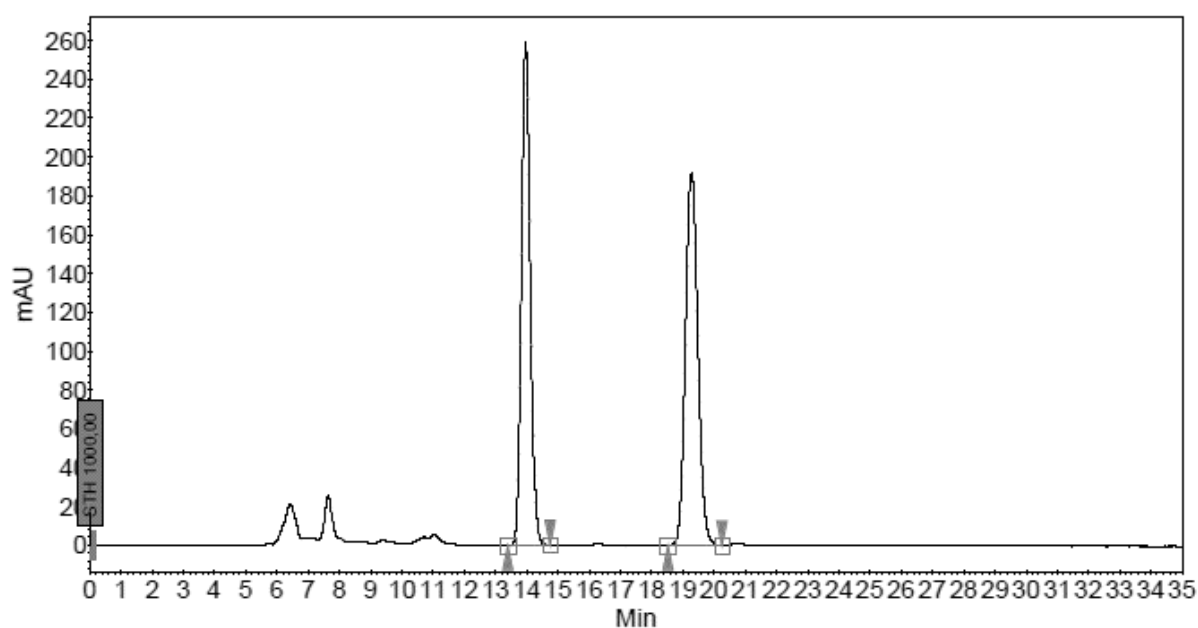
Index	Name	Time [Min]	Quantity [% Area]	Height [mAU]	Area [mAU.Min]	Area % [%]
1	UNKNOWN	9,90	92,28	256,2	67,9	92,282
2	UNKNOWN	11,77	7,72	18,6	5,7	7,718
Total			100,00	274,9	73,6	100,000

Diethyl 2-(1-(benzofuran-2-yl)-2-nitroethyl)malonate (58h)

Vial : 35
Method : Phex-Cel1_50-50_0.5
Run time : 35,00 min
Inj. vol. : 10,000 μ l

Column : Phenomenex Lux Cellulose-1,
4.6 x 250 mm, 5 μ m
Eluents : A = n-Heptane
B = i-Propanol
Flow : 0.5 ml/min

λ : 215 nm

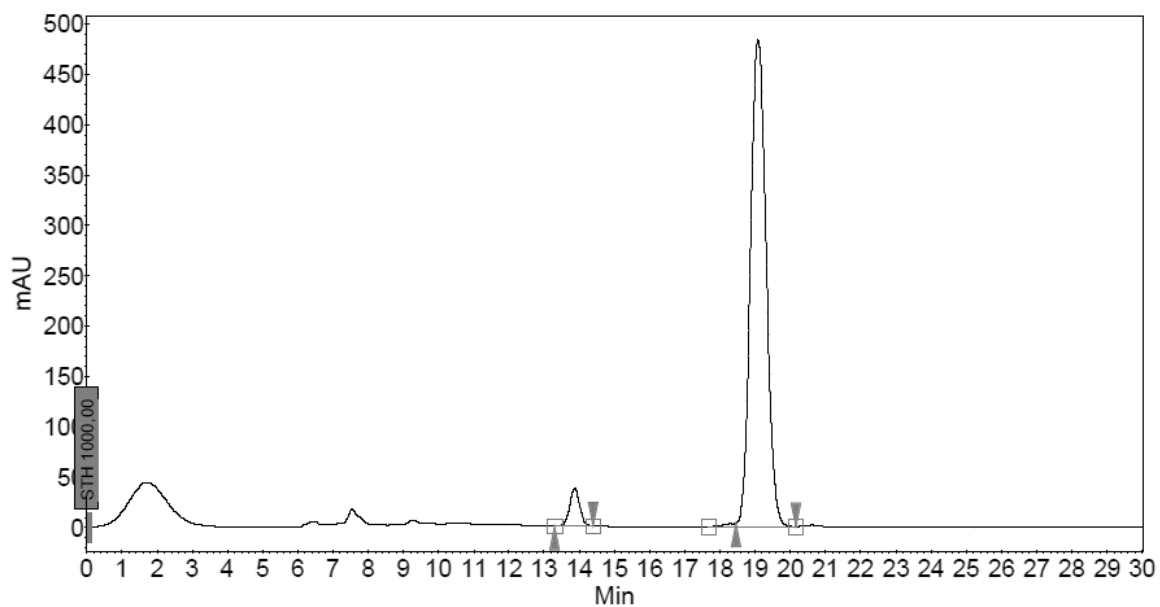
**Peak Results :**

Index	Name	Time [Min]	Quantity [% Area]	Height [mAU]	Area [mAU.Min]	Area % [%]
1	UNKNOWN	13.97	49.46	259.4	86.0	49.461
2	UNKNOWN	19.28	50.54	192.2	87.8	50.539
Total			100.00	451.6	173.8	100.000

Vial : 44
 Method : Phex-Cel1_50-50_0.5
 Run time : 30,00 min
 Inj. vol. : 10,000 µl

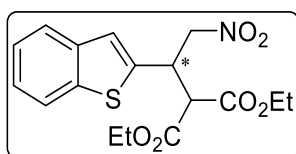
Column : Phenomenex Lux Cellulose-1,
 4.6 x 250 mm, 5 µm
 Eluents : A = n-Heptane
 B = i-Propanol
 Flow : 0.5 ml/min

λ : 215 nm



Peak Results :

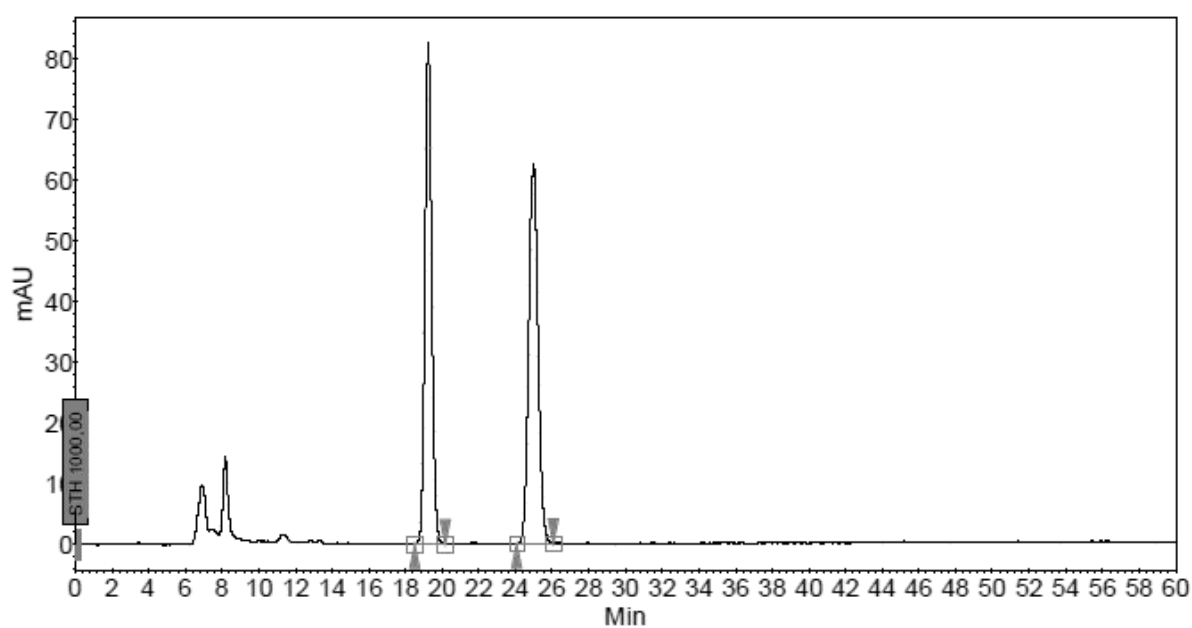
Index	Name	Time [Min]	Quantity [% Area]	Height [mAU]	Area [mAU.Min]	Area % [%]
1	UNKNOWN	13,87	4,81	37,6	12,6	4,813
2	UNKNOWN	19,08	95,19	483,3	250,1	95,187
Total			100,00	520,8	262,7	100,000

Diethyl 2-(1-(benzo[b]thiophen-2-yl)-2-nitroethyl)malonate (58i)

Vial : 36
Method : Phex-Cel1_50-50_0.5
Run time : 60,00 min
Inj. vol. : 10,000 μ l

Column : Phenomenex Lux Cellulose-1,
4.6 x 250 mm, 5 μ m
Eluents : A = n-Heptane
B = i-Propanol
Flow : 0.5 ml/min

λ : 215 nm

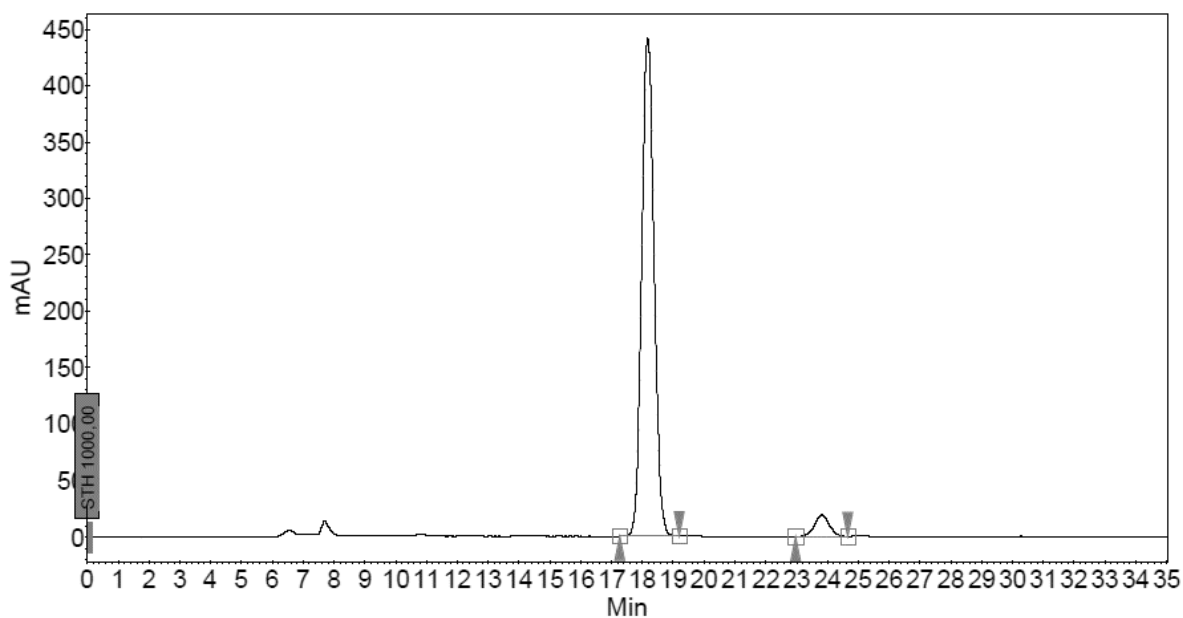
**Peak Results :**

Index	Name	Time [Min]	Quantity [% Area]	Height [mAU]	Area [mAU.Min]	Area % [%]
1	UNKNOWN	19.23	50.11	82.6	36.1	50.106
2	UNKNOWN	24.97	49.89	62.6	35.9	49.894
Total			100.00	145.2	72.0	100.000

Vial : 45
 Method : Phex-Cel1_50-50_0.5
 Run time : 35,00 min
 Inj. vol. : 10,000 µl

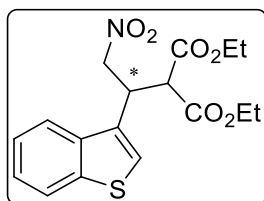
Column : Phenomenex Lux Cellulose-1,
 4.6 x 250 mm, 5 µm
 Eluents : A = n-Heptane
 B = i-Propanol
 Flow : 0.5 ml/min

λ : 215 nm



Peak Results :

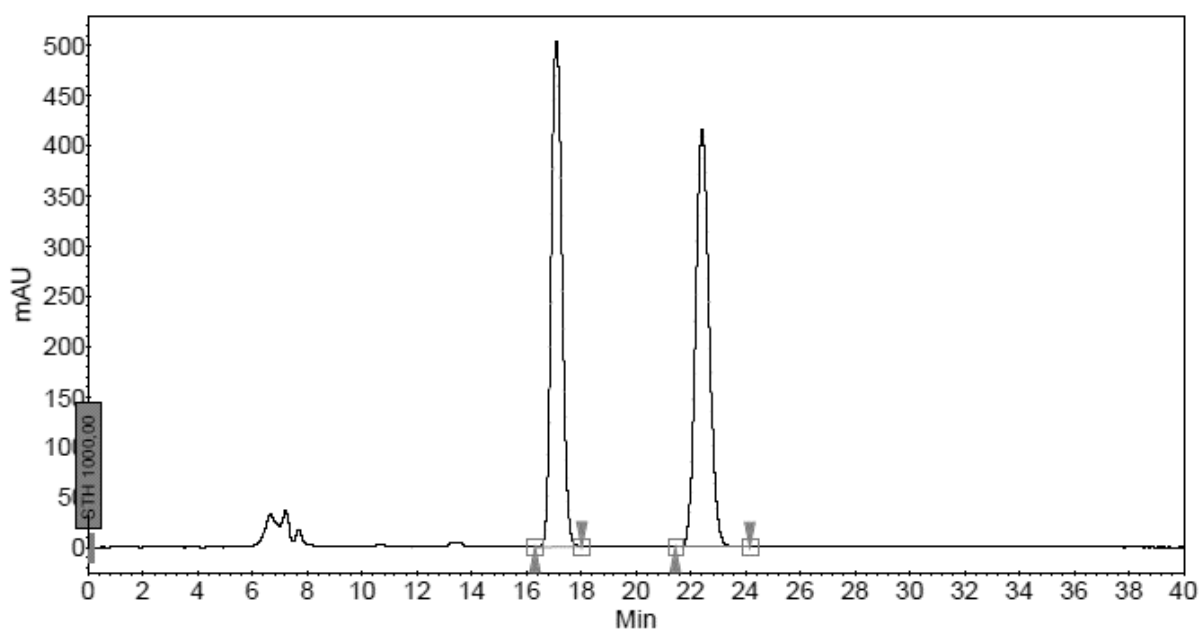
Index	Name	Time [Min]	Quantity [% Area]	Height [mAU]	Area [mAU.Min]	Area % [%]
1	UNKNOWN	18,17	95,08	441,2	206,1	95,077
2	UNKNOWN	23,81	4,92	19,1	10,7	4,923
Total			100,00	460,3	216,8	100,000

Diethyl 2-(1-(benzo[b]thiophen-3-yl)-2-nitroethyl)malonate (58j)

Vial : 34
Method : Phex-Cel1_50-50_0.5
Run time : 40,00 min
Inj. vol. : 10,000 μ l

Column : Phenomenex Lux Cellulose-1,
4.6 x 250 mm, 5 μ m
Eluents : A = n-Heptane
B = i-Propanol
Flow : 0.5 ml/min

λ : 215 nm

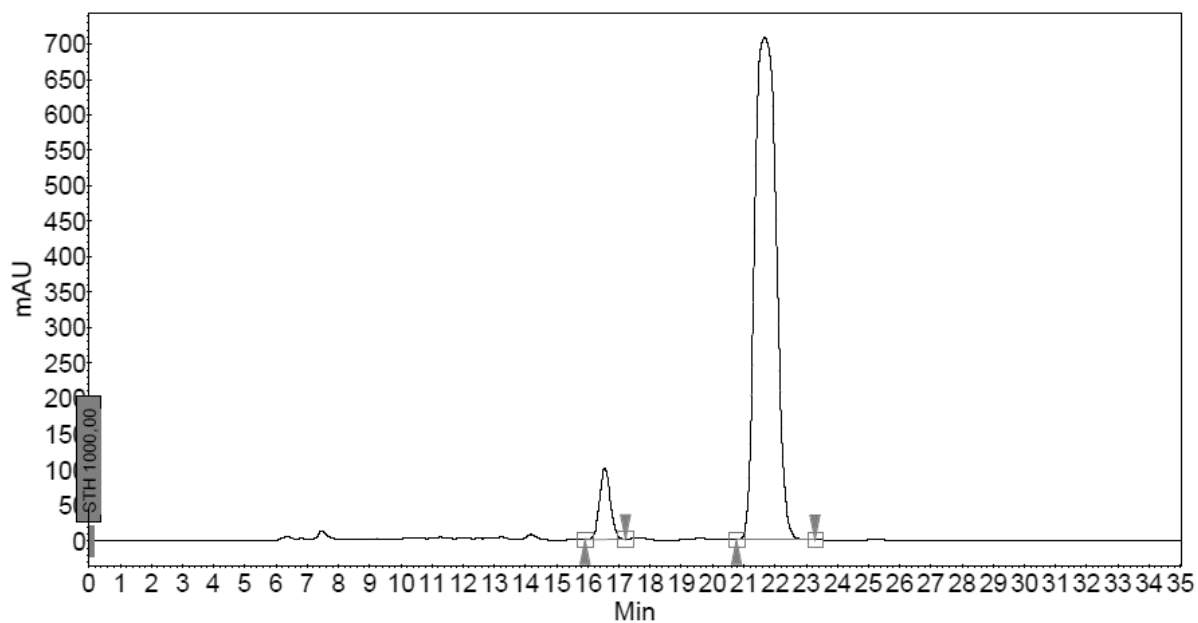
**Peak Results :**

Index	Name	Time [Min]	Quantity [% Area]	Height [mAU]	Area [mAU.Min]	Area % [%]
1	UNKNOWN	17.09	48.41	502.6	226.0	48.411
2	UNKNOWN	22.42	51.59	415.9	240.9	51.589
Total			100.00	918.4	466.9	100.000

Vial : 43
Method : Phex-Cel1_50-50_0.5
Run time : 35,00 min
Inj. vol. : 10,000 µl

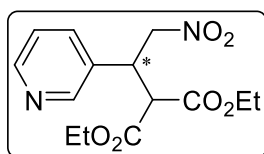
Column : Phenomenex Lux Cellulose-1,
4.6 x 250 mm, 5 µm
Eluents : A = n-Heptane
B = i-Propanol
Flow : 0.5 ml/min

λ : 215 nm



Peak Results :

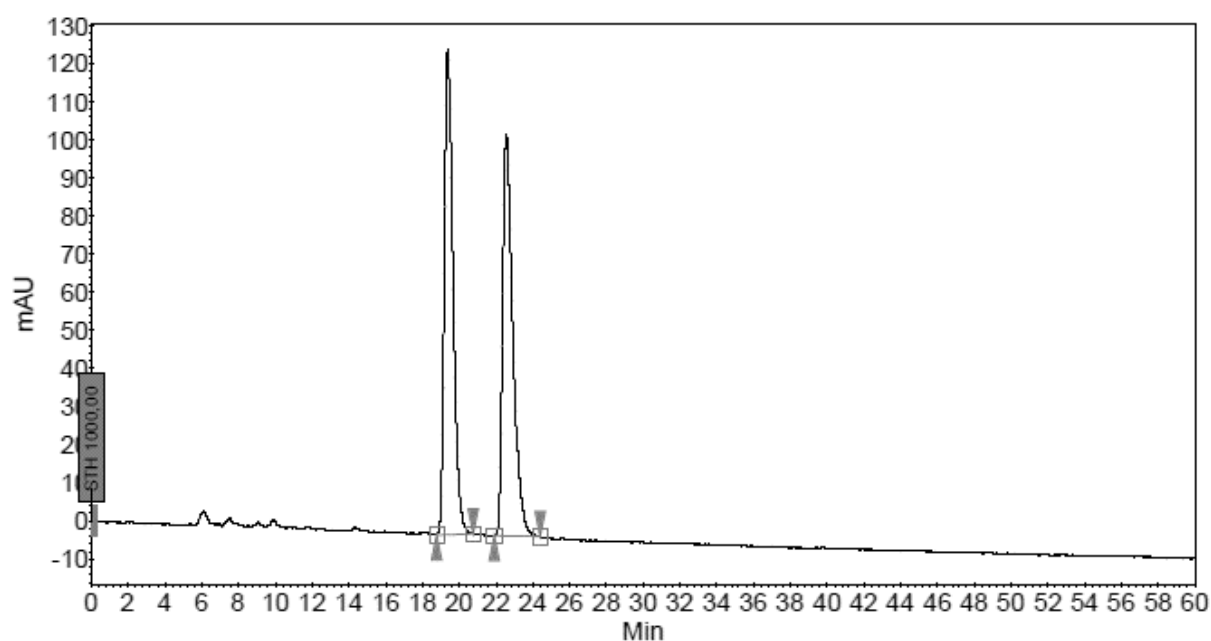
Index	Name	Time [Min]	Quantity [% Area]	Height [mAU]	Area [mAU.Min]	Area % [%]
1	UNKNOWN	16,54	6,74	100,5	40,6	6,736
2	UNKNOWN	21,66	93,26	706,8	561,8	93,264
Total			100,00	807,3	602,4	100,000

Diethyl 2-(2-nitro-1-(pyridin-3-yl)ethyl)malonate (58k)

Vial : 26
Method : Phex-Cell1_70-30_0.5
Run time : 60,00 min
Inj. vol. : 10,000 µl

Column : Phenomenex Lux Cellulose-1,
4.6 x 250 mm, 5 µm
Eluents : A = n-Heptane
B = i-Propanol
Flow : 0.5 ml/min

λ : 215 nm

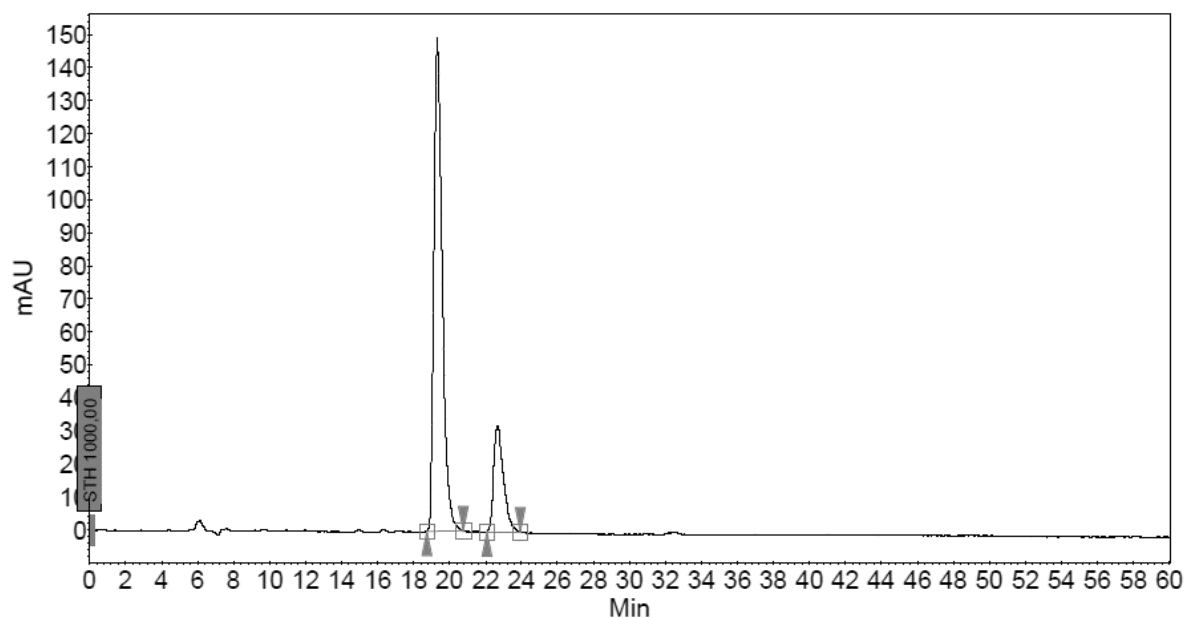
**Peak Results :**

Index	Name	Time [Min]	Quantity [% Area]	Height [mAU]	Area [mAU.Min]	Area % [%]
1	UNKNOWN	19.39	49.77	127.3	68.3	49.772
2	UNKNOWN	22.56	50.23	105.6	69.0	50.228
Total			100.00	232.9	137.3	100.000

Vial : 31
Method : Phex-Cel1_70-30_0.5
Run time : 60,00 min
Inj. vol. : 10,000 µl

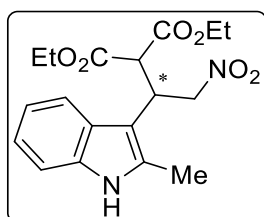
Column : Phenomenex Lux Cellulose-1,
4.6 x 250 mm, 5 µm
Eluents : A = n-Heptane
B = i-Propanol
Flow : 0.5 ml/min

λ : 215 nm



Peak Results :

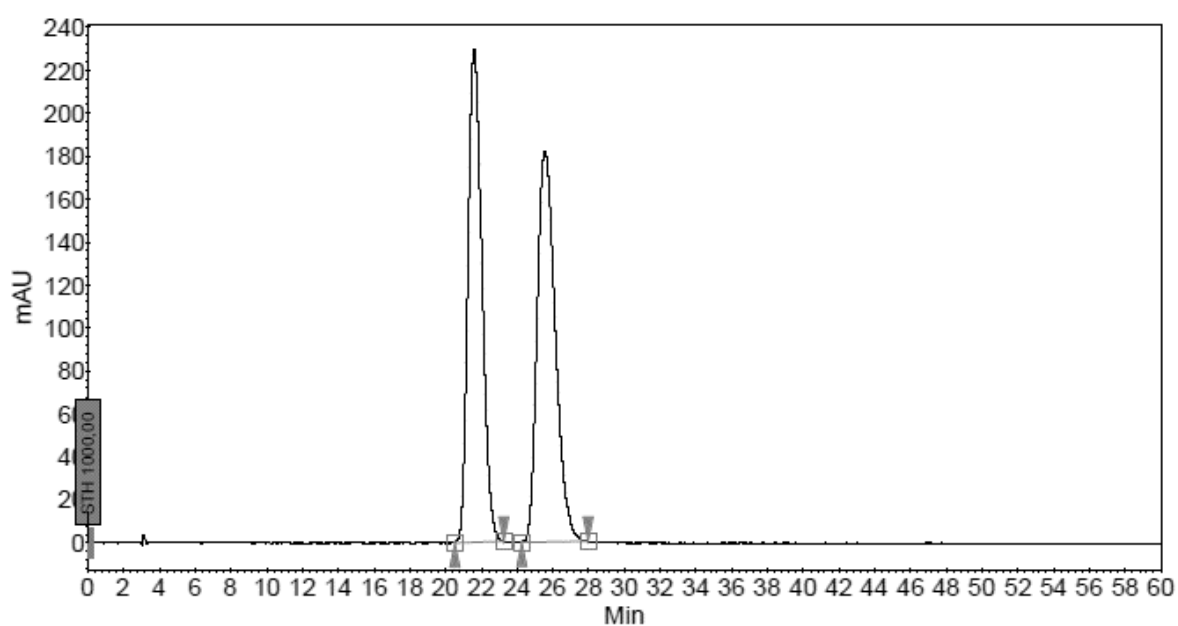
Index	Name	Time [Min]	Quantity [% Area]	Height [mAU]	Area [mAU.Min]	Area % [%]
1	UNKNOWN	19.32	79.87	149.2	80.6	79.873
2	UNKNOWN	22.67	20.13	32.1	20.3	20.127
Total			100.00	181.2	100.9	100.000

Diethyl-2-(1-(2-methyl-1H-indol-3-yl)-2-nitroethyl)malonat (58I)

Vial : 35
Method : AS-H_90-10
Run time : 60,00 min
Inj. vol. : 5,000 µl

Column : Chiralcel AS-H, 4.6 x 250 mm, 10 µm
Eluents : A = n-Heptane
 B = i-Propanol
Flow : 1.0 ml/min

λ : 215 nm

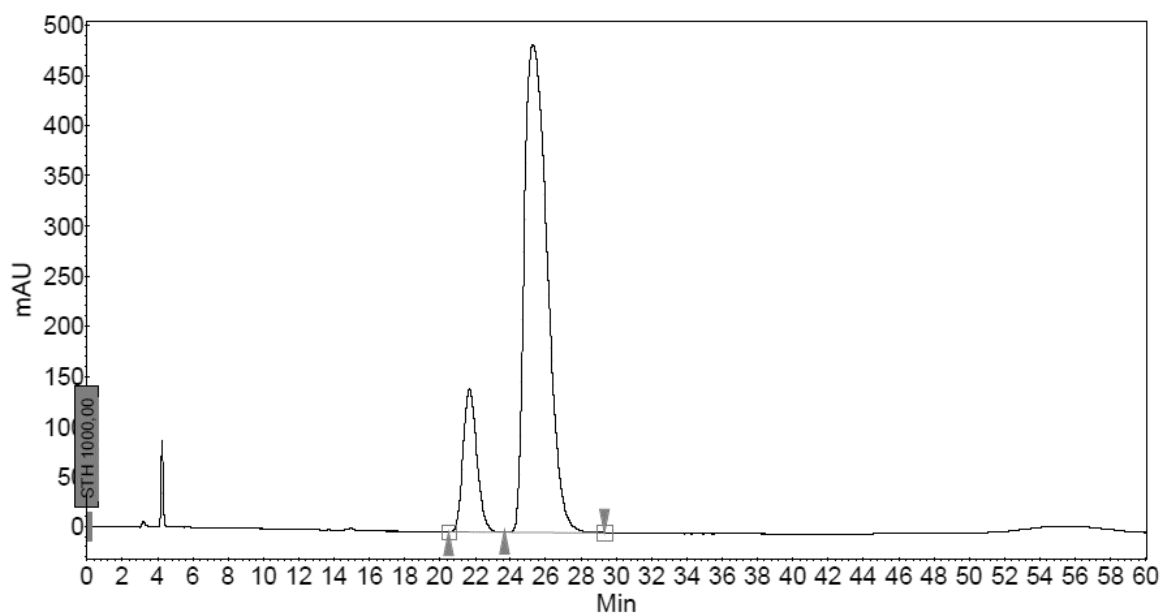
**Peak Results :**

Index	Name	Time [Min]	Quantity [% Area]	Height [mAU]	Area [mAU.Min]	Area % [%]
1	UNKNOWN	21.61	49.37	229.4	207.9	49.368
2	UNKNOWN	25.57	50.63	181.8	213.2	50.632
Total			100.00	411.2	421.1	100.000

Vial : 37
Method : AS-H_90-10
Run time : 60,00 min
Inj. vol. : 10,000 µl

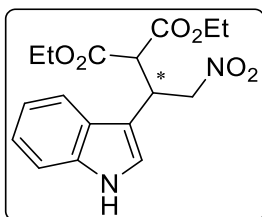
Column : Chiralcel AS-H, 4.6 x 250 mm, 10 µm
Eluents : A = n-Heptane
 B = i-Propanol
Flow : 1.0 ml/min

λ : 215 nm



Peak Results :

Index	Name	Time [Min]	Quantity [% Area]	Height [mAU]	Area [mAU.Min]	Area % [%]
1	UNKNOWN	21,67	15,00	142,6	128,2	14,997
2	UNKNOWN	25,27	85,00	485,4	726,8	85,003
Total			100,00	628,0	855,0	100,000

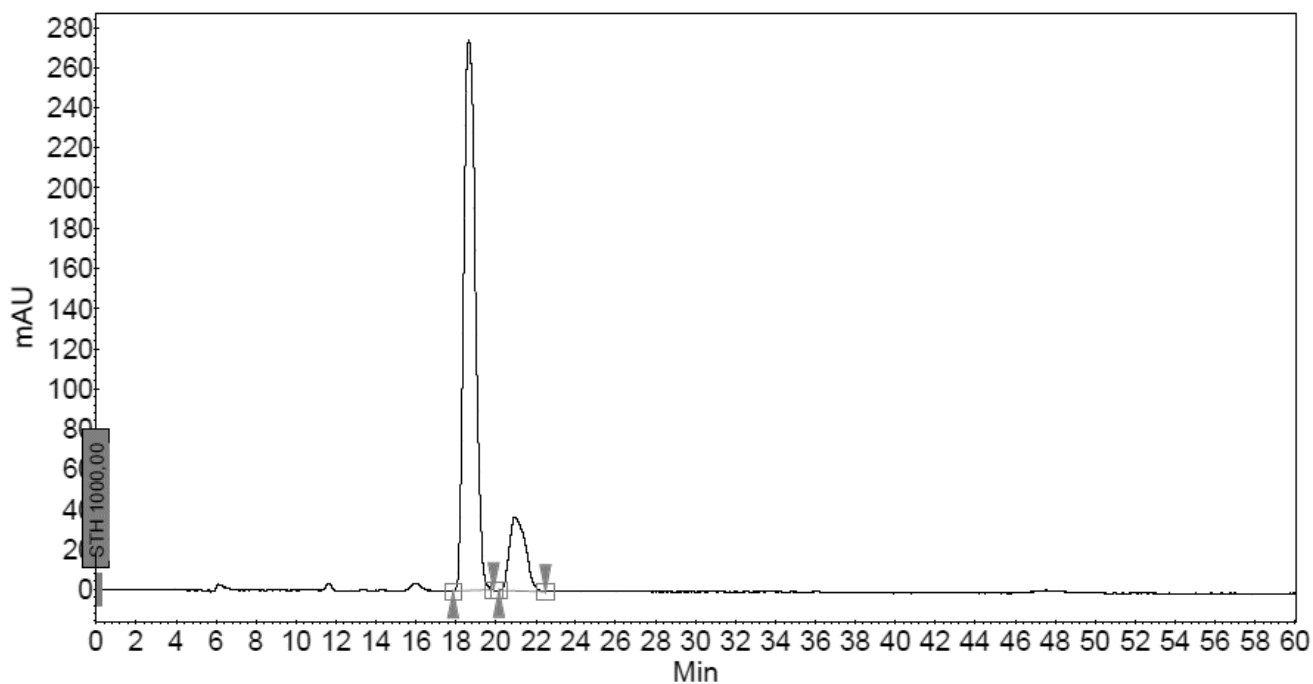
Diethyl-2-(2-(1*H*-indol-3-yl)-2-nitroethyl)malonat (58m)

Chiral HPLC measurement of the racemic mixture was not possible due to technical problems caused by the sample.

Vial : 95
 Method : AS-H_70-30_0.5
 Run time : 60,00 min
 Inj. vol. : 10,000 µl

Column : Chiralpak AS-H, 4.6 x 250 mm, 10 µm
 Eluents : A = n-Heptane
 B = i-Propanol
 Flow : 0.5 ml/min

λ : 215 nm

**Peak Results :**

Index	Name	Time [Min]	Quantity [% Area]	Height [mAU]	Area [mAU.Min]	Area % [%]
1	UNKNOWN	18,66	84,29	274,1	184,6	84,294
2	UNKNOWN	20,95	15,71	36,8	34,4	15,706
Total			100,00	310,9	219,0	100,000

6 References

- [1] T. Weinbender, M. Hofmann, O. Reiser, *Biophys. Chem.* **2019**, 106280.
- [2] E. Hogan, A. L. Kelly, D.-W. Sun in *Emerging Technologies for Food Processing*, Elsevier, **2005**, pp. 3–32.
- [3] S. D. Hamann, *Annu. Rev. Phys. Chem.* **1964**, *15*, 349.
- [4] G. Jenner, *Tetrahedron* **2002**, *58*, 5185.
- [5] O. Reiser, *Top. Catal.* **1998**, *5*, 105.
- [6] B. Chen, R. Hoffmann, R. Cammi, *Angew. Chem. Int. Ed. Engl.* **2017**, *56*, 11126.
- [7] a) Y. Yoshimura, J. Osugi, M. Nakahara, *BCSJ* **1983**, *56*, 680; b) Y. Yoshimura, J. Osugi, M. Nakahara, *J. Am. Chem. Soc.* **1983**, *105*, 5414; c) F.-G. Klaerner, B. Krawczyk, V. Ruster, U. K. Deiters, *J. Am. Chem. Soc.* **1994**, *116*, 7646; d) M. K. Diedrich, F.-G. Klärner, *J. Am. Chem. Soc.* **1998**, *120*, 6212.
- [8] J. S. Hill, N. S. Isaacs, *Tetrahedron Lett.* **1986**, *27*, 5007.
- [9] G. Jenner, *Angew. Chem. Int. Ed. Engl.* **1975**, *14*, 137.
- [10] F. Karl Fleischmann, H. Kelm, *Tetrahedron Lett.* **1973**, *14*, 3773.
- [11] G. Jenner, *J. Phys. Org. Chem.* **1999**, *12*, 619.
- [12] R. van Eldik, T. Asano, W. J. Le Noble, *Chem. Rev.* **1989**, *89*, 549.
- [13] W. G. Dauben, A. P. Kozikowski, *J. Am. Chem. Soc.* **1974**, *96*, 3664.
- [14] M. Bellassoued, E. Reboul, F. Dumas, *Tetrahedron Lett.* **1997**, *38*, 5631.
- [15] B. List, R. A. Lerner, C. F. Barbas, *J. Am. Chem. Soc.* **2000**, *122*, 2395.
- [16] K. A. Ahrendt, C. J. Borths, D. W. C. MacMillan, *J. Am. Chem. Soc.* **2000**, *122*, 4243.
- [17] Y. Hayashi, W. Tsuboi, M. Shoji, N. Suzuki, *J. Am. Chem. Soc.* **2003**, *125*, 11208.
- [18] B. List, P. Pojarliev, W. T. Biller, H. J. Martin, *J. Am. Chem. Soc.* **2002**, *124*, 827.
- [19] H. Kotsuki, K. Nakano, Y. Ichikawa, *Heterocycles* **2010**, *80*, 799.
- [20] M. Wiesner, M. Neuburger, H. Wennemers, *Chem. Eur. J.* **2009**, *15*, 10103.

- [21] a) J. Duschmalé, H. Wennemers, *Chem. Eur. J.* **2012**, *18*, 1111; b) R. Kastl, H. Wennemers, *Angew. Chem. Int. Ed. Engl.* **2013**, *52*, 7228; c) T. Schnitzer, H. Wennemers, *Synlett* **2017**, *28*, 1282; d) M. Wiesner, J. D. Revell, H. Wennemers, *Angew. Chem. Int. Ed. Engl.* **2008**, *47*, 1871; e) P. Krattiger, R. Kovasy, J. D. Revell, S. Ivan, H. Wennemers, *Org. Lett.* **2005**, *7*, 1101.
- [22] J. D. Revell, H. Wennemers, *Adv. Synth. Catal.* **2008**, *350*, 1046.
- [23] J. D. Revell, H. Wennemers, *Tetrahedron* **2007**, *63*, 8420.
- [24] R. Beumer, C. Bubert, C. Cabrele, O. Vielhauer, M. Pietzsch, O. Reiser, *J. Org. Chem.* **2000**, *65*, 8960.
- [25] V. D'Elia, H. Zwicknagl, O. Reiser, *J. Org. Chem.* **2008**, *73*, 3262.
- [26] L. K. A. Pilsl, *Dissertation*, Universität Regensburg, Regensburg, **2015**.
- [27] M. Hofmann, *Dissertation*, Universität Regensburg, Regensburg, **2018**.
- [28] Z. Zhao, D. Herbst, B. Niemeyer, L. He, *Food Bioprod. Process.* **2015**, *96*, 240.
- [29] M. J. Eisenmenger, J. I. Reyes-De-Corcuera, *Enzyme Microb. Technol* **2009**, *45*, 118.
- [30] G. Dodson, *Trends Biochem. Sci.* **1998**, *23*, 347.
- [31] M. J. Eisenmenger, J. I. Reyes-De-Corcuera, *J. Mol. Catal. B: Enzym.* **2010**, *67*, 36.
- [32] T. Q. Luong, N. Erwin, M. Neumann, A. Schmidt, C. Loos, V. Schmidt, M. Fändrich, R. Winter, *Angew. Chem. Int. Ed. Engl.* **2016**, *55*, 12412.
- [33] S. Kara, W. S. Long, M. Berheide, S. Peper, B. Niemeyer, A. Liese, *J. Biotechnol.* **2011**, *152*, 87.
- [34] a) P. Kwiatkowski, K. Dudziński, D. Łyżwa, *Org. Lett.* **2011**, *13*, 3624; b) P. Kwiatkowski, A. Cholewiak, A. Kasztelan, *Org. Lett.* **2014**, *16*, 5930; c) A. Cholewiak, K. Adamczyk, M. Kopyt, A. Kasztelan, P. Kwiatkowski, *Org. Biomol. Chem.* **2018**, *16*, 4365.
- [35] D. Łyżwa, K. Dudziński, P. Kwiatkowski, *Org. Lett.* **2012**, *14*, 1540.
- [36] A. Kasztelan, M. Biedrzycki, P. Kwiatkowski, *Adv. Synth. Catal.* **2016**, *358*, 2962.
- [37] P. R. Schreiner, A. Wittkopp, *Org. Lett.* **2002**, *4*, 217.
- [38] K. Mori, J. Maddaluno, K. Nakano, Y. Ichikawa, H. Kotsuki, *Synlett* **2009**, 2346.

- [39] N. Miyamae, N. Watanabe, M. Moritaka, K. Nakano, Y. Ichikawa, H. Kotsuki, *Org. Biomol. Chem.* **2014**, *12*, 5847.
- [40] S. Hillers, S. Sartori, O. Reiser, *J. Am. Chem. Soc.* **1996**, *118*, 2087.
- [41] S. Hillers, O. Reiser, *Tetrahedron Lett.* **1993**, *34*, 5265.
- [42] T. Weinbender, M. Knierbein, L. Bittorf, C. Held, R. Siewert, S. P. Verevkin, G. Sadowski, O. Reiser, *ChemPlusChem* **2020**.
- [43] A. Michael, *J. Prakt. Chem.* **1887**, *35*, 349.
- [44] M. Conrad, M. Guthzeit, *Ber. Dtsch. Chem. Ges.* **1884**, *17*, 1185.
- [45] a) Y.-H. Li, P. S. Akula, B.-C. Hong, C.-H. Peng, G.-H. Lee, *Org. Lett.* **2019**, *21*, 7750; b) N. Ono, H. Feuer (Eds.) *Wiley Series in Organic Nitro Chemistry*, John Wiley & Sons, Inc, New York, USA, **2001**; c) S. Z. Zard, *Helv. Chim. Acta* **2012**, *95*, 1730.
- [46] N. Ono, H. Miyake, A. Kamimura, I. Hamamoto, R. Tamura, A. Kaji, *Tetrahedron* **1985**, *41*, 4013.
- [47] T. Mukaiyama, T. Hoshino, *J. Am. Chem. Soc.* **1960**, *82*, 5339.
- [48] a) A. K. Beck, D. Seebach, *Ber. Dtsch. Chem. Ges.* **1991**, *124*, 2897; b) M.-A. Poupart, G. Fazal, S. Goulet, L. T. Mar, *J. Org. Chem.* **1999**, *64*, 1356; c) A. G.M. Barrett, C. D. Spilling, *Tetrahedron Lett.* **1988**, *29*, 5733; d) D. H. Lloyd, D. E. Nichols, *J. Org. Chem.* **1986**, *51*, 4294.
- [49] H. W. Pinnick in *Organic Reactions*, John Wiley & Sons, Inc, Hoboken, NJ, USA, **2004**, pp. 655–792.
- [50] M. Berthelot, P. De Saint-Gilles, *Recherches sur les affinités de la formation et de la décomposition des éthers*, Mallet-Bachelier, **1862**.
- [51] a) S. Brownstein, *Can. J. Chem.* **1960**, *38*, 1590; b) O. Tapia, J. Bertrán, *Solvent Effects and Chemical Reactivity*, Vol. 17, Springer, **1996**; c) C. Reichardt, T. Welton, *Solvents and solvent effects in organic chemistry*, Wiley-VCH, Weinheim, Germany, **2011**.
- [52] a) A. Behr, J. Leschinski, C. Awungacha, S. Simic, T. Knoth, *ChemSusChem* **2009**, *2*, 71; b) A. Behr, N. Tenhumberg, A. Wintzer, *RSC Adv* **2013**, *3*, 172; c) S. Grob, H. Hasse, *J. Chem. Eng. Data* **2005**, *50*, 92; d) H. Struebing, Z. Ganase, P. G. Karamertzanis, E. Siougkrou, P. Haycock, P. M. Piccione, A. Armstrong, A. Galindo, C. S. Adjiman, *Nat. Chem.* **2013**, *5*, 952.

- [53] a) A. Wangler, R. Loll, T. Greinert, G. Sadowski, C. Held, *J. Chem. Thermodyn.* **2019**, *128*, 275; b) A. Wangler, A. Hüser, G. Sadowski, C. Held, *ACS omega* **2019**, *4*, 6264; c) A. Wangler, R. Canales, C. Held, T. Q. Luong, R. Winter, D. H. Zaitsau, S. P. Verevkin, G. Sadowski, *Phys. Chem. Chem. Phys.* **2018**, *20*, 11317; d) M. Voges, R. Abu, M. T. Gundersen, C. Held, J. M. Woodley, G. Sadowski, *Org. Process Res. Dev.* **2017**, *21*, 976; e) M. Voges, C. Fischer, D. Wolff, C. Held, *Org. Process Res. Dev.* **2017**, *21*, 1059; f) M. Voges, F. Fischer, M. Neuhaus, G. Sadowski, C. Held, *Ind. Eng. Chem. Res.* **2017**, *56*, 5535; g) A. E.M. Janssen, B. J. Sijursnes, A. V. Vakurov, P. J. Halling, *Enzyme Microb. Technol.* **1999**, *24*, 463; h) A. E.M. Janssen, A. M. Vaidya, P. J. Halling, *Enzyme Microb. Technol.* **1996**, *18*, 340.
- [54] M. Lemberg, R. Schomäcker, G. Sadowski, *Chem. Eng. Sci.* **2018**, *176*, 264.
- [55] M. Lemberg, G. Sadowski, M. Gerlach, E. Kohls, M. Stein, C. Hamel, A. Seidel-Morgenstern, *AIChE J.* **2017**, *63*, 4576.
- [56] M. Lemberg, G. Sadowski, *ChemPhysChem* **2017**, *18*, 1977.
- [57] a) O. Riechert, M. Husham, G. Sadowski, T. Zeiner, *AIChE J.* **2015**, *61*, 3000; b) R. Rönneck, T. Salmi, A. Vuori, H. Haario, J. Lehtonen, A. Sundqvist, E. Tirronen, *Chem. Eng. Sci.* **1997**, *52*, 3369; c) H. Teo, B. Saha, *J. Catal.* **2004**, *228*, 174; d) V. K. S. Pappu, A. J. Yanez, L. Peereboom, E. Muller, C. T. Lira, D. J. Miller, *Bioresour. Technol.* **2011**, *102*, 4270; e) Y. Qu, S. Peng, S. Wang, Z. Zhang, J. Wang, *Chin. J. Chem. Eng.* **2009**, *17*, 773; f) M. T. Sanz, R. Murga, S. Beltrán, J. L. Cabezas, J. Coca, *Ind. Eng. Chem. Res.* **2002**, *41*, 512; g) P. Kiviranta-Pääkkönen, L. Struckmann, A. O. I. Krause, *Chem. Eng. Technol.* **1998**, *21*, 321; h) P. Delgado, M. T. Sanz, S. Beltrán, *Chem. Eng. J.* **2007**, *126*, 111; i) P. Patidar, S. M. Mahajani, *Chem. Eng. J.* **2012**, *207-208*, 377; j) A. K. Kolah, N. S. Asthana, D. T. Vu, C. T. Lira, D. J. Miller, *Ind. Eng. Chem. Res.* **2007**, *46*, 3180; k) J. Gangadwala, S. Mankar, S. Mahajani, A. Kienle, E. Stein, *Ind. Eng. Chem. Res.* **2003**, *42*, 2146; l) L. K. Rihko, P. K. Kiviranta-Pääkkönen, A. O. I. Krause, *Ind. Eng. Chem. Res.* **1997**, *36*, 614; m) T. Pöpken, L. Götze, J. Gmehling, *Ind. Eng. Chem. Res.* **2000**, *39*, 2601; n) A. Orjuela, A. J. Yanez, A. Santhanakrishnan, C. T. Lira, D. J. Miller, *Chem. Eng. J.* **2012**, *188*, 98; o) W.-T. Liu, C.-S. Tan, *Ind. Eng. Chem. Res.* **2001**, *40*, 3281.
- [58] M. Planck, *Ann. Phys. Chem.* **1887**, *268*, 462.
- [59] V. Rothmund, *Z. Phys. Chem.* **1896**, *20U*.
- [60] a) R. Winter, D. Lopes, S. Grudzielanek, K. Vogtt, *J. Non-Equilib. Thermodyn.* **2007**, *32*, 367; b) T. Q. Luong, S. Kapoor, R. Winter, *ChemPhysChem* **2015**, *16*, 3555.

- [61] a) S. W. Benson, J. A. Berson, *J. Am. Chem. Soc.* **1962**, *84*, 152; b) E. Whalley, *Ber. Bunsenges. Phys. Chem.* **1996**, *70*, 958; c) J. H. Espenson, *Chemical kinetics and reaction mechanisms, Vol. 102*, Citeseer, **1995**; d) H. Tiltcher, H. Hofmann, *Chem. Eng. Sci.* **1987**, *42*, 959; e) D. G. Peck, A. J. Mehta, K. P. Johnston, *J. Phys. Chem.* **1989**, *93*, 4297; f) G. Jenner, *J. Phys. Org. Chem.* **2002**, *15*, 1; g) F.-G. Klärner, F. Wurche, *J. Prakt. Chem.* **2000**, *342*, 609; h) R. van Eldik, *Angew. Chem. Int. Ed. Engl.* **1986**, *25*, 673.
- [62] K. Matsumoto, T. Uchida, *Chem. Lett.* **1981**, *10*, 1673.
- [63] a) M. E. G. Hendrickx, D. Knorr, L. Ludikhuyze, A. Loey, V. Heinz, *Ultra High Pressure Treatments of Foods*, Springer, US, **2012**; b) P. C. K. Cheung, B. M. Mehta (Eds.) *Handbook of food chemistry*, Springer Reference, Heidelberg, New York, Dordrecht, London, **2015**.
- [64] T. Okino, Y. Hoashi, Y. Takemoto, *J. Am. Chem. Soc.* **2003**, *125*, 12672.
- [65] T. Okino, Y. Hoashi, T. Furukawa, X. Xu, Y. Takemoto, *J. Am. Chem. Soc.* **2005**, *127*, 119.
- [66] a) J. Gross, G. Sadowski, *Ind. Eng. Chem. Res.* **2001**, *40*, 1244; b) J. Gross, J. Vrabec, *AIChE J.* **2006**, *52*, 1194.
- [67] O. Reiser, *Top. Catal.* **1998**, *5*, 105.
- [68] a) A. Brozena, J. H. Buchanan, R. W. Miles, B. R. Williams, M. S. Hulet, *J. Chem. Eng. Data* **2014**, *59*, 2649; b) J. A. Riddick, W. B. Bunger, T. K. Sakano, *Organic Solvents: Physical Properties and Methods of Purification*, Wiley, **1986**; c) S.L. Oswal, P. Oswal, P.S. Modi, J.P. Dave, R.L. Gardas, *Thermochimica Acta* **2004**, *410*, 1; d) C. L. Yaws, *Chemical properties handbook. Physical, thermodynamic, environmental, transport, safety, and health related properties for organic and inorganic chemicals*, Knovel, Norwich, NY, **2001**.
- [69] For reactions on preparative scale, we could not go beyond 440 MPa with the pressure equipment available to us.
- [70] J. Awapara, A. J. Landua, R. Fuerst, B. Seale, *J. Biol. Chem.* **1950**, *187*, 35.
- [71] S. Udenfriend, *J. Biol. Chem.* **1950**, *187*, 65.
- [72] E. Roberts, S. Frankel, *J. Biol. Chem.* **1950**, *187*, 55.
- [73] J. L. Brennan, J. G. Leung, J. P. Gagliardi, S. K. Rivelli, A. J. Muzyk, *Clin. Pharmacol.* **2013**, *5*, 99.

- [74] W. Froestl, B. Bettler, H. Bittiger, J. Heid, K. Kaupmann, S. J. Mickel, D. Strub, *Farmaco* **2003**, *58*, 173.
- [75] a) H. Mudila, P. Prasher, M. Kumar, A. Kumar, M. G. H. Zaidi, A. Kumar, *J. Renew. Sustain. Energy* **2019**, *8*, 509; b) H. Talbi, G. Monard, M. Loos, D. Billaud, *J. Mol. Struct.* **1998**, *434*, 129.
- [76] J. O. Osby, B. Ganem, *Tetrahedron Lett.* **1985**, *26*, 6413.
- [77] a) D. R. Askeland, W. J. Wright, *The science and engineering of materials*, Cengage Learning, Boston, MA, **2016**; b) W. O. Soboyejo, *Mechanical properties of engineered materials*, Marcel Dekker, New York, **2003**.
- [78] J. E. Huheey, E. A. Keiter, R. L. Keiter, *Inorganic chemistry. Principles of structure and reactivity*, Harper; HarperCollins, Cambridge, New York, NY, **2009**.
- [79] G. A. Jeffrey, *An introduction to hydrogen bonding*, Oxford Univ. Press, New York, **1997**.
- [80] L. Pauling, *The nature of the chemical bond and the structure of molecules and crystals. An introduction to modern structural chemistry*, Cornell Univ. Press, Ithaca, New York, **1960**.
- [81] K. Roy, S. Kar, R. N. Das in *Understanding the Basics of QSAR for Applications in Pharmaceutical Sciences and Risk Assessment*, Elsevier, **2015**, pp. 1–46.
- [82] P. A. Kollman, L. C. Allen, *Chem. Rev.* **1972**, *72*, 283.
- [83] a) M. M. Kreevoy, T. M. Liang, *J. Am. Chem. Soc.* **1980**, *102*, 3315; b) W. W. Cleland, *Biochemistry* **1992**, *31*, 317; c) W. W. Cleland, M. M. Kreevoy, *Science* **1994**, *264*, 1887.
- [84] F. Hibbert, J. Emsley in *Advances in Physical Organic Chemistry*, Elsevier, **1990**, pp. 255–379.
- [85] P. A. Frey, *Magn. Reson. Chem.* **2001**, *39*, S190-S198.
- [86] D. J. Gardiner, H. J. Bowley (Eds.) *Practical Raman spectroscopy*, Springer, Berlin, **1989**.
- [87] H. Günzler, H.-U. Gremlich, *IR-Spektroskopie. Eine Einführung*, Wiley; Wiley-VCH, Hoboken, NJ, Weinheim, **2003**.
- [88] H. Friebolin, C. M. Thiele, *Ein- und zweidimensionale NMR-Spektroskopie. Eine Einführung*, Wiley-VCH, Weinheim, **2013**.

- [89] S. Fanetti, M. Citroni, K. Dziubek, M. M. Nobrega, R. Bini, *J. Phys. Condens. Matter* **2018**, *30*, 94001.
- [90] H. Ohtaki, *J. Mol. Liq.* **2003**, *103-104*, 3.
- [91] H. Y. Kim, K. Oh, *Org. Lett.* **2011**, *13*, 1306.
- [92] a) D. H. Appella, L. A. Christianson, I. L. Karle, D. R. Powell, S. H. Gellman, *J. Am. Chem. Soc.* **1996**, *118*, 13071; b) S. H. Gellman, *Acc. Chem. Res.* **1998**, *31*, 173; c) C. M. Goodman, S. Choi, S. Shandler, W. F. DeGrado, *Nat. Chem. Biol.* **2007**, *3*, 252.
- [93] G. P. Dado, S. H. Gellman, *J. Am. Chem. Soc.* **1994**, *116*, 1054.
- [94] C. Zorn, *Dissertation*, Universität Regensburg, Regensburg, **2001**.
- [95] H.-S. Wu, S.-H. Jou, *J. Chem. Technol. Biotechnol.* **1995**, *64*, 325.
- [96] C. B. Tripathi, S. Mukherjee, *J. Org. Chem.* **2012**, *77*, 1592.
- [97] N. Duguet, A. Donaldson, S. M. Leckie, J. Douglas, P. Shapland, T. B. Brown, G. Churchill, A. M.Z. Slawin, A. D. Smith, *Tetrahedron: Asymmetry* **2010**, *21*, 582.
- [98] Y. Liu, T.-R. Kang, Q.-Z. Liu, L.-M. Chen, Y.-C. Wang, J. Liu, Y.-M. Xie, J.-L. Yang, L. He, *Org. Lett.* **2013**, *15*, 6090.
- [99] J.-Y. Fu, X.-Y. Xu, Y.-C. Li, Q.-C. Huang, L.-X. Wang, *Org. Biomol. Chem.* **2010**, *8*, 4524.
- [100] A. Berkessel, B. Seelig, *Synthesis* **2009**, *2009*, 2113.
- [101] A. Berkessel, S. Mukherjee, T. N. Müller, F. Cleemann, K. Roland, M. Brandenburg, J.-M. Neudörfel, J. Lex, *Org. Biomol. Chem.* **2006**, *4*, 4319.
- [102] M. Petrini, R. Ballini, E. Marcantoni, G. Rosini, *Synth. Commun.* **1988**, *18*, 847.
- [103] *Org. Synth.* **1929**, *9*, 66.
- [104] K. R. Law, C. S. P. McErlean, *Chemistry* **2013**, *19*, 15852.
- [105] J.-P. Strachan, D. F. O'Shea, T. Balasubramanian, J. S. Lindsey, *J. Org. Chem.* **2000**, *65*, 3160.
- [106] J. D. Neuhaus, P. Angyal, R. Oost, N. Maulide, *J. Org. Chem.* **2018**, *83*, 2479.
- [107] V. Leen, E. Braeken, K. Luckermans, C. Jackers, M. van der Auweraer, N. Boens, W. Dehaen, *Chem. Commun.* **2009**, 4515.

- [108] S. R. Shengule, G. Ryder, A. C. Willis, S. G. Pyne, *Tetrahedron* **2012**, *68*, 10280.
- [109] Y.-L. Zhang, Y.-J. Qin, D.-J. Tang, M.-R. Yang, B.-Y. Li, Y.-T. Wang, H.-Y. Cai, B.-Z. Wang, H.-L. Zhu, *ChemMedChem* **2016**, *11*, 1446.
- [110] S. Kandekar, R. Preet, M. Kashyap, M. U. Renu Prasad, P. Mohapatra, D. Das, S. R. Satapathy, S. Siddharth, V. Jain, M. Choudhuri et al., *ChemMedChem* **2013**, *8*, 1873.
- [111] F. Giraud, C. Loge, F. Pagniez, D. Crepin, S. Barres, C. Picot, P. Le Pape, M. Le Borgne, *J. Enzym. Inhib. Med. Chem.* **2009**, *24*, 1067.
- [112] R. Balamurugan, R. Sureshbabu, G. G. Rajeshwaran, A. K. Mohanakrishnan, *Synth. Commun.* **2009**, *39*, 531.
- [113] N. Gigant, E. Claveau, P. Bouyssou, I. Gillaizeau, *Org. Lett.* **2012**, *14*, 844.
- [114] S. Dai, C. Chen, *Angew. Chem. Int. Ed. Engl.* **2016**, *55*, 13281.
- [115] J. Fournier Dit Chabert, L. Joucla, E. David, M. Lemaire, *Tetrahedron* **2004**, *60*, 3221.
- [116] R. P. Dickinson, B. Iddon, *J. Chem. Soc., C* **1968**, 2733.
- [117] Y. Duan, J.-H. Lin, J.-C. Xiao, Y.-C. Gu, *Org. Lett.* **2016**, *18*, 2471.
- [118] S. Maity, T. Naveen, U. Sharma, D. Maiti, *Org. Lett.* **2013**, *15*, 3384.
- [119] V. M. Berestovitskaya, E. A. Ishmaeva, I. A. Litvinov, O. S. Vasil'eva, Y. A. Vereshchagina, E. S. Ostroglyadov, G. R. Fattakhova, D. V. Beskrovnyi, S. M. Aleksandrova, *Russ. J. Gen. Chem.* **2004**, *74*, 1108.
- [120] J. M. Andrés, R. Manzano, R. Pedrosa, *Chemistry* **2008**, *14*, 5116.

7 Appendix

7.1 Curriculum Vitae

Personal Data

Name Thomas Weinbender
Date / place of birth 22.05.1993 Prien a. Chiemsee
Citizenship German
Marital status Unmarried
E-Mail thomas.weinbender@gmail.com

Education

11/2016 – 08/2020 PhD (Dr. rer. nat.), Organic Chemistry
University of Regensburg
Dissertation: The Effect of High Hydrostatic Pressure on Hydrogen Bond Scaffolds

10/2014 – 09/2016 Master of Science (M. Sc.), Chemistry
University of Regensburg
Master thesis: The organocatalyzed & high pressure mediated 1,4-conjugate addition of malonate derivatives to nitroolefins using thiourea based catalysts

10/2011 – 09/2014 Bachelor of Science (B. Sc.), Chemistry
University of Regensburg
Bachelor thesis: Synthesestrategien zur Darstellung von stabilisierten Phosphorsulfidanionen in Kupfer(I)-halogenid-Matrizen

09/2003 – 06/2011 General Qualification for the University Entrance
Johannes-Heidenhain-Gymnasium Traunreut
Degree: Allgemeine Hochschulreife

Professional References

Prof. Dr. Oliver Reiser Institut für Organische Chemie
Universität Regensburg, Universitätsstr. 31
93053 Regensburg, Germany
Phone: +49 941 9434631
E-mail: oliver.reiser@chemie.uni-regensburg.de

International

- Conferences
- Solvation Science Meets High Pressure Bioscience: RESOLVE – 10th IMBP – DFG FOR 1979 (Poster, 10/2019)
 - 7. EuCheMS Chemistry Congress in Liverpool, Großbritannien (Poster, 09/2018)
 - GDCh-Wissenschaftsforum in Berlin, Deutschland (Poster, 09/2017)
 - 26. ISHC Congress in Regensburg, Deutschland (Poster, 09/2017)

Publications

- [1] T. Weinbender, M. Hofmann, O. Reiser, *Biophys. Chem.* **2019**, 106280. “*Functional changes of biomolecules and organocatalysts as a probe for pressure effects in solution*”
- [2] T. Weinbender, M. Knierbein, L. Bittorf, C. Held, R. Siewert, S. P. Verevkin, G. Sadowski, O. Reiser, *ChemPlusChem* **2020**. “*High-Pressure-Mediated Thiourea-Organocatalyzed Asymmetric Michael Addition to (Hetero)aromatic Nitroolefins: Prediction of Reaction Parameters by PCP-SAFT Modelling*”

8 Acknowledgement

Mein besonderer Dank gilt Herrn Prof. Dr. Oliver Reiser für die Aufnahme in seine Arbeitsgruppe, Bereitstellung des interessanten Themas, das rege Interesse an meiner Arbeit und konstruktive Kritik, sowie die hervorragenden Arbeitsbedingungen am Lehrstuhl.

Für die technische Unterstützung danke ich Dr. Peter Kreitmeier, Klaus Döring, Johannes Floss, Roxane Harteis und Brigitte Eichenseher. Zudem gilt mein Dank Michaela Schüle für die Unterstützung organisatorischer Angelegenheiten.

Für die nette Atmosphäre im Labor und große Hilfsbereitschaft im Laboralltag möchte ich mich bei Christian Lankes, Eugen Lutsker, Natalija Moor, Martin Stinglhamer und Sebastian Engl bedanken.

Außerdem danke ich allen Mitarbeitern des Lehrstuhls für die Hilfe während des Laboralltags. Besonderer Dank gilt dabei Christian Kaiser und Eugen Lutsker, die mich auch in besonders schweren Zeiten unterstützt haben.

Für die Zusammenarbeit im Rahmen des Projektes „High-pressure-mediated thiourea-organocatalyzed Michael addition to (hetero)aromatic nitroolefins: Prediction of reaction parameters by PCP-SAFT modelling“ bedanke ich mich bei Prof. Gabriele Sadowski und Dr. Christoph Held. Besonderer Dank gilt Michael Knierbein für den intensiven Austausch während der Erstellung des Manuskripts.

Meinen ehemaligen Bachelorstudenten und Forschungspraktikanten Franz F. Westermair, Bettina Brechenmacher und Sebastian Fischer danke ich für ihre engagierte Mitarbeit und qualitativ hochwertige Berichte.

Den Mitarbeitern der zentralen Analytik Fritz Kastner, Annette Schramm, Georgine Stuhler, Veronica Scheidler und Dr. Ilya Shenderovich danke ich für die Hilfe bei der Aufnahme von NMR Spektren aller Art und Josef Kiermaier und Wolfgang Söllner für die Durchführung der Massenspektroskopien.

Für die finanzielle Unterstützung bedanke ich mich bei der Deutschen Forschungsgemeinschaft im Rahmen der Forschungseinheit FOR 1979.

Für die großartige Zeit auch außerhalb des Labors bedanke ich mich bei meinen Freunden Anja Busler, Thomas Rawner, Christian A. Kaiser, Eugen Lutsker, Sebastian Engl, Tomislav Krolo, Tobias Babl, Carina Sonnleitner, Nikolai Wurzer und einigen mehr.

Für das Korrekturlesen der Arbeit möchte ich mich bei Sebastian Engl, Tomislav Krolo, Carina Sonnleitner und Nikolai Wurzer recht herzlich bedanken.

Vielen Dank auch an meine Kommilitonen und Freunde Alexander Wimmer, Andreas Graml und Matthias Schmalzbauer für die unvergesslichen und lustigen Shisha- und Nintendo 64-Abende. Gemeinsam haben wir so einige nächtliche Abenteuer erlebt.

Meinen Freunden Julian "Julzn" Farkas, Igor „Пидор“ Abt, Christian „Cizi“ Richter und Johannes „Huansi“ Staffa aus dem schönen Chiemgau danke ich für die tollen Wochenendausflüge, die verrückten Nächte, die wir in Regensburg verbracht haben und vor allem die Gespräche, die nie etwas mit Chemie zu tun hatten. Auf viele weitere Erlebnisse mit euch freue ich mich schon mit einem Schmunzeln im Gesicht.

Der größte Dank gilt meiner Familie und besonders meinen Eltern Katharina & Fedor und meinem Bruder Fedor für ihre Unterstützung bereits während der Schulzeit und dann des Studiums. Auch in schweren Zeiten wusste ich, dass ich mich auf euch verlassen kann.

DANKE

9 Declaration

Herewith I declare that this present PhD thesis is a presentation of my original work prepared single-handed. Wherever contributions from others are involved, all of them are marked clearly, with reference to the literature, license and acknowledgement of collaborative research.

Regensburg, 17.06.2020

Thomas Weinbender